Talanta

The International Journal of Pure and Applied Analytical Chemistry

Aims & Scope

Talanta provides a forum for the publication of original research papers, preliminary communications, and critical reviews in all branches of pure and applied analytical chemistry. Papers are evaluated based on established guidelines, including the fundamental nature of the study, scientific novelty, substantial improvement or advantage over existing technology or methods, and demonstrated analytical applicability. Original research papers on fundamental studies, and novel sensor and instrumentation development, are especially encouraged. Novel or improved applications in areas such as clinical and biological chemistry, environmental analysis, geochemistry, and materials science and engineering are welcome.

Analytical performance of methods should be determined, including interference and matrix effects, and methods should be validated by comparison with a standard method, or analysis of a certified reference material. The developed method should especially comprise information on selectivity, sensitivity, detection limits, accuracy, and reliability. However, applying official validation or robustness studies to a routine method or technique does not necessarily constitute novelty. Proper statistical treatment of the data should be provided. Relevant literature should be cited, including related publications by the authors, and authors should discuss how their proposed methodology compares with previously reported methods.

Since classical spectrophotometric measurements and applications (including derivative spectrophometry), fluorimety, solvent extraction, titrimetry, chemometrics, etc. are well established and are considered routine analytical methods, studies in such areas should demonstrate a unique and substantial advantage over presently known systems. New reagents or systems should demonstrate clear advantage, and their presentation should be comprehensive rather than generating a series of similar papers for several analytes or similar reagents. Modifications of reagents should demonstrate significant improvements. Obvious application of known chemistries or methods to established instrumental techniques are discouraged.

Application of established analytical approaches to relatively simple matrices having no major interferences, such as pharmaceutical preparations, are discouraged unless considerable improvements over other methods in the literature are demonstrated. Papers dealing with analytical data such as stability constants, pK_a values, etc. should be submitted to more specific journals, unless novel analytical methodology is demonstrated, or important analytical data are provided which could be useful in the development of analytical procedures.

Talanta 79 (2009) 54–61

Contents lists available at ScienceDirect

Talanta

journal homepage: www.elsevier.com/locate/talanta

Synthesis and binding properties of carboxylphenyl-modified calix[4]arenes and cytochrome *c*

Wen Ting An[a,b], Yong Jiao[a], Xiao Hua Sun[b], Xiao Ling Zhang[b], Chuan Dong[a], Shao Min Shuang[a,*], Ping Fang Xia[b], Man Shing Wong[b,*]

[a] *Research Center of Environmental Science and Engineering, Department of Chemistry, Shanxi University, Taiyuan 030006, China*
[b] *Department of Chemistry, Hong Kong Baptist University, Kowloon Tong, Hong Kong S.A.R., China*

ARTICLE INFO

Article history:
Received 7 December 2008
Received in revised form 27 February 2009
Accepted 3 March 2009
Available online 14 March 2009

Keywords:
Calix[4]arene carboxylphenyl derivatives
Cytochrome *c*
Protein binding
Synthesis
Fluorescence spectroscopy

ABSTRACT

Two novel carboxylphenyl-modified calix[4]arenes, *tetrakis*-carboxylphenylcalix[4]arene (TCPC) and 1,3-*bis*-carboxylphenylcalix[4]arene (BCPC), as well as a corresponding analogue for comparison, *tetrakis*-phenylcalix[4]arene (TPC), have been synthesized by palladium-catalyzed Suzuki cross-coupling of arylboronic acid and tetrabromocalix[4]arene as a key step. The binding properties of these calix[4]arene derivatives with bovine heart cytochrome *c* (cyt *c*) in dimethylformamide (DMF) was investigated by fluorescence spectroscopy. The binding affinity in the order of TCPC > BCPC ≫ TPC reflects a clear dependence on the number of carboxyl ligating groups attached onto a receptor and suggests the electrostatic force may be the predominant factor driving the complexing process. The stable 1:1 complexes of TCPC and BCPC with cyt *c* were evidenced with the binding constants of 3.15×10^6 and 5.85×10^5 L mol^{-1}, respectively. Due to a large overlap between the emission spectrum of TCPC and the absorption spectrum of cyt *c*, and a short interaction distance (estimated to be 5.6 nm) between them, the fluorescence quenching of TCPC upon complexation with cyt *c* is attributed to an efficient energy transfer.

1. Introduction

There has been a growing interest in the development of synthetic protein binding agents based on macrocyclic molecules to identify, inhibit, separate and/or functionally modify specific proteins [1–3]. In recent years, Hamilton et al. [2,4] have developed a series of artificial protein binders, including those built by a central calix[4]arene scaffold with peripheral groups of cyclic peptides, acting as inhibitors to specific proteins. They also created a pattern-based detection approach for different proteins by using an array of functionalized porphyrins as fluorescent protein receptors, which can be used for high-throughput proteomics, medical diagnostics, and bioterrorism applications in which multiple types of proteins need to be rapidly detected [5]. On the other hand, many synthetic receptors, particularly calixarene-based ones, have been found to possess excellent capabilities to solubilize, extract and separate specific proteins, as well as to improve the efficiency or modify the function of enzymes in organic media or ionic liquids. Shimojo et al. [6] reported that dicyclohexano-18-crown-6 enables transfer of cyt *c* into ionic liquids via supramolecular complexation, and the solubilized cyt *c* was stable and showed peroxidase activity. Recently, they found that denatured cyt *c* can be extracted from an urea solution into an organic solution containing calixarene derivatives and can successfully regain its native structure through back-extraction into a denaturant-free aqueous solution [7]. Oshima et al. [8–10] have extracted and separated cyt *c* from water into organic solvents via calixarene derivatives, and utilized one of them as mobile carriers to continuous separation and transport of cyt *c* through a liquid membrane.

Calix[*n*]arenes, consisting of phenol rings bridged by methylenes, are one of the major classes of macrocyclic host compounds in supramolecular chemistry [11,12]. Calix[*n*]arenes possess a unique basketlike cavity that can be controlled by changing the number of phenol units. To date, calix[4]arene has been extensively used as a platform to construct synthetic receptors because of its tunable and unique three-dimensional structure together with the ease of functionalization [12–15]. However, there are few examples taking advantage of an extended preorganized rigid platform of calix[4]arene for construction of artificial receptors [16]. Besides the merit of improving the encapsulation and recognition properties [17], the extended calix[4]arene skeleton with π-conjugated units could act as a chromophore or fluorophore. Based on a change in fluorescence properties upon binding with a specific guest, chemical sensors are developed and are considered particularly attractive because they offer promise for high sensitivity at low analyte concentration [18,19]. In present work, calix[4]arene carboxylphenyl derivatives

* Corresponding authors. Tel.: +86 351 7011322; fax: +86 351 7011322.
E-mail addresses: smshuang@sxu.edu.cn (S.M. Shuang), mswong@hkbu.edu.hk (M.S. Wong).

0039-9140/$ – see front matter © 2009 Elsevier B.V. All rights reserved.
doi:10.1016/j.talanta.2009.03.007

were designed and constructed by a calix[4]arene scaffold stabilized in the cone conformation with tetra- or di-carboxylphenyl groups born at the upper rim. Cytochrome *c* (cyt *c*) is one of the most thoroughly physicochemically characterized metalloproteins with a stable protein backbone and plays key roles in electron transfer and apoptosis [20]. As a highly basic protein (pI 9.79), it possesses abundant positively charged residues on its exterior surface. In addition, it has been shown that the unpaired electrons in the ferro moiety could quench fluorescence upon binding to a fluorogenic receptor [21]. So cyt *c* represents an excellent model protein for an investigation of the interactions of proteins with artificial protein binding agents designed with the electrostatic complementary principle via fluorescence spectroscopy. Various techniques [8,22–24], including circular dichroism, dynamic light scattering and Langmuir film balance have been used to probe the binding of calixarenes to proteins. However, there are only few reports on this topic by using fluorescence method [5,25,26].

We have recently reported a preliminary findings on a carboxylphenyl-substituted calix[4]arene derivative binding with cyt *c* and revealed the interaction mechanism by molecular modeling studies [27]. Continuing on the thorough investigation of the binding properties of carboxylphenyl-substituted calix[4]arene derivatives with cyto *c*, we herein report a complete study including (i) the design rationale, detailed synthesis and full characterization of three calix[4]arene-based fluorescent receptors, *tetrakis*-carboxylphenylcalix[4]arene (TCPC), 1,3-*bis*-carboxylphenylcalix[4]arene (BCPC), and a corresponding analogue *tetrakis*-phenylcalix[4]arene (TPC) (Fig. 1); (ii) the comparison of fluorescence behavior and binding affinity of these calix[4]arene derivatives binding upon cyt *c* in dimethylformamide (DMF); (iii) the mechanism of the fluorescence quenching upon binding; and (iv) the investigation of visible CD spectra of cyt *c*–TCPC complex in DMF. The results of the present work suggest that TCPC exhibits a higher binding affinity towards cyt *c* in DMF, which highlights its potential application in chemoenzymatic synthesis to stabilize proteins in organic media [28,29]. In addition, because of its high fluorescent nature and its efficient fluorescence quenching property upon binding with specific proteins, this artificial protein binder is anticipated to have widespread applications as a fluorescent detection tool e.g. fluorescent sensor for various proteins with cation-rich surface.

2. Experimental

2.1. Apparatus

Fluorescence spectra were measured at $20 \pm 1\,^{\circ}C$ in standard quartz cells of 1 cm path length on a Hitachi F-4500 spectrofluorimeter equipped with a xenon lamp source and a thermostat bath. Both of the excitation and emission bandwidths were set at 5 nm. Circular Dichroism (CD) measurements were carried out on a Jasco J-810 spectropolarimeter. ^1H NMR and ^{13}C NMR spectra were recorded by a JEOL JHM-EX270 FT NMR or Varian INOVA-400 FT NMR spectrometer. Mass spectroscopy measurements were carried out by using fast atom bombardment (FAB) on the API ASTAR Pulsar I Hybrid Mass Spectrometer or matrix-assisted laser desorption ionisation time-of-flight (MALDI-TOF) technique.

2.2. Reagents

Cytochrome *c* from bovine heart (C_{2037}) was purchased from Sigma and employed without further purification. Quinine sulfate was of biochemical reagent grade and purchased from Shanghai second reagent factory of China. All other reagents were of reagent grade for synthesis or analytical reagent grade for spectroscopic measurements and were used as received.

2.3. Preparation of TCPC and BCPC

The synthetic route is shown in Scheme 1. The corresponding analogue 5,11,17,23-*tetrakis*(4-phenyl)-25,26,27,28-tetrapropoxycalix[4]arene (TPC) was synthesized by the literature procedure [30]. All characterization data of ^1H NMR, ^{13}C NMR and MS for TCPC and BCPC are shown in Fig. S1–S5.

2.3.1. 5,11,17,23-Tetrakis(4-formylphenyl)-25,26,27,28-tetrapropoxycalix[4]arene (**2**)

To a 100-mL flask containing compound **1** (0.23 g, 0.25 mmol) and 4-formylphenylboronic acid (0.23 g, 1.53 mmol) in 50 mL of toluene was added $Pd(OAc)_2$ (11 mg, 5 mol%), P(*o*-tol)$_3$ (30 mg, 10 mol%), 8 mL of methanol and 3 mL of 2 M K_2CO_3. The mixture was stirred at 75 °C under N_2 overnight. After cooling to room temperature, 20 mL of water was added. The reaction mixture was acidified to pH 3–4 using 6 M HCl and then extracted by ethyl acetate (20×3 mL). The combined organic phase was dried over anhydrous Na_2SO_4 and evaporated to dryness. The residue obtained was purified by silica gel flash column chromatography using gradient elution method with petroleum ether and ethyl acetate as eluent affording a white solid (0.16 g, 64% yield). ^1H NMR (400 MHz, $CDCl_3$, δ) 9.85 (s, 4H), 7.56 (d, J = 8 Hz, 8H), 7.22 (d, J = 8 Hz, 8H), 6.98 (s, 8H), 4.60 (d, J = 13.2 Hz, 4H), 3.97 (t, J = 7.2 Hz, 8H), 3.33 (d, J = 13.2 Hz, 4H), 1.96–2.04 (m, 8H), 1.06 (t, J = 7.2 Hz, 12H). ^{13}C NMR (100 MHz, $CDCl_3$, δ) 191.7, 157.3, 146.7, 135.5, 134.4, 133.5, 129.9, 127.2, 126.7, 77.1, 31.3, 23.3, 10.3. MS (FAB) m/z 1008.1 [M^+].

2.3.2. 5,11,17,23-Tetrakis(4-carboxylphenyl)-25,26,27,28-tetrapropoxycalix[4]arene (TCPC)

To a 100 mL flask containing **2** (0.2 g, 0.20 mmol) in 10 mL $CHCl_3$ and 30 mL acetone was added 1 mL aqueous sulphamic acid (0.3 g, 3.1 mmol) and 1 mL aqueous sodium chlorite (0.28 g, 3.1 mmol). The mixture was stirred at room temperature for 1 h and then evapo-

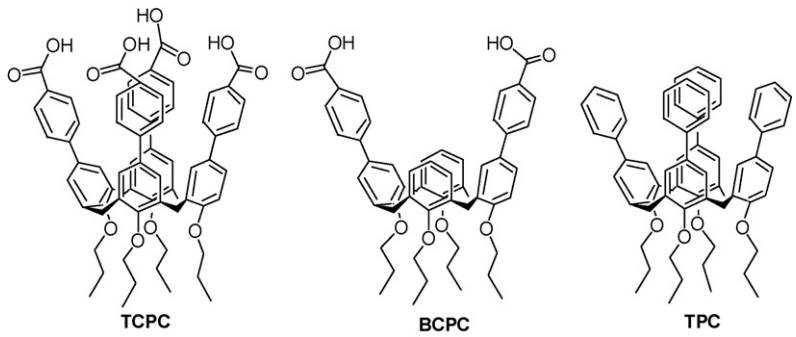

Fig. 1. The molecular structures of TCPC, BCPC and TPC.

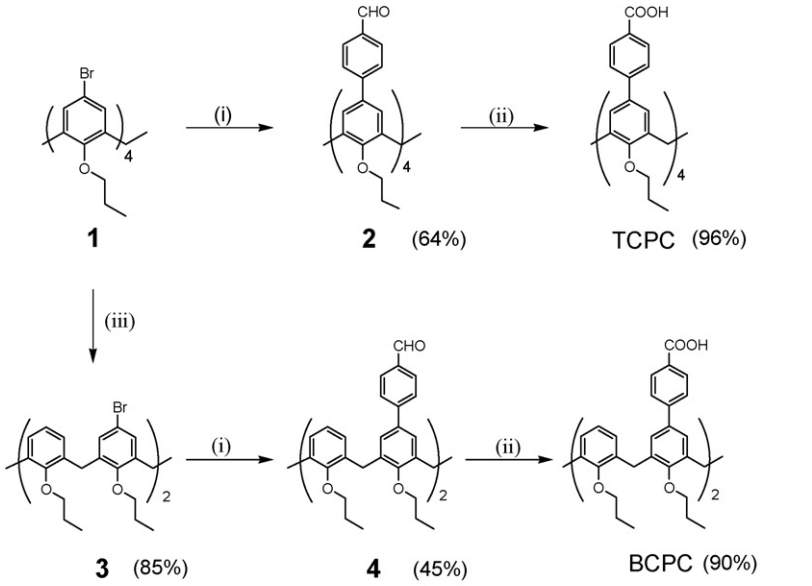

Scheme 1. Synthesis of calix[4]arene carboxylphenyl derivatives TCPC and BCPC. Reagents and conditions: (i) 4-formylbenzeneboronic acid, $Pd(OAc)_2/P(o\text{-tol})_3$, toluene/MeOH, 2 M K_2CO_3, 75 °C; (ii) NH_2SO_3H, $NaClO_2$, acetone, r.t.; (iii) (a) *n*-butyllithium THF, −78 °C; (b) MeOH.

rated to dryness. The solid obtained was washed with water and acetone affording a quantitative yield of TCPC as a white solid (0.20 g, 96% yield). ^{1}H NMR (270 MHz, DMSO-D_6, δ) 12.4 (b, 4H), 7.65 (d, J = 8.1 Hz, 8H), 7.23 (d, J = 8.1 Hz, 8H), 7.06 (s, 8H), 4.44 (d, J = 13.2 Hz, 4H), 3.90 (t, J = 7.0 Hz, 8H), 1.93–1.95 (m, 8H), 1.02 (t, J = 7.3 Hz, 12H). ^{13}C NMR (67.5 MHz, DMSO-D_6, δ) 166.6, 156.3, 144.2, 134.8, 132.8, 129.3, 128.4, 126.6, 125.8, 76.4, 30.4, 22.9, 10.3. MS (FAB) m/z 1072.8 [M$^+$]. HRMS (ESI-TOF) calcd. for $C_{68}H_{63}O_{12}$ 1071.4320, found 1071.4285 [M−H]$^-$.

2.3.3. 5,17-Bisbromo-25,26,27,28-tetrapropoxycalix[4]arene (**3**)

In a flame dried 250 mL two-neck flask, compound **1** (1.8 g, 1.98 mmol) in 100 mL anhydrous THF was added under N_2 atmosphere. Then the solution was cooled to −78 °C in the dry-ice and acetone bath, *n*-butyllithium (2.6 mL, 1.6 M in hexane) was added slowly by syringe. After stirring for 1 h, the solution was turned from colourless to dark. The reaction mixture was kept stirring for another 0.5 h after quenching 1 mL of methanol. Afterward, the cooling bath was removed to allow warming to room temperature and the reaction mixture was added with 20 mL of water. The solution mixture was extracted with DCM (3 × 20 mL) and the combined organic phase was dried over anhydrous Na_2SO_4 and evaporated in vacuum. The residue was purified by silica gel flash column chromatography using CH_2Cl_2/petroleum ether as eluent affording 1.26 g of a white solid compound **3** with 85% of an isolated yield. ^{1}H NMR (270 MHz, $CDCl_3$, δ) 6.75 (s, 4H), 6.62 (m, 6H), 4.38 (d, J = 13.2 Hz, 4H), 3.81 (m, 8H), 3.10 (d, J = 13.2 Hz, 4H), 1.82–1.94 (m, 8H), 0.93–1.00 (m, 12H). ^{13}C NMR (67.5 MHz, $CDCl_3$, δ) 156.1, 155.4, 137.0, 134.1, 130.5, 128.2, 122.2, 114.5, 76.8, 76.4, 30.8, 23.3, 23.1, 10.3, 10.2. MS (FAB) m/z 750.2 [M$^+$].

2.3.4. 5,17-Bis(4-formylphenyl)-25,26,27,28-tetrapropoxycalix[4]arene (**4**)

In a 50 mL flask, compound **2** (0.19 g, 0.25 mmol), boronic acid (0.11 g, 0.76 mmol); $Pd(OAc)_2$ (5.7 mg, 5% mmol), $P(o\text{-tol})_3$ (15 mg, 10% mmol), 10 mL toluene and 2 mL of 2 M K_2CO_3 were added. The solution was stirred at 75 °C overnight. After quenching with water, the pH value of the reaction mixture was adjusted to 3–4 by HCl (6 M) then extracted with DCM (3 × 20 mL), organic phase was dried over anhydrous Na_2SO_4, evaporated in vacuum. The crude product was purified by silica gel flash column chromatography affording 0.091 g of a white solid of compound **4** with 45% yield. ^{1}H NMR (400 MHz, $CDCl_3$, δ) 9.78 (s, 2H), 7.41 (d, J = 8.0 Hz, 4H), 7.00 (d, J = 8.4 Hz, 4H), 6.90 (d, J = 7.6 Hz, 4H), 6.79 (t, J = 7.6 Hz, 2H), 6.70 (s, 4H), 4.52 (d, J = 13.2 Hz, 4H), 3.99 (t, J = 7.6 Hz, 4H), 3.82 (t, J = 7.2 Hz, 4H), 3.23 (d, J = 13.2 Hz, 4H), 2.03–1.91 (m, 8H), 1.07 (t, J = 7.2 Hz, 6H), 0.99 (t, J = 7.2 Hz, 6H). ^{13}C NMR (100 MHz, $CDCl_3$, δ) 191.8, 157.0, 156.8, 146.7, 135.6, 135.0, 134.1, 133.0, 129.6, 128.6, 126.7, 126.4, 122.2, 77.1, 76.7, 31.1, 23.4, 23.1, 10.5, 10.1. HRMS (MALDI-TOF) calcd. for $C_{54}H_{56}O_6Na$ 823.3969, found 823.3942 [M+Na]$^+$.

2.3.5. 5,17-Bis(4-carboxylphenyl)-25,26,27,28-tetrapropoxycalix[4]arene (BCPC)

In a 50 mL flask, compound **4** (0.06 g, 0.075 mmol) was dissolved in 10 mL $CHCl_3$ and 30 mL acetone. Then NH_2SO_3H (64 mg, 0.66 mmol) in 1 mL water and $NaClO_2$ (54 mg, 0.6 mmol) in 1 mL water were added. The solution was stirred for 4 h at room temperature. After evaporating the solvent, residue was washed with water, and then dried affording 56 mg of a white product of BCPC in 90% yield. ^{1}H NMR (400 MHz, $CDCl_3$, δ) 7.46 (d, J = 8.4 Hz, 4H), 7.24 (d, J = 7.6 Hz, 4H), 7.05 (t, J = 7.2 Hz, 4H), 6.57 (d, J = 8.8 Hz, 4H), 6.37 (s, 4H), 4.52 (d, J = 13.2 Hz, 4H), 4.11 (t, J = 8.0 Hz, 4H), 3.70 (t, J = 6.8 Hz, 4H), 3.22 (d, J = 13.2 Hz, 4H), 2.07–2.01 (m, 4H), 1.94–1.88 (m, 4H), 1.13 (t, J = 7.2 Hz, 6H), 0.92 (t, J = 7.2 Hz, 6H). ^{13}C NMR (100 MHz, $CDCl_3$, δ) 172.8, 157.8, 155.7, 145.5, 136.9, 133.7, 133.2, 129.8, 129.1, 126.5, 126.1, 125.3, 122.2, 77.2, 76.6, 31.1, 23.5, 23.0, 10.8, 9.8. HRMS (MALDI-TOF) calcd. for $C_{54}H_{56}O_8Na$ 855.3872, found 855.3870 [M+Na]$^+$.

2.4. Fluorescence spectra

The stock solutions of TCPC, BCPC and TPC, as well as cyt *c* were prepared in DMF and double distilled water, respectively. Double distilled water was used throughout the work and all stock solutions were stored at 0–4 °C. A 0.5 μL stock solution (1.77×10^{-3} mol L^{-1}) of TCPC (or BCPC, TPC), was transferred into a 10 mL volumetric flask then diluted to final volume with DMF and shaking thoroughly, to which was added an appropriate amount of 1.73×10^{-3} mol L^{-1} cyt *c* in double distilled water. The mixed solution was diluted to final volume with DMF, and the resulting solution was shaken thoroughly, and the fluorescence spectra were measured on a F-4500 spectrofluorimeter after standing for 30 min. All experiments were carried out at 20 ± 1 °C. All the glassware including cuvette were routinely washed in 1.0 M HNO_3 and then rinsed with double distilled water.

2.5. Circular dichroism spectra

In CD spectra measurement, Soret region CD spectra (350–450 nm) of native cyt *c* in deionized water and of the cyt *c*–TCPC complex in DMF were obtained at 20 °C using a CD spectropolarimeter (Jasco J-810). Measurement conditions were as follows:

[cyt *c*] = 10 μM and [TCPC] = 10 μM. The optical path length is 1 cm.

3. Results and discussion

3.1. Design and synthesis

The design rationales for carboxylphenylcalix[4]arene derivatives are as follows: (i) the incorporation of carboxyl functional groups is to provide anionic ligating sites for complement binding of the cationic surface of cyt *c* as electrostatic interaction is one of the important and strong binding interactions of synthetic receptors with cyt *c* [2,7–10]. The more the carboxyl ligating groups the receptor bears, the stronger binding affinity it possesses. So the order of the binding affinity would be TCPC > BCPC > TPC. (ii) The donor–acceptor type bi-phenyl structure motif would endow the calix[4]arene derivatives with strong fluorescence property [31–33], and would have the merit of exhibiting an efficient Förster resonance energy transfer (FRET) based on the quenching of fluorescence upon binding to proteins, which makes the utilizing of sensitive fluorescence methods to examine interactions of the calix[4]arenes with cyt *c* possible. The subsequent results indicate that the above design aims are achieved, and TCPC indeed has the highest binding affinity to the targeted protein.

The syntheses of TCPC and BCPC are summarized in Scheme 1. The extended arylcalix[4]arene skeleton was constructed by a convergent approach using palladium catalyzed Suzuki cross-coupling of arylboronic acid and tetrabromocalix[4]arene as a key step [33]. 5,11,17,23-Tetrakis(4-formylphenyl)-25,26,27,28-tetrapropoxycalix[4]arene **2** was obtained by Suzuki cross-coupling of 4-formylbenzeneboronic acid with 5,11,17,23-tetrakisbromo-25,26,27,28-tetrapropoxycalix[4]arene, **1**, which were prepared by the well developed procedures [31], affording 64% yield. Aldehyde **2** was oxidized by sodium chlorite at room temperature giving TCPC in a quantitative yield. BCPC was synthesized using a similar protocol. Lithium-bromide exchange of **1** using *n*-BuLi at −78 °C followed by quenching with methanol afforded 5,17-bisbromo-25,26,27,28-tetrapropoxycalix[4]arene, **3**, in good yield (85%). Suzuki cross-coupling of 4-formylbenzeneboronic acid and **3** using the typical coupling procedure afforded the desired 5,17-bis(4-formylphenyl)-25,26,27,28-tetrapropoxycalix[4]arene **4** which was oxidized accordingly to BCPC. The newly synthesized carboxylphenyl-substituted calix[4]arenes TCPC and BCPC, and the corresponding analogue, 5,11,17,23-tetrakis(4-phenyl)-25,26,27,28-tetrapropoxycalix[4]arene synthesized by the literature procedure [30] for comparison, were fully characterized by ^{1}H NMR, ^{13}C NMR, and low/high-resolution mass spectroscopy and found to be in good agreement with the expected structures.

3.2. Comparison of the binding affinity of TCPC, BCPC and TPC to cyt c

TCPC, with an aryl-extended calix[4]arene framework and end-functionalized by four carboxylic acid groups on the upper rim, was designed and synthesized for the first time for binding to cyt *c*. Addition of cyt *c* to the solution containing TCPC or BCPC resulted in the fluorescence quenching of the arylcalix[4]arene which is due to the formation of complex between them. In contrast, the titration of TPC with cyt *c* showed almost no quenching in the same concentration range used for TCPC or BCPC titration, indicating the absence of a specific binding. The results of the fluorescence titration of TCPC, BCPC and TPC by cyt *c* are shown in Fig. 2 *via* the least-squares fit of the experimental data.

TCPC binds to cyt *c* with the binding constant (K_a) of $(3.15 \pm 0.47) \times 10^6$ L mol^{-1} and K_a for BCPC with cyt *c* = $(5.85 \pm 1.30) \times 10^5$ L mol^{-1} which is approximately one-fifth of that of TCPC. For TPC without carboxyl functional groups, there is almost no specific binding observed. As shown in Fig. 2, the marked difference in the binding affinity to cyt *c*, that is in the order of TCPC > BCPC ≫ TPC, was achieved just by tuning the number of carboxyl ligating groups at the upper rim of the phenylcalix[4]arenes. All of these evidences indicate the importance of the carboxyl ligating groups (or in turn the electrostatic interactions) for the formation of stable complexes of calix[4]arene-based receptors with cyt *c*. Importantly, TCPC was identified as the best synthetic receptor for cyt *c* among the three calix[4]arene derivatives.

3.3. Mechanism of fluorescence quenching of TCPC binding upon cyt c

Fig. 3 shows the fluorescence spectra of TCPC in the absence and presence of cyt *c* in DMF. The maximum excitation and emission wavelengths are at 316 nm and 404 nm, respectively. With increasing the concentration of cyt *c*, the fluorescence intensity of TCPC decreased gradually. Meanwhile, the maximum emission wavelength produced a small blue shift from 404 nm to 400 nm

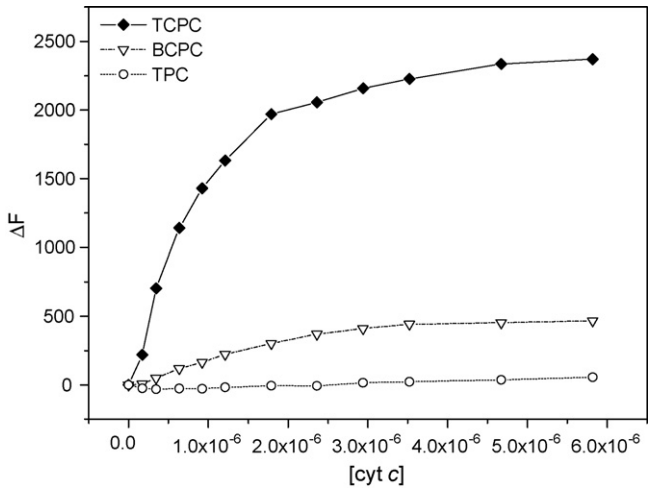

Fig. 2. Fluorescence quenching of TCPC, BCPC, TPC upon addition of cyt *c* in DMF.

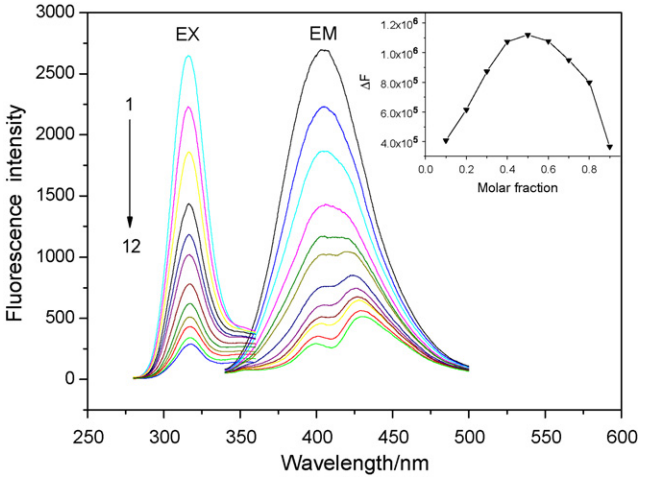

Fig. 3. The fluorescence spectra of TCPC in different concentrations of cyt *c* in DMF at λ_{ex} = 316 nm and λ_{em} = 404 nm. The concentrations of cyt *c* (mol L^{-1}): (1) 0; (2) 1.73×10^{-7}; (3) 3.46×10^{-7}; (4) 6.34×10^{-7}; (5) 9.23×10^{-7}; (6) 1.21×10^{-6}; (7) 1.79×10^{-6}; (8) 2.36×10^{-6}; (9) 2.94×10^{-6}; (10) 3.52×10^{-6}; (11) 4.67×10^{-6}; (12) 5.82×10^{-6}. The inset shows the Job's plot of TCPC and cyt *c*. The total mole concentration of TCPC and cyt *c* is 1×10^{-6} mol L^{-1}.

and the corresponding excitation wavelength is red-shifted slightly from 316 nm to 318 nm. Such a strong fluorescence quenching of TCPC suggests that the intermolecular energy transfer may occur between TCPC and cyt *c*.

It is well known that the fluorescence quenching can be caused by a static or a dynamic quenching process, both of them result in a similar linear Stern–Volmer plot. However, they can be differentiated by the difference in the temperature dependence property. The higher the temperature, the faster is the diffusion and hence the greater extent of dynamic quenching is. In another case, the high temperature enhances the dissociation of weakly bound complexes, which results in the lesser extent of the static quenching. The Stern–Volmer plots of TCPC with cyt *c* at different temperatures, *i.e.* 25 °C, 30 °C and 40 °C, as shown in Fig. 4, disclose the quenching mechanism. Because the slopes of the plots decrease with the increase of temperature, the static quenching interaction of TCPC with cyt *c* is evident. In order to further confirm the mechanism, the dynamic quenching constant calculations were carried out.

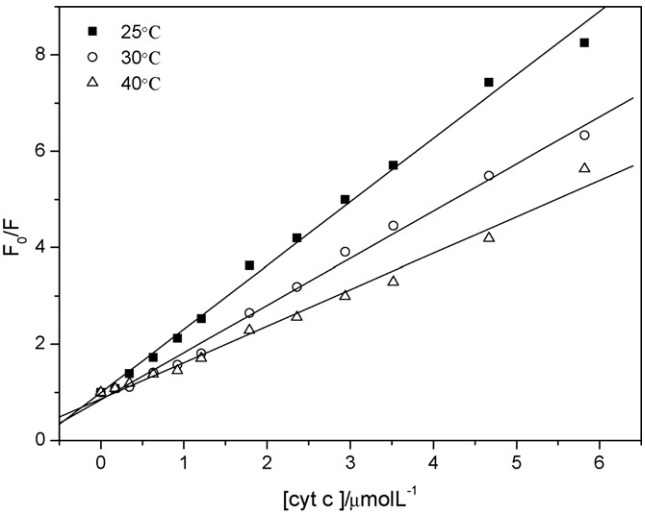

Fig. 4. The Stern–Volmer plots for the quenching of TCPC by cyt *c* in DMF at 25 °C, 30 °C and 40 °C.

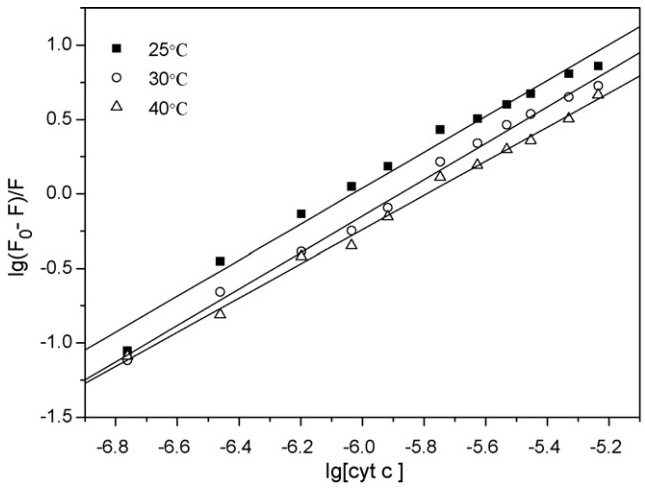

Fig. 5. Binding constants and binding sites of TCPC with cyt *c* in DMF calculated by static quenching equation.

The dynamic quenching process can be described by the Stern–Volmer equation [34]:

$$\frac{F_0}{F} = 1 + K_{sv}[Q] = 1 + K_q\tau_0[Q]. \quad (1)$$

where F and F_0 are the fluorescence intensities in the presence and absence of a quencher, respectively. K_{sv}, K_q, τ_0 and $[Q]$ denote dynamic quenching constant, quenching rate constant, typical lifetime of fluorophore and concentration of quencher, respectively.

According to Eq. (1), the dynamic quenching constants at 25 °C, 30 °C and 40 °C were estimated to be $(1.32 \pm 0.03) \times 10^6$, $(9.77 \pm 0.24) \times 10^5$ and $(7.55 \pm 0.28) \times 10^5$ L mol^{-1}, respectively. In general, the dynamic quenching constant should be less than 100 L mol^{-1}. As a result, the dynamic quenching is further excluded. In addition, all the findings consistently affirmed that the quenching is originated from the formation of a complex of TCPC with cyt *c*.

The static quenching process can be described by the equation [35]:

$$lg\frac{F_0 - F}{F} = lgK_A + nlg[Q] \quad (2)$$

where F_0 and F are the fluorescence intensities in the absence and presence of quencher, respectively. K_A, n and $[Q]$ are the binding constant, binding site and concentration of quencher, respectively.

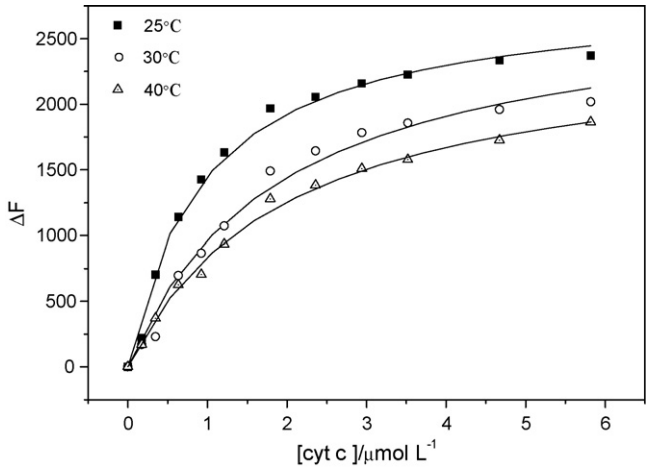

Fig. 6. Binding constants and binding sites of TCPC with cyt *c* in DMF calculated by non-linear fitting equation.

Eq. (2) is built on two assumptions: (i) the stoichiometry of *host*:*guest* in a complex is 1:*n*, and (ii) the complexation between the host (fluorophore) and guest (quencher) is a static quenching process [34].

From a plot of $\lg F_0 - F/F$ versus the lg[*Q*] shown in Fig. 5, the binding constants K_A and binding sites n can be conveniently derived from the plots at various temperatures. The plots exhibit good linearity and the values of the binding site of TCPC with cyt *c* were 1.2067, 1.2217 and 1.1472 at 25 °C, 30 °C and 40 °C, respectively, and the 1:1 stoichiometry was further confirmed by the continuous molar variation (Job's) plots (inset in Fig. 3).

In addition, the binding constant can also be determined by the non-linear curve fitting analysis using the fluorescence titration data (shown in Fig. 6). The equation used for the non-linear curve fitting analysis is as follows [36,37]:

$$\Delta F = \frac{1}{2}\left\{\alpha\left([\mathrm{H}]_0 + [\mathrm{G}]_0 + \frac{1}{K}\right) - \sqrt{\alpha^2\left([\mathrm{H}]_0 + [\mathrm{G}]_0 + \frac{1}{K}\right)^2 - 4[\mathrm{H}]_0[\mathrm{G}]_0\alpha^2}\right\} \quad (3)$$

where $[\mathrm{H}]_0$, $[\mathrm{G}]_0$ is the initial concentration of TCPC and cyt *c*, respectively. ΔF denotes the change of the fluorescence intensity of TCPC upon an addition of cyt *c*. α is a sensitive factor of the structure change of complexation composed of TCPC with cyt *c* at the interactive course. *K* is the association constant. Except the assumption that the host and guest forms a 1:1 complex, there is not any theoretical approximation treatment in the curve fitting method described by Eq. (3), and the results (K_A) obtained from Eq. (3) should be closer the true value than that from Eq. (2). Table 1 summarizes the binding constants of TCPC with cyt *c* at 25 °C, 30 °C and 40 °C determined by Eqs. (2) and (3), respectively. Interestingly, the binding constants of TCPC–cyt *c* complex are remarkably large at all the measured temperatures, which suggest that there are strong interactions of TCPC with cyt *c*.

Under the same conditions as that of TCPC, the binding behavior of BCPC with cyt *c* (≤25 °C) was monitored by fluorescence spectroscopy. As shown in Fig. 7, the maximum excitation and emission wavelengths of the fluorescence spectra of BCPC in the absence of cyt *c* in DMF are at 312 nm and 385 nm, respectively. With increasing the concentration of cyt *c*, the fluorescence intensity of BCPC decreased gradually. Meanwhile, the maximum emission wavelength produced a small red shift from 385 nm to 388 nm and the corresponding excitation wavelength is red-shifted slightly from 312 nm to 316 nm. The quenching of the fluorescence of BCPC upon an addition of cyt *c* suggests that the interaction appeared between them. The binding constant of BCPC with cyt *c* at 25 °C estimated by Eq. (3) is listed in Table 1. When we performed the ascending temperature experiment to examine the quenching mechanism, it was found that the fluorescent behaviors of this system were irregular, suggesting that the interaction of BCPC with cyt *c* may be destroyed by the enhanced molecular thermodynamic-motion. The lower stability of the complex could originate from the structure of BCPC, where there are two carboxylphenyl ligating groups less than TCPC resulting in the weaker electrostatic interactions between the cationic protein and the higher conformationally flexible BCPC.

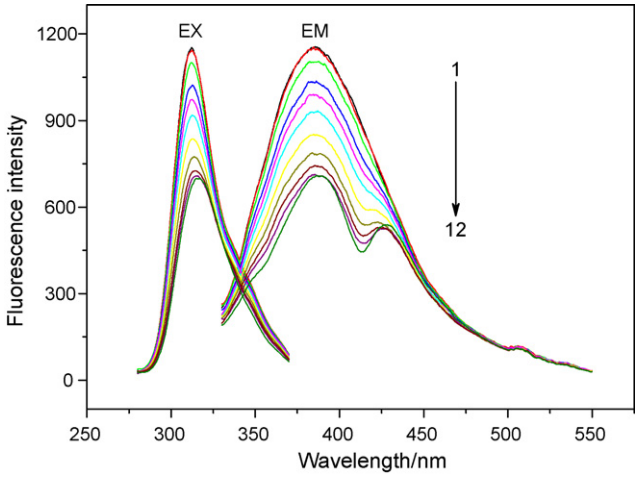

Fig. 7. The fluorescence spectra of BCPC in different concentrations of cyt *c* in DMF at λ_{ex} = 312 nm and λ_{em} = 385 nm. The concentrations of cyt *c* (mol L^{-1}): (1) 0; (2) 1.73×10^{-7}; (3) 3.46×10^{-7}; (4) 6.34×10^{-7}; (5) 9.23×10^{-7}; (6) 1.21×10^{-6}; (7) 1.79×10^{-6}; (8) 2.36×10^{-6}; (9) 2.94×10^{-6}; (10) 3.52×10^{-6}; (11) 4.67×10^{-6}; (12) 5.82×10^{-6}.

3.4. Energy transfer between TCPC and cyt c

Based on the Förster resonance energy transfer (FRET) theory [34], the energy transfer will occur under the following conditions: (1) the donor can emit fluorescence; (2) the emission spectrum of the donor and the absorption spectrum of the acceptor overlap to each other; and (3) the distance between the donor and the acceptor is shorter than 7 nm. The large spectral overlap between the emission spectrum of the donor TCPC and the absorption spectrum of the acceptor cyt *c* (see Fig. 8) indicates the efficient energy transfer may occur between them and lead to the fluorescence quenching of TCPC.

According to FRET theory, the energy transfer efficiency (*E*) is related not only to the distance between the donor and the acceptor (r_0), but also to the critical energy transfer distance (R_0) when the transfer efficiency is 50%, that is

$$E = \frac{(R_0)^6}{(R_0)^6 + (r_0)^6} \quad (4)$$

R_0 can be obtained by

$$(R_0)^6 = 8.8 \times 10^{-25} K^2 N^{-4} \Phi J. \quad (5)$$

where K^2 is the spatial orientation factor of the dipole, *N* the refractive index of the medium, Φ the fluorescence quantum yield of the donor, *J* the overlap integral of the fluorescence emission spectrum of the donor and the absorption spectrum of the acceptor. Therefore,

$$J = \frac{\sum F(\lambda)\varepsilon(\lambda)\lambda^4 \Delta\lambda}{\sum F(\lambda)\Delta\lambda} \quad (6)$$

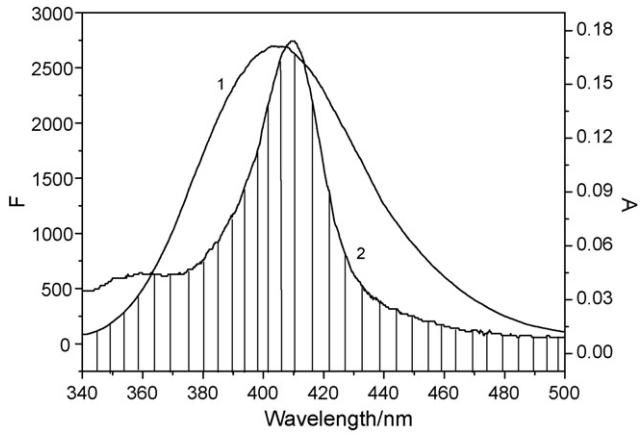

Fig. 8. Overlap of the fluorescence emission spectrum of TCPC (**1**) and the absorption spectrum of cyt *c* (**2**).

Table 1
Binding constants of TCPC/BCPC with cyt *c*.

T (°C)	TCPC				BCPC	
	K_A (10^{-7} L mol^{-1})	R	K_A' (10^{-6} L mol^{-1})	R^2	K_A' (10^{-5} L mol^{-1})	R^2
25	1.916	0.9908	3.15 ± 0.47	0.9968	5.85 ± 1.30	0.9893
30	1.5136	0.9972	0.98 ± 0.63	0.9905	–	–
40	0.4365	0.9976	0.87 ± 0.09	0.9962	–	–

Notes: K_A and K_A' were obtained by Eqs. (2) and (3), respectively.

where $F(\lambda)$ is the fluorescence intensity of the fluorescence donor at wavelength λ, and $\varepsilon(\lambda)$ the molar absorptivity of the acceptor at wavelength λ.

According to Eq. (6), $J = 1.32 \times 10^{-13}$ cm^3 L mol^{-1} was evaluated by integrating the overlap of the emission spectrum of the donor and the absorption spectrum of the acceptor from 340–500 nm with 2 nm wavelength step. The other parameters in Eq. (5) are as follows: (i) the refraction index $N = 1.336$ is the average value of water and organism; (ii) the directional factor $K^2 = 2/3$ is the average value of the donor–acceptor in every direction randomly; (iii) the quantum yield of TCPC $\Phi = 0.45$ under the experimental conditions is determined by a relative method [38] using quinine sulfate as a standard substance ($\Phi_{313} = 1.00$ [39]). By substituting all the parameters in Eq. (5), the critical distance R_0 is estimated to be 5.71 nm.

The energy transfer efficiency, E, is given by

$$E = 1 - \frac{F}{F_0} \tag{7}$$

where F_0 and F represent the fluorescence intensities of the donor in the absence and presence of the acceptor, respectively.

Finally, the donor–acceptor distance $r_0 = 5.60$ nm is determined by the Eq. (4) based on the energy transfer efficiency E obtained from Eq. (7). Obviously, the r_0 value is smaller than 7 nm, which further confirms that the efficient energy transfer between TCPC and cyt *c* occurred leading to the fluorescence quenching of TCPC.

3.5. Visible CD spectra of cyt c–TCPC complex in DMF

Circular dichroism (CD) spectra were measured for examining structural changes of cyt *c* complexed with TCPC in DMF. The far-UV CD spectrum of native cyt *c* shows negative bands at around 222 nm (n–π* amide transitions) and 208 nm (π–π* amide transitions), which is typical of proteins containing mainly α-helical structure [40]. Unfortunately, we could not take an accurate measurement of the far-UV CD spectrum in the α-helix region for the cyt *c*–TCPC complex, because of the strong background signals of DMF due to the intensive absorption of the solvent in the ultraviolet region. However, the measurable CD spectrum in Soret region can provide some insight into the structural changes of the heme cleft. Optical activity in the Soret region of heme proteins is generated through the coupling of heme π–π* electric dipole transition moments with those of nearby aromatic residues in the protein [7]. Fig. 9 shows the Soret region CD spectra (from 350 nm to 450 nm) of native cyt *c* in aqueous solution, and that of the cyt *c*–TCPC complex in DMF. A negative (414 nm) peak and positive (403 nm) peak produced due to a split Cotton effect are observed for native cyt *c*. In the cyt *c*–TCPC complex in DMF, the CD spectrum is characterized by the disappearance of the negative Cotton effect with a concomitant increase in the intensity of the positive Cotton effect at 405 nm. These changes indicate a change in heme-polypeptide interactions in the vicinity of the heme active site and an increase in the planarity of the ferric heme moiety [40].

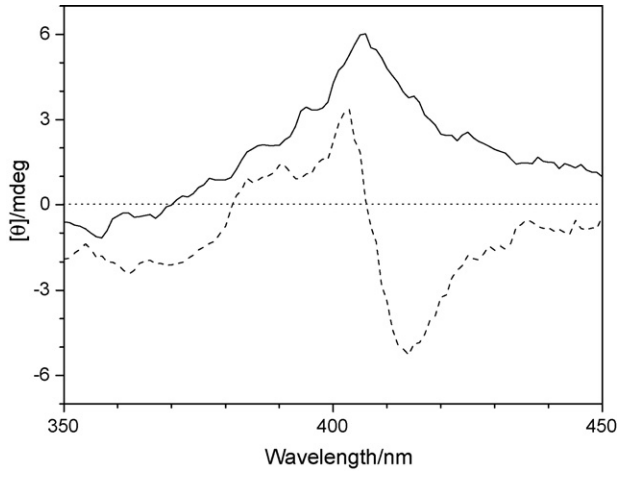

Fig. 9. CD spectra (350–450 nm) of cyt *c*: broken line, cyt *c* (10 μM) in water; solid line, cyt *c* with TCPC (10 μM) in DMF.

4. Conclusions

In summary, two novel carboxylphenyl-modified calix[4]arenes, TCPC and BCPC, as well as a corresponding analogue, TPC, have been synthesized by palladium-catalyzed Suzuki cross-coupling of arylboronic acid and tetrabromocalix[4]arene as a key step. Among the three extended calix[4]arene derivatives, TCPC shows the highest affinity to cyt *c*, which reflects a clear dependence of the number of carboxyl groups attached to the molecule. The stable 1:1 complexes of TCPC and BCPC with cyt *c* were evidenced with the binding constants of 3.15×10^6 and 5.85×10^5 L mol^{-1}, respectively. The fluorescence quenching of TCPC upon complexation with cyt *c* is attributed to an efficient energy transfer. The results suggest that TCPC not only has a potential application in chemoenzymatic synthesis to stabilize proteins in organic media due to its higher binding affinity to cyt *c* in DMF, but also is expected to have widespread applications as a fluorescent sensors for various proteins with cation-rich surface because of its high fluorescent nature and its efficient fluorescence quenching property upon binding with specific proteins.

Acknowledgements

This work was supported by the Natural Science Foundation of China (No.90813018), the Youth Foundation of Shanxi Province (No. 2006021009), and Hong Kong Baptist University, Faculty Research Grant (FRG/08-09/II-16). Helpful suggestions by anonymous referees are also gratefully acknowledged.

Appendix A. Supplementary data

Supplementary data associated with this article can be found, in the online version, at doi:10.1016/j.talanta.2009.03.007.

References

[1] M.W. Peczuh, A.D. Hamilton, Chem. Rev. 100 (2000) 2479.

[2] S. Fletcher, A.D. Hamilton, Curr. Opin. Chem. Biol. 9 (2005) 632.
[3] R. Ludwig, Macrochim. Acta 152 (2005) 1.
[4] H. Yin, A.D. Hamilton, Angew. Chem. Int. Ed. Engl. 44 (2005) 4130.
[5] H. Zhou, L. Baldini, J. Hong, A.J. Wilson, A.D. Hamilton, J. Am. Chem. Soc. 128 (2006) 2421.
[6] K. Shimojo, N. Kamiya, F. Tani, H. Naganawa, Y. Naruta, M. Goto, Anal. Chem. 78 (2006) 7735.
[7] K. Shimojo, T. Oshima, H. Naganawa, M. Goto, Biomacromolecules 8 (2007) 3061.
[8] T. Oshima, M. Goto, S. Furusaki, Biomacromolecules 3 (2002) 438.
[9] T. Oshima, K. Inoue, K. Uezu, M. Goto, Anal. Chim. Acta 509 (2004) 137.
[10] T. Oshima, A. Suetsugu, Y. Baba, Y. Shikaze, K. Ohto, K. Inoue, J. Membr. Sci. 307 (2008) 284.
[11] C.D. Gutsche, Calixarenes, Royal Society of Chemistry, Cambridge, U.K., 1989.
[12] Z. Asfari, V. Böhmer, J. Harrowfield, J. Vicens, M. Saadioui, Calixarenes 2001, Kluwer Academic Publishers, Dordrecht, The Netherlands, 2001.
[13] A.F. Danil de Mamor, R.M. Cleverley, M.L. Zapata-Ormachea, Chem. Rev. 98 (1998) 2495.
[14] R.K. Mahajan, M. Kumar, V. Sharma, I. Kaur, Talanta 58 (2002) 445.
[15] S. Kim, H. Kim, K.H. Noh, S.H. Lee, S.K. Kim, J.S. Kim, Talanta 61 (2003) 709.
[16] Y.L. Cho, D.M. Rudkevich, J. Rebek, J. Am. Chem. Soc. 122 (2000) 9868.
[17] P.K. Lo, M.S. Wong, Sensors 8 (2008) 5313.
[18] A.P. de Silva, H.Q. Nimal Gunaratne, T. Gunnlaugsson, A.J.M. Huxley, C.P. Mccoy, J.T. Rademacher, T.E. Rice, Chem. Rev. 97 (1997) 1515.
[19] Y. Ma, H.X. Bai, C. Yang, X.R. Yang, Analyst 130 (2005) 283.
[20] R.A. Scott, A.G. Mauk, Cytochrome *c*: A Multidisciplinary Approach, University Science Books, Sausalito, 1996.
[21] T. Aya, A.D. Hamilton, Bioorg. Med. Chem. Lett. 13 (2003) 2651.
[22] T. Mecca, G.M.L. Consoli, C. Geraci, F. Cunsolo, Bioorg. Med. Chem. 12 (2004) 5057.
[23] R. Zadmard, M. Arendt, T. Schrader, J. Am. Chem. Soc. 126 (2004) 7752.
[24] G. Izzet, B.D. Douziech, T. Prangé, A. Tomas, I. Jabin, Y.L. Mest, O. Reinaud, Proc. Natl. Acad. Sci. U.S.A. 102 (2005) 6831.
[25] A.J. Wilson, J. Hong, S. Fletcher, A.D. Hamilton, Org. Biomol. Chem. 5 (2007) 276.
[26] Y. Wei, G.L. McLendon, A.D. Hamilton, M.A. Case, C.B. Purring, Q. Lin, H.S. Park, C.S. Lee, T.N. Yu, Chem. Commun. (2001) 1580.
[27] W.T. An, Y. Jiao, X.H. Sun, C. Dong, S.M. Shuang, P.F. Xia, M.S. Wong, Chinese Chem. Lett. 19 (2008) 1341.
[28] M.Y.J. Lee, S. Dordick, Curr. Opin. Biotechnol. 13 (2002) 376.
[29] B.G. Davis, Curr. Opin. Biotechnol. 14 (2003) 379.
[30] R.K. Juneja, K.D. Robinson, C.P. Johnson, J.L. Atwood, J. Am. Chem. Soc. 115 (1993) 3818.
[31] M.S. Wong, P.F. Xia, X.L. Zhang, P.K. Lo, Y.K. Cheng, K.T. Yeung, X.L. Guo, S.M. Shuang, J. Org. Chem. 70 (2005) 2816.
[32] X.H. Sun, W.Y. Li, P.F. Xia, H.B. Luo, Y.L. Wei, M.S. Wong, Y.K. Cheng, S.M. Shuang, J. Org. Chem. 72 (2007) 2419.
[33] M.S. Wong, X.L. Zhang, D.Z. Chen, W.H. Cheung, Chem. Commun. (2003) 138.
[34] J.R. Lakowicz, Principles of Fluorescence Spectroscopy, Plenum Press, New York, 1983.
[35] M. Alain, B. Michel, D. Michel, J. Chem. Ed. 63 (1986) 365.
[36] Y. Liu, B.H. Han, Y.T. Chen, J. Phys. Chem. B 106 (2002) 4678.
[37] Y. Inoue, K. Yamamoto, T. Wada, S. Everitt, X.M. Gao, Z.J. Hou, L.H. Tong, S.K. Jiang, H.M. Wu, J. Chem. Soc., Perkin Trans. 2 (1998) 1807.
[38] P.G. Wu, L. Brand, Anal. Biochem. 218 (1994) 1.
[39] W.T. An, Y. Jiao, C. Dong, C. Yang, Y. Inoue, S.M. Shuang, Dyes and Pigments 81 (2009) 1.
[40] S.G. Sivakolundu, P.A. Mabrouk, J. Am. Chem. Soc. 122 (2000) 1513.

Talanta 79 (2009) 86–91

Contents lists available at ScienceDirect

Talanta

journal homepage: www.elsevier.com/locate/talanta

On-line sequential injection dispersive liquid–liquid microextraction system for flame atomic absorption spectrometric determination of copper and lead in water samples

Aristidis N. Anthemidis*, Kallirroy-Ioanna G. Ioannou

Laboratory of Analytical Chemistry, Department of Chemistry, Aristotle University, Thessaloniki 54124, Greece

ARTICLE INFO

Article history:
Received 14 January 2009
Received in revised form 26 February 2009
Accepted 4 March 2009
Available online 14 March 2009

Keywords:
Sequential injection
Dispersive liquid–liquid microextraction
Atomic spectrometry
Copper
Lead

ABSTRACT

A simple, sensitive and powerful on-line sequential injection (SI) dispersive liquid–liquid microextraction (DLLME) system was developed as an alternative approach for on-line metal preconcentration and separation, using extraction solvent at microlitre volume. The potentials of this novel schema, coupled to flame atomic absorption spectrometry (FAAS), were demonstrated for trace copper and lead determination in water samples. The stream of methanol (disperser solvent) containing 2.0% (v/v) xylene (extraction solvent) and 0.3% (m/v) ammonium diethyldithiophosphate (chelating agent) was merged on-line with the stream of sample (aqueous phase), resulting a cloudy mixture, which was consisted of fine droplets of the extraction solvent dispersed entirely into the aqueous phase. By this continuous process, metal chelating complexes were formed and extracted into the fine droplets of the extraction solvent. The hydrophobic droplets of organic phase were retained into a microcolumn packed with PTFE-turnings. A portion of 300 μL isobutylmethylketone was used for quantitative elution of the analytes, which transported directly to the nebulizer of FAAS. All the critical parameters of the system such as type of extraction solvent, flow-rate of disperser and sample, extraction time as well as the chemical parameters were studied. Under the optimum conditions the enhancement factor for copper and lead was 560 and 265, respectively. For copper, the detection limit and the precision (R.S.D.) were 0.04 μg L^{-1} and 2.1% at 2.0 μg L^{-1} Cu(II), respectively, while for lead were 0.54 μg L^{-1} and 1.9% at 30.0 μg L^{-1} Pb(II), respectively. The developed method was evaluated by analyzing certified reference material and applied successfully to the analysis of environmental water samples.

1. Introduction

In recent years, pollution of the environment by large amount of toxic elements has been considered as a result of human activities. Exposure to these toxic elements imposes risks not only to human health, but also to plants, animals and microorganisms [1]. Therefore, the determination of various toxic metals such as lead and copper in environmental samples is very important task. Despite its significant analytical capabilities for metal determination, flame atomic absorption spectrometry (FAAS) often requires a suitable sample pretreatment step (preconcentration and/or separation), due to analyte low concentration and matrix effects [2,3].

Conventional liquid–liquid extraction (LLE) is the most widely used sample pretreatment technique in routine analyses for trace metal determination due to its simplicity and adaptability. However, some shortcomings like the use of large sample volumes and toxic organic solvents make LLE expensive, time-consuming, laborious and environmentally unfriendly. Sample pretreatment still remains to be the bottleneck for a large number of analytical procedures and often the one, which seriously hinders automation and miniaturization. The implementation of on-line LLE simulating the same sequences performed in batch procedures, offers advantages which are inherent in automatic methods [3]. Recently, efforts have been focused on the miniaturizing of the LLE procedure by reducing the organic solvent, leading to the development of microextraction methodologies [4,5].

The first attempt to miniaturize LLE in a flowing stream assembly was carried out by Liu and Dasgupta [6], while further research led to the development of the so-called single-drop microextraction (SDME) where a droplet of organic solvent was suspended at the tip of a microsyringe needle and immersed into the aqueous sample [7]. Psillakis and Kalogerakis [8] and recently Xu et al. [9] overviewed the principles of SDME as well as its latest developments and applications. An automatic sequential injection single-drop microextraction (SI-SDME) system for metal deter-

* Corresponding author. Tel.: +30 2310997826; fax: +30 2310997719.
E-mail address: anthemid@chem.auth.gr (A.N. Anthemidis).

0039-9140/$ – see front matter © 2009 Elsevier B.V. All rights reserved.
doi:10.1016/j.talanta.2009.03.005

mination in environmental samples using ETAAS was developed recently by our group [5]. Cloud point extraction (CPE) procedure is based on the phase separation, which occurs in aqueous solutions of non-ionic surfactants, when heated above the so-called cloud point temperature. At this temperature the initial solution separates into a surfactant rich phase of small volume containing the metal trapped by organized structures and a bulk aqueous phase [10]. The principles and theoretical aspects as well as relevant applications regarding the use of micelle-mediated separation have been well documented in various interesting reviews [11,12].

On the other hand, homogeneous liquid–liquid extraction (HLLE) is a simple and powerful preconcentration technique for organic and inorganic analytes, which utilizes the phase separation from a homogeneous solution where no interface between the aqueous phase and organic solvent phase exist and the analytes are extracted into the sedimented phase. It can be considered that the surface area of the interface is infinitely large. Hence, vigorous shaking or mixing is not necessary. Generally, HLLE has been applied through two different modes: by the perfluorinated surfactant system [13–15] and the ternary component solvent one [16,17,18,19]. In these cases, phase separation is based on pH, on ion-pair formation or on the solubility difference among the solvents of a ternary system.

Recently, Assadi and coworkers [20] presented a microextraction technique, termed dispersive liquid–liquid microextraction (DLLME) based on ternary component solvent systems, similar to HLLE and CPE. An appropriate mixture of an extraction solvent and a disperser solvent with high miscibility in both aqueous phase and extractant is rapidly injected into the sample (aqueous phase) using a microsyringe. By this procedure a cloudy solution (high turbulence) is produced, which is consisted of fine droplets of extraction solvent dispersed throughout the aqueous sample. The nature of the disperser solvent can also have an influence on the mean droplet size and their distribution. After centrifuging of the cloudy solution, the sedimented phase at the bottom of a conical tube is removed manually by a syringe and analyzed by various analytical techniques like gas chromatography (GC) [21,22], high-performance liquid chromatography (HPLC) [23], electrothermal atomic absorption spectrometry (ETAAS) [24–27] and FAAS [28,29]. DLLME has been applied for preconcentration and determination of organic compounds as well as for metals [24–29] and metalloids [30] in water samples. The principal advantage of DLLME is that the surface area between extraction solvent and aqueous sample is very large, thus the equilibrium state is achieved quickly and the extraction time is very short. However, when DLLME is performed in manual mode, is limited to a small number of extraction solvents, since the required conditions, i.e. to have higher density rather than water, to form a stable cloudy solution and to be easily removed from the bottom of the conical vial after centrifugation, are met by a few organic solvents [31]. Also it suffers from the inherent problems of the manual procedures.

The aim of present work was to develop a novel automatic sequential injection dispersive liquid–liquid microextraction (SI-DLLME) system for metal preconcentration and determination using FAAS. To best of our knowledge, the automation of the DLLME was demonstrated for the first time. The effectiveness and efficiency of the proposed SI-DLLME system has been demonstrated for copper and lead determination in environmental water samples. Ammonium diethyldithiophosphate (DDPA) was selected as chelating agent due to its good selectivity in strong acidic medium. All main factors were investigated and optimized. The proposed method was evaluated by analyzing certified reference material and spiked environmental water samples.

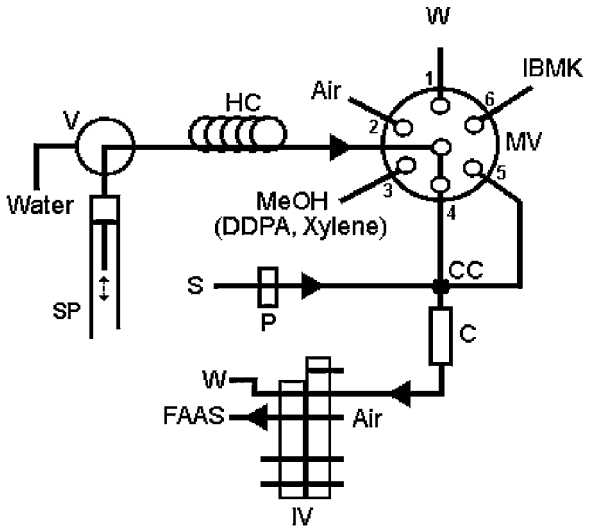

Fig. 1. Schematic manifold for SI-DLLME metal determination by FAAS (step 4). For details see text and Table 1. S, sample; MeOH, solution containing 2.0% (v/v) xylene and 0.3% (m/v) DDPA; W, waste; P, peristaltic pump; SP, syringe pump; MV, multiposition valve; IV, injection valve in "load" position; V, valve in "out" position; HC, holding coil; C, microcolumn; CC, confluence connector.

2. Experimental

2.1. Instrumentation

The manifold and its operation for on-line sequential injection dispersive liquid–liquid microextraction (SI-DLLME) metal determination by FAAS is presented schematically in Fig. 1.

A FIAlab®-3000 sequential injection system (Alitea FIAlab, USA) equipped with an internally incorporated six-port multiposition valve (MV) and a syringe pump (SP, Cavro, Sunnyvale, CA) with a capacity of 1000 μL was adopted. The FIAlab®-3000 system was controlled by a personal computer and the FIAlab for windows v. 5.9.245 application software, written by FIAlab instruments (http://www.flowinjection.com).

A PerkinElmer, Norwalk, Connecticut, U.S.A. (http://las.perkinelmer.com) model 5100 PC flame atomic absorption spectrometer was exploited as detection system. Copper hollow cathode lamp (HCL) and lead electrodeless discharge lamp (EDL) was used as light source operated at 15 and 10 W, respectively. The slit was set at 0.7 nm, while the wavelength was set at 324.7 and 283.3 nm resonance line for copper and lead, respectively. A time-constant of 0.2 s was used for peak height evaluation. The flame conditions were adjusted to be slightly leaner than the recommended by the manufacturer, in order to compensate the effect of organic solvent isobutyl methyl ketone (IBMK), which serves as an additional fuel. The air and acetylene flow-rate were 10.0 and 0.9 L min^{-1}, respectively. By these conditions the nebulizer's free uptake rate was 5.6 mL min^{-1}. A flow spoiler was employed inside the spray chamber for better nebulization conditions.

A PerkinElmer Norwalk, Connecticut, U.S.A. model FIAS-400 flow injection analysis system was coupled to FAAS and SI system for automatic processing of the whole procedure. The FIAS-400 system was controlled by a personal computer and the AA Lab. Benchtop version 7.2 software program. The two programs (FIAlab and AA Lab.) were synchronized and activated in the same time. The FIAS-400 system consisted of two peristaltic pumps (only one was used in the proposed manifold) and a 5-port 2-position injection valve, IV. The connecting tubing between the IV and the FAAS nebulizer was as short as possible PTFE tube (20 cm length, 0.5 mm i.d.).

Table 1
Operational sequence of the SI-DLLME–FAAS on-line preconcentration method for copper and lead determination (for manifold details, see Fig. 1).

Step	V position	MV position	SP flow-rate	SP operation	IV position	P operation	Commentary
1	IN	2	50 μL s^{-1}	Aspirate 200 μL	Load	OFF	Water into SP
2	OUT	2	3 μL s^{-1}	Aspirate 5 μL	Load	OFF	Segment of air into HC
3	OUT	3	30 μL s^{-1}	Aspirate 770 μL	Load	OFF	Disperser solvent into HC
4	OUT	4	6 μL s^{-1}	Dispense 720 μL	Load	ON[a]	Cloudy solution formation/Extraction (120 s)/retention
5	OUT	1	20 μL s^{-1}	Dispense 200 μL	Load	OFF	Discard of air segment
6	IN	1	50 μL s^{-1}	Aspirate 600 μL	Load	OFF	Water into SP
7	OUT	6	30 μL s^{-1}	Aspirate 300 μL	Load	OFF	IBMK into HC
8	OUT	5	50 μL s^{-1}	Dispense 600 μL	Elution	OFF	Elution of microcolumn/measurement
9	OUT	6	50 μL s^{-1}	Aspirate 500 μL	Elution	OFF	IBMK into HC
10	OUT	4	50 μL s^{-1}	Empty	Elution	OFF	Washing of manifold

[a] Sample propulsion with flow-rate, 6.0 mL min^{-1}; V, valve; MV, multiposition valve; SP, syringe pump; IV, injection valve; P, peristaltic pump.

The microcolumn for retention of the extraction solvent, which includes the derivative chelate complex M–DDPA, was fabricated by firmly packing 180 mg of PTFE-turnings in a piece of narrow PTFE tube (40 mm length, 2.1 mm i.d./3.2 mm o.d.). PTFE-turnings were mechanically produced in our laboratory by lathe as described elsewhere [32] and the image of turnings has been given previously [33]. The PTFE-turnings were washed thoroughly by ethanol followed by 1 mol L^{-1} HNO_3 and de-ionized water. The performance of the column was stable for at least 1000 cycles.

A VICI AG (Valco International) four-section "cross" type confluence connector made of PEEK, with 0.5 mm i.d. bore size was used for intermixing of aqueous (sample) and organic phase (methanol plus xylene). An Orion EA940 pH-meter was employed for the pH measurements being defined by NIST buffers.

2.2. Reagents and samples

All chemicals were of analytical reagent grade and were provided by Merck (Darmstadt, Germany, http://www.merck.de). Ultra-pure quality water was used throughout which was produced by a Milli-Q system (Millipore, Bedford, USA, http://www.millipore.com). All standard solutions were prepared immediately before use, by stepwise dilution of 1000 mg L^{-1} Cu(II) and Pb(II) stock standard solution in HNO_3 0.5 mol L^{-1} (Merck Titrisol) to the required sub-μg L^{-1} levels. The chelating agent, 0.3% (m/v) ammonium DDPA solution was prepared daily by dissolving appropriate amount of DDPA (Aldrich) in methanol without any further purification. IBMK was previously saturated with ultra-pure water.

Natural water samples were filtered through 0.45 μm membrane filters and acidified to 0.05 mol L^{-1} HNO_3 (pH ~ 1.4).

2.3. Procedure

The operation steps of the optimized on-line sequential injection dispersive liquid–liquid microextraction method (SI-DLLME–FAAS) for copper and lead determination are summarized in Table 1.

In step 2 and 3 segments of air and disperser solution (methanol containing 2.0% (v/v) xylene and 0.3% (m/v) DDPA) at volumes of 5 and 770 μL, respectively were aspirated into the holding coil (HC). In step 4 (Fig. 1), peristaltic pump (P) is activated in order to transport the sample towards the microcolumn (C) through the confluence connector (CC). In the same time syringe pump (SP) dispense the disperser solution through the port 4 of MV towards microcolumn through also CC. Hence, the disperser solution was injected into the moving sample solution, resulting thus a cloudy solution of fine droplets of extraction solvent (xylene). Under these conditions the metal complexes were extracted continuously from aqueous phase to organic phase (xylene). The extraction procedure performed for 120 s (extraction time). Meanwhile, the xylene droplets, which contain the metal complexes, were retained on the PTFE-turnings into the microcolumn (C). In step 8, the injection valve (IV) was switched to the "Elution" position, so that the segment of 300 μL of IBMK was delivered through the microcolumn in order to elute the analyte. The eluent forwarded to the FAAS nebulizer for atomization and measuring. During the next steps a completed washing of the manifold were done. Five replicate measurements were made in all instances.

3. Results and discussion

For higher sensitivity, selectivity and precision for metal determination with the SI-DLLME method, the effect of the main parameters, like the type of disperser and extraction solvent, sample and disperser flow-rate, sample acidity, amount of chelating agent, sample ionic strength and extraction time, were studied and optimized thoroughly. Standard aqueous solutions 10.0 μg L^{-1} Cu(II) and 100.0 μg L^{-1} Pb(II) in pH ~ 1.4 were used for the following experiments. In order to obtain effective microcolumn elution and atomization, a segment of 300 μL IBMK at 3.0 mL min^{-1} flow-rate was used in any case, as they were optimized during preliminary experiments.

3.1. Effect of extraction solvent type and concentration

The selection of an appropriate organic solvent for SI-DLLME is very important task. It should able to form a cloudy solution system with water and disperser solvent. Also it should have highly immiscibility with aqueous phase (sample solution), high extraction efficiency, selectivity and hydrophobicity. Opposition to conventional (off-line) dispersive liquid–liquid microextraction systems, extraction solvent was not necessary to have higher density than water, due to the fact that the formation of the cloud solution took place in a moving stream and the retention of the extraction droplets on PTFE-turnings was based on its hydrophobicity. It means that the separation of the organic phase is based on the retention and not on the centrifuging. Chloroform, carbon tetrachloride, dichloromethane, hexane, benzene, xylene, toluene, IBMK, di-isobutyl ketone (DIBK) were compared in the extraction of copper and lead. The concentration of the examined extraction solvents in methanol was fixed at 2.0% (v/v). The obtained results of relative absorbance of copper and lead together with the solubility "in water" values of the extraction solvents, are given in Table 2. The results revealed that xylene achieved the highest extraction efficiency and therefore selected as optimum for all further experiments.

The concentration of the extraction solvent in methanol affects positively the volume of the droplets. On the other hand an increment in the droplets results in lower preconcentration factor, due to lower volume-ratio of aqueous to organic phase. In addition the volume of extraction solvent can affect the retention processes and finally the enhancement factor. The effect of the xylene concentra-

Table 2
Extraction efficiency of various extraction solvents (2.0%, v/v in methanol) for Cu(II) and Pb(II) determination by SI-DLLME–FAAS.

Extraction solvent	Solubility in water, % (m/m)	Relative absorbance, %	
		Cu(II)	Pb(II)
Chloroform	0.82	44	46
Carbon tetrachloride	0.08	86	89
Dichloromethane	1.60	32	35
Hexane	0.005	76	75
Benzene	0.18	60	58
Xylene	0.02	100	100
Toluene	0.05	94	91
IBMK	1.91	24	28
DIBK	0.05	97	96

tion on the absorbance was studied from 0.5 to 8.0% (v/v) and the results are illustrated in Fig. 2. Relative absorbance remained almost constant for xylene concentration from 0.5% up to 2.0%, while for higher concentrations it was gradually decreasing. In the absent of xylene the recorded absorbance was insignificant indicating that the retention of the metal complex on the column was not achieved, due to the presence of MeOH.

For better precision and higher enrichment factors a xylene concentration of 2.0% (v/v) was chosen as optimum for the following experiments.

3.2. Effect of disperser solvent type and flow-rate

The miscibility of the disperser solvent with the extraction solvent and aqueous phase (sample solution) is a significant criterion for its choice, in DLLME methods. Acetone, ethanol and methanol were examined for this purpose. Xylene concentration in any disperser solvent was 2.0% (v/v). Other experimental conditions were as in Fig. 2. The resulting data had shown no significant statistical differences between the studied solvents. Methanol was selected as disperser solvent in the subsequent experiments due to its accessibility and low-priced.

The flow-rate of disperser solvent affects on the sedimentation of the extraction solvent (fine droplets formation) and on the retention of them in the microcolumn. This consideration is based on the variation of the linear velocity of the liquid mixture by changing the flow-rate into the microcolumn. The influence of disperser solvent flow-rate on the absorbance was examined in the range of 0.12–0.72 mL min^{-1}. It was found that the absorbance was increased by increasing the flow-rate of methanol up to

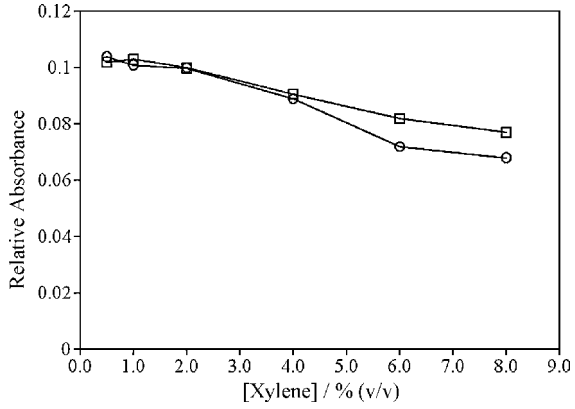

Fig. 2. Effect of the concentration of xylene on the absorbance of 10.0 μg L^{-1} Cu(II) (–□–) and 100.0 μg L^{-1} Pb(II) (–○–) obtained from SI-DLLME–FAAS. Extraction solvent: methanol containing 0.2% (m/v) DDPA and xylene; 5.1 mL min^{-1} sample flow-rate; 0.36 mL min^{-1} methanol flow-rate.

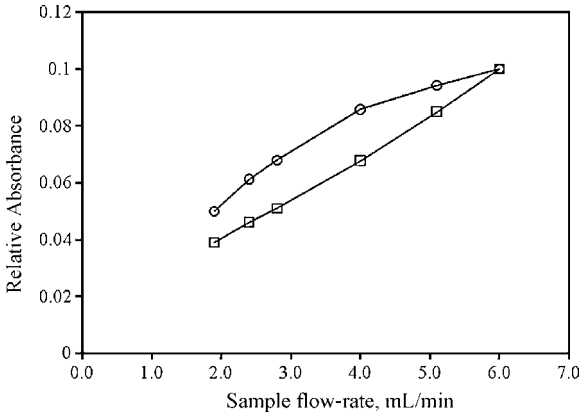

Fig. 3. Effect of the sample flow-rate on the absorbance of 10.0 μg L^{-1} Cu(II) (–□–) and 100.0 μg L^{-1} Pb(II) (–○–) obtained from SI-DLLME–FAAS. Extraction solvent: methanol containing 0.2% (m/v) DDPA and 2.0% (v/v) xylene; 0.36 mL min^{-1} methanol flow-rate.

0.36 mL min^{-1} and after that it was slightly decreased. Therefore, 0.36 mL min^{-1} was chosen as optimum.

3.3. Effect of aqueous phase flow-rate

The effect of aqueous phase (sample solution) flow-rate was evaluated in the range of 1.9–6.0 mL min^{-1}. Methanol flow-rate was fixed at 0.36 mL min^{-1}. Thereby, the ratio of aqueous to organic volume was increased by increasing the sample flow-rate. The recorded relative absorption was almost linearly within the studied range as it is shown in Fig. 3, implying that the contact time of fine droplets of extraction solvent with the PTFE-turnings was sufficient. This is an advantage because enables more sample to be loaded during a given loading time resulting in higher preconcentration factor. A flow-rate of 6.0 mL min^{-1} was selected for high sensitivity.

3.4. Sample acidity and DDPA concentration

Ammonium DDPA has been used successfully in on-line liquid–liquid extraction and solid phase extraction methodologies and compared with other dithiocarbamate reagents proved to be more selective and stable for cadmium, copper and lead in very low pH values [34]. The main advantage of the DDPA is that forms stable complexes with several metals even in strong acidic medium due to its resistance against hydrolysis, avoiding thus the addition of buffer solutions which are a significant source of contamination [35].

Among chemical variables, sample acidity, which is defined by the pH of the sample solution, plays a significant role in the overall performance of the on-line solvent extraction affecting the complex formation and the extraction efficiency. The effect of the pH on the absorbance was studied in the range 0.9–3.0 by adjusting it (in metal solution) with dilute nitric acid. The obtained results shown that, the absorbance was maximum and practically stable in a pH window varied between 0.9 and 1.6, while for higher values the absorbance was decreased gradually. Thus, samples and standards solutions were fixed to pH = 1.4 ± 0.1. This optimum pH value enables the use of the method directly in many aqueous samples after common acid preservation.

The effect of DDPA concentration in the disperser solvent (methanol) was studied in the range of 0.01–0.6% (m/v). The maximum absorbance was observed over the concentration range 0.15–0.6% (m/v). Given its competitive complexation with other coexisting ions in the real samples a DDPA concentration of 0.3% (m/v) was adopted for all further experiments.

Table 3
Effect of interferents on the recovery of 2.0 μg L^{-1} Cu(II) and 20.0 μg L^{-1} Pb(II) in water samples using SI-DLLME–FAAS.

Interferent	[Interferent]/[M(II)]	Recovery (%)	
		Cu(II)	Pb(II)
Al(III)	1000	97	96
Ag(I)	100	100	99
Cu(II)	100	–	95
Cd(II)	100	95	95
Co(II)	1000	99	100
Pb(II)	100	97	–
Fe(II)	1000	99	98
Fe(III)	1000	97	100
Zn(II)	1000	99	101
Mn(II)	1000	98	99
Ni(II)	1000	95	96
Hg(II)	100	96	95

3.5. Effect of ionic strength

The influence of ionic strength of the aqueous solutions on the absorbance was evaluated by adding various amounts of sodium chloride (NaCl) in the range 0–5.0% (m/v). The experimental conditions of the SI-DLLME method were the optimum. As it is shown by increasing the NaCl concentration no significant statistical differences were recorded throughout the studied range.

3.6. Extraction time

The process of mass transfer is time-dependent, while the extraction rate is reduced, as the system is going to the chemical equilibrium. Thereby, maximum absorbance is attained. However, in the on-line systems, the equilibrium is not necessary, as long as the extraction conditions are extremely reproducible.

The influence of the extraction time on the absorbance was investigated in the range 30–120 s. The results have shown, that the absorbance was increased almost proportional by increasing the extraction time. As a compromise between sensitivity and sampling frequency, an extraction time of 120 s was adopted throughout the experiments.

3.7. Interference studies

The effect of potential ions, encountered in natural water samples, on the recovery of 2.0 μg L^{-1} Cu(II) and 20.0 μg L^{-1} Pb(II) standard solution in the presence of various amounts of individual interfering ions, was examined. For this purpose the proposed SI-SLLME–FAAS method under the optimum conditions was adopted while a variation on the recovery greater than ±5% was considered as interference. The results are presented in Table 3. A significant advantage of DDPA is that it does not react with alkali, alkaline earth metals and others such as Mn, V, Ti, Co, Cr, Zn allowing the separation of major components of the matrix [34]. Moreover, the effect of common coexisting cations such as Ca(II), Mg(II), Ba(II), Na(I) and K(I) were also investigated. No significant variation in the absorbance was observed at concentrations up to 1000 mg L^{-1}.

Table 5
Analytical results of copper determination (dissolved fraction) in certified reference material and spiked natural waters samples with the SI-DLLME–FAAS method ([M] in μg L^{-1}).

Sample	Certified	Added	Found[a]	Recovery (%)
CRM 1643e	22.76 ± 0.31	–	22.15 ± 1.5	97.3
Tap water		–	0.82 ± 0.05	–
		2.00	2.75 ± 0.16	96.5
River water		–	1.94 ± 0.08	–
		2.00	3.85 ± 0.24	95.5
Coastal seawater		–	1.64 ± 0.11	–
		2.00	3.65 ± 0.26	100.5

[a] Mean value ± standard deviation based on three replicate measurements.

Table 6
Analytical results of lead determination (dissolved fraction) in certified reference material and spiked natural waters samples with the SI-DLLME–FAAS method ([M] in μg L^{-1}).

Sample	Certified	Added	Found[a]	Recovery (%)
CRM 1643e	19.63 ± 0.21	–	18.95 ± 0.9	96.5
Tap water		–	$<c_L$	–
		10.0	9.8 ± 0.4	98.0
River water		–	4.3 ± 0.3	–
		10.0	13.9 ± 0.7	96.0
Coastal seawater		–	5.0 ± 0.4	–
		10.0	14.5 ± 0.8	95.0

c_L: detection limit.
[a] Mean value ± standard deviation based on three replicate measurements.

3.8. Analytical performance and analysis of natural waters

The performance data of the SI-LLME on-line preconcentration method for FAAS copper and lead determination under the optimum conditions are summarized in Table 4.

For a sample consumption 12.0 mL, the detection limit, based on 3 s criterion, was 0.04 and 0.54 μg L^{-1} while the precision (RSD) was 2.1% (at 2.0 μg L^{-1}) and 1.9% (at 30.0 μg L^{-1}) for copper and lead, respectively. The enhancement factor calculated by comparison the slops of the calibration graphs with and without preconcentration, was 560 and 265 for copper and lead, respectively.

The accuracy of the proposed method was evaluated, by the analysis of the certified reference material, NIST CRM 1643e (National Institute of Standard and Technology, Trace elements in water). The proposed method was applied to the analysis of tap water, river water and coastal seawater samples, which had been collected from Northern Greece. All the determinations were performed using aqueous standard solutions for calibration, without further matrix specific optimization for the samples. The certified

Table 4
Analytical performance characteristics of the SI-DLLME-FAAS method for copper and lead determination under the optimized conditions.

Parameter	Copper	Lead
Sample consumption (mL)	12.0	12.0
Extraction/preconcentration time (s)	120	120
Sampling frequency (h^{-1})	12	12
Enhancement factor	560	265
Linear range ([M] in μg L^{-1})	0.16–12.0	2.3–160.0
Detection limit (3 s), μg L^{-1}	0.04	0.54
Precision (R.S.D., n = 10) (%)	2.1 (2.0 μg/L)	1.9 (30.0 μg/L)
Regression equation ([M] in μg L^{-1}, n = 9)	A = (0.0304 ± 0.00097)[Cu(II)] + (0.0014 ± 0.00598)	A = (0.0021 ± 0.00005)[Pb(II)] + 0.0014 ± 0.0045
Correlation coefficient (r)	0.9993	0.9995

values and the analytical results are presented in Tables 5 and 6. The determined concentration of copper and lead were in good agreement with the certified values and the recovery ranged between 95.0 and 100.5% showing the good performance of the method in all type of natural waters samples.

4. Conclusions

A new on-line liquid–liquid microextraction technique for metal determination with FAAS was developed. The proposed method was based on the metal extraction from aqueous phase into the fine droplets of extraction solvent (cloudy solution), which were formed on-line from a ternary system (water–methanol–xylene). From commercial, economical and environmental point of view, SI-DLLME offers several important advantages: faster operation in micro-scale analysis, extremely low time, low cost and particularly low consumption of organic solvent thanks to the use of a syringe pump of SI manifold, simple manifold (no need of separation unit), high recovery and enhancement factor. In addition, the proposed system seems to have easier linkage to analytical methods. The results have shown that SI-DLLME is a precise, economic and reproducibly way for trace copper and lead determination in natural environmental samples.

References

[1] M. Miró, J.M. Estela, V. Cerda, Talanta 63 (2004) 201.
[2] A.N. Anthemidis, G.A. Zachariadis, C.G. Farastelis, J.A. Stratis, Talanta 62 (2004) 437.
[3] A. Anthemidis, Talanta 77 (2008) 541.
[4] J.-H. Wang, E.H. Hansen, Anal. Chim. Acta 456 (2002) 283.
[5] A.N. Anthemidis, I.S.I. Adam, Anal. Chim. Acta 632 (2009) 216.
[6] H.-H. Liu, P.K. Dasgupta, Anal. Chem. 68 (1996) 1817.
[7] M.A. Jeannot, F.F. Cantwell, Anal. Chem. 68 (1996) 2236.
[8] E. Psillakis, N. Kalogerakis, Trends Anal. Chem. 21 (2002) 53.
[9] L. Xu, C. Basheer, H.K. Lee, J. Chromatogr. A 1152 (2007) 184.
[10] M.A. Bezerra, M.A.Z. Arruda, S.L.C. Ferreira, Appl. Spectrosc. Rev. 40 (2005) 269.
[11] E.K. Paleologos, D.L. Giokas, M.I. Karayannis, Trends Anal. Chem. 24 (2005) 426.
[12] M.F. Silva, E.S. Cerutti, L.D. Martinez, Microchim. Acta 155 (2006) 349.
[13] S. Igarashi, T. Yotsuyanagi, Mikrochim. Acta 106 (1992) 37.
[14] A. Takahashi, S. Igarashi, Y. Ueki, H. Yamaguchi, Fresenius J. Anal. Chem. 368 (2000) 607.
[15] A. Takahashi, Y. Ueki, S. Igarashi, Anal. Chim. Acta 387 (1999) 71.
[16] S. Igarashi, N. Ide, Y. Takagai, Anal. Chim. Acta 424 (2000) 263.
[17] M.R. Jamali, Y. Assadi, F. Shemirani, Sep. Sci. Technol. 42 (2007) 3503.
[18] M.A. Farajzadeh, M. Bahram, S. Zorita, B. Ghorbani Mehr, J. Hazard. Mater. 161 (2009) 1535.
[19] H. Ebrahimzadeh, Y. Yamini, F. Kamarei, S. Shariati, Anal. Chim. Acta 594 (2007) 93.
[20] M. Rezaee, Y. Assadi, M.-R.M. Hosseini, E. Aghaee, F. Ahmadia, S. Berijani, J. Chromatogr. A 1116 (2006) 1.
[21] A.P. Birjandi, A. Bidari, F. Rezaei, M.R. Milani Hosseini, Y. Assadi, J. Chromatogr. A 1193 (2008) 19.
[22] M. Garcia-Lopez, I. Rodriguez, R. Cela, J. Chromatogr. A 1166 (2007) 9.
[23] M.A. Farajzadeh, M. Bahram, J.A. Jonsson, Anal. Chim. Acta 591 (2007) 69.
[24] M. Shamsipur, M. Ramezani, Talanta 75 (2008) 294.
[25] E.Z. Jahromi, A. Bidari, Y. Assadi, M.R. Milani Hosseini, M.R. Jamali, Anal. Chim. Acta 585 (2007) 305.
[26] H. Jiang, Y. Qin, B. Hu, Talanta 74 (2008) 1160.
[27] M.T. Naseri, M.R. Milani Hosseini, Y. Assadi, A. Kiani, Talanta 75 (2008) 56.
[28] M.T. Naseri, P. Hemmatkhah, M.R. Milani Hosseini, Y. Assadi, Anal. Chim. Acta 610 (2008) 135.
[29] M.A. Farajzadeh, M. Bahram, B. Ghorbani Mehr, J.A. Jonsson, Talanta 75 (2008) 832.
[30] A. Bidari, E. Zeini Jahromi, Y. Assadi, M.R. Milani Hosseini, Microchem. J. 87 (2007) 6.
[31] F. Pena-Pereira, I. Lavilla, C. Bendicho, Spectrochim. Acta B 64 (2009) 1.
[32] A.N. Anthemidis, G.A. Zachariadis, J.A. Stratis, J. Anal. At. Spectrom. 17 (2002) 1330.
[33] G.A. Zachariadis, A.N. Anthemidis, J.A. Stratis, Talanta 57 (2002) 919.
[34] R. Ma, W. Van Mol, F. Adams, Anal. Chim. Acta 285 (1994) 33.
[35] A.N. Anthemidis, G.A. Zachariadis, C.G. Farastelis, J.A. Stratis, J. Anal. At. Spectrom. 18 (2003) 1400.

Talanta 79 (2009) 2–9

Contents lists available at ScienceDirect

Talanta

journal homepage: www.elsevier.com/locate/talanta

Review

Application of pyridylazo and thiazolylazo reagents in flow injection preconcentration systems for determination of metals

Patrícia Xavier Baliza, Sérgio Luis Costa Ferreira, Leonardo Sena Gomes Teixeira*

Universidade Federal da Bahia, Instituto de Química, Campus Universitário de Ondina, 40170-280, Salvador, Bahia, Brazil

ARTICLE INFO

Article history:
Received 18 November 2008
Received in revised form 9 February 2009
Accepted 27 February 2009
Available online 13 March 2009

Keywords:
Pyridylazo
Thiazolylazo
Flow injection systems
Metal
Preconcentration

ABSTRACT

Pyridylazo and thiazolylazo reagents are synthetic dyes widely used in analytical chemistry. These reagents are also very attractive for use in preconcentration systems. This paper covers the application of pyridylazo and thiazolylazo reagents in flow injection systems for the determination of metals. The article discusses flow injection preconcentration systems with solid-phase extraction, precipitation and cloud point extraction. The use of pyridylazo and thiazolylazo reagents in flow injection detection systems is also presented. The relative advantages and drawbacks of these systems are discussed. The application of pyridylazo and thiazolylazo reagents in new systems is presented in the concluding part of this review article.

Contents

1. Introduction 2
2. Pyridylazo and thiazolylazo reagents 3
3. Flow injection preconcentration systems 3
   3.1. Solid-phase extraction 3
   3.2. Cloud point extraction 4
   3.3. Precipitation 6
4. Measurements on solid support and sensors 7
5. Conclusion 8
   Acknowledgments 8
   References 8

1. Introduction

Flow injection systems are frequently preferred over batch procedures due to the advantages obtained. These advantages include high analytical frequency, ease of association with several types of detectors, good precision and accuracy, reduced disposal costs and a higher degree of safety for the operator in the handling of the solutions [1–3]. Procedures involving flow injection systems that include derivatization reactions, solid-phase extraction, liquid–liquid extraction, sensors and enzymatic reactions have attracted scientists due to the growing demand for more sensitive and more selective analytical methodologies. These procedures involve the use of complexing reagents associated with solid supports employed for the formation of detectable species and the development of extraction procedures. Among these reagents, the pyridylazo and thiazolylazo groups deserve special attention because of their capacity to form complexes with several metals [4–7]. This property is shared with reagents widely used in several fields within analytical chemistry.

Pyridylazo and thiazolylazo reagents have been used for spectrophotometric determinations because of their good selectivity and sensitivity, although for conventional spectrophotometric analysis in aqueous solution, the low solubility of these azo compounds and their complexes is a significant drawback. This drawback can be overcome by adding organic solvents or surfactants [8]. However, the low solubility of these compounds can become an advantage

* Corresponding author. Tel.: +55 71 32836829; fax: +55 71 32355166.
E-mail address: lsgt@ufba.br (L.S.G. Teixeira).

0039-9140/$ – see front matter © 2009 Elsevier B.V. All rights reserved.
doi:10.1016/j.talanta.2009.02.055

when separation and preconcentration procedures are applied because these reagents can be immobilized through physical sorption on a proper support or complexes with these reagents can precipitated in aqueous media.

The application of pyridylazo reagents in separation systems has been practically performed in parallel with the use of the thiazolylazo compounds. This work aims to present a general view on use of the pyridylazo and thiazolylazo reagents in flow injection analysis systems. Some variables and analytical parameters of the systems are discussed, as well as the advantages and disadvantages of the different procedures.

2. Pyridylazo and thiazolylazo reagents

Azo reagents represent the largest and most important group of synthetic dyes. These substances possess the basic structure Ar–N=N–Ar′, where Ar and Ar′ designate any aromatic groups. The unit that contains the bond –N=N– is referred to as the azo group and is a chromophore that gives brilliant color to these compounds. In the formation of the azo group, many combinations of $ArNH_2$ and $Ar'NH_2$ (or Ar′OH) can be used. These different combinations give rise to a variety of colors, such as yellow, orange, red, brown and blue. The production of an azo dye involves the treatment of an aromatic amine with nitrous acid, resulting in a diazo ion as an intermediate product. This process is known as diazotization. Among these dyes, two groups deserve special attention: pyridylazo and thiazolylazo reagents [9–11].

Compounds derived from 2-aminopyridine have been widely used as chromogenic reagents in spectrophotometry for the determination of metallic elements, including iron, cobalt, nickel, copper, zinc, chromium, palladium, mercury and cadmium, as well as organic substances, such as nucleic acids and tartaric acid. Additionally, the reactions of pyridylazo reagents with metallic ions have been used in procedures involving atomic spectrometry, chromatography and electroanalytical techniques in order to increase the sensitivity and the selectivity of the analysis [12,13].

Thiazolylazo dyes are organic substances prepared from the diazotization of 2-aminothiazol and its derivatives, with subsequent coupling to phenolic groups or other aromatic substances. This preparation does not require any special conditions for diazotization. The diazotization is carried out in strongly acid solutions at low temperatures, due to the elevated reactivity of the diazotate. In this way, a great number of thiazolylazo dyes have been prepared from several phenols, napthols and other substances. Among these compounds, the reagents 1-(2-thiazolylazo)-2-naphtol (TAN), 2-(2-thiazolylazo)-*p*-cresol (TAC) and 4-(2-thiazolylazo) resorcinol (TAR) have been extensively employed for the separation and determination of trace elements [9].

The synthesis of pyridylazo reagents is not as simple as the synthesis of compounds derived from 2-aminothiazol. The synthesis of these reagents involves the coupling of pyridyldiazotate with a phenolic substance in a carbon dioxide atmosphere. This coupling is usually accomplished with some difficulty [14]. 1-(2-Pyridylazo)-2-naphthol (PAN) and 4-(2-pyridylazo)-resorcinol (PAR) are examples of pyridylazo reagents that are prepared by the coupling of diazotized 2-aminopyridine with 2-naphthol and 2-aminopyridine, respectively.

3. Flow injection preconcentration systems

3.1. Solid-phase extraction

Solid-phase extraction involves the partition of analytes between two phases, a liquid and a solid sorbent [15]. In general, the liquid is put in contact with a sorbent in a flask or in a column. The mechanism of retention of the analytes will depend on the nature of the sorbent. This mechanism can be a simple retention, chelation or ion exchange. Chelating agents such as pyridilazo and thiazolylazo reagents may be added directly to the sample, and the chelates then retained on an appropriate sorbent. Alternatively, a ligand may be introduced to the support, generating a chelating sorbent. This introduction can be done by three methods [16]:

(a) *Loaded sorbents*: sorption of a ligand on the sorbent by impregnation of the solid matrix with a solution containing the chelating reagent;
(b) *Synthesized sorbents*: synthesis of new sorbents containing chelating groups;
(c) *Functionalized sorbents*: chemical incorporation of chelating groups on existing sorbents.

Loading is the more generally method employed to incorporate pyridylazo and thiazolylazo reagents to solid supports because these sorbents are the simplest to prepare and use. Several solid supports have been loaded with pyridylazo and thiazolylazo reagents such as polyurethane foam [16], polystyrene divinylbenzene [3], naphthalene [17,18], activated carbon and silica C18 [16]. However, the main disadvantage of these materials is the possibility of lixiviation of the chelating reagent during the extraction process. This possibility can reduce the lifetime of the sorbent.

Modified sorbents have been used extensively to increase the selectivity and the sensitivity of analytical procedures. An increase in the selectivity of the extraction is usually obtained by the modification of the surface of the solid support with functional groups. The selectivity of the modified solid-phase in relation to certain metallic ions is attributed to known factors, such as the size of the reagent used to modify the sorbent and the activity and the type of the inserted groups. However, the selective extraction of a trace element in the presence of other ions represents a challenge in finding an available sorbent capable of exhibiting a high enough affinity to selectively extract this metal. The combination of two sorbents may be a good alternative for some specific applications [19].

Preconcentration procedures are executed using off- or flow injection systems. Off-line preconcentration procedures are appropriate when higher preconcentration factors are needed. However, these procedures require a large quantity of both reagents and samples. When flow injection systems are considered, the principal advantage is the possibility of automation, thus increasing the precision and accuracy, while minimizing both the reagent/sample consumption and the production of chemical residues [20]. Additionally, flow injection systems are usually more robust than conventional separation methods, offering ease of operation. Several procedures based on flow injection systems using thiazolylazo and pyridylazo loaded sorbents have been described in the literature [21].

Polyurethane foam has been impregnated with PAR, and the resulting sorbent was used in flow injection preconcentration systems for cadmium [22], lead [23] and zinc [24]. The procedures were based on simple steps of sorption and elution. Some chemical and flow variables were optimized using a two-level factorial and Doehlert designs. In the sorption step, the ions were retained on the minicolumn at pH 8.0, in the form of complexes with PAR, and the residual solution was discarded. In the elution, a hydrochloric acid solution flowed through the minicolumn, liberating the metallic ions by decreasing the pH. Cadmium, lead or zinc ions present in the sample were transported through the HCl solution and were detected by Flame Atomic Absorption Spectrometry (FAAS). The signals were measured as peak area. This system was applied to the determination of cadmium and zinc concentrations in natural waters and lead concentrations in mineral water and saline effluents.

In another work described in the literature, Amberlite XAD-4 resin was impregnated with PAN, and the resulting material was applied in an flow injection preconcentration system. This system was used for the determination of cadmium [25,26] and lead [27] in seawater samples. The preconcentration step for cadmium and lead was accomplished in the field. After this step, the minicolumns were removed from the system and transported to the laboratory, where the elution stage was completed using an HCl solution. The metallic ions were measured by FAAS. The experimental procedure was optimized by using a univariate method in order to establish the best chemical and flow conditions. The sorbent mentioned above was also used for copper determination in seawater samples. Chemical and flow variables were optimized using a Plackett-Burman design for seven factors [28]. The problems associated with sample transport and storage were avoided by using these field flow preconcentration systems. Furthermore there is no need to adjust the pH of the seawater samples.

The PAN reagent was also used to modify octadecyl silica. The resulting sorbent was used as the packing material in a minicolumn inserted in an flow injection system for the determination of rare earth metals (Ce, Dy, La, Sm, and Y) and uranium. After the preconcentration step, a solution of nitric acid was used to remove the ions from the minicolumn, and the elements were detected by inductively coupled plasma-optical emission spectrometry (ICP-OES) [29]. The procedure was applied to the determination of these metals in natural waters.

A simple flow injection system using PAN-loaded TiO_2 was used in the separation and preconcentration of Cu, Co, Cr, Y, Yb and Bi [30]. The procedure was based on two simple steps of sorption and elution of the ions with hydrochloric acid and followed by direct detection by ICP-OES. The combination of the reagent PAN and the sorbent TiO_2 has resulted in a simple, sensitive and economical procedure. Some metal ions that could not be adsorbed on TiO_2, such as Co(II), were retained quantitatively on PAN–TiO_2. However, it was observed that some ions that could be adsorbed quantitatively on TiO_2, such as Mn(II), were not adsorbed quantitatively on the PAN-loaded sorbent. In general, the adsorption on the sorbent PAN–TiO_2 was 2.4 times higher than the absorption on unmodified TiO_2. The procedure was employed for the determination of metallic ions in a biological reference material.

The reagent 2-(5-bromo-2-pyridylazo)-5-diethylaminophenol (5-Br-PADAP) has been used as a colorimetric reagent in flow injection systems for the spectrophotometric determination of nickel [31]. A possible limitation of the system is the interference from Fe(III) and Cu(II). Both substances are known to form stable complexes with 5-Br-PADAP. Several masking substances were tested in order to increase the tolerance to these ions. The interference of Fe(III) was greatly decreased by the addition of sodium pyrophosphate. However, none of the substances tested were capable of reducing the interference from Cu(II). Then, a minicolumn packed with TAN immobilized on silica C18 was inserted in the flow injection system. It was observed that Cu(II) and Ni(II) are retained by the sorbent at pH values ranging from 4.0 to 6.5 and 5.0 to 7.0, respectively. No retention of Ni(II) occurred at pH values below 5.0. The pH of the solution was then adjusted to 4.5 in order to retain the Cu ions on the minicolumn while allowing the detection of Ni(II) free from any interference by Cu. This procedure was used for the determination of nickel in biological materials including rice flour, fish and apple leaves.

A minicolumn packed with 2-2-thiazolylazo-5-dimethylaminophenol (TAM)-loaded Amberlite XAD-2 resin was used in a flow injection system for the preconcentration and determination of trace cadmium [32]. This method has advantages such as a high sample throughput ($40\,h^{-1}$), a low detection limit ($1.2\,\mu g\,L^{-1}$), a high preconcentration factor (108) and ease of operation. Biological reference materials, lobster hepatopancreas and rice flour, were analyzed.

TAN reacts with copper and zinc, and the complexes formed can be preconcentrated and separated from the sample by employing a SEP PAK C18 cartridge [33]. Sequential determination of copper and zinc in copper-based alloys by ICP-OES employing a flow injection separation procedure was proposed. The flow injection system was based on the association of valves, allowing the determination of copper and zinc in dissolved brass samples by making use of flow injection spectrometric detectors. The method, based on the chemical separation of these two metals, overcomes the spectral interference of copper in the main emission line of zinc when atomic emission or absorption spectrometric techniques are applied [34].

Several flow injection systems are described in the literature, involving pyridylazo and thiazolylazo reagents in combination with many solid supports. These materials have resulted in powerful sorbents that are used in procedures for the preconcentration of metals. A summary of these procedures is given in Table 1.

In most these flow injection solid-phase extraction systems the loading of analytes in the column is usually made at slightly acidic to alkaline pH values. This is due to the fact that most of the pyridylazo and thiazolylazo reagents interact with metals at this pH range. The elution is carried out in most cases with acidic solutions, because the lowering of pH creates unfavorable conditions for the metal–ligand interaction, promoting a rapid desorption of analytes from the column. Dilute solutions of mineral acids such as hydrochloric and nitric acid are often used. Solutions of organic solvents such as acetone, ethanol and methanol in mineral acids are also used. However, it should be noted that the solvents may lixiviate quickly pyridylazo and thiazolylazo reagents loaded in solid supports, reducing the lifetime of the column. These eluent mixtures are more suitable for use with functionalized sorbents, in which the degree of leaching is much lower.

The solid supports more used for association with pyridylazo and thiazolylazo reagents in flow injection systems are the Amberlite XAD resin series and polyurethane foam. This preference is, probably, due to low cost, easy availability and high affinity of hydrophobic media to these reagents. Moreover, the favorable properties of the media for use in flow injection systems such as resistance to variations in pH and low degree of swelling, make them very popular media for this use [35–48].

3.2. Cloud point extraction

The process called cloud point extraction (CPE) is based on the separation of two isotropic phases generated from micellar systems. This phenomenon can be applied for the extraction and/or preconcentration of inorganic and organic species and biomolecules [49].

Surfactants have a fundamental importance in CPE processes. These substances have the capacity to alter the superficial and interfacial properties of a liquid. The most experimentally condition modified to reach the cloud point of a solution of surfactant is the temperature. The explanation of the cloud point phenomenon is still controversial [50]. According a model described in the literature, at low temperatures, each molecule of surfactant is surrounded by a layer of water molecules highly organized forming hydrogen bondings with the polar head groups and the ethylene oxide units of non-ionic surfactant [50,51]. When the temperature is increased, the increase of entropy cause dehydration of the chains of polyoxyethylene and destroys the cover of water molecules. Weak forces of attraction of van der Waals prevail between the molecules of surfactants that lead to the formation of micellar aggregates and, consequently, the separation of phases.

Table 1
Flow injection separation/preconcentration methods employing solid-phase extraction with pyridylazo and thiazolylazo reagents.

Reagent	Support	Metal	LD (ng L^{-1})	EF	Sample	Detection	Reference
TAM	Amberlite XAD-2	Cd	1.2	108	Biological reference materials	FAAS	[32]
TAN	Silica C18	Zn(II)	150.0	120.0	Soil	FAAS	[35]
		Cu(II)	–	–	Alloys	ICP-OES	[34]
		Zn(II)	–	–			
PAR	Polyurethane foam	Cd(II)	20.0	–	Mineral water	FAAS	[22]
	Polyurethane foam	Pb(II)	400.0	51.0	Mineral water and saline samples	FAAS	[23]
	Polyurethane foam	Zn(II)	280.0	–	Mineral water	FAAS	[24]
	Amberlite XAD-4	Cu(II)[a]	2800.0	7.4	Seawater	FAAS	[28]
		Cu(II)[b]	80.0	220.7			
		Cu(II)[c]	50.0	294.8			
PAN	Amberlite XAD-4	Cd(II)	3.8	1059.0	Seawater	FAAS	[25]
	Silica	Ce(III)	37.0	328.0	Water	ICP-OES	[29]
		Dy(IiI)	11.0	275.0			
		La(III)	14.0	337.0			
		Sm(III)	23.0	324.0			
		Y(III)	13.0	372.0			
		U(VI)	69.0	382.0			
	TiO_2	Cu(II)	2800.0	–	Biological reference materials	ICP-OES	[25]
		Co(II)	3500.0	–			
		Cr(II)	500.0	–			
		Y(III)	600.0	–			
		Yb(III)	12700.0	–			
		Bi(III)	17900.0	–			
	Amberlite XAD-4	Pb(II)	5.0	12048	Seawater	FAAS	[27]
BTAC	PUF	Cd(II)	270.0	41.0	Biological reference material	FAAS	[36]
		Pb(II)	1000.0	26.0	Wine		[37]
	Amberlite XAD-2	Pb(II)	1700.0	60.0	Biological reference materials	FAAS	[38]
		Ni(II)	1100.0	30.0	Food		[39]
TAC	PUF	Co(II)	3200.0	37.0	Water	FAAS	[40]
	PUF		2400.0	51.0			
	Amberlite XAD-2		130.0	87.0			[41]
5-Br-PADAP	Amberlite XAD-2	Co(II)	180.0	–	Bee honey	FAAS	[42]
TAR	Amberlite XAD-16	Cr(III)	20.0	50.0	Parenteral solutions	FAAS	[43]
		Cr(III) and Cr(VI)	20.0	250.0	Water		[44]
Me-BTANC	PUF	Cd(II)	800.0	37	Black tea, spinach leaves and water	FAAS	[45]
		Pb(II)	3750.0	37			
		Cu(II)	1200.0	–	Shrimp	SP	[46]
Me-BTABr	PUF	Zn(II)	370.0	23	Water	FAAS	[47]
Me-BDBD	PUF	Cu(II)	3400.0	7	Corn flour, rice flour and black tea	SP	[48]

a, b and c: sample volumes of 2.5, 75 and 100 mL, respectively; EF: enrichment factor; LD: detection limit; SP: spectrophotometry, FAAS: flame atomic absorption spectrometer.; ICP-OES: inductively coupled plasma-optical emission spectrometry; BTAC: 2-(2-benzothiazolylazo)-2-*p*-cresol, Me-BTANC: 2-(6′-methyl-2′-benzothiazolylazo)chromotropic acid, Me-BTABr: 2-[2-(6-methyl-benzothiazolylazo)]-4-bromophenol, Me-BDBD: 6-[2′-(6′-methyl-benzothiazolylazo)]-l,2-dihydroxy-3,5-benzenedisulfonic acid.

Some authors have been trying to promote CPE in flow injection systems. The first work using CPE combined with flow injection analysis (FIA) was published in 2001 [52]. Previously, some works that involved CPE, employed flow injection systems to facilitate the manipulation or transport of the rich phase to some detector [53]. The difficulties of the incorporation of CPE in flow injection systems have been resolved by using some procedures such as the employ of additives (salts, alkalis, acids, polymers, urea and other surfactants). The additive is used in order to induce the phase separation at the cloud point, avoiding problems with the difficulty of incorporating a temperature-control device in the system. Those additives can also affect the extraction efficiency and the preconcentration factor of the procedure [54].

The collection of the surfactant-rich phase after the phase separation in CPE batch procedures is usually accomplished by centrifugation. In flow injection procedures, the centrifuge is replaced by a column packed with an appropriate filtering material. The elution of the micelles from the column is carried out with an appropriate solvent, such as acetonitrile, water or acid solutions.

In an FIA system involving CPE, typically the filtering material should retain the surfactant aggregates, allowing the passage of minor components, such as salts, water, surfactant monomers and minor aggregates. Therefore, the selection of the filtering material is extremely important in these systems. Several filtering materials have been tested for use as the packing material in these columns, including cotton, glass wool, nylon fiber, cigarette filters and silica.

The main limitation of flow injection cloud point extractions of metallic ions is the low partition coefficient of many neutral species of chelates. This drawback can be solved by using highly hydrophobic ligands. As highly hydrophobic ligands, pyridylazo and thiazolylazo reagents are appropriate for use in flow injection CPE systems.

5-Br-PADAP was used as a complexing agent in the determination of vanadium in parenteral solutions. The non-ionic surfactant polyoxyethylene (5.0) nonylphenol (PONPE 5.0) was used in the formation of micellar aggregates. In this system, the cloud point extraction technique was used for batch preconcentration of vanadium. The surfactant-rich phase was introduced into a flow injection system with detection by ICP-OES. In this case, the flow injection system was just used to introduce the concentrated phase into the spectrometer [55]. The reagent 5-Br-PADAP was also used in a similar system for the determination of mercury by ICP-OES. The system was modified to allow for the use of a gas–liquid separator. The mercury from the CPE flowed towards the separator where

the metal was reduced, and the vapor was transported to the nebulizer of the spectrometer. A study of the parameters affecting the cloud point extraction and cold vapor mercury generation from the surfactant phase was performed. A 200-fold preconcentration factor has been obtained. The concentration of the metal in potable water samples was determined [56].

A flow injection preconcentration system associated with cloud point extraction and capillary electrophoresis for the determination of dysprosium and iron in urine samples was developed [57]. The sample was transported through a reagent coil, where it was mixed with a solution of 5-Br-PADAP and the surfactant polyethyleneglycol-mono-*p*-nonylphenylether (PONPE 7.5). The mixture was heated to 30 °C and was then transported through a minicolumn packed with cotton. The analytes were retained in this step. An acetonitrile solution was used for the elution. The rich phase was collected directly in an electrophoresis flask. The present work demonstrated the viability of coupling capillary electrophoresis and flow injection cloud point extraction and showed that such a coupling resulted in a sensitive method for the determination of Dy and Fe.

The application of pyridylazo and thiazolylazo reagents in flow injection cloud point extraction systems still has not been thoroughly explored; therefore the use of this extraction technique in FIA systems is a recent development [52]. The possibility of the association of CPE with flow injection systems represents a promising alternative in the field of automated separation methods, particularly, if excellent enrichment factors and extraction efficiencies are obtained. Therefore, the analytical characteristics and the applicability presented in the developed works are comparable or superior to procedures involving other preconcentration techniques. In this type of extraction system, additional experimental parameters should be tested, especially those related to the collection column, such as the chemical nature of the packing material, the dimensions of the column, the elution and preconcentration flow rates and the configuration of the flow injection system. Table 2 presents the characteristics of some flow injection cloud point extraction procedures involving pyridylazo and thiazolylazo reagents [55–59].

3.3. Precipitation

Precipitation can be used in preconcentration procedures that are characterized by the formation of insoluble substances. When direct precipitation is inadequate due to the low concentration of the analytes in solution, coprecipitation is an alternative [60]. The phenomenon of coprecipitation refers either to the adsorption of chemical species on the surface of a precipitate or their incorporation in the structure of an insoluble system [20]. Several substances can used as coprecipitating agents, such as the colloids $Ga(OH)_3$, $Hf(OH)_4$, $Zr(OH)_4$, or organic substances capable of generating neutral chelates, like diehyldithiocarbamate and hexamethylenedithiocarbamate.

After the generation of the insoluble compound, a dissolution step must be done through the addition of small amounts of an appropriate solution. This solution can contain a strong mineral acid or an organic solvent. The coprecipitation is usually employed more often in batch systems, which give a greater amount of precipitate for further manipulation. When flow injection procedures are used, direct precipitation is preferred due to the small amount of solid formed, which reduces the impedance in the system.

In flow injection systems, the precipitate can be collected in filters or reactors. Membrane filters or systems packed with cotton or polymeric beads are frequently used [3]. Some basic configurations of the reactors used in flow injection precipitation systems include the following:

(a) *Helicoidal reactors*: a tube with several circular sections of constant diameter.
(b) *Serpentine reactors*: a configuration with a figure-8 shape. These reactors can promote a secondary flow pattern by sharp turns in the flow direction.
(c) *Knotted reactors*: several knots, with the flow directions varying in a three-dimensional base.

Knotted reactors have been extensively used in flow injection preconcentration systems in order to retain metal complexes on their inner walls through sorption [61]. Besides collecting the precipitate, the reactor has other functions in the system. One of these functions is to make possible the fast mixture of sample solutions and reagents. The knotted reactor also minimizes the dispersion of the components after dissolution when the eluate is transported to detector. In addition to efficient mixing, these reactors also create a secondary flow due to the changes in the direction caused by the knots. Centrifugal forces are created in the flow, directing the particles to the walls of the tube and allowing the effective generation of the precipitate. However, the precipitate can be lost from the walls of the tube during the flow passage, causing a decrease in the sensitivity of the procedure. This limitation can be avoided by incorporating a small membrane filter on the system [20]. When compared to conventional microcolumns used in flow injection systems, knotted reactors reactor have the following advantages: unlimited life and ease of construction and the ability to use higher sample flow rates due to the low pressure generated by the reactor in the system [62].

Most of studies using flow injection precipitation involve detection by FAAS, ETAAS or ICP-OES [63]. The reagents most widely used as precipitating agents are diethyldithiocarbamate (DDTC) and pyrrolidine dithiocarbamate ammonium (APDC) [64,65]. Pyridylazo and thiazolylazo reagents are known to form insoluble chelates with many metal ions, and this characteristic makes them powerful reagents for use in flow injection precipitation systems. However, the potential of pyridylazo and thiazolylazo reagents for use in these systems only began to be exploited in 2000 [66].

The pyridylazo reagent most frequently used in flow injection precipitation systems is 5-Br-PADAP. This reagent was used as a

Table 2
Flow injection preconcentration methods employing cloud point extraction with pyridylazo and thiazolylazo reagents.

Reagent	Surfactant	Metal	Sample	LD (ng L^{-1})	EF	Detection	Reference
Br-PADAP	PONPE 5.0	V	Parenteral solutions	16.0	250.0	ICP-OES	[55]
		Hg	Water	4.0	200.0	CV-ICP-OES	[56]
	PONPE 7.5	Fe	Urine	200.0	2200.0	CE	[57]
		Dy		480.0			
		Gd		40.0	20.0	ICP-OES	[58]
Br-TAO	Triton X-114	Mn	Food	500.0	14.0	FAAS	[59]

ICP-OES: inductively coupled plasma-optical emission spectrometry; CV-ICP-OES: cold vapor inductively coupled plasma-optical emission spectrometry; CE: capillary electrophoresis, LD: detection limit, EF: enrichment factor. Br-TAO: 4-(5ĭ-bromo-2ĭ-thiazolylazo)orcinol.

Table 3
Flow injection preconcentration methods employing precipitation with pyridylazo and thiazolylazo reagents..

Reagent	Metal	EF	F (h^{-1})	LD (ng L^{-1})	Sample	Detection	Reference
Br-PADAP	Zn	42.00	22	90.00	River water	ICP-OES	[66]
	Cd	216.0	40	5.00	Wine	ICP-OES	[68]
	Cd	140.0	–	–	Honey	ICP-OES	[69]
	Sc	1120	11	0.45	River water	ICP-OES	[67]
	V	180.0	22	19.00	Mineral water	ICP-OES	[63]
	Hg	25.00	–	5.00	Mineral water	CV-AAS	[72]
PAN	Cd	18.00	48	100.00	Drink water	FAAS	[70]
	Pb	26.00	48	430.00	Drink water	FAAS	[71]
TAC	Cd	23.00	25	40.00	Water	FAAS	[73]

CV-AAS: cold vapor atomic absorption spectrometry, EF: enrichment factor, F: sampling frequency, LD: detection limit.

precipitating agent in flow injection systems with a knotted reactor for the determination of zinc [66] and scandium [67] in the river water, vanadium in mineral water [63] and cadmium in wine [68] and honey [69]. The detection in all systems was performed by ICP-OES. In these systems, important parameters were studied, such as the sample pH, the concentration of 5-Br-PADAP, the reagent flow rate, the length of the reactor, and the type and concentration of eluent. The length of the reactor systems was 200 cm, and the eluent used was a 30% (v/v) nitric acid solution.

A flow injection system was developed for the determination of cadmium in drinking water using a knotted reactor and PAN as a precipitating agent [70]. The preconcentration system was based on the precipitation of the complex Cd-PAN, with sorption on the walls of the reactor, and later elution with a hydrochloric acid solution. The optimization of some of the variables involved in the system was performed in two steps using a factorial design for preliminary evaluation. A Box-Behnken design was employed for the determination of the critical experimental conditions. After application of the design, the optimized conditions of the method were as follows: the length of the knotted reactor, 150 cm; sample flow rate, 5.0 mL min^{-1}; sample pH, 8.3; buffer solution concentration 0.011 mol L^{-1}; PAN solution concentration, 3.0×10^{-5} mol L^{-1}.

PAN was also used as the precipitating agent in another fully automated flow injection preconcentration system for the determination of lead in drinking water [71]. After optimization of the variables using a Box-Behnken design, the optimum values found were: sample pH, 8.8; buffer solution concentration, 0.024 mol L^{-1}; sample flow rate, 9.27 mL min^{-1}.

A flow injection preconcentration procedure for cadmium determination was based on the precipitation of cadmium(II) ions in a knotted reactor (KR) using 1-(2-thiazolylazo)-*p*-cresol (TAC) as the complexing reagent [72]. The system was used for cadmium determination in drinking water samples. A detection limit of 40.0 ng L^{-1} and a preconcentration factor of 23 for a sample volume of 10 mL were obtained.

Table 3 shows a summary of the procedures using pyridylazo and thiazolylazo reagents in flow injection precipitation systems [66–73,63].

4. Measurements on solid support and sensors

The solid-phase spectrometry (SPS) is a technique that permits direct measurements on a solid support [74,75]. In this technique, a solid matrix is employed for the preconcentration of the species of interest, and the absorbance is measured directly on the solid support. Typically two strategies have been employed: (a) a chromogenic reagent is first adsorbed on the solid-phase and when the sample solution is placed in contact with the solid-phase, the analytes are removed from the solution, forming a product with the immobilized reagent [76,77]; (b) a reaction between the analyte and the chromogenic reagent occurs first and this preformed compound is sorbed onto the surface of the solid support [78,79]. SPS offers a simple and easy way to automate the process, provides low detection limits and uses only small amounts of samples and reagents. A specific requirement for these sorbents is transparency for absorbance measurements [80].

The sorbed species can be eluted after each determination or after a number of determinations. The second option increases the number of measurements per hour, but it is applicable only if the response is linear with respect to a wide range of concentrations.

Opaque materials are used only in reflectance applications due to the excessive attenuation of the light intensity. Even when using non-opaque materials, light attenuation and scattering are inevitable. Adjustments in spectrophotometers in order to adapt them for absorbance measurements are frequently demanded. The construction and adaptation of a simple flow cell for measurements using solid-phase spectrophotometry has been described in the literature [81]. This type of cell allows for the use of large quantities of material without causing an excessive increase in hydrodynamic impedance or in scattering of radiation. The reaction of cobalt(II) with TAN retained on functionalized silica C18 was used to demonstrate the features of the flow cell [81]. This solid support was also used for the determination of zinc in pharmaceutical preparations [80], the simultaneous determination of nickel and zinc in alloys [82] and the simultaneous determination of iron, nickel and zinc in water [83], using flow injection solid-phase spectrophotometry.

The reagent 5-Br-PADAP was used for the determination of cobalt in water samples. The complex formed between the metal and ligand was concentrated in the ion exchange resin AG 50W-X2 contained in a flow cell. The increase in absorbance caused by the accumulation of the complex in the resin was continuously measured [84].

Another possibility for associating direct measurement on solid supports and flow injection systems is the use of sensors. Chemical sensors combine the advantages offered by optical fibers with chemical systems of transduction. The phase sensor (chemical transducer) consists of a sensitive and selective immobilized reagent that generates the optical signal. This signal is related to the concentration of the analyte.

The immobilization of a reagent can be done in two ways: physically, by adsorption, occlusion or electrostatic attraction, or chemically, by covalent bonding. The quantification of metals is based on the monitoring of the change in the color or another optical property of the complexing reagent that interacts with the metal ions [85–87].

Several solid supports can be used as the basis for the immobilization of the reagent PAN for use as chemical sensors. PAN has been incorporated into membranes of the ion exchange polymer Nafion to form an optical chemical sensor, showing good results for the determination of Ni and Cu in aqueous solutions [85]. The reagent has been immobilized in a membrane of polyvinyl chloride (PVC) incorporated into a cellulose support in a flow cell. This

Table 4
Flow injection preconcentration methods employing sensors and pyridylazo reagents.

Reagent	Support	Metal	LD ($mg\,L^{-1}$)	Sample	Reference
PAR	Amberlite XAD-7	Co(II)	0.02	Aqueous samples	[91]
DPAN	Nafion	Cu(II)	–	Aluminium bronze, bronze and tap water	[92]
		Zn(II)	10.0	Pharmaceuticals	[93]
PAN	PVC	Mn(II)	0.18	Water, steel, lemon and leaves	[94]
		Cu(II)	–	Water	[95]

DPAN: 4-decyloxy-2-(2-pyridylazo)-1-naphthol.

cell was used in the flow injection photometric determination of manganese and cadmium [86,87].

The reagent PAR was incorporated into a sol–gel, and the resulting material was used as a flow injection optical sensor system for spectrophotometric determination of Cu(II) in urine and Zn(II) in insulin injections. The PAR immobilized in the support formed a red complex with Cu(II). This complex had a maximum absorbance at 500 nm, and was also used in the determination of Zn [88,89]. The same reagent was immobilized in a membrane of chitosan as a transducer. The resulting material was used in the development of an optical sensor in a cell flow for determination of Co(II). The sensor can be regenerated using a solution of HCl saturated with KCl [90]. Table 4 presents the characteristics of some flow injection procedures with sensors and pyridylazo reagents [91–95].

5. Conclusion

The ease of coupling of pyridylazo and thiazolylazo reagents to solid supports has made them very attractive for use in flow injection systems involving solid-phase extraction. This combination has been enabled the development of interesting methods for the determination of metals. Several studies describing the use of these systems in the determination of metals in different substances such as food, biological fluids, fuels and medicines are found in the literature. The detection of metals is generally performed using techniques such as spectrophotometry, FAAS, GFAAS and ICP.

The low solubility of pyridylazo and thiazolylazo reagents and their metallic complexes in water has also allowed the development of methods involving flow injection precipitation for the determination of metals, and recently these reagents have been used in cloud point extraction systems. The need for hydrophobic substances in some of these systems makes the use of pyridylazo and thiazolylazo reagents quite appropriate. The combination of cloud point extraction and flow injection systems was first described very recently. Some very common reagents, such as Br-PADAP and TAN were used in flow injection CPE systems for the determination of metals, resulting in very sensitive methodologies. However, the potential of this combination has not yet been fully exploited. This fact is evidenced by the limited number of publications on the subject. The same considerations are made for the use of pyridylazo and thiazolylazo reagents in flow injection CPE systems.

The use of these reagents can still be exploited in several types of flow injection systems for the determination, the separation or the preconcentration of metals. These systems can be based on the ability of pyridylazo and thiazolylazo reagents to form complexes with a large number of metal cations. This property is quite interesting in systems with multi-element detection, such as ICP-OES, ICP-MS, and some applications for sequential measurements by FAAS.

Acknowledgments

The authors would like to acknowledge the financial support received from Conselho Nacional de Desenvolvimento Científico e Tecnológico (CNPq) and Fundação de Amparo à Pesquisa do Estado da Bahia (FAPESB).

References

[1] C.E.S. Miranda, E. Carrilho, A.P. Gervasio, M.F. Giné, Quim. Nova 25 (2002) 412.
[2] M. Valcárcel, M.D.L. Castro, Non-Chromatographic Continuous Separation Techniques, Royal Society of Chemistry, Cambridge, 1991, 290 p.
[3] Z. Fang, Flow Injection Separation and Preconcentration, John Wiley, Weinheim, 1993, 259 p.
[4] L.S.G. Teixeira, A.C.S. Costa, S.L.C. Ferreira, M.S. Carvalho, M.L. Freitas, J. Braz. Chem. Soc. 10 (1999) 519.
[5] A.C.S. Costa, L.S.G. Teixeira, H.V. Jaeger, S.L.C. Ferreira, Mikrochim. Acta 130 (1998) 41.
[6] L.S.G. Teixeira, A.C.S. Costa, A.S. Queiroz, A.M.M. Amorim, O.N. Bomfim, S.L.C. Ferreira, Mikrochim. Acta 129 (1998) 103.
[7] S. Shibata, Anal. Chim. Acta 25 (1961) 348.
[8] L.S.G. Teixeira, A.C.S. Costa, J.C.R. Assis, S.L.C. Ferreira, M. Korn, Mikrochim. Acta 137 (2001) 29.
[9] T. Ying, Z.J. Li, Z. Juan, J.M. Pan, Rev. Anal. Chem. 24 (2005) 103.
[10] V.M. Ivanov, J. Anal. Chem. 60 (2005) 486.
[11] A.D. Towns, Dyes Pigments 42 (1999) 3.
[12] S. Oszwałdowski, M. Jarosz, Chem. Anal. (Warsaw) 42 (1997) 739.
[13] H.R. Hovind, Analyst 100 (1975) 769.
[14] R.G. Anderson, G. Nickless, Analyst 92 (1967) 207.
[15] V.A. Lemos, L.S.G. Teixeira, M.A. Bezerra, A.C.S. Costa, J.T. Castro, L.A.M. Cardoso, D.S. de Jesus, E.S. Santos, P.X. Baliza, L.N. Santos, Appl. Spectrosc. Rev. 43 (2008) 303.
[16] V. Camel, Spectrochim. Acta B 58 (2003) 1177.
[17] A.P. Anjos, L. Cornejo-Ponce, S. Cadore, N. Baccan, Talanta 71 (2007) 1252.
[18] A. Bhalotra, B.K. Puri, Anal. Sci. 5 (2000) 507.
[19] C. Gueguen, J. Dominck, D. Perret, Fresenius J. Anal. Chem. 370 (2001) 909.
[20] M.G. Pereira, M.A.Z. Arruda, Microchim. Acta 141 (2003) 115.
[21] V.A. Lemos, E.S. Santos, M.S. Santos, R.T. Yamaki, Microchim. Acta 158 (2007) 189.
[22] W.N.L. dos Santos, J.L.O. Costa, R.G.O. Araujo, D.S. Jesus, A.C.S. Costa, J. Hazard. Mater. 137 (2006) 1357.
[23] W.N.L. dos Santos, C.M.M. Santos, J.L.O. Costa, H.M.C. Andrade, S.L.C. Ferreira, Microchem. J. 77 (2004) 123.
[24] W.N.L. dos Santos, C.M.M. Santos, S.L.C. Ferreira, Microchem. J. 75 (2003) 211.
[25] M.C. Yebra, A. Garcia, N. Carro, A. Moreno-Cid, L. Puig, Talanta 56 (2002) 777.
[26] M.C. Yebra, J. Salgado, L. Puig, A. Moreno-Cid, Anal. Bioanal. Chem. 370 (2002) 530.
[27] M.C. Yebra, L. Rodriguez, L. Puig, A. Moreno-Cid, Microchim. Acta 140 (2002) 219.
[28] M.C. Yebra, N. Carro, A. Moreno-Cid, Spectrochim. Acta B 57 (2002) 85.
[29] N. Bahramifar, Y. Yamini, Anal. Chim. Acta 540 (2005) 325.
[30] L. Yang, B. Hu, Z. Jiang, H. Pan, Microchim. Acta 144 (2004) 227.
[31] S. Vicente, N. Maniasso, Z.F. Queiroz, E.A.G. Zagatto, Talanta 57 (2002) 475.
[32] M.H.A. Melo, S.L.C. Ferreira, R.E. Santelli, Microchem. J 65 (2000) 59.
[33] L.S.G. Teixeira, J.O.N. Reis, A.C.S. Costa, S.L.C. Ferreira, M.G.A. Korn, J.B. de Andrade, Talanta 46 (1998) 1279.
[34] M. Korn, A.F. Santos Jr., L.S.G. Teixeira, M.G.A. Korn, S.L.C. Ferreira, A.C.S. Costa, J.B. de Andrade, Am. Lab. News 31 (1999) 148.
[35] C.R. Preetha, V.M. Biju, T.P. Rao, Atom. Spectrosc. 24 (2003) 118.
[36] V.A. Lemos, R.E. Santelli, M.S. Carvalho, S.L.C. Ferreira, Spectrochim. Acta B 55 (2000) 1497.
[37] V.A. Lemos, M. de la Guardia, S.L.C. Ferreira, Talanta 58 (2002) 475.
[38] V.A. Lemos, J.S. Santos, L.S. Nunes, Sep. Sci. Technol. 40 (2005) 1401.
[39] W.N.L. dos Santos, S.L.C. Ferreira, V.A. Lemos, Anal. Chim. Acta 445 (2001) 145.
[40] R.J. Cassella, V.A. Salim, L.S. Jesuíno, R.E. Santelli, S.L.C. Ferreira, M.S. Carvalho, Talanta 54 (2001) 61.
[41] V.A. Lemos, C.F. Brito, A.C. Ferreira, M.G.A. Korn, Can. J. Anal. Sci. Spectros. 47 (2002) 49.
[42] S. Cerutti, R.F. Orsi, M. Kaplan, J.A. Gásquez, R.A. Olsina, L.D. Martinez, Instrum. Sci. Technol. 32 (2004) 401.
[43] G.M. Wuilloud, R.G. Wuilloud, J.C.A. Wuilloud, R.A. Olsina, L.D. Martinez, J. Pharmaceut. Biomed. 31 (2003) 117.
[44] R.G. Wuilloud, G.M. Wuilloud, J.C.A. Wuilloud, R.A. Olsina, L.D. Martinez, Atom. Spectrosc. 23 (2002) 44.
[45] E.M. Gama, A.S. Lima, V.A. Lemos, J. Hazard. Mater. 136 (2006) 757.
[46] V.A. Lemos, A.A. Jesus, E.M. Gama, G.T. David, R.T. Yamaki, Anal. Lett. 38 (2005) 683.
[47] V.A. Lemos, W.N.L. dos Santos, J.S. Santos, M.B. Carvalho, Anal. Chim. Acta 481 (2003) 283.
[48] V.A. Lemos, D.R. Vieira, C.G. Novaes, M.S. Santos, R.T. Yamaki, Microchim. Acta 153 (2006) 193.
[49] M.F. Silva, E.S. Cerutti, L.D. Martinez, Microchim. Acta 155 (2006) 349.
[50] L. Qiao, A.J. Easteal, Colloid Polym. Sci. 276 (1998) 313.
[51] R. Kjellander, J. Chem. Soc., Faraday Trans. 278 (1982) 2025.

[52] Q. Fang, M. Du, C.W. Huie, Anal. Chem. 73 (2001) 3502.
[53] M.E.F. Laespada, J.L.P. Pavón, B.M. Cordero, Analyst 118 (1993) 209.
[54] A.M. Al-Ghamdi, H.A. Nasr-El-Din, Colloids Surf. A 125 (1997) 5.
[55] M. Gustavo, J.C.A. Wuilloud, R.G. Wuilloud, M.F. Silva, R.A. Olsina, L.D. Martinez, Talanta 58 (2002) 619.
[56] J.C.A. Wuilloud, R.G. Wuilloud, M.F. Silva, R.A. Olsina, L.D. Martinez, Spectrochim. Acta B 57 (2002) 365.
[57] C. Ortega, S. Cerutti, R.A. Olsina, L.D. Martinez, M.F. Silva, J. Pharm. Biom. Anal. 36 (2004) 721.
[58] C. Ortega, M.R. Gomez, R.A. Olsina, M.F. Silva, L.D. Martinez, J. Anal. At. Spectrom. 17 (2002) 530.
[59] V.A. Lemos, P.X. Baliza, A.L. Carvalho, R.V. Oliveira, L.S.G. Teixeira, M.A. Bezerra, Talanta 77 (2008) 388.
[60] M.S. Bispo, E.S. Boa Morte, M.G.A. Korn, L.S.G. Teixeira, M. Korn, A.C.S. Costa, Spectrochim. Acta B 60 (2005) 653.
[61] S. Liawruangrath, W. Som-Aum, A. Townshend, Talanta 58 (2002) 1177.
[62] Z. Fang, S.K. Xu, L.P. Dong, W.Q. Li, Talanta 41 (1994) 2165.
[63] R.G. Wuilloud, J.A. Salonia, R.A. Olsina, L.D. Martinez, Spectrochim. Acta B 55 (2000) 671.
[64] P. Galli, N. Oddo, Microchem. J. 46 (1992) 327.
[65] S. Nielsen, E. Hansen, Anal. Chim. Acta 366 (1998) 163.
[66] J.A. Salonia, R.G. Wuilloud, J.A. Gásquez, R.A. Olsina, L.D. Martinez, Fresenius J. Anal. Chem. 367 (2000) 653.
[67] S. Cerutti, J.A. Salonia, J.A. Gásquez, R.A. Olsina, L.D. Martinez, J. Anal. At. Spectrom. 18 (2003) 1198.
[68] R.F. Lara, R.G. Wuilloud, J.A. Salonia, R.A. Olsina, L.D. Martinez, Fresenius J. Anal. Chem. 371 (2001) 989.
[69] R.F. Orsi, R.G. Wuilloud, J.C.A. Wuilloud, R.A. Olsina, L.D. Martinez, J. AOAC. Int. 85 (2002) 1410.
[70] A.S. Souza, W.N.L. dos Santos, S.L.C. Ferreira, Spectrochim. Acta B 60 (2005) 737.
[71] A.S. Souza, G.C. Brandão, W.N.L. dos Santos, V.A. Lemos, E.M. Ganzarolli, R.E. Bruns, S.L.C. Ferreira, J. Hazard. Mater. 141 (2007) 540.
[72] J.C.A. Wuilloud, R.G. Wuilloud, J.A. Gasquez, R.A. Olsina, L.D. Martinez, Atom. Spectrosc. 22 (2001) 398.
[73] S. Cerutti, S.L.C. Ferreira, J.A. Gásquez, R.A. Olsina, L.D. Martinez, J. Hazard. Mater. 112 (2004) 279.
[74] R.J. Cassella, L.S.G. Teixeira, S. Garrigues, A.C.S. Costa, R.E. Santelli, M. de la Guardia, Analyst 10 (2000) 1835.
[75] F.R.P. Rocha, L.S.G. Teixeira, Quím. Nova 27 (2004) 807.
[76] L.S.G. Teixeira, F.R.P. Rocha, Talanta 71 (2007) 1507.
[77] F.S. Oliveira, L.S.G. Teixeira, M. Korn, Lab. Rob. Automat. 12 (2000) 305.
[78] J.G. Portela, A.C.S. Costa, L.S.G. Teixeira, J. Pharm. Biomed. Anal. 34 (2004) 543.
[79] L.S.G. Teixeira, E.S. Leão, A.F. Dantas, H.L.C. Pinheiro, A.C.S. Costa, J.B. Andrade, Talanta 64 (2004) 711.
[80] L.S.G. Teixeira, F.R.P. Rocha, M. Korn, B.F. Reis, S.L.C. Ferreira, A.C.S. Costa, Anal. Chim. Acta 383 (1999) 309.
[81] B.F. Reis, F.R.P. Rocha, L.S.G. Teixeira, A.C.S. Costa, M. Korn, Quim. Nova 23 (2000) 116.
[82] L.S.G. Teixeira, F.R.P. Rocha, M. Korn, B.F. Reis, S.L.C. Ferreira, A.C.S. Costa, Talanta 51 (2000) 1027.
[83] L.S.G. Teixeira, A.C.S. Costa, S. Garrigues, M. de la Guardia, J. Braz. Chem. Soc. 13 (2002) 54.
[84] S. Matsuoka, N. Shiota, K. Yoshimura, Anal. Sci. 22 (2006) 177.
[85] J.E. Madden, T.J. Cardwell, R.W. Cattrall, L.W. Deady, Anal. Chim. Acta 319 (1996) 129.
[86] C. Sanchez-Pedreño, M.S. García, J.A. Ortuño, M.I. Albero, E. Ballester, Fresenius J. Anal. Chem. 369 (2001) 680.
[87] M.I. Albero, J.A. Ortuño, M.S. García, C. Sánchez-Pedreño, R. Expósito, Talanta 56 (2002) 481.
[88] P.C.A. Jerónimo, A.N. Araújo, M.C.B.S.M. Montenegro, C. Pasquini, I.M. Raimundo Jr., Anal. Bioanal. Chem. 380 (2004) 108.
[89] P.C.A. Jeronimo, A.N. Araujo, M. Conceicão, B.S.M. Montenegro, Sens. Actuators B: Chem. 103 (2004) 169.
[90] N.A. Yusof, M. Ahmad, Sens. Actuators B: Chem. 86 (2002) 127.
[91] N.A. Yusof, M. Ahmad, Spectrochim. Acta A 69 (2008) 413.
[92] T.J. Sands, T.J. Cardwell, R.W. Cattrall, J.R. Farrell, P.J. Iles, S.D. Kolev, Sens. Actuators B: Chem. 85 (2002) 33.
[93] M.I. Albero, J.A. Ortuño, M.S. García, C. Sánchez-Pedreño, R. Expósito, J. Pharm. Biomed. Anal. 29 (2002) 779.
[94] M.I. Albero, J.A. Ortuño, M.S. García, C. Sánchez-Pedreño, R. Expósito, Fresenius J. Anal. Chem. 369 (2001) 680.
[95] C. Sánchez-Pedreño, J.A. Ortuño, M.I. Albero, M.S. García, J.C. Garcia de las Bayonas, Fresenius J. Anal. Chem. 366 (2000) 811.

Contents lists available at ScienceDirect

Talanta

journal homepage: www.elsevier.com/locate/talanta

Editorial

Updated aims and scope

Talanta recently celebrated fifty years of service to the analytical sciences community [Talanta 74 (4) (2008) 141]. Manuscript submission has grown substantially over the years, which has necessitated close adherence to our Aims and Scope – see our 1998 Editorial [Talanta 47 (1998) 1].

With even more growth in the past decade, along with the maturing of certain methodologies, we have recently updated our aims and scope to better reflect today's analytical sciences. Authors and reviewers are encouraged to read these guidelines, which will help assure continued quality publications that are of benefit to our readers. Papers are evaluated based on established guidelines, including the fundamental nature of the study, scientific novelty, substantial improvement or advantage over existing technology or methods, and demonstrated analytical applicability. Our aims and scope provides details of instructions for improving the quality and impact of a paper, as well as the types of papers that may be judged routine or less novel. In order to maintain the high quality of the journal, we strive to publish the most significant studies, which means that many scientifically sound investigations may not be accepted for publication. The good submissions of authors, and the conscientious evaluations by our dedicated reviewers, continue to establish *Talanta* as a leading analytical sciences journal.

Editors-in-Chief
Gary D. Christian*
Jean-Michel Kauffmann

Associate Editors
José Luis Burguera
Jianhua Wang
University of Washington, Chemistry, Box 351700, Seattle, WA 98195-1700, United States

* Corresponding author.
E-mail address: christian@chem.washington.edu (G.D. Christian)

0039-9140/$ – see front matter
doi:10.1016/j.talanta.2009.03.041

Talanta 79 (2009) 77–85

Contents lists available at ScienceDirect

Talanta

journal homepage: www.elsevier.com/locate/talanta

A new statistical method for the automated detection of peaks in UV-DAD chromatograms of a sample mixture

Benjamin Debrus[a,*], Pierre Lebrun[a], Attilio Ceccato[b], Gabriel Caliaro[c], Bernadette Govaerts[d], Bernard A. Olsen[e], Eric Rozet[a,1], Bruno Boulanger[f], Philippe Hubert[a]

[a] Laboratory of Analytical Chemistry, CIRM, Department of Pharmacy, University of Liège, Avenue de l'Hôpital 1, B36, B-4000 Liège, Belgium
[b] Mithra Pharmaceuticals, Rue Saint-Georges 5, B-4000 Liège, Belgium
[c] Orailac Quality Solutions, Brussels, Belgium
[d] Institute of statistics, Catholic University of Louvain, UCL, Voie du roman pays 20, B-1348 Louvain-la-Neuve, Belgium
[e] Analytical Sciences R&D, Eli Lilly and Company, Lilly Technology Center, South, DC 4816, Indianapolis, IN 46285, United States
[f] UCB Pharma SA, R&D Clinical Pharmacometrics, Allée de la Recherche 60, B-1070 Brussels, Belgium

ARTICLE INFO

Article history:
Received 16 October 2008
Received in revised form 27 February 2009
Accepted 4 March 2009
Available online 14 March 2009

Keywords:
Independent components analysis
High-order statistics
Peak detection
High-performance liquid chromatography
UV-diode array detector

ABSTRACT

One of the major issues within the context of the fully automated development of chromatographic methods consists of the automated detection and identification of peaks coming from complex samples such as multi-component pharmaceutical formulations or stability studies of these formulations. The same problem can also occur with plant materials or biological matrices. This step is thus critical and time-consuming, especially when a Design of Experiments (DOE) approach is used to generate chromatograms. The use of DOE will often maximize the changes of the analytical conditions in order to explore an experimental domain. Unfortunately, this generally provides very different and "unpredictable" chromatograms which can be difficult to interpret, thus complicating peak detection and peak tracking (i.e. matching peaks among all the chromatograms). In this context, Independent Components Analysis (ICA), a new statistically based signal processing methods was investigated to solve this problem. The ICA principle assumes that the observed signal is the resultant of several phenomena (known as sources) and that all these sources are statistically independent. Under those assumptions, ICA is able to recover the sources which will have a high probability of representing the constitutive components of a chromatogram. In the present study, ICA was successfully applied for the first time to HPLC–UV-DAD chromatograms and it was shown that ICA allows differentiation of noise and artifact components from those of interest by applying clustering methods based on high-order statistics computed on these components. Furthermore, on the basis of the described numerical strategy, it was also possible to reconstruct a cleaned chromatogram with minimum influence of noise and baseline artifacts. This can present a significant advance towards the objective of providing helpful tools for the automated development of liquid chromatography (LC) methods. It seems that analytical investigations could be shortened when using this type of methodologies.

1. Introduction

In many frameworks such as the automated development and optimization of analytical methods, the use of Design of Experiments (DOE) is of great interest to generate data over a broad experimental space. This requires the choice of a well-structured set of experiments to allow the modeling of the studied responses. However, analytical conditions of a liquid chromatography (LC) method must be varied significantly in order to cover an experimental space as large as possible. This can lead to very different chromatograms and peak tracking from one chromatogram to another is often problematic. Peak detection in the case of overlapping peaks can also present a problem. Even if this step can be done manually by an experienced analyst, there is a possibility of error in peak assignment. The automation of this process is therefore one of the first problems to solve to achieve the fully automated development of LC methods.

In the literature, different approaches to peak deconvolution and tracking have been described. A mathematical treatment like deconvolution (one-dimensional or less frequently multidimensional) is a widely used technique to accurately estimate the overlapping of peaks. It only needs the number of peaks and

* Corresponding author. Tel.: +32 4366 4324; fax: +32 4366 4317.
E-mail address: b.debrus@ulg.ac.be (B. Debrus).
[1] Chargé de Recherches F.R.S.-FNRS, Belgium.

0039-9140/$ – see front matter © 2009 Elsevier B.V. All rights reserved.
doi:10.1016/j.talanta.2009.03.009

some information about the peak shapes as basic input parameters in the computer assisted peak deconvolution procedure [1–3]. However, the knowledge of overlapped peak shapes is sometimes difficult to determine, and poor results can sometimes be obtained [4–6]. Methods such as alternating least-square multivariate curve-resolution [7,8], mutual automated peak matching [9] or factor analysis [10] have been recently developed and seem to be very efficient in the multidimensional numerical separation domain applied to HPLC–diode array detection (DAD) data. However, examples with real data demonstrate that some work is still necessary to achieve better automated detection and tracking of peaks [9–10].

Independent Component Analysis (ICA) is an interesting alternative that may be used to achieve peak detection and tracking. ICA is used in many domains due to its ability to separate successfully many types of signals [11]. In this context, ICA is a blind source separation method. The term *blind* indicates that both the source signals, and the way they are mixed, are unknown. This processing method has been successfully applied to the analysis of mixed sounds, satellite signals, to biomedical signal processing problems such as electroencephalographic (EEG) data [12,13], and used in order to eliminate artifacts from EEG data [14] or functional magnetic resonance imaging data [15]. Recent papers have shown that ICA has been applied in the field of chromatography for metabolite peak detection [16] or to resolve overlapping signals from gas chromatographic–mass spectrometry [17,18] or 3D-fluorescence spectroscopy [19] and for the signal analysis in proteomic and metabolomic investigations [20,21]. Independent components (sources) can be obtained by applying this statistical method which maximizes the statistical independence of the estimated sources. To measure the independence between the sources, the calculation of non-Gaussianity can be used, as explained by Hyvärinen and Oja [22]. Another popular criterion for measuring statistical independence of signals can be mutual information between sources. Typical algorithms for ICA use preprocessing steps in order to simplify and reduce the complexity of the problem. Data centering, whitening (i.e. signals decorrelation, accomplishable by using a classical principal component analysis method) and dimensionality reduction are generally used. ICA can be carried out by various algorithms which include JADE [23] (joint approximate diagonalization of eigenmatrices), FastICA [24] and OGWE [25] (optimized generalized weighted estimator). It is important to know that being based on different independence criteria, each algorithm may lead to slightly different results.

In fact, every multidimensional recorded signal which can be considered as a combination of primary independent signals (sources) can be treated by ICA, which tries to extract these independent sources and thus estimates the linear combination, i.e. a mixing matrix, which leads to the observed multidimensional signal. Consequently, recorded signals in LC can be regarded as the sum of independent signals that constitute a DAD-chromatogram (i.e. peaks, noise, baseline drift ...). The use of UV-DAD detection and thus the acquisition of multiwavelength data fulfill the requirements to consider ICA numerical separation of such chromatograms. It is thus very interesting to be able to separate peaks from noise or drift, and co-eluted peaks can be numerically separated for further processing. To carry out the numerical treatment in an automated way, it is advisable to find a methodology which allows the use of ICA in a generic manner, i.e., to find the number of components/sources that ICA will try to make independent. In this paper, our objective is thus to investigate the possibility to perform automatically the pretreatment of data, independent component analysis, classification of independent components, peak detection, extraction of UV spectra for each component, and reconstruction of cleaned DAD-chromatograms.

2. Methodology

2.1. Independent component analysis

Different definitions can be given for ICA. The most classical is referred to as noise-free or noiseless ICA [22,24,26] whose simplified summary of its application on UV-DAD chromatograms is given below. In UV-DAD chromatography, the recorded data are matrices, **X**, whose dimensions are $T \times J$, where T is the analysis time divided by the acquisition frequency and J is the number of wavelengths. Therefore each matrix can be expressed as a random vector, $\mathbf{x} = (\mathbf{x}_1, \ldots, \mathbf{x}_j, \ldots, \mathbf{x}_J)'$ where $\mathbf{x}_j = \mathbf{x}_j(t)$ represents the absorbance values at wavelength j as a function of the time t. Then ICA is carried out on **x** and consists of estimating the following generative model:

$$\boldsymbol{x} = \boldsymbol{As} \tag{1}$$

where **A** is a constant $(J \times n)$ mixing matrix, with n the number of sources to be computed and **s** is the sources random vector $\mathbf{s} = (\mathbf{s}_1, \ldots, \mathbf{s}_n)'$. Both **A** and **s** must be estimated and n must be chosen. To solve this problem, an unmixing matrix, **W**, is introduced and the ICA algorithm estimates it such that the elements of the vector **s** are as statistically independent as possible.

$$\boldsymbol{s} = \boldsymbol{Wx} \tag{2}$$

An important step consists in normalizing sources to avoid infinity of solutions, when estimating **W**. The ith component, $\mathbf{c}_i$, whose dimensions are $T \times J$, is then defined as the product between the ith row, $\mathbf{a}_i$, of the estimated mixing matrix **A** and the ith element of the estimated vector of sources $\mathbf{s}{:}\mathbf{c}_i = \mathbf{s}_i\mathbf{a}_i$. The sum of the n components is then equal to $\mathbf{x}, \boldsymbol{x} = \sum_{i=1}^{n} \boldsymbol{s}_i\boldsymbol{a}_i$. It is important to bear in mind that the term source designates the vectors on which are calculated the independence and which are used to calculate the high-order moments and statistics. The term component indicates the vectors some of which can be assigned to chemical compounds and which are used to reconstruct "cleaned" chromatograms. In this paper, no modifications were made to the original FastICA algorithm. More details on this algorithm can be found in the book of Hyvärinen et al. [27].

2.2. High-order moments and statistics

Since noise usually follows a Normal distribution, the computed independent sources given by ICA are investigated in order to find which one may be considered as noise or not. It has been described in the literature that the kurtosis of a distribution is a good criterion to reject artifacts and noise [15]. The use of kurtosis and other statistics or moments of the sources was used in the present study.

Thus, the following statistics or moments can be used to check the normality of the distribution of each source. If normality is not observed, it should imply that the source is unlikely to be noise and therefore likely corresponds to an exogenous phenomenon such as a compound being detected. In summary, sources of interest such as peaks are assumed to have a non-normal distribution, and will be identified as such.

2.2.1. Kurtosis

The kurtosis is the fourth standardized moment of a random variable and is a measurement of the peakedness (i.e. the flattening of a distribution) of the probability distribution of this variable, and can be estimated as:

$$K_i = \frac{m_4}{m_2^2} - 3 = \frac{n\sum_{t=1}^{T}(s_i(t) - \bar{s}_i)^4}{\left(\sum_{t=1}^{T}(s_i(t) - \bar{s}_i)^2\right)} - 3 \tag{3}$$

m_k represents the moment (about the mean) of order k and $\bar{s}_i$ is the mean of the ith source s_i.

2.2.2. Shapiro–Wilk statistic

The non-parametric Shapiro–Wilk (S–W) test examines the null hypothesis that a sample $s_i(1), \ldots, s_i(T)$, comes from a Normally distributed population. This hypothesis is rejected if the test statistic is too small. This test statistic or the associated p-value can be used to characterize the distribution. More details about this test can be found in the literature [28].

Kurtosis and S–W statistics can then be used to describe the degree of normality of a distribution and, hence, to identify noise sources. However, these are far from the only statistics that allow this and other simple or complex statistics (skewness of the distribution of the source, range, Kolmogorov–Smirnov Normality test, etc.) can also be used in this context.

2.3. k-Means clustering

k-Means is a non-supervised method to cluster objects into k partitions on the basis of their attributes. The objects are the sources computed by ICA and the attributes are the estimated statistics computed on these sources, namely the kurtosis and Shapiro–Wilk statistic. The objective is to use these computed characteristics to discriminate the relevant sources (peaks) from sources representing noise or irrelevant artifacts, chromatogram by chromatogram. The concept is to compare the Euclidian distance between the objects. A short distance (slight difference in the computed attributes) is a sign of closeness between objects and the closest objects are put together in the same cluster.

Different implementations exist for k-means clustering. The Hartigan and Wong algorithm is used here, because it generally provides better results than other implementations [29]. However, this application of clustering is rather simple because it implies a low number of variables (i.e. Kurtosis and S–W) and observations. The clustering results will then not depend on the implementation selected but on the data distribution.

In practice, k-means with $k = 2$ is used. The partitioning should result in two clusters, one with sources having a high Kurtosis and low S–W values corresponding to the components of interest and conversely, another with low Kurtosis and high S–W value corresponding to noise and irrelevant artifact components. The outcome of the k-means clustering algorithm may vary from one run to the other because the k centers are randomly placed at the start of the algorithm. To avoid this dependence on initial conditions, the algorithm is repeated a hundred times for each data set (coming from one chromatogram) and the selected clusters are those with the highest frequency.

2.4. Peak detection methodology

This section presents the methodology to detect peaks for a given value of n, the number of estimated sources. The DAD-chromatograms are referenced with the index p ($p = 1, \ldots, P$) corresponding, for example, to P experimental conditions. As the treatment for each DAD-chromatogram is the same, the following explanations are given for an unspecified pth chromatogram. First, data for DAD-chromatograms are truncated at 14, 24, and 34 min for overall run times of 16, 26, and 36 min, respectively. This was performed in order to remove the perturbation of the end of the gradient containing only noise or irrelevant artifacts. Second, the ICA algorithm is applied on the resulting DAD-chromatogram and high-order statistics (i.e. Kurtosis and S–W) are computed for each of the n sources. Before applying clustering, attributes are divided by their standard deviation computed from all the sources available in order to give each attribute the same weight in the clustering decision process. This is illustrated by the following equation, applied to kurtosis. The same computation was done for each considered statistic.

$$K_{Si} = \frac{K_i}{\sqrt{\sum_{i=1}^{n}(K_i - \bar{K})^2}} \quad (4)$$

where K_{Si} is the standardized Kurtosis value for the ith source and $\bar{K}$ is the mean kurtosis computed from all the sources of one DAD-chromatogram. Third, k-means clustering (with $k = 2$) is applied on this bi-dimensional distribution. Fourth, the number of sources found in the relevant cluster for the pth DAD-chromatogram is defined as $c_r(n,p)$, as it also depends on n. These $c_r(n,p)$ relevant sources correspond to the $c_r(n,p)$ detected peaks in the pth DAD-chromatogram. Finally, as this methodology is applied on each of the P DAD-chromatograms, $c_r^*(n)$ is defined as the mode of the $c_r(n,p)$ distribution and corresponds to the most probable value of $c_r(n,p)$.

2.5. Automated adjustment of n methodology

As previously explained, the main parameter of the ICA is the number, n, of sources chosen to make up the signal. By default, it can be arbitrarily chosen by the operator if the number of compounds in the sample is known. In the present section, an automated process to adjust the number of sources is presented when the number of compounds to identify is unknown. In a DOE framework, the same mixture is injected several times using different analytical conditions. Thus, each DAD-chromatogram should contain the same information, i.e. the same number of relevant sources. Finding an optimal value of n for the application of ICA is similar to finding the most likely number of sources counted in the relevant cluster for all DAD-chromatograms. This method is presented in Fig. 1. An initial value for n must first be given. One can use an estimated number of pure components, trough signal matrix singular value ratios computation [30], for instance. Another easier technique is to begin the ICA computation with a very low number of sources, such as $n = 3$. Then, the methodology presented in the previous section is applied on each of the P DAD-chromatograms by incrementing the value of n, and then each value of $c_r^*(n)$ is recorded. It is possible to plot $c_r^*(n)$ against n (see Fig. 5). One can observe that $c_r^*(n)$ stabilizes when n increases. The smallest value of n when $c_r^*(n)$ reaches a plateau is defined as the optimal number of sources, n_{opt}, to carry out ICA. The value of $c_r^*(n)$ at the ceiling is defined as c_c^* and will be assumed to be the optimal estimation of the number of compounds in the mixture. The optimal number of sources, n_{opt}, maximizes the probability to have (for any chromatogram) $c_r(n, p) = c_c^*$ and highly depends on the number of compounds in the sample.

3. Experimental

3.1. Chemicals

Methanol and acetonitrile were HPLC grade from Sigma (St. Louis, MO, USA). Ultra pure water was obtained with a Millipore (Billerica, MA, USA) Milli-Q Academic A10. In the present study, two test mixtures were selected in order to develop and to test the presented algorithms and methodologies. These mixtures mimic an unknown mixture. The first mixture contains atenolol, phenytoin, sulfinpyrazone and warfarin and was used to develop the methodology. The second mixture was used to put the methodology to the test. It contains atenolol, pindolol, warfarin, indoprofen, naproxen, propranolol, retinoic acid, an impurity of

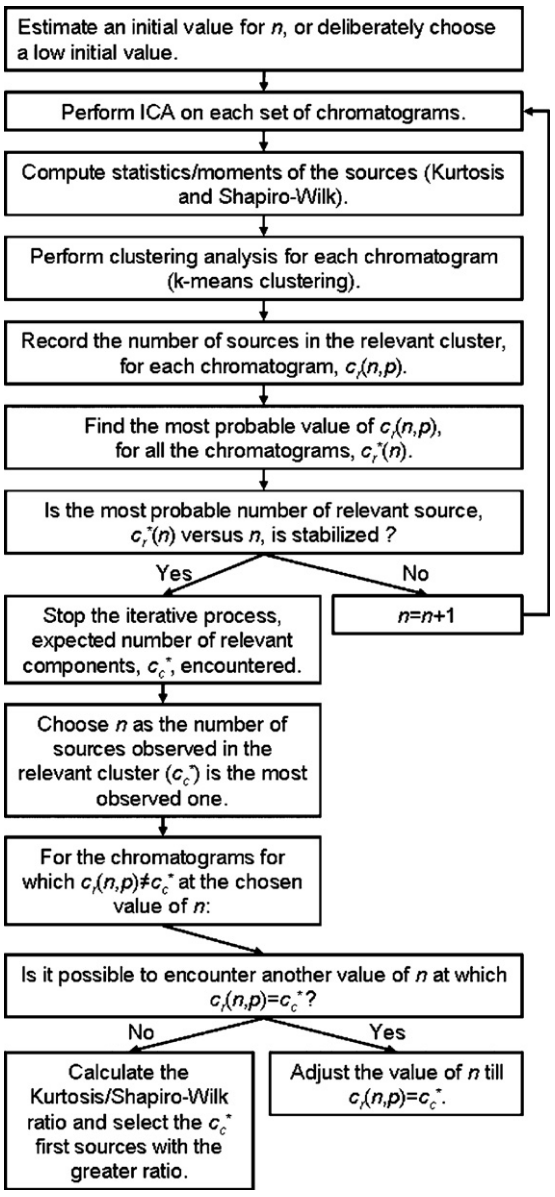

Fig. 1. Methodology for the selection of number of sources for the ICA computation.

the retinoic acid and an unidentified compound. These mixtures and compounds were obtained from the Eli Lilly Company (Indianapolis, IN, USA). Acetic acid (>98%) was purchased from Merck (Darmstadt, Germany), ammonium formate (99%) was purchased from Alfa Aesar (Karlsruhe, Germany) and ammonium hydrogencarbonate (99.7%) was purchased from VWR (Fontenay-sous-Bois, France).

3.2. Sample preparation

The first mixture (sample 1) was prepared as follow. 35 mg of atenolol, 35 mg of phenytoin, 15 mg of sulfinpyrazone and 15 mg of warfarin were dissolved in a 10 ml volumetric flask with a mixture of water-methanol (50:50, v/v). The second mixture (sample 2) was obtained directly from Eli Lilly Company and was prepared as follow. 103 mg of warfarin, 97 mg of atenolol, 100 mg of pindolol, 98 mg retinoic acid, 101 mg of naproxen sodium, 99 mg of indoprofen and 103 mg of propranolol hydrochloride were dissolved in a 100 ml volumetric flask with a mixture of water-acetonitrile (50:50, v/v). Then, from these two samples, two aliquots were filtered with 0.20 μm PTFE syringe filtration disks into some vials for injection in the HPLC system. The injection volume was 2 μl for sample 1 and 0.5 μl for sample 2.

Table 1
Linear gradient shapes with organic modifier percentage (O.M.%) in mobile phase.

Applied linear gradient					
T_G = 10 min		T_G = 20 min		T_G = 30 min	
Time (min)	O.M.%	Time (min)	O.M.%	Time (min)	O.M.%
0	5	0	5	0	5
10	95	20	95	30	95
10.5	95	20.5	95	30.5	95
10.6	5	20.6	5	30.6	5
16	5	26	5	36	5

3.3. Experiments

A full factorial design [31] was applied on three HPLC factors: the pH of the aqueous part of the mobile phase (four levels from 2.6 to 10.0), the gradient time (T_G) (three levels from 10 to 30 min) and the nature of organic modifier (two levels, acetonitrile or methanol). For sample 1, this design was repeated on five analytical columns: XBridge C18, XBridge C8, XBridge RP18, XBridge Phenyl columns (100 × 2.1 mm i.d.; particle size 3.5 μm), all from Waters (Milford, MA, USA) and a Cogent Bidentate C18 column (100 × 2.1 mm i.d.; particle size 4.0 μm) from Microsolv (Eatontown, NJ, USA). For the sample 2, the design was only carried out on the XBridge C18 with methanol for a total of 12 experimental conditions. The experiments were carried out at a flow rate of 0.25 ml/min and at 30 °C. The buffers consisted of 10 mM pH 2.6 formic acid, pH 5.0 ammonium formate, pH 7.0 ammonium formate and pH 10.0 ammonium hydrogen–carbonate. The pH was adjusted to the selected value with concentrated formic acid or ammonia 35% aqueous solution. The shapes of the linear gradients are described in Table 1.

Chromatographic separations were performed on a Waters 2695 separation module coupled to a Waters selector valve 7678 and a Waters 996 Photodiode array detector. All the DAD-chromatograms were recorded between 210 nm and 400 nm with an estimated step of 1.2 nm (158 points) and with an acquisition time of 500 ms. They were finally exported by Empower 1.0 (Waters) in ASCII files containing the UV-DAD data.

The experimental design leads to 2·4·3 (i.e. 2 organic modifiers, 4 pH, 3 gradient times) = 24 experiments which were repeated for the five columns which leads to a total of 120 chromatograms. It is important to state that this full factorial design was not only set up to challenge ICA abilities to analyze DAD-chromatograms recorded under various conditions but also to develop and to test new mathematical models of retention times [32]. Such a large set of experiments is not required for ICA and for conventional or automated optimization of analytical methods. In most complex separations, classical or D-optimal design with 12–24 experiments will largely suffice to accomplish a DOE and ICA driven separation.

3.4. Software

An in-house computer program was developed to perform the analysis presented in the previous sections. The coding was carried out with R 2.4.1 statistical language for Windows, freely distributed at http://www.r-project.org. These codes can be run on compatible PC (3 GHz in this case) or other environments where R is available. For ICA computations, the FastICA algorithm for R, developed at the Helsinki University of Technology, was used.

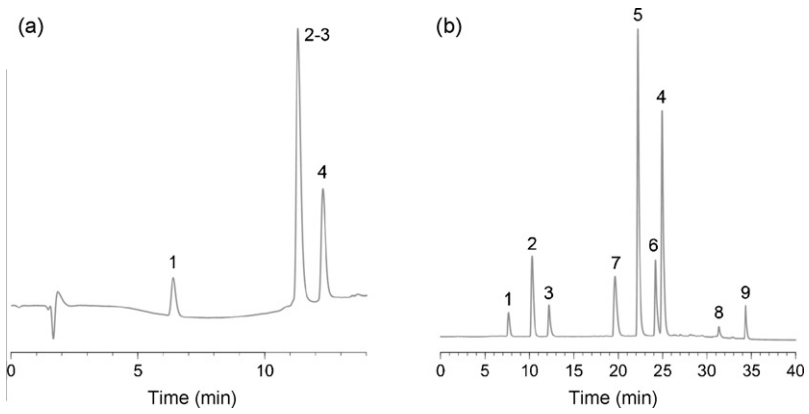

Fig. 2. (a) Chromatogram (sample 1) recorded on an XBridge C18 with methanol and buffer at pH 7.0 with a gradient time of 10 min observed at 240 nm. Compounds numbered from 1 to 4 are respectively atenolol, phenytoin, sulfinpyrazone and warfarin. (b) Chromatogram (sample 2) recorded on an XBridge C18 with methanol and buffer pH 2.9 with a gradient time of 30 min observed at 280 nm. Compounds numbered from 1 to 9 are respectively atenolol, pindolol, an unidentified compound, warfarin, indoprofen, naproxen, propranolol, an impurity of the retinoic acid and the retinoic acid.

4. Results and discussion

4.1. ICA algorithm results and components clustering

Each chromatogram matrix **X** can be described as a ($T \times 158$) matrix where T is either 1680, 2880 or 4020, depending on the gradient time (10, 20 and 30 min, respectively). In this section, the results obtained (for sample 1) by applying the methodology described in Section 2.4, for one chromatogram, are presented. A summary of the results obtained for sample 2 can be found in Section 4.7. The arbitrarily selected value for n is equal to 12 and the chosen DAD-chromatogram is the one recorded with sample 1 on the XBridge C18 column with methanol and buffer at pH 7.0 with a gradient time of 10 min (Fig. 2(a)). In fact, in this case $n = 12$ is a good value for n because it succeeds in finding the four compounds and the dead volume perturbation (i.e. the small baseline perturbation observed at t_0) of the considered DAD-chromatogram.

The twelve independent components are depicted in Fig. 3 at the wavelength of 240 nm. At this wavelength, each peak absorbs and gives approximately the same signal to noise ratio. The compo-

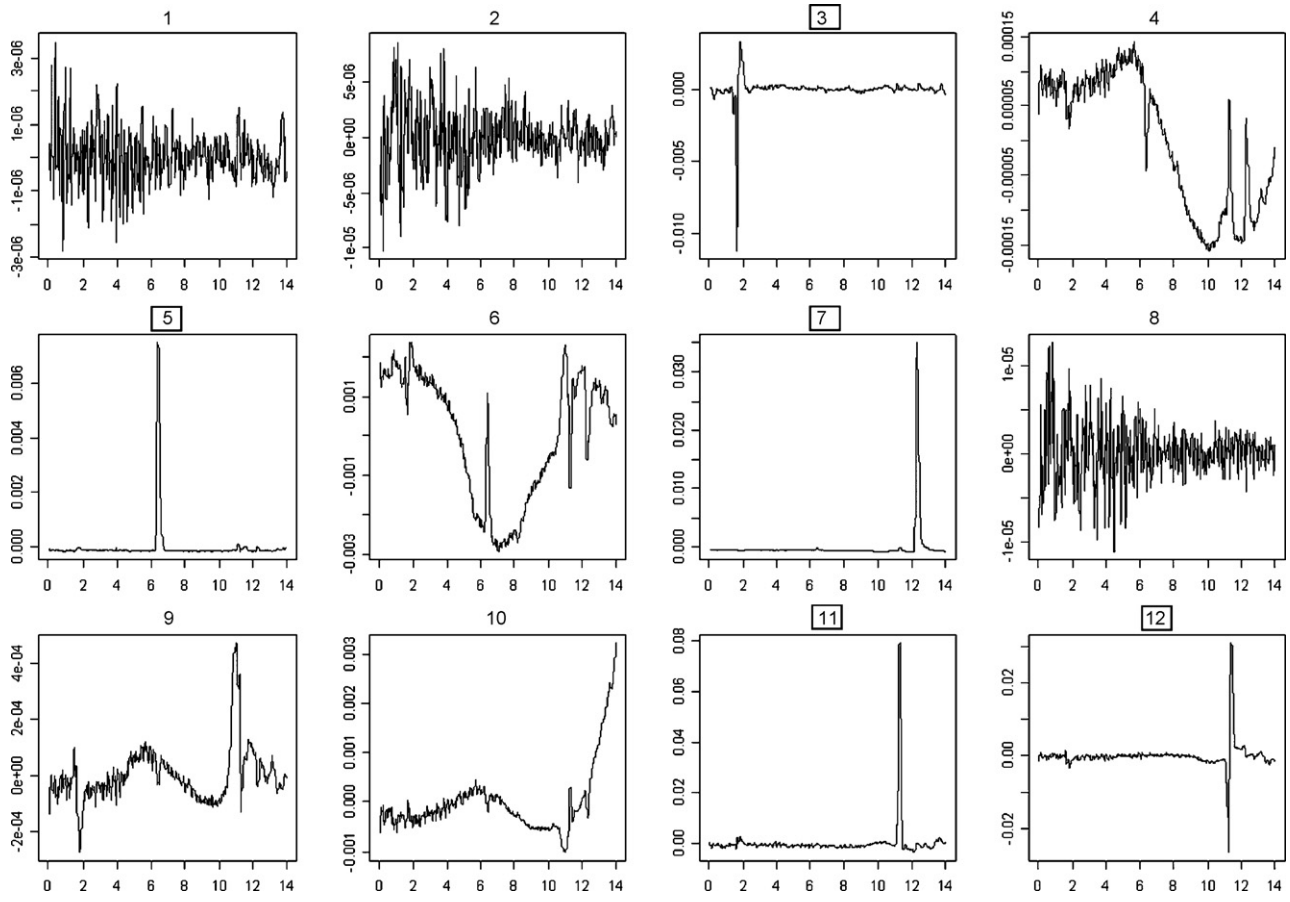

Fig. 3. Components computed by ICA with $n = 12$ and at 240 nm. The components whose numbers are labeled with a square are the ones that correspond to peaks. Other components correspond to noise or irrelevant artifacts. The *X*-axis represents the time (min) and the *Y*-axis is the absorbance.

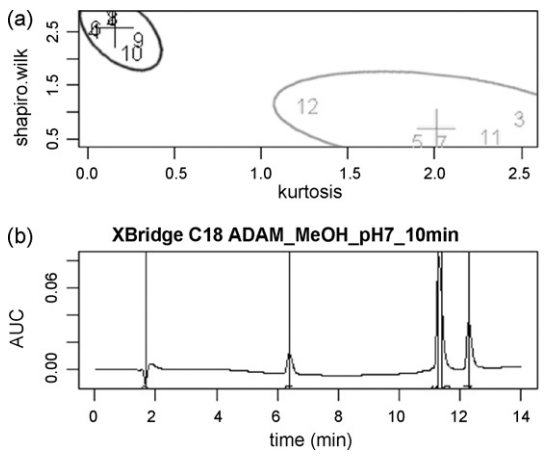

Fig. 4. (a) Clustering *k*-means realized on standardized kurtosis and Shapiro–Wilk statistics. The right-bottom cluster (cluster 1, in grey) contains the relevant sources. Crosses indicate the clusters centers. (b) Original DAD-chromatogram at 240 nm with automatically picked apexes by a vertical line.

nents corresponding to peaks are labeled by a surrounding square (sources 3, 5, 7, 11 and 12). The seven other components correspond to noise and are of much lower amplitude.

First, one can observe that the 12th component is distorted and it seems to issue from the strong coelution with the eleventh component. This type of distortion was observed an each set of coeluting peaks for all the chromatograms. A similar distortion is not visible on the 11th component which is probably due to its higher size. However, the distortions which can exist from components which result from coeluted peaks do not seem to affect the detection of these peaks even if their size ratio is about 2.5:1 in this case. Second, some components which were classified as corresponding to noise depict small peaks at the same retention times as the relevant components (e.g., component 6). This results from the fact that ICA algorithm is seldom able to generate components which are totally independent. It apparently does not affect peak detection either. The classification of components determined from *k*-means clustering is shown in Fig. 4(a). The crosses indicate the center of the clusters and the relevant one (grey ellipse) is located at the bottom right and contains five components ($c_r(n,p) = 5$). The apex of each relevant component has been found and its retention time has been automatically placed on the chromatogram (Fig. 4(b)).

4.2. Optimal number of sources

When the 120 chromatograms are treated as in the previous section, a distribution of 120 values of $c_r(n,p)$ is obtained. With $n = 12$, the mode of this distribution is equal to five ($c_r^*(n) = 5$) and its observed frequency is equal to 37.5%. The distribution of $c_r(n,p)$ obtained with $n = 20$ strengthens the fact that (from a given value) when n increases the mode of the distribution is not modified (still equal to 5 with a frequency of 29.2%).

To find the optimal value of sources which make up the chromatogram, n was incremented from 3 to 30. The variation of $c_r^*(n)$ against n is plotted in Fig. 5(a). This figure clearly shows first, an increasing variation and second, a stabilization of relevant components number, $c_r^*(n)$. The cap of $c_r^*(n)$ is observed at the value of 5 ($c_c^* = 5$) and starts with a value of n equal to twelve, so $n_{opt} = 12$. Therefore, this result indicates that the sample seemingly contains five independent sources of interest (five compounds or four compounds and the dead volume baseline perturbation).

4.3. Final adjustment of n and Kurtosis/Shapiro–Wilk ratio

However, for $n = n_{opt}$, $c_r(n,p)$ differs from c_c^* in 62.5% of the clustering results. It means that for 62.5% of the results (75 chromatograms), the number of components counted in the relevant cluster is not equal to five. Then, for these inconvenient results, the value of n is adjusted till $c_r(n,p)$ reaches c_c^* whose the computation is explained in the previous section. However, for some chromatograms, when n is incremented, $c_r(n,p)$ never equals five. So, the components are ranked in descending order accordingly to their K_S/S–W ratio. Indeed, if this ratio is high then the corresponding components are close to the bottom right corner of the clustering plot, which means that the probability for this component to belong to the relevant cluster is higher. So, the c_c^* components with the higher ratios are defined as being the relevant ones.

4.4. Results of automated peak detection

For the 120 DAD-chromatograms, a total of 516 components are classified as relevant, 457 of whom are detected peaks and 59 correspond to the detection of the dead volume baseline perturbation. As the dead volume baseline perturbation is detected in about 50% of the chromatograms and as the foretold number of relevant components by chromatogram is equal to five ($c_c^* = 5$), then it means that among these five components stands the dead volume baseline perturbation, so the number of expected peaks in the mixture is equal to 4. As 457 peaks are detected on the 120 chromatograms, 95.2% of the peaks are automatically detected. To confirm these results, peak detection was done manually and four peaks were detected for each chromatogram. However, even done by an experienced analyst, the manual peak detection cannot always be error free (but we assume it is error free due to the small number of compounds in the mixture). The dead volume baseline perturbation is of particular interest (defining the dead time of a HPLC system), but the detection of this relevant component is not consistent. This can be due to its random shape when using different mobile phase as in DOE, to its small size and also to its undifferentiated UV signature with the mobile phase.

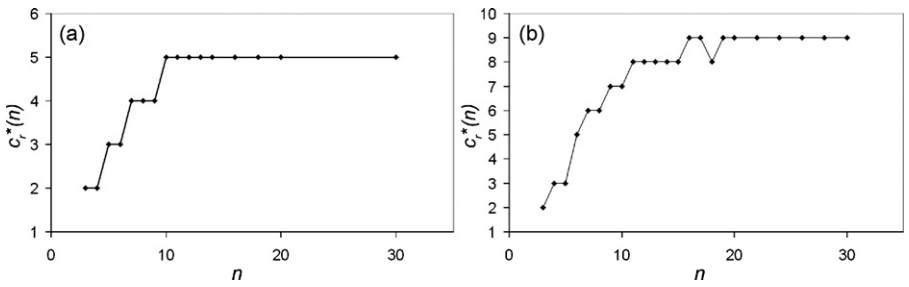

Fig. 5. Plot of the variation of $c_r^*(n)$ versus n. (a) For sample 1 (b) for sample 2.

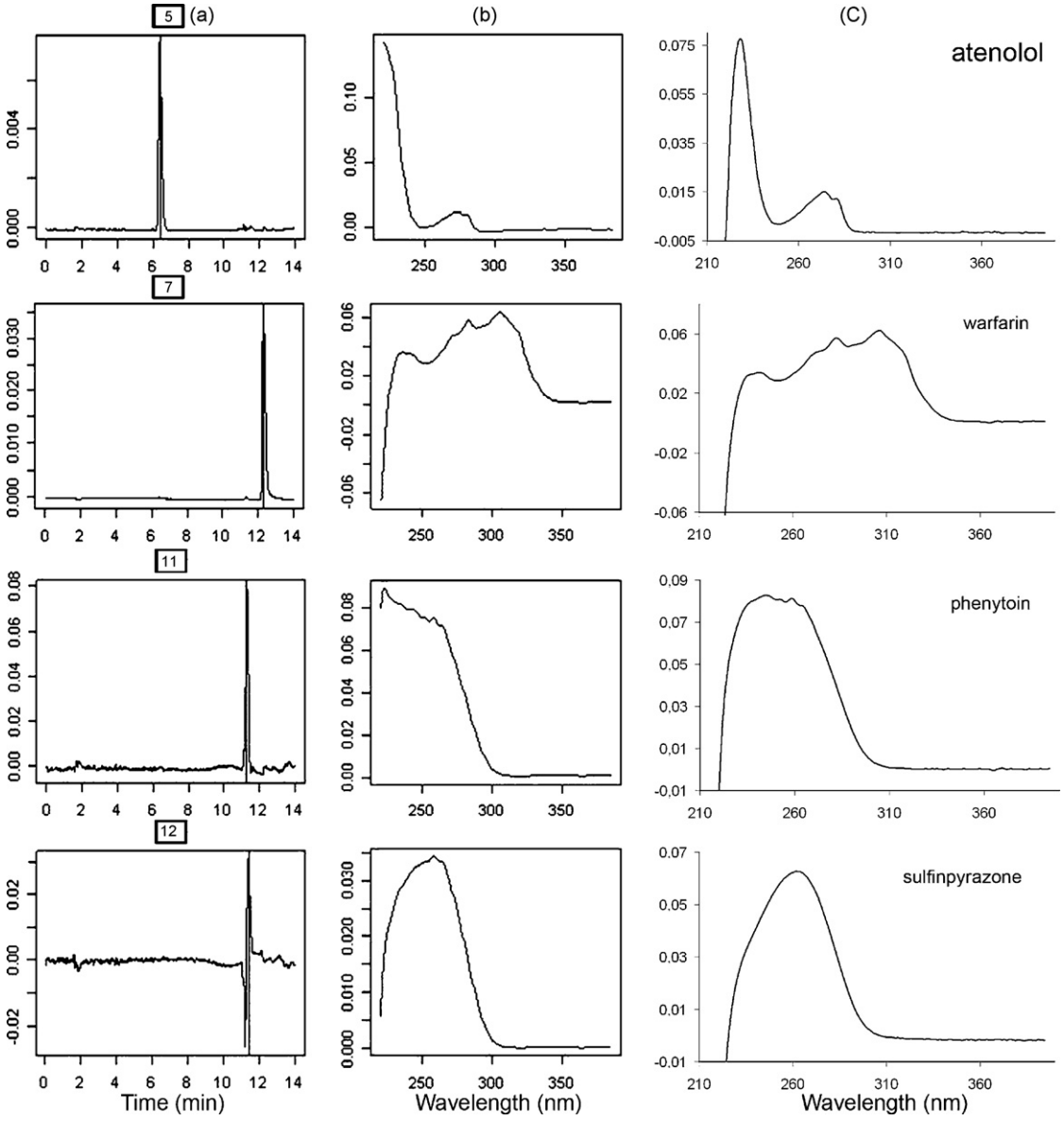

Fig. 6. Comparison between the obtained relevant components UV-spectra and the reference ones. (a) Components contained in the relevant cluster, observed at 240 nm; (b) estimated UV spectra of each independent component at apex (210–400 nm); (c) UV spectra (210–400 nm) as observed in the original chromatogram. Those spectra were recorded from chromatograms obtained from each individual reference solution using the same experimental condition.

4.5. Extracting component UV-spectra

Finally, the identification of the compounds can be done manually. In the case of phenytoin and sulfinpyrazone, which are coeluting (Fig. 2(a)), the UV spectra extracted from the original chromatogram are mixtures of the "pure" spectra (i.e. the spectra that will be obtained if the compounds were not coeluting). As the obtained independent components have the same dimensions than the original chromatogram, UV spectra can be extracted from the respective independent components. These spectra are good estimations of the "pure" spectra and the compounds identification is made easier. Fig. 6(b) depicts, for one chromatogram, the UV spectra estimated by ICA extracted from the corresponding relevant component (which are displayed on Fig. 6(a)) at the apex of the peak. These extracted UV spectra can be compared to the UV spectra coming from the original chromatogram (Fig. 6(c)). One can observe that some slight differences exist between the extracted and the original UV spectra. It is probably due to the interference of the mobile phase (organic modifier, buffer composition and buffer pH) and to the strong coelution existing between phenytoin and sulfinpyrazone.

4.6. Reconstruction of DAD-chromatogram

As the sum of the n components gives (approximately) the original chromatogram, the sum of the $c_r(n,p)$ relevant components should give a chromatogram free from noise and artifacts represented by the other components. Fig. 7(a) illustrates the original DAD-chromatogram compared to the reconstructed one (Fig. 7(c)), both observed at 240 nm. The peaks (identified by the triangles in the top of the chromatograms) have been automatically detected. However, at this wavelength, the noise reduction of the chromatogram is not really observable. The chromatograms of Fig. 7(b) and (d) illustrates that, for other wavelengths, the reconstructed chromatogram (d) has been cleaned from noise, irrelevant artifacts and gradient baseline drift.

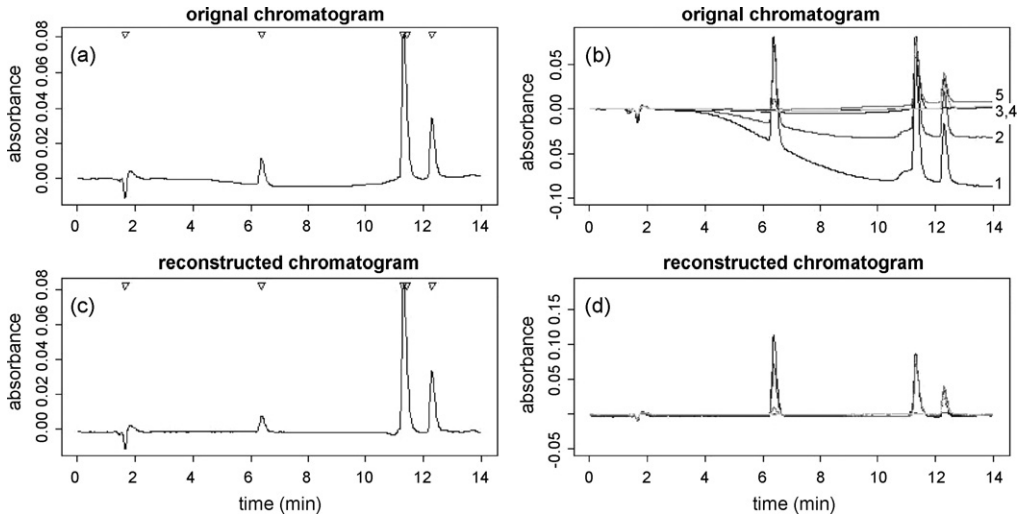

Fig. 7. (a–c) Comparison between original DAD-chromatogram (a) and reconstructed one with $n = 12$ (c). The original is recorded at 240 nm, on an XBridge C18 with methanol and pH 5 buffer with a gradient of 20 min. Apexes have been automatically picked. (b–d) Comparison at different wavelengths (1: 214, 2: 220, 3: 240, 4: 268 and 5: 327 nm) of the same original (b) and reconstructed (d) chromatograms.

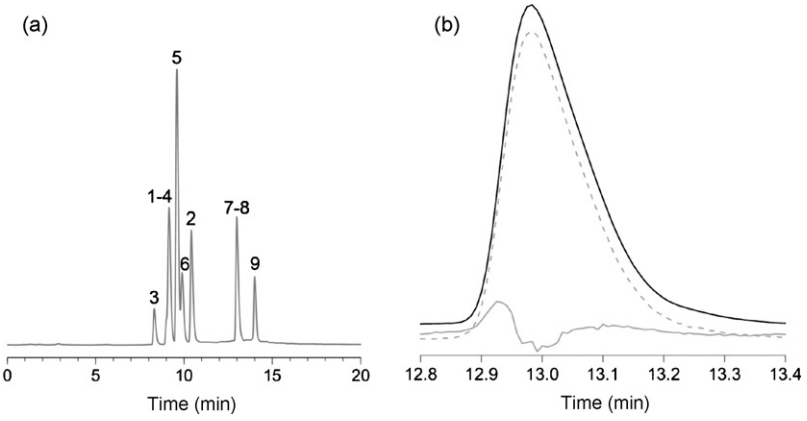

Fig. 8. (a) One chromatogram obtained (with sample 2) in the experimental design depicted at 280 nm. Nine compounds were actually automatically detected. (b) Magnification of the zone between 12.8 and 13.4 min. The solid black line represents the original recorded chromatogram, the dashed grey line depict the component corresponding to compound 7 (propranolol) and the solid grey line display to the component corresponding to compound 8 (an impurity of the retinoic acid).

4.7. Test of the methodology with a more complex sample

Sample 2 was directly shipped from Eli Lilly Company and seven compounds were described in the sample preparation procedure. This mixture was used to test the ability of the methodology to detect peaks in a more complex mixture. The global methodology was exactly applied in the same way as for sample 1. As depicted in Fig. 2(b), nine compounds were manually detected. Thus the mixture contained at least nine compounds which was more than foreseen. The analysis of the variation of $c_r^*(n)$ against n, which is displayed on Fig. 5(b), shows that the cap of $c_r^*(n)$ is observed at the value of 9 ($c_c^* = 9$) and starts with a value of n equal to nineteen, so $n_{opt} = 19$. As the baseline perturbation at t_0 was not detected, this result confirms that nine compounds were contained in sample 2. Among the two unexpected compounds, one is still unidentified and the second has been identified as an impurity of the retinoic acid. It seems that the baseline perturbation at t_0 was not detected due the really small injected volume (0.5 μl). For the twelve recorded DAD-chromatograms, a total of 103 components were classified as relevant. As the number of compounds in the mixture is equal to nine, it means that 95.4% of the peaks were automatically detected. Fig. 8(a) depicts a chromatogram where compound 7 and compound 8 are coeluting. Despite this coelution and the difference between the peaks size, ICA was able to differentiate and to detect these compounds as displayed on Fig. 8(b). Furthermore, these results obtained with sample 2 tend to confirm that the percentage of detected peak (about 95%) seems not to be affected by the sample complexity.

5. Conclusions

The automated detection of peaks is a very crucial step in the automated development of analytical methods. A new and original approach combining ICA, high-order statistics and clustering was successfully used for the determination of a test mixture of pharmaceutical compounds in the framework of a DOE methodology. The present approach could be envisaged in high throughput screening experiments, such as those resulting from synthetic process development (purity assessment) or for the development of stability indicating methods when impurities are not necessarily known. Moreover, it does not require expensive equipment, such as a mass spectrometer, to detect the compounds, as long as the compounds absorb in the UV. Clustering methods allow separating very efficiently the noise components from the relevant ones, using adequate summary statistics. The technique to find an optimal number of sources is very convenient but is time consuming.

Fortunately, the time needed for the numerical data treatments presented in this study is much smaller than the sample analysis time. Indeed, the required times to obtain the ICA results, for one chromatogram, when n is incremented from 3 to 30 as shown in this paper, are 35, 55 and 75 s for the respective gradient times of 10, 20 and 30 min. Therefore, as the chromatograms are numerically treated one by one, this gives the opportunity to easily implement the numerical data treatments in a semi-concurrent mode, i.e. just after the sample analysis.

On the other hand, this process could also be performed only on sub-parts of a DAD-chromatogram, according to the analyst interest; for instance, searching for coeluted impurities in peaks of interest allowing a significant reduction in the time devoted to the computational process.

Eventually, the combination of the original aforesaid strategies described in this paper could give a powerful tool and seems to begin to open new prospects for the fully automated development of LC–UV-DAD methods. Nevertheless, further work concerning the possibilities for automated peak tracking is required.

Acknowledgments

The authors are very grateful to the reviewers for providing important comments that led to significant improvements of this article. The authors would also like to thank the Walloon Region of Belgium for the FIRST-DEI convention funds no. 516130 and the Eli Lilly Company for partial funding of ADAM project and equipments. A research grant from the Belgium National Fund for Scientific Research (FRS-FNRS) to E. Rozet is also gratefully acknowledged.

References

[1] J.R. Torres-Lapasio, M.C. Garcia-Alvarez-Coque, J. Chromatogr. A 1120 (2006) 308.
[2] J. Krupcik, J. Mydlova, I. Spanik, B. Tienpont, P. Sandra, J. Chromatogr. A 1084 (2004) 80.
[3] G. Vivó-Truyols, J.R. Torres-Lapasió, M.C. García-Alvarez-Coque, J. Chromatogr. A 991 (2003) 47.
[4] V.B. di Marco, G.G. Bombi, J. Chromatogr. A 931 (2001) 1.
[5] P. Nikitas, A. Pappa-Louisi, A. Papageorgiou, J. Chromatogr. A 912 (2001) 13.
[6] J.R. Torres-Lapasio, J.J. Baeza-Baeza, M.C. Garcia-Alvarez-Coque, Anal. Chem. 69 (1997) 3822.
[7] G. Vivó-Truyols, J.R. Torres-Lapasió, M.C. García-Alvarez-Coque, P.J. Schoenmakers, J. Chromatogr. A 1158 (2007) 258.
[8] R. Tauler, Chemom. Intell. Lab. Syst. 30 (1995) 133.
[9] A. Bogomolov, M. McBrien, Anal. Chim. Acta 490 (2003) 41.
[10] A. de Juan, R. Tauler, J. Chromatogr. A 1158 (2007) 184.
[11] G. Wang, Q. Ding, Z. Hou, TrAC, Trends Anal. Chem. 27 (2008) 368.
[12] S. Makeig, T. Jung, A.J. Bell, D. Ghahremani, T.J. Sejnowski, Proc. Natl. Acad. Sci. U.S.A. 94 (1997) 10979.
[13] T.-P. Jung, C. Humphries, T.-W. Lee, S. Makeig, M. McKeown, V. Iragui, T.J. Sejnowski, Adv. Neural Inform. Process. Syst. 10 (1998) 894.
[14] A. Delorme, T.J. Sejnowski, S. Makeig, NeuroImage 34 (2007) 1443.
[15] M. McKeown, S. Makeig, G. Brown, T.-P. Jung, S. Kindermann, T.W. Lee, T.J. Sejnowski, Proc. Natl. Acad. Sci. U.S.A. 95 (1998) 803.
[16] H. Yamamoto, K. Hada, H. Yamaji, T. Katsuda, H. Ohno, H. Fukuda, Biochem. Eng. J. 32 (2006) 149.
[17] G. Wang, W. Cai, X. Shao, Chemom. Intell. Lab. Syst. 82 (2006) 137.
[18] M. Vosough, Anal. Chim. Acta 598 (2007) 219.
[19] D. Jouan-Rimbaud Bouveresse, H. Benabid, D.N. Rutledge, Anal. Chim. Acta 589 (2007) 216.
[20] D. Mantini, F. Petrucci, P. Del Boccio, D. Pieragostino, M. Di Nicola, A. Lugaresi, G. Federici, P. Sacchetta, C. Di Ilio, A. Urbani, Bioinformatics 24 (2008) 63.
[21] S. Wienkoop, K. Morgenthal, F. Wolschin, M. Scholz, J. Selbig, W. Weckwerth, Mol. Cell. Proteomics 7 (2008) 1725.
[22] A. Hyvärinen, E. Oja, Neural Networks 13 (2000) 411.
[23] J.-F. Cardoso, Neural Comput. 11 (1999) 157.
[24] A. Hyvärinen, E. Oja, Neural Comput. 9 (1999) 1483.
[25] J.J. Murillo-Fuentes, R. Boloix-Tortosa, F.J. Gonzalez-Serrano, Fourth International Symposium on Independent Component Analysis and Blind Signal Separation [ICA2003], 2003, p. 1053.
[26] A. Hyvärinen, IEEE Trans. Neural Networks 10 (1999) 626.
[27] A. Hyvärinen, J. Karhunen, E. Oja, Independent Component Analysis, Wiley, New York, 2001.
[28] S.S. Shapiro, M.B. Wilk, Biometrika 52 (1965) 591.
[29] J.A. Hartigan, M.A. Wong, Appl. Statist. 28 (1979) 100.
[30] H. Yuzhu, S. Weiyang, Y. Weifeng, D.L. Massart, Chemom. Intell. Lab. Syst. 77 (2005) 97.
[31] G. Cox, W. Cochran, Experimental Designs, 2nd ed., McGraw-Hill, 1962.
[32] P. Lebrun, B. Govaerts, B. Debrus, A. Ceccato, G. Caliaro, Ph. Hubert, B. Boulanger, Chemom. Intell. Lab. Syst. 91 (2008) 4.

Talanta 79 (2009) 22–26

Contents lists available at ScienceDirect

Talanta

journal homepage: www.elsevier.com/locate/talanta

Electrochemical behaviour of epinephrine and uric acid at a Sonogel–Carbon L-Cysteine modified electrode

H. El Bouhouti [a,b], I. Naranjo-Rodríguez [a,*], J.L. Hidalgo-Hidalgo de Cisneros [a], M. ElKaoutit [a], K.R. Temsamani [b], D. Bouchta [b], L.M. Cubillana Aguilera [a]

[a] Departamento de Química Analítica, Facultad de Ciencias, Universidad de Cádiz, 11510 Puerto Real, Cádiz, Spain
[b] University Abdelmalek Essaâdi, Department of Chemistry, Faculty of Sciences of Tétouan, Equipe de Recherche Electrochimie et Systèmes Interfaciaux (ERESI), M'Hannech II, B.P. 2121, 93002, Tétouan, Morocco

ARTICLE INFO

Article history:
Received 25 November 2008
Received in revised form 18 February 2009
Accepted 24 February 2009
Available online 14 March 2009

Keywords:
Sonogel–Carbon
L-Cysteine
Epinephrine
Uric acid
Urine sample

ABSTRACT

The Sonogel–Carbon electrode is a special class of sol–gel electrode that exhibits favourable mechanic and electric properties to be used as electrochemical sensor. In this study, Sonogel–Carbon modified with L-Cysteine was used to prepare a novel electrochemical sensor. The objective of this novel electrode modification was to seek new electrochemical performances for detection of epinephrine in the presence of uric acid. The response of catalytic current with epinephrine concentration shows a linear relation in the range from 1×10^{-7} to 5×10^{-4} M with a correlation coefficient of 0.998, and a detection limit of 8.7×10^{-8} M. The modified electrode had also been applied to the determination of epinephrine and uric acid in biological samples with satisfactory results. A surface characterisation of this modified electrode was carried out helped by scanning electron microscopy (SEM) and X-Ray energy dispersive spectroscopy (EDS).

1. Introduction

Epinephrine (EP) is an important neurotransmitters in mammalian central nervous systems [1,2], and it exits in the nervous tissue and body fluid in the form of large organic cations. The changes of its concentration may result in many diseases [3]. Thus, a quantitative determination of EP concentration is significant for developing nerve physiology, pharmacological research and life science.

There are some methods applied for the determination of EP, such as high performance liquid chromatography (HPLC) [4,5], capillary electrophoresis [6,7], flow injection [8,9], chemiluminescence [10,11], fluorimetry [12] and spectrophotometry [13,14]. As an electroactive device, it can also be studied via electrochemical techniques. Some reports showed the electrochemical response of EP on different kinds of electrodes, such as electrochemically pretreated glassy carbon electrode [15], carbon fiber microelectrode [16], polymer film modified glassy carbon electrode [17,18] and self-assembled monolayer modified electrode [19,20].

Uric acid (2,6,8-trihydroxypurine, UA) is the primary product of purine metabolism [21]. Physiological UA serum levels range from 41 to 88 mg mL^{-1} and urinary excretion is typically 250–750 mg per day [22]. Its abnormal concentration level in a human body may be symptoms of several diseases, such as gout, hyperuricaemia, and Lesch-Nyhan syndrome. Leukemia, pneumonia, and so on are also associated with enhanced urate levels [23,24]. So it is desirable to have a simple and direct method for monitoring the concentration of UA in biological fluids. UA and EP are coexistent in biological fluids of human, so the simultaneous detection of UA and EP in a mixture is quite attractive to biological and chemical researches. Individual determination of UA or EP has been reported by many researches; however, simultaneous determination of them is rarely presented.

It nowadays exists a great interest in the development and application of sol–gel-derived carbon-based electrodes for electrochemical applications. The sol–gel process is a chemical synthesis technique that enables the possibility of preparing a wide variety of oxide compounds at far lower temperatures than conventional methods. Recently, some of us have developed a new type of graphite-based sol–gel electrode, the Sonogel–Carbon electrode, which is obtained using high-energy ultrasounds. Classical procedures for the synthesis of acid catalysed sol–gel-based electrode materials include the addition of an alcoholic solvent to the initial precursor mixture to make it homogeneous and the employment of an ultrasound bath for several minutes to promote the hydrolysis. On the contrary, by means of sonocatalysis, high-energy ultrasounds are applied directly to the precursors, and ultrasonic cavitation is achieved so that hydrol-

* Corresponding author. Tel.: +34 956 01 63 53; fax: + 34 956 01 4 60.
E-mail address: ignacio.naranjo@uca.es (I. Naranjo-Rodríguez).

0039-9140/$ – see front matter © 2009 Elsevier B.V. All rights reserved.
doi:10.1016/j.talanta.2009.02.057

ysis with acidic water is promoted in only a few seconds and in the absence of any additional solvent. Thanks to the phenomenon of ultrasonic cavitation, sol–gel reactions occur in a unique environment, leading to gels with special characteristics. These so-called sonogels are mainly of high density, with a fine texture and homogeneous structure. The mix of sonogel with spectroscopic grade graphite leads to the Sonogel–Carbon electrode [25,26]. The Sonogel–Carbon electrodes show the general good properties of the other CCE's (Ceramic Carbon Electrodes). Besides, in comparison with other carbon electrodes, they exhibit especially favourable electrochemical properties, such as broad operational range of voltage and very low values of observed charging capacity (C_{obs}). These electrodes show very favourable electroanalytical properties for their use as amperometric sensors and, furthermore, they can easily permit the incorporation of numerous receptor molecules at the Sonogel–Carbon materials, and the deliberate chemical modification of the electrode surface with a suitable reagent results in the control of the rates and selectivities of electrochemical reactions at the solid/liquid interface [27–31].

In the present paper, we propose a new application of Sonogel–Carbon electrodes based on the incorporation of L-Cysteine and the response of the new modified electrode for EP and UA.

2. Experimental

2.1. Reagents and materials

Methyltrimethoxysilane (MTMOS) was from Merk (Darmstad, Germany), Hydrochloric acid (HCl) and sulfuric acid (H_2SO_4) were from Panreac (Barcelona, Spain). L-Cysteine (>99%) was obtained from Fluka Chemical Company (Switzerland). UA (99%) was purchased from Sigma (Barcelona, Spain), EP was purchased from Aldrich (Milwaukee, USA), and used as received. KH_2PO_4 and K_2HPO_4 for phosphate buffer were from Fluka. All reagents were of analytical grade or higher and used as received without further purification. Graphite powder (spectroscopic grade RBW) was from SGL Carbon (Ringsdorff, Germany). Nanopure water was obtained by passing twice-distilled water through a Milli-Q system (18 MΩ cm, Millipore, Bedford, MA).

Glassy capillary tubes, i.d. 1.15 mm, were used as the bodies for the composite electrodes.

2.2. Instrumentation

All electrochemical measurements were performed with an Autolab PGSTAT20 (Ecochemie, Utrecht, The Netherlands). The experiments were carried out in a three-electrode cell at room temperature (25 ± 1 °C), the counter electrode was a platinum wire and a Ag/AgCl, 3 M KCl electrode was used as the reference, the composite-filled capillary tubes were used as working electrode. Differential Pulse Voltammetry (DPV) and Cyclic Voltammetry (CV) were the electrochemical techniques applied to study the behaviour of the Sonogel–Carbon electrodes. Measurements were carried out under N_2 atmosphere when required.

The synthesis of the Sonogels-Carbon was carried out sonicating with a high-power ultrasonic generator, SONICATOR 3000, from MISONIX (MISONIX Inc., Farmingdale, NY, USA) (equipped with a 13-mm titanium tip), that provides a maximum power of 600 W.

Scanning electron microscopy (SEM) studies were carried out on a QUANTA 200 (FEI Company, Hillsboro, Oregon, USA) operating at 20 keV and equipped with a Microanalyzer to perform X-Ray energy dispersive spectroscopy (EDS).

2.3. Preparation of the Sonogel electrode

To prepare the Sonosol, the general procedure was as follows: 500 μl of MTMOS and 100 μl of 0.2 M HCl were mixed and then insonated during 5 s with the high-power ultrasonic processor; in this way the mixture is subjected to the phenomenon of ultrasonic cavitation, by which the sol–gel process begins, avoiding the use of alcoholic solvent and reducing drastically the time needed to get an unique phase. In the next step, the adequate amounts of L-Cysteine and graphite powder were added and homogenously dispersed in the obtained Sonosol. After several minutes, the resulting material starts to acquire enough consistency thus it could fill easily the glass capillaries leaving a little extra mixture sticking out of the glass tube to facilitate the subsequent polishing step. After 24 h, the Sonogel–Carbon L-Cysteine composite electrode becomes hardened and, therefore, structured. Adherence between the developed material and the glass was excellent. Before use, the electrodes were polished with No. 1200 emery paper to remove extra composite material and wiped gently with weighing paper. Electrical contact was established by inserting a cooper wire into the capillary.

3. Results and discussion

3.1. SEM and EDS studies

Four different samples of Sonogel–Carbon L-Cysteine electrodes were analyzed by SEM: used Sonogel–Carbon electrode with 2.5% of L-Cysteine; used Sonogel–Carbon electrode with 5% of L-Cysteine; used Sonogel–Carbon electrode with 7.5% of L-Cysteine and used Sonogel–Carbon electrode with 10% of L-Cysteine. A sample of used Sonogel–Carbon electrode without modification was analyzed too.

The used electrodes that contained 2.5% and 5% of modifier show a minimum erosion after use, and a light separation among the material and the glass capillary that serves as body for the electrode. The electrodes with a higher modifier percentage show a higher number of holes, fissures and fractures on their surfaces, besides a much more marked separation between the glass capillary and the Sonogel–Carbon material. This would explain the worst electrochemical behaviour of the modified electrodes with 7.5% and 10% with respect to the Sonogel–Carbon material modified with 5%; this percentage shows the better electrochemical behaviour compared with the other modifier percentages tested.

In the micrographs, great differences are not observed among the electrodes modified with 2.5% and 5%. The difference of electrochemical behaviour between these two types of electrodes can be due fundamentally to the higher modifier proportion that implies a greater presence of the modifier on the active surface of the electrode in the case of the electrodes modified with 5% of L-Cysteine.

In the micrographs of Fig. 1, an image of a Sonogel–Carbon electrode without modifier, together with its EDS spectrum (a); and an image of a Sonogel–Carbon electrode modified with 5% of L-Cysteine, together with its spectrum of EDS (b) are shown. It can be seen that in both cases the separation between the material and the capillary body is minimum. The main difference between both images is the presence of particles of L-Cysteine on the surface of the material that is proven by the presence of sulphur in the elementary composition of the modified material, as it can be observed in the EDS spectra. In Fig. 2, an amplification of a part of the micrograph 1.b is collected; a bright particle is observed and identified as L-Cysteine thanks to the presence of sulphur in the EDS spectrum.

3.2. Cyclic voltammetry

Since uric acid and epinephrine have similar oxidation potential at most solid electrodes and many modified electrodes [32,33], overlapped signals are usually obtained. Separated sig-

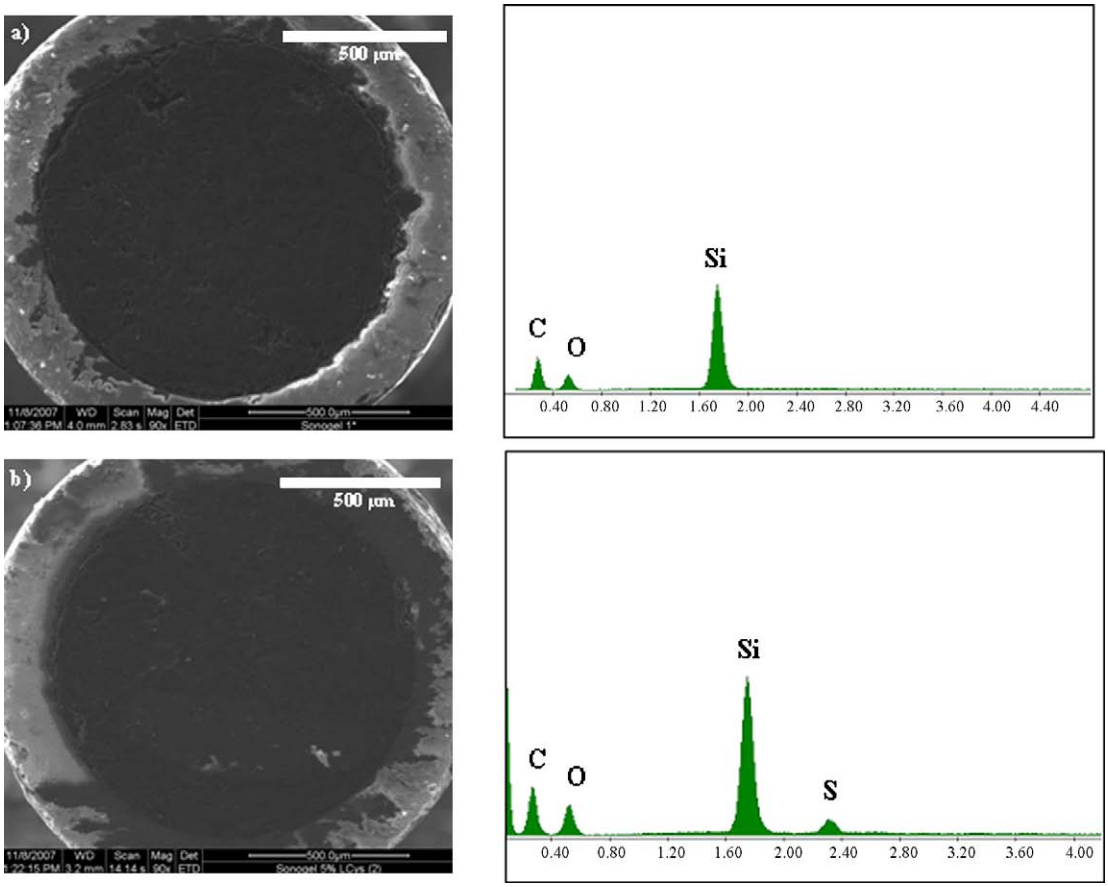

Fig. 1. (a) SEM micrograph and EDS spectrum of a modified Sonogel–Carbon electrode; (b) SEM micrograph and EDS spectrum of a 5% L-Cysteine Sonogel–Carbon modified electrode.

nals can be obtained for UA and EP using a Sonogel–Carbon electrode modified with L-Cysteine. To evaluate the sensitivity and selectivity of this sensor for simultaneous analysis, cyclic voltammograms of mixtures of these species are recorded at 5% L-Cysteine Sonogel–Carbon modified electrode, and compared with an unmodified Sonogel–Carbon electrode (Fig. 3). It can be observed that the peak potentials for EP and UA are indistinguishable at an unmodified Sonogel–Carbon electrode. However, for a 5% L-Cysteine Sonogel–Carbon modified electrode the overlapped voltammetric peaks are resolved into well defined peaks (Fig. 3b) at about 0.38 V and 0.532 V corresponding to the oxidation of EP and UA, respectively.

3.3. Analysis of epinephrine

In bibliography, different detection limits are reported depending of the electrode used and the purpose of the sensing activity. DPV seems to be suitable pulse technique to achieve good result, since it favours the measurement of the faradic over the non-faradic current, which improves sensitivity during the measurements. In this work, the anodic differential pulse peak was used for epinephrine analysis in 0.05 M phosphate buffer solution (pH 6). The calibration curve provided linear relationships for EP: $i = 0.4344 + 0.0521C$, $R^2 = 0.998$, in the range from 10^{-7} to 5×10^{-4} M. The detection limit for EP (S/N = 3) was 8.7×10^{-8} M.

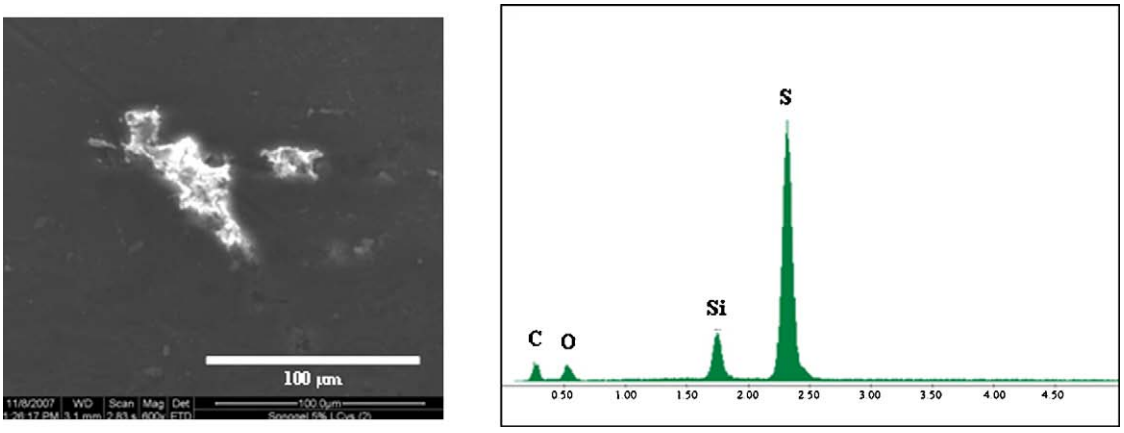

Fig. 2. SEM micrograph detail and EDS spectrum of a L-Cysteine particle in the surface of a modified electrode.

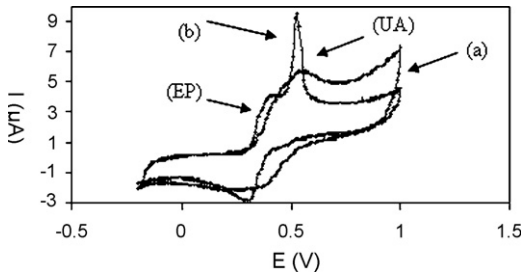

Fig. 3. Cyclic voltammograms for mixture of 10^{-6} M EP and 10^{-4} M UA in 0.05 M phosphate buffer pH 6 (a) unmodified electrode, (b) 5% L-Cysteine Sonogel–Carbon modified electrode. Scan rate 50 mV s^{-1} and $T = 20\,^{\circ}C$.

This value is much lower than values previously obtained [34,35], and compares well with the best values reported [19].

According to SEM studies, the used electrodes containing 5% of modifier exhibit minimum erosion after use; this fact, and the presence of L-Cysteine on the electrode surface, allow us to assume that the properties of the electrodes remain after use. The repeatability of the electrode was estimated by ten repetitive measurements in the same day using the same electrode; relative standard deviation (RSD) of 3.3% was obtained. The useful lifetime is at least one month after repetitive measurements every day. These results show clearly the good performances of our novel sensor.

3.4. Simultaneous determination of EP and UA

Under the optimum condition, the electro-oxidation processes of EP and UA in the mixture were investigated when the concentration of one species changed while the other species was kept constant. The results show that the peak current for EP increased with the increase of EP concentration while the concentration of UA was kept constant. Although the charge current was slightly enhanced after EP oxidation, the anodic peak current for UA did no change. In a similar way, keeping the concentration of EP constant, the oxidation peak current of UA was positively proportional to its concentration, while that of EP did not change. From the experimental results described previously, it was known that in the mixture containing EP and UA the oxidation peak potentials of the two compounds were clearly separated from each other.

The current responses of EP and UA have been investigated to validate the performance of the 5% L-Cysteine Sonogel–Carbon modified electrode for the simultaneous analysis of the two species by changing the concentration of EP and UA in the mixture at the same time. Fig. 4 shows the DPV response at the 5% L-Cysteine Sonogel–Carbon modified electrode simultaneously varying the

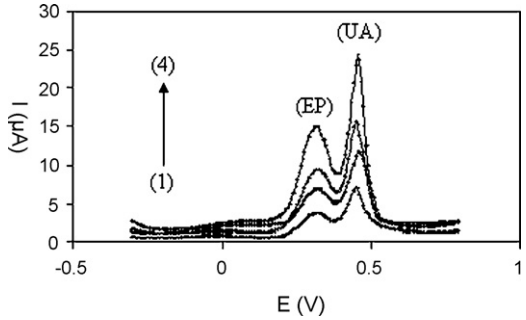

Fig. 4. Differential Pulse Voltmammograms of EP and UA mixtures at a 5% L-Cysteine Sonogel–Carbon modified electrode in phosphate buffer (pH 6). EP contents from 1 to 4 are 1×10^{-6}, 2×10^{-6}, 3×10^{-6} and 6×10^{-6} M, respectively. UA contents from 1 to 4 are 1×10^{-4}, 2×10^{-4}, 3×10^{-4} and 6×10^{-4} M, respectively. Scan rate: 50 mV s^{-1}. Pulse amplitude: 25 mV.

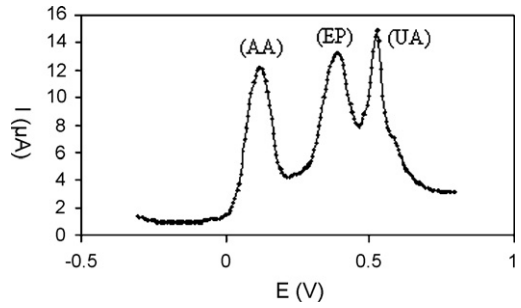

Fig. 5. Differential Pulse Voltammogram of 5×10^{-4} M AA, 5×10^{-6} M EP and 5×10^{-4} M UA mixtures at a 5% L-Cysteine Sonogel–Carbon modified electrode in 0.05 M phosphate buffer (pH 6). Scan rate: 50 mV s^{-1}. Pulse amplitude: 25 mV.

concentration of both EP and UA; the peak current values were proportional to the concentration of EP and UA in the mixture.

3.5. Interference study

It is well known that UA coexists with EP in the extracellular fluid of the central nervous system and its concentration is much higher than that of EP. Hence, UA and AA are important interfering substances for the electrochemical analysis of EP, and the interference from AA and UA was investigated. Fig. 5 shows the DPV of 5×10^{-4} M AA + 5×10^{-6} M EP + 5×10^{-4} M UA in phosphate buffer, pH 6. Well defined anodic peaks at −0.002, 0.277 and 0.438 mV for the oxidation of AA, EP and UA, respectively, were obtained at the 5% L-Cysteine Sonogel–Carbon modified electrode. However, the presence of AA and UA does not modify significantly the signal for EP. The interference studies were also performed with other compounds; for 5×10^{-4} M EP, no interference could be observed for glucose (1:300), glutamic acid (1:300), citric acid (1:200), NaCl (1:700) and KCl (1:700), where the data in brackets were the EP:interferent con-

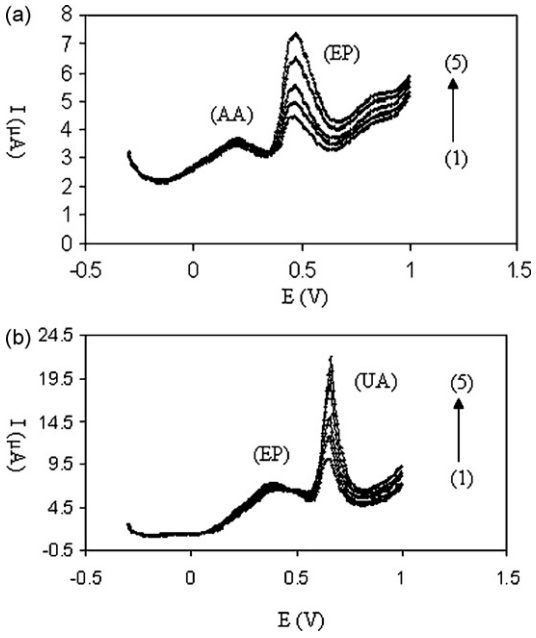

Fig. 6. (a) Differential Pulse Voltammograms of 10^{-4} M AA at a 5% L-Cysteine Sonogel–Carbon modified electrode in urine sample diluted 50 times with phosphate buffer (pH 6) in different concentration of EP (1–5): 2×10^{-6}, 4×10^{-6}, 6×10^{-6}, 8×10^{-6} and 1×10^{-5} M. Scan rate: 50 mV s^{-1}. Pulse amplitude: 25 mV. (b) Differential Pulse Voltammograms of 8×10^{-6} M EP at 5% L-Cysteine Sonogel–Carbon modified electrode in urine sample diluted 50 times with phosphate buffer (pH 6) in different concentration of AU (a–e: 1×10^{-4}, 2×10^{-4}, 4×10^{-4}, 6×10^{-4} and 8×10^{-4} M). Scan rate: 50 mV s^{-1}. Pulse amplitude: 25 mV.

centration ratios. Theses results show a no significant influence of many interferents for EP electrochemical signal at a 5% L-Cysteine Sonogel–Carbon modified electrode.

3.6. Analytical performance in urine sample

The applicability of our Sonogel–Carbon L-Cysteine modified electrode was tested in urine sample. The sample was diluted 50 times with phosphate buffer solution (pH 6) before the measurements to prevent the matrix effect. The DPV recorded for urine sample are shown in Fig. 6. Examination of Fig. 6a shows that peak current of EP increased with an increase in EP concentration, while the concentration of AA was kept constant. As shown in Fig. 6b, keeping the concentration of EP constant, the oxidation peak current of UA was positively proportional to its concentration, while that of EP did not change. These results indicate that selective analysis of AA, EP and UA is possible at a 5% L-Cysteine Sonogel–Carbon modified electrode in urine sample.

4. Conclusion

In this paper, we have prepared a new modified Sonogel–Carbon electrode based on the incorporation of L-Cysteine, and the simultaneous electrochemical analysis of EP and UA in phosphate buffer and urine sample has been tested.

The novel L-Cysteine Sonogel–Carbon electrode shows good behaviour and electrochemical response; thanks to the adequate resolution of EP signal in presence of interferents, the developed electrode is a useful tool for the selective analysis of EP, and for simultaneous electrochemical analysis. The detection limit for EP (8.7×10^{-8} M) is much lower, or compares well with other values reported in literature. The application of the modified Sonogel–Carbon electrode has been also tested in urine sample, with good results.

Acknowledgements

This work was possible thanks to a Research grant of the Ministerio de Asuntos Exteriores y Cooperación of Spain (Programa II. A, Convocatoria general de Becas MAEC-AECI). We would like to express our gratitude to the Junta de Andalucía and Ministerio de Ciencia e Innovación of Spain (CTQ2007-67563/BQU) for their financial support.

References

[1] W.A. Banks, Brain Res. 899 (2001) 209.
[2] L.M. Contretas, R.V.M. Briceno, E.L.P. Pru, Int. J. Dev. Neurosci. 16 (1998) 403.
[3] J.O. Schenk, E. Milker, R.N. Adams, J. Chem. Educ. 60 (1983) 311.
[4] M.A. Fotopoulou, P.C. Loannou, Anal. Chim. Acta 462 (2002) 179.
[5] S. Shelkovnikov, H.C. Gonick, Life Sci. 75 (2004) 2765.
[6] L.Y. Zhang, S.F. Qv, Z.L. Wang, J.K. Cheng, J. Chromatogr. B 792 (2003) 381.
[7] S.L. Wei, G.Q. Song, J.M. Li, J. Chromatogr. A 1098 (2005) 166.
[8] E.M. Garrido, J.L. Lima, D.M. Cristina, J. Pharmceut. Biomed. 15 (1997) 845.
[9] J.X. Du, L.H. Shen, J.R. Lu, Anal. Chim. Acta 489 (2003) 183.
[10] Y.Y. Su, J. Wang, G.N. Chen, Talanta 65 (2005) 531.
[11] J. Michalowski, P. Halabudra, Talanta 55 (2001) 1165.
[12] P. Canizares, L. de Castro, Anal. Chim. Acta 317 (1995) 335.
[13] M.H. Sorouraddin, J.L. Manzoori, E. Kargarzadeh, A.M.H. Shabani, J. Pharmceut. Biomed. 18 (4, 5) (1998) 877.
[14] M. Zhu, X.M. Huang, J. Li, H. Shen, Anal. Chim. Acta 357 (3) (1997) 261.
[15] X.Z. Wu, L.J. Mu, W.Z. Zhang, J. Electroanal. Chem. 352 (1993) 295.
[16] Y. Sun, B. Ye, Y. Wang, X. Tang, X. Zhou, Microchem. J. 58 (2) (1998) 182.
[17] H.S. Wang, D.Q. Huang, R.M. Liu, J. Electroanal. Chem. 570 (2004) 83.
[18] H. Jeong, H. Kim, S. Jeon, Microchem. J. 78 (2004) 181.
[19] S.F. Wang, D. Du, Q.C. Zou, Talanta 57 (2002) 687.
[20] Y.X. Sun, S.F. Wang, X.H. Zhang, Sens. Actuators, B 113 (2006) 156.
[21] H. Kaur, B. Halliwell, Chem. Biol. Interact. 73 (1990) 235.
[22] L. Zheng, S. Wu, X. Lin, L. Nie, L. Rui, Electroanalysis 13 (16) (2001) 1351.
[23] S. Kang, K.K. Shiu, Electroanalysis 13 (2001) 1319.
[24] E. Miland, A.J. Miranda Ordieres, P. Tuñón Blanco, M.R. Smyth, C.O. Fágáin, Talanta 43 (5) (1996) 785.
[25] M.M. Cordero-Rando, J.L. Hidalgo-Hidalgo de Cisneros, E. Blanco, I. Naranjo-Rodriguez, Anal. Chem. 74 (2002) 2423.
[26] J.L. Hidalgo-Hidalgo de Cisneros, M.M. Cordero-Rando, I. Naranjo-Rodriguez, E. Blanco, L. Esquivias Fedriani, Patent P200100556, Spain, March 2001.
[27] L.M. Cubillana-Aguilera, J.M. Palacios-Santander, I. Naranjo-Rodríguez, J.L. Hidalgo-Hidalgo de Cisneros, J. Sol–Gel Sci. Technol. 40 (2006) 55.
[28] M. ElKaoutit, I. Naranjo-Rodríguez, K.R. Tensamani, J.L. Hidalgo-Hidalgo de Cisneros, Biosens. Bioelectron. 22 (2007) 2958.
[29] M.M. Cordero-Rando, I. Naranjo-Rodríguez, J.M. Palacios-Santander, L.M. Cubillana-Aguilera, J.L. Hidalgo-Hidalgo de Cisneros, Electroanalysis 17 (2005) 806.
[30] B. Ballarin, C. Zanardi, L. Schenetti, R. Seeber, J.L. Hidalgo-Hidalgo de Cisneros, Synth. Metals 139 (2003) 29.
[31] S.K. Lunsford, H. Choi, J. Stinson, A. Yeary, D.D. Dionysiou, Talanta 73 (2007) 172.
[32] J.X. Qiao, H.Q. Luo, N.B. Li, Colloids Surf., B: Biointerfaces 62 (2008) 31.
[33] J. Li, X.-Q. Lin, Anal. Chim. Acta 596 (2007) 222.
[34] N. Izaoumen, D. Bouchta, H. Zejli, M. ElKaoutit, A.M. Stalcup, K.R. Temsamani, Talanta 66 (2005) 111.
[35] K.I. Ozoemena, D. Nikosi, J. Pillay, Electrochim. Acta 53 (2008) 2844.

Talanta 79 (2009) 32–37

Contents lists available at ScienceDirect

Talanta

journal homepage: www.elsevier.com/locate/talanta

The natural abundance of ^{13}C with different agricultural management by NIRS with fibre optic probe technology

Mariela Fuentes [a], Inmaculada González-Martín [b,*], Jose Miguel Hernández-Hierro [b], Claudia Hidalgo [a], Bram Govaerts [c], Jorge Etchevers [a], Ken D. Sayre [c], Luc Dendooven [d]

[a] Colegio de Postgraduados, Laboratorio de Fertilidad, IRENAT Km 36.5 Carretera México-Texcoco, Montecillo, México, CP 56230, Mexico
[b] Universidad de Salamanca, Departamento de Química Analítica, Nutrición y Bromatología, Plaza de la Merced s/n, 37008 Salamanca, Spain
[c] International Maize and Wheat Improvement Centre (CIMMYT), Apdo. Postal 6-641, 06600 México, D.F., Mexico
[d] Cinvestav, Dept. Biotechnology and Bioengineering, Av. Instituto Politécnico Nacional 2508, C.P. 07000, México, D.F., Mexico

ARTICLE INFO

Article history:
Received 27 July 2008
Received in revised form 20 February 2009
Accepted 2 March 2009
Available online 13 March 2009

Keywords:
$\delta^{13}C$
Soil
Near infrared reflectance spectroscopy (NIRS)

ABSTRACT

In the present study the natural abundance of ^{13}C is quantified in agricultural soils in Mexico which have been submitted to different agronomic practices, zero and conventional tillage, retention of crop residues (with and without) and rotation of crops (wheat and maize) for 17 years, which have influenced the physical, chemical and biological characteristics of the soil. The natural abundance of C13 is quantified by near infrared spectra (NIRS) with a remote reflectance fibre optic probe, applying the probe directly to the soil samples.

Discriminate partial least squares analysis of the near infrared spectra allowed to classify soils with and without residues, regardless of the type of tillage or rotation systems used with a prediction rate of 90% in the internal validation and 94% in the external validation. The NIRS calibration model using a modified partial least squares regression allowed to determine the $\delta^{13}C$ in soils with or without residues, with multiple correlation coefficients 0.81 and standard error prediction 0.5‰ in soils with residues and 0.92 and 0.2‰ in soils without residues. The ratio performance deviation for the quantification of $\delta^{13}C$ in soil was 2.5 in soil with residues and 3.8 without residues. This indicated that the model was adequate to determine the $\delta^{13}C$ of unknown soils in the −16.2‰ to −20.4‰ range. The development of the NIR calibration permits analytic determinations of the values of $\delta^{13}C$ in unknown agricultural soils in less time, employing a non-destructive method, by the application of the fibre optic probe of remote reflectance to the soil sample.

1. Introduction

The characteristics of a soil vary with tillage and management practices applied, which, in turn, determines soil fertility [1]. Zero tillage is a technique used in conservation agriculture, which guarantees stable yields and better water management while preventing soil degradation. It consists basically in maintaining a permanent or semi-permanent organic cover, i.e. a crop residue or a layer of stubble, over the soil [2].

The determination of $\delta^{13}C$ in soil helps to understand the dynamic of soil organic matter and its origin, being it from C3 or C4 vegetation [3–5] for instance, used $\delta^{13}C$ measurements to demonstrate that the rate of decomposition of soil organic matter increased after tillage. The technique has often been used to study dynamics of C in tropical agro-forestry systems [6–9], but not often in temperate or semi-arid regions [10]. Velázquez et al. [11] evaluated soil quality in different tropical agrosystems using NIRS with discriminant analysis. The spectra of soils were grouped considering type of crop and absence of vegetation, which is similar to our set-up.

The quantification of stable C isotopes using isotope mass spectrometry is an expensive and labour intensive methodology. In the last decade spectroscopic techniques, such as spectroscopy in the near infrared (NIRS), have been developed that facilitate the characterization and quantification of organic material in soil [12]. This technique is fast, accurate, direct without requiring sample preparation and non-destructive. It allows analyzing qualitatively and quantitatively multi-parametric in different matrices thereby reducing costs compared to conventional laboratory techniques without generating wastes [13,14].

The NIRS technology together with the application of mathematical models has been used to quantify chemical elements in

* Corresponding author. Tel.: +34 23 294483; fax: +34 23 294483.
E-mail address: inmaglez@usal.es (I. González-Martín).

0039-9140/$ – see front matter © 2009 Elsevier B.V. All rights reserved.
doi:10.1016/j.talanta.2009.03.002

Table 1
$\delta^{13}C$ of the soils cultivated with maize and wheat subjected to: ZTM+r/−r = zero tillage monoculture with residues or without, ZTR+r/−r = zero tillage rotation with residues or without, CTM+r/−r = conventional tillage monoculture with residues or without and CTR+r/−r = conventional tillage rotation with residues or without.

	$\delta^{13}C$ (‰)					
	Crop: maize			Crop: wheat		
	0–5 cm[a]	5–10 cm	10–20 cm	0–5 cm	5–10 cm	10–20 cm
ZTM+r	−16.56 (0.12)	−18.41 (0.15)	−18.72 (0.27)	−23.28 (0.32)	−21.44 (0.15)	−20.00 (0.13)
ZTR+r	−18.93 (0.43)	−20.01 (0.21)	−19.99 (0.12)	−20.34 (0.65)	−20.52 (0.60)	−19.93 (0.22)
CTM+r	−18.08 (0.16)	−18.02 (0.55)	−18.59 (0.34)	−22.58 (0.57)	−22.07 (0.37)	−21.25 (0.22)
CTR+r	−19.87 (0.17)	−19.77 (0.23)	−19.80 (0.20)	−19.69 (0.31)	−20.00 (0.29)	−19.93 (0.10)
ZTM−r	−20.04 (0.14)	−20.08 (0.19)	−19.78 (0.03)	−21.44 (0.04)	−20.51 (0.06)	−20.06 (0.74)
ZTR−r	−21.47 (0.48)	−20.70 (0.23)	−20.19 (0.15)	−20.98 (0.07)	−20.53 (0.10)	−20.51 (0.42)
CTM−r	−19.05 (0.24)	−19.13 (0.26)	−19.22 (0.16)	−22.06 (0.08)	−21.50 (0.16)	−21.09 (0.14)
CTR−r	−20.15 (0.18)	−20.24 (0.32)	−20.22 (0.31)	−20.70 (0.63)	−21.14 (0.39)	−20.17 (0.02)

Standard errors are given in parentheses ($n = 3$).
[a] Soil depth.

soil, such as organic C and soil organic matter [15–17]. Fourier transformation-NIR (FT-NIR) spectroscopy has been used to study $\delta^{13}C$–CO_2 emission and to quantify CO_2 fluxes of different ecosystem compartments [18] and degradation of ^{13}C straw in coniferous forest in Sweden [19].

The objective of this work is to study the potential of the NIRS with a remote reflectance fibre optic probe in the quantification of $\delta^{13}C$ in soils submitted to different agricultural systems, zero and conventional tillage, rotation of crops (wheat and maize), management of residues (with and without) and generate models that permit the determination of $\delta^{13}C$ in unknown agricultural soils by the direct application of a fibre optic probe to the sample.

2. Materials and methods

2.1. Experimental site

The study was conducted at the El Batán Experimental Station of CIMMYT (Centro Internacional de Mejoramiento de Maíz y Trigo) located in the central highlands of Mexico (19°31′North, 98°50′West, 2259 masl). The soil is a Cumulic Phaeozem [20] with a particle size distribution of 250 g sand kg^{-1} (1000–50 μ), 370 g silt kg^{-1} (50–2 μ) and 380 g clay kg^{-1} (<2 μ). The climate is semi-arid with a monthly mean temperature between 12.5 and 17.5 °C and a mean of 500 mm rainfall $year^{-1}$ mostly during summer.

Sixteen treatments in 7.5 m × 22 m plots were applied in duplicate combining zero tillage or conventional tillage with residues or without residues. The four combinations were sown with monoculture of maize (*Zea mays* L.) or wheat (*Triticum aestivum* L.) and with maize in rotation with wheat or wheat with maize.

The following operations were applied to the zero tillage treatment. Harrowing at 20 cm depth with a disc harrow starting some days after harvest incorporating the crop residue where residue is kept in the field and repeated when needed for weed control (at least once) during the dry season. To prepare the seed bed a spike tooth harrow was used once. The zero tillage plots were sown directly with maize or wheat using an Almaco© seeder and Aitcheson© machine, respectively, both using disc openers for seed placement. In the treatments with residue retention all the residues of the former crop were kept in the field. In conventional tillage plots the residues were ploughed into the ground and in zero tillage they were left on the surface. In the without residues treatments, that is where the residues were removed, most of the aerial residues were removed simulating the farmers practice. All plots were fertilized with nitrogen as urea (120 kg of N Ha^{-1}).

2.2. Soil sampling and chemical analysis

Fifteen soil samples were taken at random from each plot and pooled to form composite samples. Samples were collected from the 0–5 cm, 5–10 cm and 10–20 cm soil layer generally considered to have the largest root content and microorganisms. All samples were air dried and characterized. A 0.5 mm-sieved sub-sample of soil dried at 105 °C for 24 h, carbonates were removed and soil analyzed for $\delta^{13}C$. Carbonates were removed by treating 2 g of finely ground soil with 60 mL of 0.5 M HCl for 24 h [21]. To determine the quantity of soil sample to use in the isotopic analysis, it is necessary to know the content of organic C. The soils with maize have between 24.1 and 10.9 g kg^{-1} dry soil, and the soils with wheat between 23.4 and 11.9 g kg^{-1} dry soil, the group of data present a standard deviation of 0.3.

The samples were air dried, ground and analyzed for $\delta^{13}C$ using a HCNOS EURO EA 3000 elemental analyser with a system of combustion at high temperature and a system of dilution for $\delta^{13}C$ analysis connected to a mass spectrometer with gaseous source in continual flow for the determination of relationships of stable isotopes, model ISOPRIME; made by Micromass. The ^{13}C natural abundance was expressed in $\delta^{13}C$ units using the international PDB standard: $\delta^{13}C = [(^{13}R_{sample}/^{13}R_{standard}) - 1]1000$, where $^{13}R = {}^{13}C/{}^{12}C$. The values in the soils after 16 years of applying different tillage practices are shown in Table 1.

From each of the 100 samples (50 soils with residues and 50 soils without residues), 85 formed the so-called calibration set and the other 15 were used for the external validation. Table 2 presents a summary of the characteristics of the soil samples of the study with the return of the residues (50) and without the return of the residues (50) and within these with maize crops and with wheat crops, indicating the maximum and minimum values of $\delta^{13}C$ and the standard deviation. The values of abundance of ^{13}C obtained with the method of reference (isotope ratio mass spectrometer) are situated in the range of −16.6‰ to −23.3‰ (standard deviation 1.5) for soils with residues and −19.1‰ to −22.1‰ (standard deviation 0.8) for soils without residues.

Table 2
Values of $\delta^{13}C$ isotope composition of soils subjected to different agricultural treatments, quantified with isotopic mass spectrometry technology.

	Soils with retention of crop residues ($N = 50$) maize (25); wheat (25)	Soils without retention of crop residues ($N = 50$) maize (25); wheat (25)
$\delta^{13}C$ (‰)	−16.6 to −23.3	−19.1 to −22.1
S.D.	1.5	0.8

N: Number of samples; S.D.: standard deviation .The mean of the standard deviation of the reference method (stable isotope analysis) for each sample ($n = 3$) was 0.2%.

2.3. NIR spectroscopy

A Foss NIR System 5000 with a standard 1.5 m 210/7210 bundle fibre-optic probe (Ref no. R6539-A) was used for NIR spectroscopy. The probe employs a remote reflectance system and uses a ceramic plate as reference. The quartz window with a 5 cm × 5 cm surface area, allows to measure reflectance in the NIR zone close to 1100–2000 nm. The spectra were recorded at intervals of 2 nm, performing 32 scans for both the reference and samples. All samples were analysed in triplicate to minimize sampling errors. Spectra were stored as the logarithm reciprocal of reflectance ($\log 1/R$) (R = reflectance). The software used for spectral collection, data manipulation and chemometric analysis was Win ISI 1.50 installed on a Hewlett-Packard Pentium III computer. The NIR spectra were determined by applying the fibre optic probe of remote reflectance directly onto the soil without previous treatment or manipulation.

2.4. Statistical analyses for NIR

Sample spectra were pre-processed using a principal component analysis (PCA) to select samples for allocation in either the calibration or validation set and to detect outliers. PCA is a procedure for separating data into orthogonal components whose linear combinations approximate the original data to a selected degree of accuracy [22]. Anomalous spectra were determined by applying the Mahalanobis distance because the risk of there being mistakes in the equations under practical conditions is very low or almost absent when the standardised H-statistic (Mahalanobis distance) is used during routine analysis of unknown samples. This tells us how different the spectrum of the unknown sample is from the average spectrum in the calibration set. Samples with a H-value greater than three may be considered as not belonging to the population from which the equations were developed. Moreover, using the $T \geq 2.5$ criterion, samples that were different from the population owing to chemical criteria were removed from the set. The modified partial least squares (MPLS) regression method was used to obtain the NIR equations for all the parameters studied. Partial least squares (PLS) regression is similar to principal component regression (PCR), but uses both reference data (chemical, physical, etc.) and spectral information to obtain the factors useful for fitting purposes [23]. MPLS is often more stable and accurate than the standard PLS algorithm. In MPLS, the NIRS residuals at each wavelength, obtained after each factor has been calculated, are standardised, i.e. dividing by the standard deviations of the residuals at each wavelength, before calculating the next factor. When developing MPLS equations, cross-validation is recommended to select the optimal number of factors and to avoid overfitting [24]. For cross-validation, the calibration set is partitioned into several groups; each group is then validated using a calibration developed with the other samples. Finally, validation errors are combined into a standard error of cross-validation (SECV) [25]. It has been reported that the SECV is the best single estimate of the prediction capability of the equation and that it is similar to the average standard error of prediction (SEP) from 10 randomly chosen prediction sets. The prediction capacity of the model obtained was evaluated with the ratio performance deviation (RPD) [26]. A capacity parameter defined as the relationship between the standard deviation of the chemical method (S.D. ref) and the standard prediction error (SEP) encountered in the NIRS model. If the RPD value is greater than 2.5, then the model is considered to be suitable. The RPD ratio for the calibration statistics of the properties was used to evaluate the prediction ability of reference methods for NIRS calibration based on the relationship between the error in analysis and the spread in composition. The initial objective was to obtain a model of calibration with all the soil samples, without considering treatment. However, the elevated statistical errors (SECV) indicated that they could not be considered as a spectral group. For that reason, a discriminant analysis was done which used the discriminant partial least squares (DPLS) algorithm, which is a lineal, parametric, discriminant method that permits the modelling of classes. Two perfectly differentiated groups resulted: (a) soils with residues and (b) soils without residues (Fig. 1), regardless of the type of tillage or system of rotation, with 43 and 42

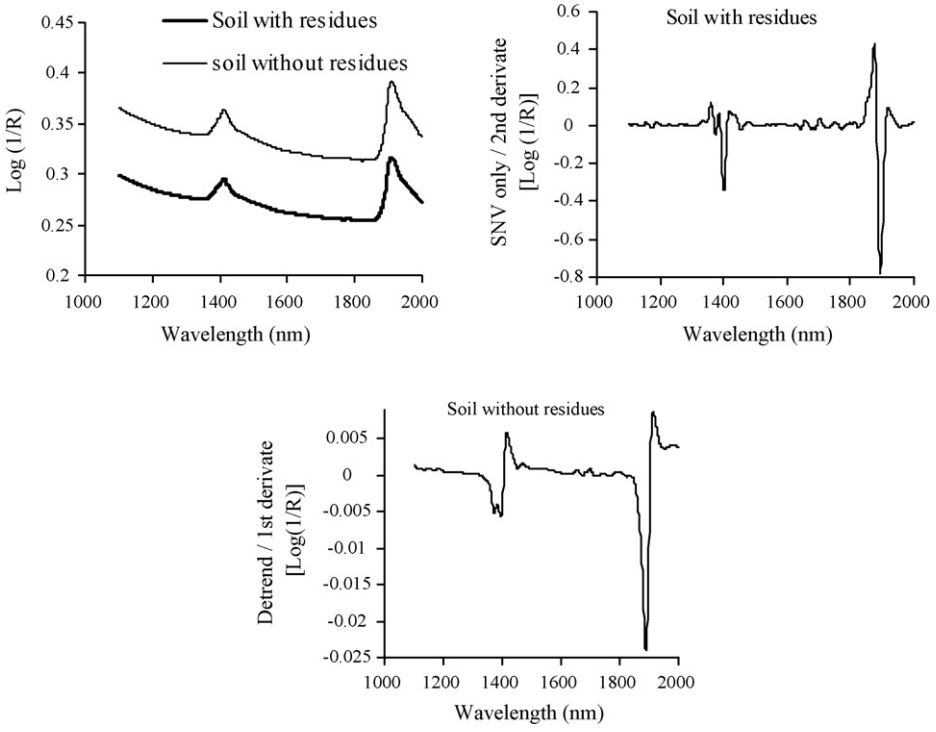

Fig. 1. Soil with and without residues NIR spectrum and mathematical treatments for $\delta^{13}C$ content.

Table 3
Calibration statistical descriptors for NIR determination in $\delta^{13}C$.

Components	*N*	Scatter correction	Mathematical treatment	RSQ	SEC	SECV	CV groups	Est. Min	Mean	Est Max	S.D.
$\delta^{13}C$ in soil with residues	38	SNV	2,4,4,1	0.81	0.5	1.2	7	−16.2	−19.8	−23.4	1.2
$\delta^{13}C$ in soil without residues	37	Detrend	1,4,4,1	0.92	0.2	0.4	7	−18.1	−20.4	−22.7	0.8

Model with residues: three factors PLS; Model without residues: five PLS factors. *N*: Number of samples; S.D.: standard deviation; RSQ: multiple correlation coefficients; SEC: standard error of calibration; SECV: standard error of cross-validation; CV: cross-validation and S.D.: standard deviation.

samples, respectively. The two groups of spectra were analysed separately to generate the mathematical models of quantification of $\delta^{13}C$ in soils with different treatments. The complexity of the NIR signal makes it necessary to apply chemometric techniques that allows modification of the data to quantify $\delta^{13}C$ in soils samples. The effects of scattering were removed using standard normal variate (SNV) mathematical treatment which corrects the problems associated with particle size DeTrend (DT) or SNV-DT. Dhanoa et al. [27] indicated that SNV-DT should be introduced not only to reduce multicollinearity, but also to calculate spectral differences by reducing the confounding effects of baseline shift and curvature. A mathematical treatment was tested in the development of the NIRS calibrations using a nomenclature of 2,4,4,1 and 1,4,4,1 in the case of $\delta^{13}C$ in soil with residues and without residues, respectively, where the first digit is the number of the derivative; the second is the gap over which the derivative is calculated; the third is the number of data points in a running average or smoothing and the fourth is the second smoothing [28]. The statistics used to select the best equations were multiple correlation coefficients (RSQ) and the standard error of cross-validation (SECV) (Table 3).

3. Results and discussion

3.1. Discriminant analysis

On generating the model of calibration of $\delta^{13}C$ by NIRS with all the samples of soil (with and without residues) large errors were obtained for the parameter (SECV). This indicated that there was not a single spectral group. Moreover, the presence or absence of residues (of maize or wheat) in the soil samples generate visually different NIR recordings (Fig. 1). For the former a mathematical model was sought which permitted the discrimination of soils with and without residues by NIR spectroscopy.

The discriminant analysis based on regression by minimum partial squares (DPLS) with the NIR spectral data allows the classification of two perfectly differentiated groups, soils with residues (43 samples) and soils without residues (42 samples), without taking into account the type of crop or systems of rotation employed.

Taking this into account, a DPLS discriminant analysis was done generating two groups of soil, i.e. soils with or without residues (Fig. 2). This indicates that the spectral characteristics are associated both to abundance of ^{13}C and to the presence or absence of residues in the sample. The model of discrimination allows the classification and prediction of soils with or without residues with a prediction rate of 90% in internal validation and of 94% in external validation.

Two models were used to quantify $\delta^{13}C$ in soil, one for treatments with and one for treatments without residues.

3.2. Calibration equations of $\delta^{13}C$

In the pre-treatment of the NIR spectra with PCA, three principal components were obtained for $\delta^{13}C$ in soil with residues or without residues, which explain the spectral variance was higher than 99%. In PCA and MPLS analysis of the NIR spectra, five soil samples with residues and five without residues were eliminated from the calibration set. Two were eliminated for spectral reasons (H criterion) and three for chemical reasons (T criterion) from both groupings. In Table 3, the treatment utilised for the correction of the dispersion, PLS factors, the number of samples used, statistical parameters of RSQ calibration, SEC, mean and margin of applicability of the models of calibration of $\delta^{13}C$ in soils with and without residues is presented. The mathematical treatment used to generate the calibration model was similar to the work of Coûteaux et al. [19], they used first and second derivative with a gap of 4 to quantify $\delta^{13}C$ in soils (forest soils with stubble enriched with $\delta^{13}C$ added).

3.3. Internal validation (prediction)

The model was evaluated by cross-validation. In this method, the set of calibration samples is divided into a series of subsets, in our case seven. Of these, six were taken for the calibration set and one for the prediction set. The NIRS calibration model using MPLS, allowed the determination of $\delta^{13}C$ in soils with and without residues, with multiple correlation coefficients (RSQ) and corrected standard errors of prediction (SEP(C)) of 0.83 and 0.50‰ in soils with residues and of 0.93 and 0.21‰ in soils without them (Figs. 3 and 4). The RPD was used to generate models to calibrate NIRS and as the principal indicator to determine the capacity for prediction [29,30,17]. Some authors consider an RPD > 3 adequate in NIRS analysis for agricultural products [31,32]. However, some reports consider a RPD > 2 as acceptable [29,30]. The calibration model of $\delta^{13}C$ by NIR in this study gave a RPD of 2.5 for the $\delta^{13}C$ in soil with residues and 3.8 in soil without residues. These results indicate that the capacity of prediction is adequate for determining the $\delta^{13}C$ of unknown soils.

3.4. External validation

We checked the robustness of the method by applying NIRS technology to 15 new samples, 8 of soil with residues and 7 of

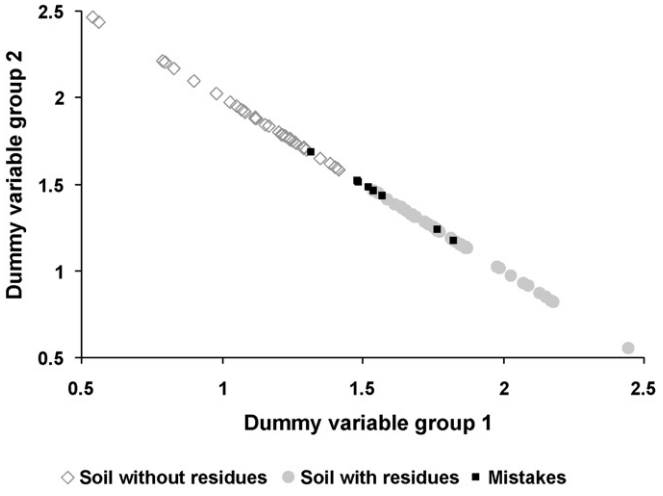

Fig. 2. Discriminant analysis of soils with and without residues.

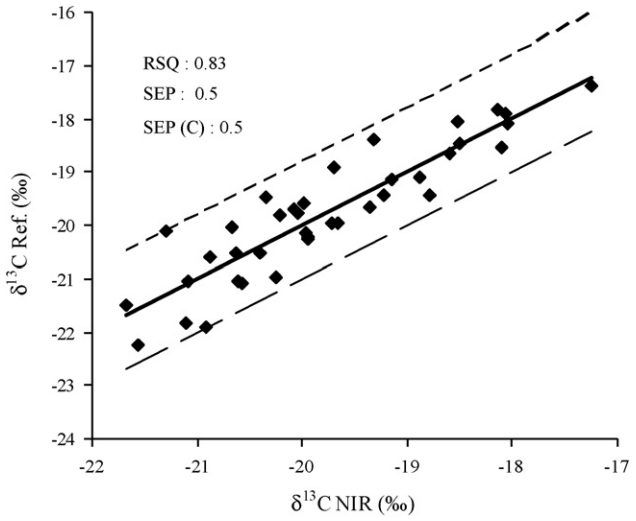

Fig. 3. Comparison of reference values with the values predicted by the calibration for $\delta^{13}C$ in soil with residues.

soil without residues. The procedure was as follows. Spectra were recorded in triplicate and the spectral mean was taken. The calibration equations obtained were applied and the predicted values were compared with the reference according to residuals and root mean standard error (RMSE).

The difference found between the results obtained by the reference method (stable isotopes) and with the NIRS technology was 6.2% for unknown soils samples with residues and 3.3% in soil without residues. The root mean standard error was 1.7 for soils with residues and 0.82 without residues. Furthermore, with the analysis of the Student's *t*-test for paired values, the values of $\delta^{13}C$ obtained with mass spectrometer and those predicted in the external validation with the NIRS model were compared. The levels of significance for soils with residue retention was 0.06 and 0.51 for soils with residue removal. These values were greater than the minimum level of significance 0.05. The null hypothesis is thus accepted and there is no difference between the values of $\delta^{13}C$ generated by the different methods.

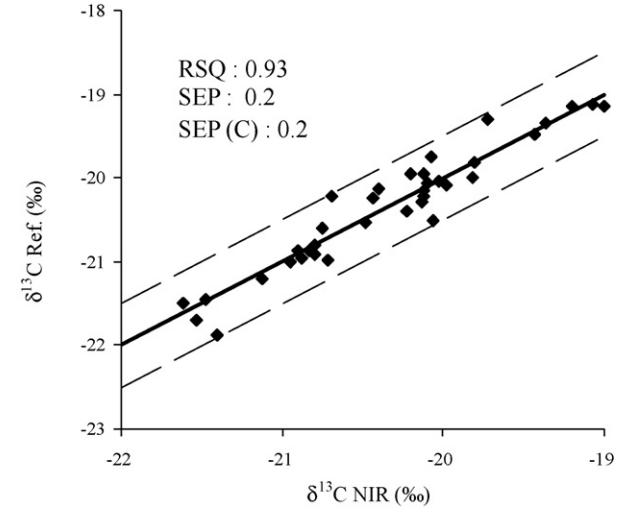

Fig. 4. Comparison of reference values with the values predicted by the calibration for $\delta^{13}C$ in soil without residues.

4. Conclusions

The NIRS technology using an optic fibre probe is a technique with a great potential for the prediction of $\delta^{13}C$ in unknown soils submitted to different types of tillage, crop rotation, plant species (C3 and C4) and residue management. The process involves a previous discrimination of the soil samples with and without residues by the NIR and DPLS discriminant analysis recordings. Afterwards the MPLS models developed for quantify $\delta^{13}C$ are applied.

These findings show that the capacity of prediction is adequate for determining the $\delta^{13}C$ of unknown soils in the −16.2‰ to −20.4‰ range.

It may be concluded that the results obtained with the NIRS method are comparable to those obtained using analytical methods. Isotope mass spectrometry is a rapid, non-destructive and cheap method that does not require previous sample treatment.

Acknowledgements

M. Fuentes received grant-aided support for her doctoral research from CONACYT-Mexico and permission to use the experimental facilities at the International Maize and Wheat Improvement Centre (CIMMYT). This study was made possible by funds from Project Iberoamericano A/7929/07. We thank Mr. G.H. Jenkins for revising the English version of the manuscript.

References

[1] M. Carter, E. Gregorich, D. Angers, R. Donald, M. Bolinder, Soil and Tillage Research 47 (1998) 253–261.
[2] FAO. Conservation Agriculture when agriculture is profitable and sustainable. FAO Land and Water Digital Media Series 18. Land and Water Development Division, Food and Agricultural Organization of the United Nations, Rome, Italy 2002.
[3] M. Stemmer, M. Von Lützow, P.E. Kandeler, H. Gerzabek, European Journal of Soil Science 50 (1999) 73–85.
[4] I. Lobea, R. Bolb, B. Ludwigc, C.C. Du Preezd, W. Amelunge, Soil Biology & Biochemistry 37 (2005) 1898–1909.
[5] J. Balesdent, A. Mariotti, D. Boisgontier, Journal of Soil Science 41 (1990) 587–596.
[6] J. Diels, B. Vanlauwe, N. Sanginga, E. Coolen, R. Merckx, Soil Biology & Biochemistry 33 (2001) 1245–1251.
[7] J. Diels, B. Vanlauwe, M.K. Van der Meersch, N. Sanginga, R. Merckx, Soil Biology & Biochemistry 36 (2004) 1739–1750.
[8] B.H. Ellert, H.H. Janzen, Journal of Geochemical Exploration 88 (2006) 198–201.
[9] M. Oelbermanna, R.P. Voroney, D. Kass, A.M. Schlönvoigt, Geoderma 130 (2006) 356–367.
[10] M. Oelbermanna, R.P. Voroney, Ecological Engineering 29 (2007) 342–349.
[11] E. Velázquez, P. Lavelle, E. Barrios, R. Joffre, F. Reversat, Soil Biology & Biochemistry 37 (2005) 889–898.
[12] J. Theo, in: J. Theo (Ed.), The Application of Vibrational Spectroscopy to Clay Minerals and Layered Double Hydroxides, vol. 13, The Clay Minerals Society, 2005, pp. 2–7.
[13] P. Pelikán, M. Čeppan, M. Linka, Applications of Numerical Methods in Molecular Spectroscopy, CRC Press, Boca Raton, 1994, p. 341.
[14] A. Morón, A. García, J. Sawchik, D. Cozzolino, Journal of the Science of Food and Agriculture 87 (2007) 147–152.
[15] B. Ludwig, P.K. Khanna, J. Bauhus, P. Hopmans, Forest Ecology and Management 171 (2002) 121–132.
[16] D. Cozzolino, A. Morón, Soil and Tillage Research 85 (2006) 78–85.
[17] D. Brunet, B.G. Barthès, J.L. Chotte, C. Feller, Geoderma 139 (2007) 106–117.
[18] J. Mohn, R.A. Werner, B. Buchmann, L. Emmenegger, Journal of Molecular Structure 834 (2007) 95–101.
[19] M. Coûteaux, B. Berg, P. Rovira, Soil Biology & Biochemistry 35 (2003) 1587–1600.
[20] IUSS Working Group WRB, World Reference Base for Soil Resources, FAO, Rome, Italy, 2006, p. 128.
[21] A.J. Midwood, T.W. Boutton, Soil Biology & Biochemistry 30 (1998) 1301–1307.
[22] T. Naes, T. Isaksson, T. Fearn, T. Davies, A User-friendly Guide to Multivariate Calibration and Classification, NIR Publications, Chichester, UK, 2002, p. 344.
[23] H. Martens, T. Naes, Multivariate Calibration, Wiley, Chichester, 2001, p. 116.
[24] J.S. Shenk, M.O. Westerhaus, in: G.C. Fahey (Ed.), Forage Quality, Evaluation and Utilization, ASA, CSSA and SSSA, Madison, WI, 1994, p. 406.
[25] M.C. Davies, P. Williams, Proceedings of the Seventh International Conference on Near Infrared Spectroscopy, NIR Publications, Chichester, West Sussex, UK, 1996, p. 198.

[26] P.C. Williams, D. Sobering, in: A.M.C. Davies, P.C. Williams (Eds.), Near Infrared Spectroscopy: The Future Waves, NIR Publications, West Sussex, Chichester, UK, 1996, p. 185.
[27] M.S. Dhanoa, S.J. Lister, R.J. Barnes, Applied Spectroscopy 49 (1995) 765.
[28] R.J. Barnes, M.S. Dhanoa, S.J. Lister, Applied Spectroscopy 43 (1989) 772.
[29] C.W. Chang, D.A. Laird, M.J. Mausbach, C.R. Hurburgh Jr., Soil Science Society of American Journal 65 (2001) 480–490.
[30] D.J. Brown, R.S. Bricklemyer, P.R. Miller, Geoderma 129 (2005) 251–267.
[31] P.C. Williams, in: P. Williams, K.H. Norris (Eds.), Near-infrared Technology in the Agriculture and Food Industries. American Association of Cereal Chemist, St. Paul, MN, USA, 2001, p. 145.
[32] T. Fearn, NIR News 13 (2002) 12–14.

Talanta 79 (2009) 97–102

Contents lists available at ScienceDirect

Talanta

journal homepage: www.elsevier.com/locate/talanta

A novel amperometric biosensor for the detection of nitrophenol

A.K.M. Kafi, Aicheng Chen*

Department of Chemistry, Lakehead University, 955 Oliver Road, Thunder Bay, Ontario P7B 5E1, Canada

ARTICLE INFO

Article history:
Received 19 December 2008
Received in revised form 4 March 2009
Accepted 5 March 2009
Available online 19 March 2009

Keywords:
Nitrophenol
HRP
Biosensors
TiO_2 nanotube arrays
Methylene blue

ABSTRACT

We report on a novel amperometric biosensor for detecting phenolic compounds based on the co-immobilization of horseradish-peroxidase (HRP) and methylene blue (MB) with chitosan on Au-modified TiO_2 nanotube arrays. The titania nanotube arrays were directly grown on a Ti substrate using anodic oxidation first; a gold thin film was then coated onto the TiO_2 nanotubes by an argon plasma technique. The morphology and composition of the fabricated Au-modified TiO_2 nanotube arrays were characterized by scanning electron microscopy (SEM) and energy-dispersive X-ray spectroscopy (EDS). Cyclic voltammetry and amperometry were used to study the proposed electrochemical biosensor. The effect of pH, applied electrode potential and the concentration of H_2O_2 on the sensitivity of the biosensor have been systemically investigated. The performance of the proposed biosensor was tested using seven different phenolic compounds, showing very high sensitivity; in particular, the linearity of the biosensor for the detection of 3-nitrophenol was observed from 3×10^{-7} to 1.2×10^{-4} M with a detection limit of 9×10^{-8} M (based on the S/N = 3).

1. Introduction

Phenolic compounds are widely used in the chemical industry and, when released into the environment, are considered to be very toxic to both humans and the environment [1–3]. This class of compounds includes highly poisonous, caustic substances derived from coal tar and the production of plastics, dyes, pharmaceuticals, germicides, preservatives and antiseptics. Phenolic compounds are listed by the Agency for Toxic Substances and Disease Registry (ATSDR) as priority hazardous substances. Approximately 165 phenolic compounds are known to have a toxic effect on the environment; among them, nitrophenols are considered as major toxic pollutants. The detection of phenolic compounds is thus very important for measuring toxicity in the environment. Some noticeable detection techniques, such as gas chromatography, liquid chromatography and spectrophotometry, have been employed to determine the presence of phenol and its derivatives [4–7]. However, these methods are time-consuming and require tedious sample preparation and expensive equipment; they are difficult to use for in situ detection in the field. Methods for screening these compounds in the field are of considerable value. The development of in situ enzyme-based electrochemical biosensors has attracted great attention [8–10]. Tyrosinase is the most widely used enzyme for the detection of phenolic compounds [11–14]. However, tyrosinase-based biosensors are limited to the monitoring of phenolic compounds with at least one free *ortho*-position. In addition, tyrosinase-based biosensors show no response to nitrophenol [15]. Therefore, there is great interest in developing electrochemical techniques and other enzyme-based biosensors for the determination of nitrophenols.

It is well known that the major drawbacks inherent to enzyme-based sensors include the difficulty in enzyme immobilization and their limited lifetime due to the desorption and/or deactivation of the immobilized enzymes. The performance of a biosensor mainly depends on the properties of the bioactive layer associated with the transducer [16–20]. It is crucial to retain a high electroactivity of the protein or enzyme immobilized on the electrode surface. Different matrices have been used for the immobilization of HRP [21–23]. Nanostructured materials have been attracting considerable attention because of their regular structure and high active surface area for protein binding [24–27]. Titanium dioxide has been widely used as a photocatalyst and is promising for biosensor design due to its nontoxicity, low cost and high chemical and thermal stability [28–31]. In this paper, we report on a novel nitrophenol biosensor based on the co-immobilization of HRP and methylene blue (MB) with chitosan on Au-modified TiO_2 nanotube arrays. To the best of our knowledge, no electrochemical biosensors have been reported for 3-nitrophenol detection with the exception of one study aimed at developing a *arthrobacter sp.* JS443-based whole cell amperometric biosensor for 4-nitrophenol, where 3-nitrophenol was mentioned as an interfering species [32]. However, the stability of the whole cell based biosensor was very low, losing its response to nitrophenol after 3 days. In this study, the titania nanotubes were fabricated by anodizing titanium foil in a standard two-

* Corresponding author. Tel.: +1 807 3438318; fax: +1 807 3467775.
E-mail address: aicheng.chen@lakeheadu.ca (A. Chen).

0039-9140/$ – see front matter © 2009 Elsevier B.V. All rights reserved.
doi:10.1016/j.talanta.2009.03.015

electrode electrochemical cell containing sodium fluoride (NaF) and hydrofluoric acid (HF). A gold thin film was then uniformly coated on the TiO_2 nanotubes using a plasma sputtering technique. The immobilization of HRP and MB on the TiO_2 nanotubes arrays was achieved by a casting method. Our electrochemical measurements show that the Au-modified TiO_2 nanotubes arrays provide excellent matrixes for the immobilization of HRP and that the immobilized HRP exhibits high stability and retains high catalytical activity. The amperometric response of the designed biosensor to phenolic compounds concentration shows long range linearity. In addition, our study reveals that the presence of MB significantly enhances the sensitivity of the designed biosensor.

2. Experimental

2.1. Reagents and materials

Horseradish peroxidase (EC1.11.1.7, Type X) was purchased from Sigma-Aldrich and used as received. The HRP stock solutions were stored at a temperature of 4 °C. Mehtylene blue was purchased from British Drug Houses Ltd., Poole, England. Hydrogen Peroxide (30%) was bought from Fluka and the stock solutions of H_2O_2 were diluted from that. Nitrophenols and other phenolic compounds were obtained from Sigma-Aldrich. Hydrofluoric acid (HF, 49%) came from Fisher Chemical and dimethyle sulfoxide (DMSO) from Caledon Laboratories Ltd, Canada. All other reagents were of analytical grade and were used as supplied. Water used to prepare all the solutions in this study was purified with a Nanopure® water system. All experiments were performed in 0.1 M phosphate buffer solution (PBS) with different pH values adjusted with K_2HPO_4 and KH_2PO_4.

2.2. Fabrication of biosensors

The TiO_2 nanotube arrays were synthesized by anodic oxidation of Ti substrates [30,33–35]. Briefly, titanium foils were ultrasonically cleaned in acetone and ethanol prior to anodization. After rinsing with distilled water, a clean titanium foil electrode (0.4 cm × 0.5 cm × 0.05 cm) was first etched in 18% HCl at 85 °C for 10 min. The etched titanium foil was rinsed thoroughly with pure water and then anodized at a direct current (DC) voltage of 40 V in a two-electrode electrochemical cell in an electrolyte containing dimethyl sulfoxide (DMSO) and hydrofluoric acid (HF, 2%) for 8 h. A platinum coil was used as the counter electrode and the experiment was conducted at room temperature. After anodization, samples were rinsed thoroughly with pure water and then ultrasonicated to remove surface debris. In order to improve the crystalline properties and remove the remnants of the barrier oxide layer after the anodic reaction, the samples were annealed at 450 °C for 1 h. The Au thin film was then coated onto the TiO_2 nanotube arrays by argon plasma sputtering for 30 s. Finally, 20 μL of 2 mg/mL of HRP and 20 μL of 1 mg/mL of MB and 10 μL of 2 mg/mL of chitosan were co-immobilized onto the synthesized Au-coated TiO_2 nanotube arrays (Ti/TiO_2/Au/HRP-MB). Chitosan was used here because of its excellent membrane-forming ability, good adhesion, biocompatibility, nontoxicity and high mechanical strength, which make the biosensor more stable [36]. For comparison, a biosensor based on TiO_2/Au without MB (Ti/TiO_2/Au/HRP) and TiO_2 nanotube arrays without the Au thin film (Ti/TiO_2/HRP) were also fabricated. All resulting electrodes were stored in 0.1 M PBS (pH 7.0) and at 4 °C when not in use.

2.3. Instrument and electrochemical measurements

The morphology and the composition of the synthesized TiO_2 nanotube arrays were characterized by scanning electron microscope (SEM) (JEOL JSM 5900 LV), at an acceleration voltage of 13 kV, and an energy-dispersive X-ray (EDX) spectrometer. Electrochemical measurements were carried out with a CHI (630B) workstation. A three-electrode configuration was employed for these experiments. The fabricated biosensors were employed as the working electrodes. A platinum coil was connected as the counter electrode and a KCl saturated Ag/AgCl electrode was used as the reference electrode. Cyclic voltammetric measurements were carried out in 0.1 M PBS by applying 0.0 to −0.8 V vs. Ag/AgCl sweep range in the negative scanning direction. Amperometric responses were measured in a stirred cell by applying a potential of −0.05 V to the working electrode. A magnetic stirrer was used for this experiment. All measurements were performed at room temperature.

3. Results and discussion

3.1. Structural characterization of TiO_2 nanotube arrays

The morphology and composition of the Ti substrate after anodization were examined by SEM observation and EDS analysis. Fig. 1A shows a typical SEM image of the TiO_2 nanotube arrays with a sputtered Au thin film as fabricated in this study. The TiO_2 nanotube arrays were directly grown on the Ti substrate by anodizing the Ti substrate in the electrolyte containing DMSO and 2% HF at 40 V for 8 h. The typical dimensions are calculated to be ~90 nm outer diameter, ~70 nm inner diameter, ~20 nm wall-thickness. Fig. 1B shows the EDS spectrum of the Au-modified nanotube arrays. Both Ti and O peaks are observed, and the ratio of Ti to O is close to 1:2, confirming that the formed nanotubes are TiO_2. The strong Au peak is derived from the Au thin film sputtered on the TiO_2 nanotube arrays. The adhesion and integrity of the synthesized TiO_2 nanotube layer are essential for the effective immobilization of biomolecules.

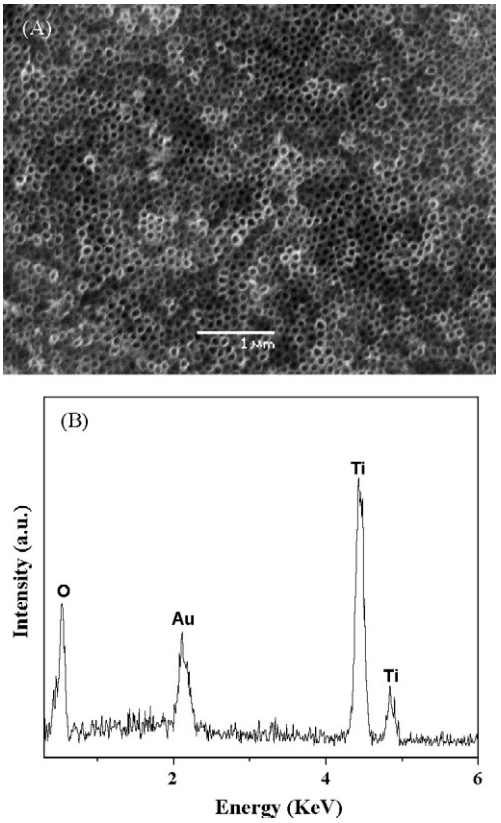

Fig. 1. (A) SEM image of TiO_2 nanotube arrays directly grown on Ti substrates, (B) EDS spectrum of Au-modified TiO_2 nanotube arrays.

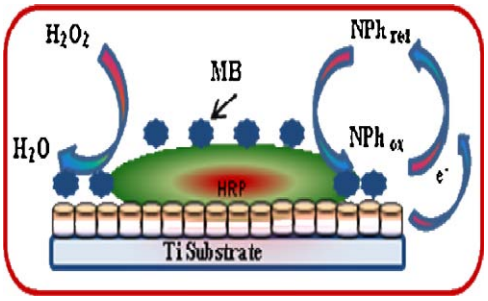

Scheme 1. Schematic diagram of the biosensor in response to nitrophenol.

This anodization method is preferable to other methods such as sol–gel and electrophoretic deposition because the TiO_2 layer is directly grown on the Ti substrate, thus exhibiting much better adhesion to the Ti substrate than that of other methods [37]. Since the TiO_2 nanotube arrays make a tightly adherent surface layer on the Ti substrate and, by taking in all other considerations such as non-toxicity, high surface area and strong thermal and chemical stability, it can be seen that the synthesized TiO_2 nanotube arrays are promising for biosensing applications.

3.2. The principle of HRP-modified electrodes for phenolic compounds detection

It has been reported that peroxidase cycles of HRP can be activated by H_2O_2 to generate active oxyferryl radicals [38]. The immobilized peroxidase on an electrode surface can be reduced to its native state by direct or mediated electron transfer in encountering phenol, aromatic amines, ferrocenes, and amine ruthenium complexes [39–42]. The response of a phenolic biosensor is based on the double displacement mechanism in which two substrates, peroxide (normally H_2O_2) and the given phenolic compounds, are involved [43]. The structure of the electrode developed in the present work as well as the enzymatic mechanism used to create a biosensor based on HRP for phenolic compound detection is proposed in Scheme 1. The reactions consist of the oxidation of the heme group of HRP molecules by H_2O_2 and the reduction by the phenolic compound. In the latter reaction, the phenolic compounds are mainly converted into free radical products which are electroactive and can be electrochemically reduced on the electrode surface [10]. The resulting reduction current is proportional to the concentration of phenolic compounds in solution as long as the H_2O_2 concentration is not limiting.

3.3. CV of the modified electrodes

Fig. 2 shows the cyclic voltammograms (CVs) of the Ti/TiO_2 (dashed line) and $Ti/TiO_2/Au$ (solid line) electrodes recorded in a 0.1 M KCl + 5.0×10^{-3} M $Fe(CN)_6^{3-/4-}$ solution at a sweep rate of 50 mV/s. TiO_2 is a semiconductor and its electrical conductivity is relatively low. As expected, neither an oxidation nor reduction peak is observed in the CV of the Ti/TiO_2 electrode. However, a well-defined and large pair of oxidation peaks located at 0.35 V, and a reduction peak centered at 0.1 V appear in the CV of the $Ti/TiO_2/Au$ electrode. The above results show that the presence of the Au thin film significantly increases the electrical activity of the TiO_2 nanotube arrays.

3.4. Biosensor behavior

As seen in Scheme 1, H_2O_2 plays an important role in the detection of phenolic compounds. Before we tested the prepared biosensor for nitrophenols detection, we studied its response to

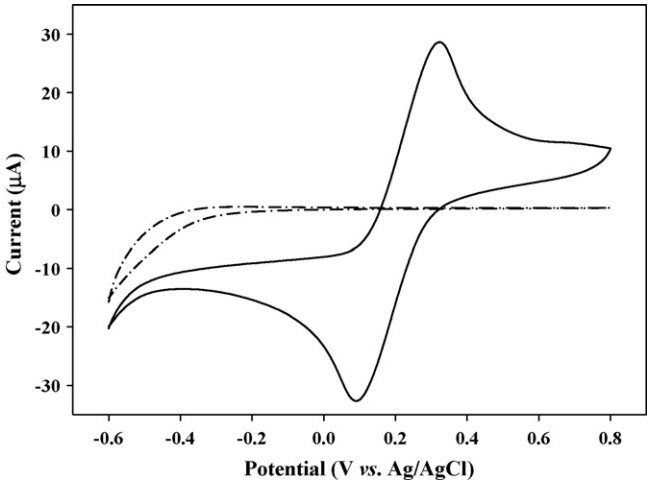

Fig. 2. Cyclic voltammamograms of the Ti/TiO_2 (dashed line) and $Ti/TiO_2/Au$ (solid line) electrodes recorded in 5×10^{-3} M $Fe(CN)_6^{3-/4-}$ + 0.1 M KCl solution at a scan rate of 50 mV/s.

H_2O_2. Fig. 3 compares the CV curves of the $Ti/TiO_2/Au/HRP/MB$ electrode in 0.1 M PBS (pH 7.0) in the presence of 3.0×10^{-3} M H_2O_2 (solid line) and in the absence of H_2O_2 (dashed line) at a scan rate of 50 mV/s, showing that the prepared biosensor has a strong response to H_2O_2. To reveal the effect of methylene blue, the CVs of the $Ti/TiO_2/Au/HRP$ electrode in the absence of (dotted line) and in the presence of 3.0×10^{-3} M H_2O_2 (dashed line) in 0.1 M PBS (pH 7.0) at a scan rate of 50 mV/s are presented in the inset of Fig. 3. The current response of the $Ti/TiO_2/Au/HRP$-MB electrode is ~120% higher for H_2O_2 reduction than that of the $Ti/TiO_2/Au/HRP$ electrode, demonstrating that MB plays an important role as an electron mediator.

Fig. 4 shows the linear sweep voltammograms of the $Ti/TiO_2/Au/HRP$-MB electrode scanned from −0.3 to +0.3 V in various solutions (a–e). Comparison of Curve a and b shows that there is almost no increase in amperometric current for this biosensor when only 3-NPh was introduced into the electrolyte. The amperometric current slightly increases while only H_2O_2 was injected (Curve c), due to the catalytic reduction of H_2O_2 on the electrode. Interestingly, when both 3-NPh and H_2O_2 were added (Curve d), a high amperometric current appears, indicating the presence of

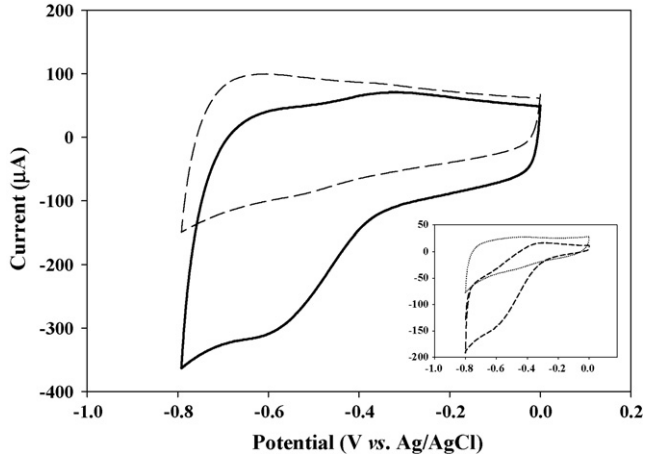

Fig. 3. Cyclic voltammamograms of the $Ti/TiO_2/Au/HRP$-MB electrode in the absence (dashed) and presence (solid) of 3×10^{-3} M H_2O_2 in 0.1 M PBS (pH 7.0) at a scan rate of 50 mV/s. The inset shows the CVs of $Ti/TiO_2/Au/HRP$ in the absence (dotted line) and presence (dashed line) of 3×10^{-3} M H_2O_2 in 0.1 M PBS (pH 7.0) at a scan rate of 50 mV/s.

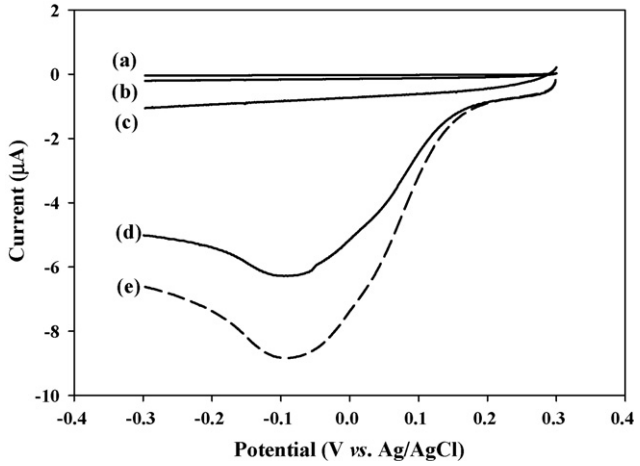

Fig. 4. Linear sweep voltammograms of the Ti/TiO_2/Au/HRP-MB electrode recorded (a) in the blank solution 0.1 M PBS (pH 7.0); (b) in the presence of 2.5×10^{-5} M 3-nitrophenol; (c) in the presence of 2.5×10^{-5} M H_2O_2; (d) in the presence of 2.5×10^{-5} M 3-nitrophenol and 2.5×10^{-5} M H_2O_2; (e) in the presence of 5×10^{-5} M 3-nitrophenol and 2.5×10^{-5} M H_2O_2.

H_2O_2 is necessary for the detection of 3-NPh. When we increase the concentration of 3-NPh to 5.0×10^{-5} M 3-NPh, the amperometric current is further increased (Curve e), showing that 3-NPh is responsible for this enhanced current. The high sensitivity observed at the Ti/TiO_2/Au/HRP-MB electrode for 3-NPh indicates that the electron mediator MB greatly accelerates the electron transfer [28].

3.5. Optimal parameters

The effect of an applied potential on the amperometric response of the biosensor was investigated. Fig. 5A shows the influence of applied potential on the biosensor response to 3-NPh. The biosensor exhibits a maximum current at −0.05 V when the electrode potential was changed from −0.3 V to 0.1 V. As mentioned in Section 3.2, the biosensing mechanism consists of the oxidation of the heme group of HRP molecules by H_2O_2 and the reduction by nitrophenol. In the latter reaction, the nitrophenol is converted into radical intermediates which are electroactive and can be electrochemically reduced on the electrode surface. The decrease of the current is likely due to the polymerization of the formed radicals at the more negative potentials.

A similar effect was also observed for the tyrosinase-based biosensors for catechol and phenol [44,45].

It is known that the presence of a high concentration of H_2O_2 results in inhibition of enzyme activity [37,46]. To achieve high sensitivity and avoid the formation of inactive enzymes caused by high concentrations of H_2O_2, we studied the effect of the H_2O_2 concentration on the Ti/TiO_2/Au/HRP-MB biosensor in 0.1 M PBS (pH 7.0) containing 25 μM 3-NPh under the optimized electrode potential −0.05 V as shown in Fig. 5B. This reveals that the maximum amperometric response was achieved in the presence of 20 μM H_2O_2. We further investigated the effect of the solution's pH on the biosensor response. The influence of pH was evaluated over the pH range of 3.0 to 9.0. As shown in Fig. 5C, a much lower response was obtained in the case of pH lower than 6.0 or higher than 8.0, showing that pH 7.0 is the optimum solution pH for the biosensor fabricated in this study.

3.6. Amperometric response of the biosensor

The amperometric response of the Ti/TiO_2/Au/HRP-MB biosensor was tested in a stirred cell containing 0.1 M PBS (pH 7.0) under the optimized operating electrode potential of −0.05 V. For comparison, Fig. 6A presents the typical amperometric responses of three different electrodes (a–c) in the presence of 2×10^{-5} M H_2O_2 for successive additions of 3-NPh. The corresponding calibration plots for the three amperometric response curves are shown in Fig. 6B. The amperometric response of the Ti/TiO_2/Au/HRP electrode (Curve b) to 3-NPh is much higher than that of the Ti/TiO_2/HRP

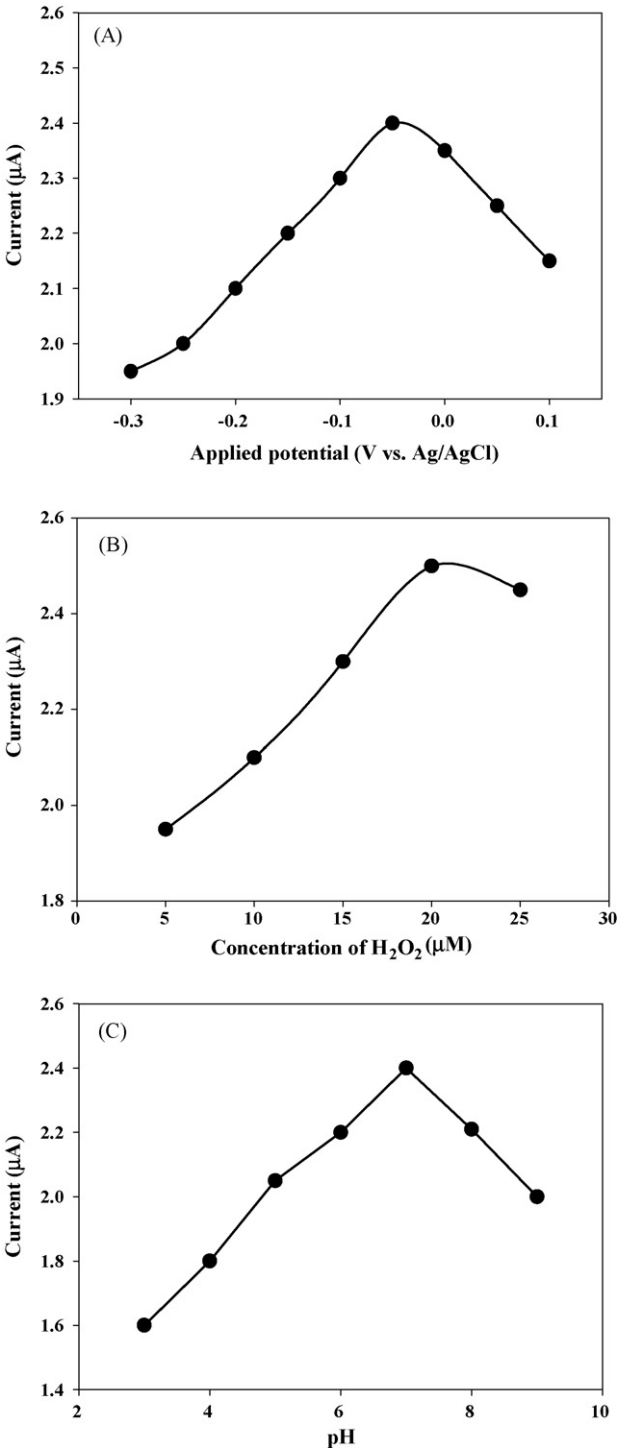

Fig. 5. (A) Dependence of catalytic current of the biosensor at different applied potentials measured in a pH 7.0 PBS containing 2.5×10^{-5} M 3-nitrophenol and 2.5×10^{-5} M H_2O_2. (B) Effect of the H_2O_2 concentration on the amperometric response of the Ti/TiO_2/Au/HRP-MB electrode to 2.5×10^{-5} M 3-nitrophenol in 0.1 M PBS (pH 7.0) at the potential of -0.05 V; (C) influence of pH on the catalytic current of the biosensor in the presence of 2.5×10^{-5} M 3-nitrophenol in 0.1 M PBS containing 2×10^{-5} M H_2O_2 at the potential of −0.05 V.

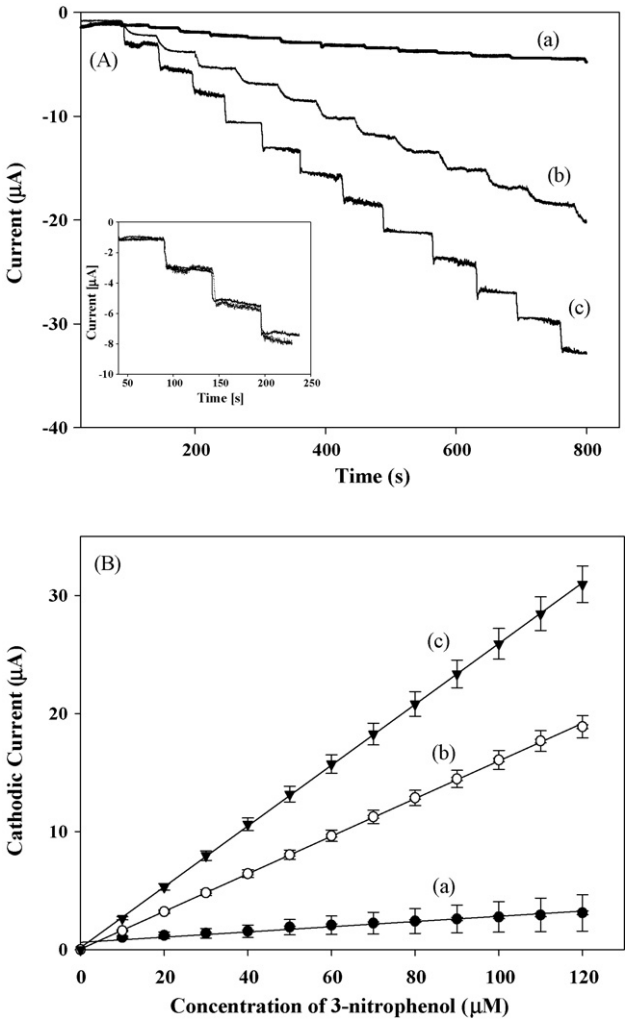

Fig. 6. (A) Typical amperometric response of the Ti/TiO_2/HRP (a), Ti/TiO_2/Au/HRP (b), and Ti/TiO_2/Au/HRP-MB (c) electrodes with successive additions of 1×10^{-5} M 3-nitrophenol in 0.1 M PBS (pH 7.0) in the presence of 2×10^{-5} M H_2O_2 at the operating potential of −0.05 V. Inset: the amperometric response of the Ti/TiO_2/Au/HRP-MB electrode after 45 days under same experimental conditions (solid line); (B) calibration plots of the proposed biosensors (the same experimental conditions as in A).

electrode (Curve a). The presence of MB on the electrode surface (Curve c) further increases the response of the biosensor. As seen in Curve c, the response of the Ti/TiO_2/Au/HRP-MB biosensor is very quick; over 95% of the steady state current is achieved within 5 s. Under these optimized experimental parameters, the Ti/TiO_2/Au/HRP-MB biosensor fabricated in this study shows a linear response in the range of 3×10^{-7} to 1.2×10^{-4} M 3-NPh with a correlation coefficient of 0.993 and very high sensitivity (0.35 μA/μM). This is 87 times higher than the *arthrobacter sp.* JS443-based whole cell amperometric biosensor [32]. The detection limit is estimated to be 9×10^{-8} M 3-NPh (based on S/N = 3). The performance of the Ti/TiO_2/Au/HRP-MB biosensor developed in this study has also been tested with six other phenolic compounds: phenol, 2-nitrophenol, 4-nitrophenol, m-cresol, p-cresol and 3-chlorophenol. As summarized in Table 1, the developed Ti/TiO_2/Au/HRP-MB biosensor exhibits a long linear range, high sensitivity and very low detection limit for all the tested phenolic compounds. Further study is needed to improve its selectivity.

3.7. Stability and reproducibility of the biosensor

The long-term stability of this biosensor was also investigated. The Ti/TiO_2/Au/HRP-MB electrode was stored in PBS (pH 7.0) at 4 °C when not being in use. The Ti/TiO_2/Au/HRP-MB biosensor fabricated in this study is extremely stable, and it retains 92% of its initial current response after 45 days as shown in the inset to Fig. 6A (solid line). The repeatability of the biosensor for the established current response was also examined, showing that the relative standard deviation (RSD) was 3.55% for 10 successive measurements with 2×10^{-5} M 3-NPh. To compare the performance of the biosensor fabricated in this study, we searched the literature. On one hand, we did not find any biosensor for 3-nitrophenol detection. To the best of our knowledge, the Ti/TiO_2/Au/HRP-MB electrode developed in this study is the first electrochemical biosensor for 3-nitrophenol detection. On the other hand, we found a number of biosensors for phenol detection in the literature. Table 2 compares the performance of the Ti/TiO_2/Au/HRP-MB biosensor for phenol detection with the reported electrochemical biosensors [15,45,47–50], revealing that the biosensor proposed in this study exhibits a very long linearity, high sensitivity, low detection limit and high stability, very promising for the detection of phenolic compounds.

Table 1
The performance of the biosensor proposed in this study for the detection of different phenolic compounds.

Phenolic compounds	Linear range	Sensitivity (μA/μM)	LOD
Phenol	8×10^{-7} to 1.3×10^{-4} M	0.19 (r = 0.996; n = 15)	1.95×10^{-7} M
2-nitrophenol	4×10^{-7} to 1.4×10^{-4} M	0.29 (r = 0.997; n = 15)	1.20×10^{-7} M
3-nitrophenol	3×10^{-7} to 1.2×10^{-4} M	0.35 (r = 0.993; n = 15)	9.00×10^{-8} M
4-nitrophenol	3×10^{-7} to 1.4×10^{-4} M	0.30 (r = 0.999; n = 15)	1.10×10^{-7} M
m-Cresol	6×10^{-7} to 1.2×10^{-4} M	0.26 (r = 0.991; n = 15)	1.35×10^{-7} M
p-Cresol	8×10^{-7} to 1.1×10^{-4} M	0.19 (r = 0.997; n = 15)	1.90×10^{-7} M
3-Chlorophenol	7×10^{-7} to 1.1×10^{-4} M	0.23 (r = 0.996; n = 15)	1.55×10^{-7} M

Table 2
Comparison of the performance of the electrochemical biosensor developed in this study with other biosensors reported in the literature for the detection of phenol.

Immobilization matrix	Linearity	Sensitivity	LOD	Stability	Ref
Tyr/nano-$MgFe_2O_4$–SiO_2	1–250 μM	54.2 mA/M	600 nM	70% (30 days)	15
Tyr/electropolymerized PTS-doped polypyrrole	3.3–220 μM	17.1 μA/mM	8.0×10^{-7} M	80% (90 days)	47
Tyr/Au nanoparticles with GC electrode	1–40 μM	82 μA/mM	2.1×10^{-7} M	N/A	45
Tyr/core-shell magnetic nanoparticles	1–250 μM	54.2 μA/mM	6×10^{-7} M	70% (30 days)	48
Tyr/sonogel-carbon	0.5–30 μM	32 nA/μM	3×10^{-7} M	80% (40 days)	49
HRP/sol–gel with GC	5–50 μM	3.65 nA/μM	8×10^{-7} M	80% (30 days)	50
HRP-TiO_2 nanotube	0.8–130 μM	0.19 μA/μM	2×10^{-7} M	92% (45days)	Proposed

Tyr = Tyrosinase; HRP = Horseradish peroxidase; GC = Glassy carbon.

4. Conclusions

In this paper, we have presented a promising electrochemical biosensor for the detection of phenolic compounds based on the co-immobilization of HRP and MB with chitosan on Au-modified titanium dioxide nanotube arrays. The titania nanotube arrays were directly grown on a titanium substrate by simple anodic oxidation. These titania nanotube arrays possess large surface area and good uniformity, ideal matrixes for enzyme immobilization. The presence of an Au thin film greatly increases the electrical activity of the formed TiO_2 nanotube arrays. Our electrochemical measurements reveal that the immobilized HRP exhibits high biological activity and stability and that the presence of methylene blue further enhances the sensitivity of the designed electrochemical biosensor for phenolic compounds. The developed biosensor exhibits fast amperometric response, high sensitivity, low detection limit and long-time stability for 3-nitrophenol. This study provides proof-of-concept for the development of HRP-based biosensors for the detection of high toxic nitrophenolic pollutants.

Acknowledgments

This work was supported by a Discovery Grant from the Natural Sciences and Engineering Research Council of Canada (NSERC). A.K.M. Kafi acknowledges the Ontario Post Doctoral Fellowship. A. Chen acknowledges NSERC and the Canada Foundation of Innovation (CFI) for the Canada Research Chair Award in Material and Environmental Chemistry.

References

[1] Z. Liu, B. Liu, J. Kong, J. Deng, Anal. Chem. 72 (2000) 4707.
[2] L. Coche-Guerente, P. Labbe, V. Mengeaud, Anal. Chem. 73 (2001) 3206.
[3] J. Febortova, V. Tatarvicova, Analyst 119 (1994) 1519.
[4] A.J.H. Louter, P.A. Jonse, J.D. Jorritsma, J.J. Vreuls, U.A.T. Brinkman, Chromatography 20 (1997) 363.
[5] O. Jauregui, M.T. Galceran, Anal. Chim. Acta 340 (1997) 191.
[6] E. Orejuela, M. Silva, Analyst 127 (2002) 127.
[7] V. Janda, K. Krijit, J. Chromatogr. 283 (1984) 309.
[8] F.D. Munteanu, A. Lindgren, J. Emneus, L. Gorton, T. Ruzgas, E. Csoregi, A. Ciucu, A. Van, R.B. Huystee, I.G. Gazaryan, L.M. Lagrimini, Anal. Chem. 70 (1998) 2596.
[9] S.S. Rosatto, L.T. Kubota, G.O. Neto, Anal. Chim. Acta 390 (1999) 65.
[10] X.J. Wu, M.M.F. Choi, X.M. Wu, Analyst 129 (2004) 1143.
[11] B. Wang, J. Zhang, S. Dong, Biosens. Bioelectron. 15 (2001) 397.
[12] C. Védrine, S. Fabiano, C. Tran-Minh, Talanta 59 (2003) 535.
[13] J. Abdullah, M. Ahmad, L.Y. Heng, N. Karuppiah, H. Sidek, Talanta 70 (2006) 527.
[14] L.D. Mello, M.D.P.T. Sotomayor, L.T. Kubota, Sens. Actuators B: Chem. 96 (2003) 636.
[15] Z.J. Liu, B.H. Liu, J.L. Kong, J.Q. Deng, Anal. Chem. 72 (2000) 4707.
[16] S. Liu, L. Bakovic, A. Chen, J. Electroanal. Chem. 591 (2006) 210.
[17] Y. Jung, J.Y. Jeong, B.H. Chung, Analyst 133 (2008) 697.
[18] T.P. Rao, R. Kala, Talanta 76 (2008) 485.
[19] S. Liu, B. Miller, A. Chen, Electrochem. Commun. 7 (2005) 1232.
[20] A. Ramanavicius, A. Kausaite, A. Ramanaviciene, Analyst 133 (2008) 1083.
[21] S. Korkut, B. Keskinler, E. Erhan, Talanta 76 (2008) 1147.
[22] M. Tian, N. Kanavillil, L. Davey, K.T. Leung, H. Schraft, A. Chen, J. Electroanal. Chem. 611 (2007) 133.
[23] Y.T. Kong, M. Boopathi, Y.B. Shim, Biosens. Bioelectron. 19 (2003) 227.
[24] J. Wang, M. Musameh, Y. Lin, J. Am. Chem. Soc. 125 (2003) 2408.
[25] W. Tremel, Angew. Chem. Int. Ed. 38 (1999) 2175.
[26] Y. Coffinier, S. Janel, A. Addad, R. Blossey, L. Gengembre, E. Payen, R. Boukherroub, Langmuir 23 (2007) 1608.
[27] K.B. Male, S. Hrapovic, J.H.T. Luong, Analyst 132 (2007) 1254.
[28] A.K.M. Kafi, G. Wu, A. Chen, Biosens. Bioelectron. 24 (2008) 566.
[29] G. Wu, T. Nishikawa, B. Ohtani, A. Chen, Chem. Mater. 19 (2007) 4530.
[30] S. Yoriya, M. Paulose, O.K. Varghese, G.K. Mor, C.A. Grimes, J. Phys. Chem. C 111 (2007) 13770.
[31] S. Liu, A. Chen, Langmuir 21 (2005) 8409.
[32] Y. Lei, P. Mulchandani, W. Chen, J. Wang, A. Mulchandani, Electroanalysis 16 (2004) 2030.
[33] C. Richter, E. Panaitescu, R.J. Welly, L. Menon, J. Nanosci. Nanotechnol. 22 (2007) 1624.
[34] A. Ghicov, J.M. Macak, H. Tsuchiya, J. Kunze, V. Haeublein, L. Frey, P. Schmuki, Nano Lett. 6 (2006) 1080.
[35] M. Tian, G. Wu, B. Adams, J. Wen, A. Chen, J. Phys. Chem. C 112 (2008) 825.
[36] X.L. Luo, J.J. Xu, Q. Zhang, G.J. Yang, H.Y. Chen, Biosens. Bioelectron. 21 (2005) 190.
[37] X.F. Xiao, T. Tian, R.F. Liu, H.D. She, Mater. Chem. Phys. 106 (2007) 27.
[38] S.I. Imabayashi, Y.T. Kong, M. Watanabe, Electroanalysis 13 (2001) 408.
[39] B. Dunford, A.J. Adeniran, Arch. Biochem. Biophys. 251 (1986) 536.
[40] D. Job, B. Dunford, Eur. J. Biochem. 66 (1976) 607.
[41] J. Kulys, U. Bilitewski, R.D. Schmid, Bioelectrochem. Bioenerg. 16 (1991) 277.
[42] M.H. Smit, A.E.G. Cass, Anal. Chem. 62 (1990) 2429.
[43] J.E. Frew, M.A. Harmer, H.A.O. Hill, S.I. Libor, J. Electroanal. Chem. 201 (1986) 1.
[44] N. Peña, A.J. Reviejo, J.M. Pingarrón, Talanta 55 (2001) 179.
[45] V. Carralero Sanz, M. Luz-mena, A. González-Cortés, P. Yáñez- Seden, J.M. Pingarrón, Anal. Chim. Acta 528 (2005) 1.
[46] H. Anni, T. Yonetani, in: H. Siegel, A. Siegel (Eds.), Marcel Dekker, New York, 1992.
[47] W. Rajesh, K. Takashima, K. Kaneto, React. Funct. Polym. 59 (2004) 163.
[48] Z. Liu, Y. Liu, H. Yang, Y. Yang, G. Shen, R. Yu, Anal. Chim. Acta 533 (2005) 3.
[49] H. Zejli, J.L. Cisnerosc, I. Naranjo-Rodriguezc, B. Liu, K.R. Temsamanib, J.L. Martya, Anal. Chim. Acta 612 (2008) 198.
[50] A.K.M. Kafi, D.Y. Lee, S.H. Park, Y.S. Kwon, Thin Solid Films 516 (2008) 2816.

Talanta 79 (2009) 16–21

Contents lists available at ScienceDirect

Talanta

journal homepage: www.elsevier.com/locate/talanta

Single-run ion chromatographic separation of inorganic and low-molecular-mass organic anions under isocratic elution: Application to environmental samples

Agnieszka Krata[a,*], Velichka Kontozova-Deutsch[a], László Bencs[a,b], Felix Deutsch[c], René Van Grieken[a]

[a] Micro and Trace Analysis Centre, Department of Chemistry, University of Antwerp, Universiteitsplein 1, B-2610 Antwerp, Belgium
[b] Research Institute for Solid State Physics and Optics, Hungarian Academy of Sciences, P.O. Box 49, H-1525 Budapest, Hungary
[c] Flemish Institute for Technological Research (VITO), Centre for Integrated Environmental Studies, Boeretang 200, B-2400 Mol, Belgium

ARTICLE INFO

Article history:
Received 14 December 2008
Received in revised form 5 February 2009
Accepted 20 February 2009
Available online 5 March 2009

Keywords:
Low-molecular-mass organic acid
Inorganic anions
Isocratic elution
Snow
Hail
Rainwater

ABSTRACT

For the isocratic ion chromatography (IC) separation of low-molecular-mass organic acids and inorganic anions three different anion-exchange columns were studied: IonPac AS14 (9 μm particle size), Allsep A-2 (7 μm particle size), and IC SI-50 4E (5 μm particle size). A complete baseline separation for all analyzed anions (i.e., F^-, acetate, formate, Cl^-, NO_2^-, Br^-, NO_3^-, HPO_4^{2-} and SO_4^{2-}) in one analytical cycle of shorter than 17 min was achieved on the IC SI-50 4E column, using an eluent mixture of 3.2 mM Na_2CO_3 and 1.0 mM $NaHCO_3$ with a flow rate of 1.0 mL min^{-1}. On the IonPac AS14 column, it was possible to separate acetate from inorganic anions in one run (i.e., less than 9 min), but not formate, under the following conditions: 3.5 mM Na_2CO_3 plus 1.0 mM $NaHCO_3$ with a flow rate of 1.2 mL min^{-1}. Therefore, it was necessary to adapt a second run with a 2.0 mM $Na_2B_4O_7$ solution as an eluent under a flow rate of 0.8 mL min^{-1} for the separation of organic ions, which considerably enlarged the analysis time. For the Allsep A-2 column, using an eluent mixture of 1.2 mM Na_2CO_3 plus 1.5 mM $NaHCO_3$ with a flow rate of 1.6 mL min^{-1}, it was possible to separate almost all anions in one run within 25 min, except the fluoride-acetate critical pair. A Certified Multianion Standard Solution PRIMUS for IC was used for the validation of the analytical methods. The lowest RSDs (less than 1%) and the best LODs (0.02, 0.2, 0.16, 0.11, 0.06, 0.05, 0.04, 0.14 and 0.09 mg L^{-1} for F^-, Ac^-, For^-, Cl^-, NO_2^-, Br^-, NO_3^-, HPO_4^{2-} and SO_4^{2-}, respectively) were achieved using the IC SI-50 4E column. This column was applied for the separation of concerned ions in environmental precipitation samples such as snow, hail and rainwater.

1. Introduction

Ion chromatography (IC) remains one of the most powerful instrumental techniques for the determination of inorganic anions and organic acids in different environmental samples, such as natural waters [1,2], snow [3,4], ice [4,5], rain [6,7], and air [8,9]. It is well known that inorganic and low-molecular-mass organic acids play an important role in the formation of acidic precipitation. Organic acids, chiefly formic and acetic acid, are ubiquitous in the troposphere, formed by photochemical oxidation of many primary compounds originating from natural and anthropogenic sources [10]. The acidity can also be connected with the high emission of sulphur and nitrogen oxides, which are converted into sulphuric and nitric acids under atmospheric conditions. Moreover, an anionic contribution to atmospheric pollution in the form of fluoride and chloride may originate from different industrial processes [11]. Therefore, it is important to monitor the level of organic and inorganic species in various environmental compartments. As it was mentioned, IC is widely used for this purpose, because it offers a number of advantages, including high sensitivity and selectivity, possibility of multi-ion determinations, stability, and reliability [12,13]. The availability of analytical columns with different stationary phases has provided a range of options for the separation of various ions. The most often applied commercial columns for IC measurements designed for the analysis of major inorganic anions (i.e., F^-, Cl^-, NO_2^-, Br^-, NO_3^-, HPO_4^{2-}, and SO_4^{2-}) are: IonPac AS4A-SC [1,14], IonPac AS9-HC [15], IonPac AS11 [16,17], and IonPac AS14 [1,18,19], produced by Dionex (Sunnyvale, CA, USA). They are packed with a resin consisting of ethylvinylbenzene (EVB) crosslinked with 55% divinylbenzene (DVB), which make the columns 100% solvent-compatible. These analytical columns were used for the separation of the concerned ions in various natural samples, generally under isocratic elution [14–17], and occasionally under gradient elution [19]. As the manufacturer states, the aforementioned columns can also be adapted for the separation of low-molecular-mass organic acids, especially, formate and acetate, even along with major inorganic anions. On the analytical column IonPac AS4-SC, with an increasing concentration of $Na_2B_4O_7$ eluent from 4.9 to 24.5 mM, the F^-, acetate, formate,

* Corresponding author. Tel.: +32 3 820 23 81; fax: +32 3 820 23 76.
E-mail address: agnieszka.krata@ua.ac.be (A. Krata).

0039-9140/$ – see front matter © 2009 Elsevier B.V. All rights reserved.
doi:10.1016/j.talanta.2009.02.044

Cl^-, NO_3^-, PO_4^{3-}, and SO_4^{2-} were quantified in one run (12 min) from natural water samples from peatlands [20]. Also, this column was applied for the separation of seven major anions together with acetate, formate, lactate, and oxalate in snow and ice samples from mountain glaciers—it was possible under gradient elution and with $Na_2B_4O_7$ as an eluent within 14 min analysis time [4].

Jauhiainen et al. [5] used the IonPac AS9-HC for the separation of acetate, formate, methylsulphonate (MSA^-), Cl^-, Br^-, NO_3^-, and SO_4^{2-} in ice core samples. However, the isocratic elution of all anions in one run was not possible, because of the excessively long retention times for NO_3^- and SO_4^{2-} and largely broadened peaks. A gradient elution was also found to be inadequate in this case as the suppressor was not able to lower the baseline conductivity efficiently, e.g., the baseline raised from 16 to 30 μS when using a gradient from 2.5 to 9 mM Na_2CO_3. Thus, ions were determined in two steps: first, acetate, formate, and MSA^- with 12 mM $NaHCO_3$ as an eluent and later, after 1–2 days, common anions were eluted with a solution of 12.5 mM Na_2CO_3. The same column was used by Hoffmann et al. [21] for the analysis of F^-, acetate, formate, Cl^-, NO_2^-, Br^-, NO_3^-, and SO_4^{2-} in rain and snow samples. In this case, it was not possible to separate F^-, acetate, and formate under isocratic elution with a mixture of 2 mM Na_2CO_3 and 0.75 mM $NaHCO_3$ as an eluent. Therefore, a gradient separation was developed with two eluents: (1) 0.02 mM Na_2CO_3 plus 0.05 mM $NaHCO_3$; and (2) 2 mM Na_2CO_3 plus 0.75 mM $NaHCO_3$, which had the property to resolve all investigated ions within a total analysis time of less than 20 min.

The analytical column, IonPac AS11, was applied for the separation of F^-, acetate, formate, Cl^-, NO_3^-, and SO_4^{2-} in rainwater samples [7]. However, it was necessary to use two different isocratic methods: (1) firstly, Cl^-, NO_3^- and SO_4^{2-} were adequately determined by using 21 mM NaOH as an eluent; and (2) secondly, F^-, acetate and formate were eluted in a solution of 0.5 mM NaOH. An elution step change with 42 mM NaOH was used to quickly purge retained matrix components from the column. It should be mentioned that poor resolution of F^- and acetate peaks was occasionally obtained, and as a consequence, a relatively poor reproducibility for both ions was achieved. Jaffrezo et al. [3] also used an IonPac AS11 for the separation of acetate, formate, Cl^-, NO_2^-, NO_3^-, SO_4^{2-}, and heavier dicarboxylic acids in snow samples, but by an eluent with a quaternary gradient composition in the order of (1) 2.5 mM NaOH, (2) 100 mM NaOH, (3) methanol (90% in H_2O), and (4) H_2O. Measurement was completed after 12 min. The separation for inorganic anions and acetate, propionate, formate, and oxalate in one run was achieved by Jackson et al. [22] using an IonPac AS17 column and 16 min analysis time. For elution, gradient conditions with concentrations from 1 mM to 25 mM KOH with an automated eluent generator EG40 in conjunction with the analytical column were applied. This method was used for the determination of anions in environmental samples such as drinking, raw and surface water, domestic and industrial wastewater, and soil extract.

On the base of the literature survey, it seems that the separation of major inorganic and low-molecular-mass organic anions under isocratic conditions was not possible in a single run [5,7,21]. Difficulties lie mostly in two aspects: (1) the problem with separating the critical pairs of ions, such as the F^- and acetate, and also the acetate and formate, because they are very close in their affinities; and (2) retention times for NO_3^- and SO_4^{2-} become extensively long and impractical, moreover, the tailing of chromatographic signals has been observed. In order to resolve these problems, it was necessary: (1) to employ two separate runs, one by one, with a rinsing step on the same column [5,7]; or (2) to use an automatic column switching for the simultaneous separation of inorganic and organic ions on two different analytical columns [23]; or (3) to use a combination of isocratic and gradient methods [24]. On the other hand, the separation of inorganic and organic anions in a single run was possible under gradient elution [3,4,20–22]. However, it should be stressed that gradient elution is nowadays, on a lot of widely used types of ion chromatographs, almost impossible to apply, e.g., on a Dionex DX-120. Also for routine analysis, isocratic elution is the preferred separation mode. Some reasons that may justify this prevalence are the lower cost, simpler instrumentation, and the fact that there is no need of column re-equilibration between consecutive injections, which needs extra time. Therefore, in many laboratories a gradient procedure is not advisable or not possible.

The aim of this study was to systematically investigate the separation of low-molecular-mass organic acids (i.e., acetate and formate), and inorganic anions (i.e., F^-, Cl^-, NO_2^-, Br^-, NO_3^-, HPO_4^{2-}, and SO_4^{2-}) in one run under isocratic elution. Three different analytical anion-exchange columns were compared: IonPac AS14 (9 μm particle size), Allsep A-2 (7 μm particle size) and IC SI-50 4E (5 μm particle size). In a previous work [9], optimal conditions were found for the separation of acetate and formate under isocratic elution on three aforementioned columns. Therefore, it was interesting to study whether it could be possible to find suitable conditions for the separation of both organic and inorganic anions under isocratic elution in a single run. All three analytical columns were validated with the use of the certified primary reference material PRIMUS for IC and after that the most suitable column was applied for the separation of the concerned ions in real samples such as snow, hail and rainwater.

2. Experimental

2.1. Sampling

Snow, hail and rainwater samples were collected manually and strictly by events in January and February 2008 in Antwerp (Belgium), using polyethylene bottles with wide funnels. Bottles for collecting rainwater were placed on the roof of building of the Department of Chemistry, University of Antwerp. For sampling snow and hail, polyethylene spoons were used. The frozen samples were thawed just before the analysis. All the solutions were filtered by Millex-GV Syringe Driven Filter Unit 0.22 μm (Millipore, Carrigtwohill, Co. Cork, Ireland) before measurements.

2.2. Apparatus

All the measurements were carried out on a Dionex model DX-120 (Sunnyvale, CA, USA) ion chromatograph equipped with a Dionex AS-50 autosampler. A 20 μl aliquot of the sample/standard solution was loaded into the eluent-stream. The ions were detected by suppressed conductivity of the eluent using an ASRS-ULTRA self-regenerating suppressor column (Dionex). Data acquisition, construction of calibration curves and peak integration were achieved with the aid of the Peaknet® Dionex software package, version 6.11.

For the separation of the concerned ions, three columns were used: (i) an IonPac AS14 (250 mm × 4 mm I.D.) analytical column with an AG14 (50 mm × 4 mm I.D.) guard column produced by Dionex, (ii) an Allsep A-2 column (150 mm × 4.6 mm I.D.) with a GA-1 (7.5 mm × 4.6 mm I.D.) guard column, produced by Alltech (Deerfield, IL, USA), and (iii) IC SI-50 4E (250 mm × 4 mm I.D.) with an IC SI-90G (10 mm × 4.6 mm I.D.) guard column, produced by Shodex (Kyoto, Japan).

2.3. Reagents

All the reagents were of analytical grade. Standard solutions of F^-, Cl^-, NO_2^-, Br^-, NO_3^-, HPO_4^{2-} and SO_4^{2-} were prepared by appropriate dilution of their stock solution "Seven Anion Standard II" (20 μg mL^{-1} of F^-; 100 μg mL^{-1} of Cl^-, NO_2^-, Br^-, NO_3^- and SO_4^{2-}; and 200 μg mL^{-1} of HPO_4^{2-}; Dionex) in Milli-Q water. Stan-

dard solutions of acetate and formate were prepared by appropriate dilution of their stock solutions (each 1000 μg mL^{-1}, Merck, Darmstadt, Germany) in Milli-Q water. The $Na_2B_4O_7$ eluent solution was prepared by dissolving appropriate amounts of $Na_2B_4O_7$ (Merck) in Milli-Q water. Eluents containing mixtures of Na_2CO_3/$NaHCO_3$ at various concentrations were prepared by dissolving appropriate amounts of Na_2CO_3 (Merck) and $NaHCO_3$ (Merck) powders in Milli-Q water. Accurate weighing of chemicals was performed on a Chyo JL-180 model (Japan) analytical balance.

A certified primary reference material for ion chromatography PRIMUS (Multielemental Ion Chromatography Anion Standard Solution) containing of 10 mg L^{-1} ±0.2% F^-, Cl^-, Br^-, NO_3^-, HPO_4^{2-} and SO_4^{2-}, for each was used.

The calibration curves were constructed with five standard solutions. Each standard/sample solution was measured in triplicate and average concentrations and their standard deviations (SDs) were calculated.

2.4. Separation procedure

For the optimization of the separation procedure of all anions under isocratic elution and taking into account the fact that the resolution could depend on the amount of one analyte, which could affect the response of the next one in the chromatogram, a variety of standard combinations was tested. Their anion contents were in mg L^{-1}:

(1) 0.2 of F^- + 5 of Ac^- + 2 of For^- + 1 of Cl^-, NO_2^-, Br^-, NO_3^-, SO_4^{2-} each + 2 of HPO_4^{2-};
(2) 1 of F^- + 10 of Ac^- + 5 of For^- + 5 of Cl^-, NO_2^-, Br^-, NO_3^-, SO_4^{2-} each + 10 of HPO_4^{2-};
(3) 2 of F^- + 50 of Ac^- + 20 of For^- + 10 of Cl^-, NO_2^-, Br^-, NO_3^-, SO_4^{2-} each + 20 of HPO_4^{2-};
(4) 4 of F^- + 100 of Ac^- + 50 of For^- + 20 of Cl^-, NO_2^-, Br^-, NO_3^-, SO_4^{2-} each + 40 of HPO_4^{2-}.

In order to achieve the best separation of all ions, different eluents for each column were tested. In the case of the IonPac AS14, the composition of eluents was as follows: (I) 0.8 mM $NaHCO_3$/2.0 mM Na_2CO_3; (II) 0.8 mM $NaHCO_3$/2.5 mM Na_2CO_3; (III) 1.0 mM $NaHCO_3$/3.2 mM Na_2CO_3; and (IV) 1.2 mM $NaHCO_3$/3.6 mM Na_2CO_3. In our previous study [9], it was found that with the use of an eluent of 2 mM $Na_2B_4O_7$, it was possible to separate acetate and formate under isocratic elution. Therefore, solutions of $Na_2B_4O_7$ with various concentrations were also tested as an eluent: (I) 1.0 mM $Na_2B_4O_7$; (II) 1.2 mM $Na_2B_4O_7$; (III) 1.5 mM $Na_2B_4O_7$; (IV) 2.0 mM $Na_2B_4O_7$; and (V) 3.0 mM $Na_2B_4O_7$. In all cases the eluent flow rate was studied in the range of 0.8–1.5 mL min^{-1}.

For the Allsep A-2 column, the following eluents were tested: (I) 0.9 mM $NaHCO_3$/1.2 mM Na_2CO_3; (II) 1.5 mM $NaHCO_3$/1.2 mM Na_2CO_3; (III) 1.8 mM $NaHCO_3$/1.6 mM Na_2CO_3; and (IV) 2.1 mM $NaHCO_3$/1.6 mM Na_2CO_3. The eluent flow rate in the range of 0.8–1.8 mL min^{-1} was investigated.

In the case of the IC SI-50 4E column, the composition of eluents was as follows: (I) 0.8 mM $NaHCO_3$/2.4 mM Na_2CO_3; (II) 1.0 mM $NaHCO_3$/2.8 mM Na_2CO_3; (III) 1.0 mM $NaHCO_3$/3.2 mM Na_2CO_3; and (IV) 1.2 mM $NaHCO_3$/3.6 mM Na_2CO_3. The eluent flow rate ranged from 0.7–1.2 mL min^{-1}.

3. Results and discussion

3.1. Conditions for the separation of investigated ions

In the case of the IonPac AS14 column and with the use of a mixture of 1.0 mM $NaHCO_3$ and 3.2 mM Na_2CO_3 buffer solution as an eluent at a flow rate of 1.2 mL min^{-1}, sharp peaks and nearly baseline separation of all seven inorganic anions and Ac^- was obtained. However, under these conditions, no peak from For^- was observed. This composition of the mobile phase was suggested by the manufacturer, mostly for the routine analysis of inorganic ions. The separation was possible within 9 min and the retention times of 2.6 min, 2.9 min, 3.4 min, 3.8 min, 4.5 min, 5.1 min, 6.7 min and 7.7 min for F^-, Ac^-, Cl^-, NO_2^-, Br^-, NO_3^-, HPO_4^{2-} and SO_4^{2-} were observed, respectively (Fig. 1). It was noticed that with the use of a flow rate lower than 1.2 mL min^{-1}, tailing of the chromatographic signals occurred, especially, in the case of HPO_4^{2-} and SO_4^{2-}. Additionally, the retention times for all peaks were longer and the separation between F^- and Ac^- was not acceptable. On the other hand, using a flow rate of e.g. 1.5 mL min^{-1} caused that the column pressure quickly rose above the maximum permissible level of the IC system.

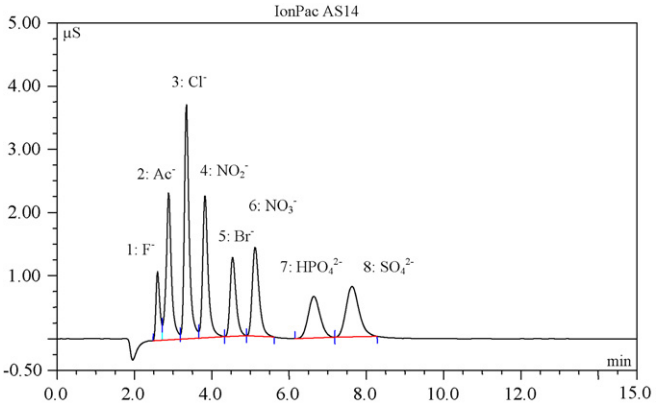

Fig. 1. Separation of 1 mg L^{-1} of F^-, 10 mg L^{-1} of Ac^-, 5 mg L^{-1} of Cl^-, NO_2^-, Br^-, NO_3^-, SO_4^{2-} each and 10 mg L^{-1} of HPO_4^{2-} standard solution on an IonPac AS14 column using a mixture of 1.0 mM $NaHCO_3$ and 3.2 mM Na_2CO_3 as an eluent.

As it was mentioned, on the IonPac AS14 column also a $Na_2B_4O_7$ solution at various concentrations and under different flow rates was tested in order to get separation of all investigated ions in a single run. Baseline separation of Ac^-, For^- and five inorganic ions as F^-, Cl^-, NO_2^-, HPO_4^{2-} and SO_4^{2-} with the use of 2.0 mM $Na_2B_4O_7$ solution as an eluent at a flow rate of 0.8 mL min^{-1} was achieved. However, under these conditions, the peaks of Br^- and NO_3^- were not observed on the chromatogram. The separation was possible in less than 18 min and retention times of 6.6 min, 7.4 min, 7.7 min, 9.6 min, 11.4 min, 14.4 min and 16.7 min for F^-, Ac^-, For^-, Cl^-, NO_2^-, HPO_4^{2-} and SO_4^{2-} were obtained, respectively (Fig. 2). At flow rates

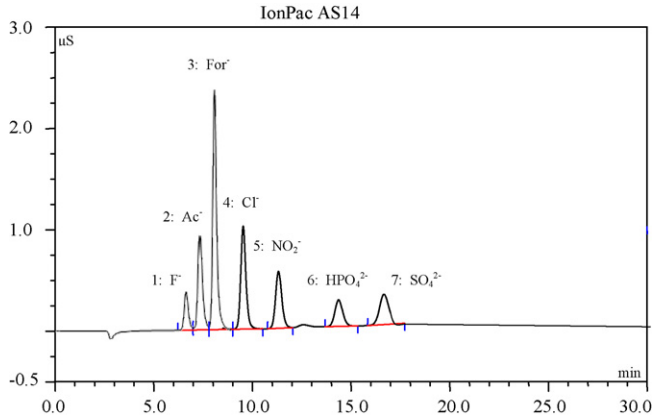

Fig. 2. Separation of 1 mg L^{-1} of F^-, 10 mg L^{-1} of Ac^-, 5 mg L^{-1} of For^-, Cl^-, NO_2^-, SO_4^{2-} each, and 10 mg L^{-1} of HPO_4^{2-} standard solution on an IonPac AS14 column using 2.0 mM $Na_2B_4O_7$ as an eluent.

Table 1
Concentrations of ions detected in a certified standard solution PRIMUS after separation on the IonPac AS14 column (eluent (a) 1.0 mM $NaHCO_3$ plus 3.5 mM Na_2CO_3 buffer solution; or (b) 2.0 mM $Na_2B_4O_7$ solution).

Anion	Concentration, mg L^{-1} (±SD)					
	PRIMUS	IonPac AS14	PRIMUS	IonPac AS14	PRIMUS	IonPac AS14
(a)						
F^-	2	2.10 ± 0.06	5	5.11 ± 0.12	10[b]	10.1 ± 0.05
Ac^-	10[a]	10.4 ± 0.20	20[a]	20.3 ± 0.20	50[a]	50.4 ± 0.20
For^-	5[a]	–	10[a]	–	20[a]	–
Cl^-	2	2.09 ± 0.06	5	5.01 ± 0.07	10[b]	10.1 ± 0.10
Br^-	2	1.99 ± 0.07	5	5.08 ± 0.08	10[b]	10.2 ± 0.09
NO_3^-	2	2.10 ± 0.06	5	4.95 ± 0.04	10[b]	10.0 ± 0.07
HPO_4^{2-}	2	1.98 ± 0.06	5	4.96 ± 0.06	10[b]	10.2 ± 0.08
SO_4^{2-}	2	2.01 ± 0.05	5	5.01 ± 0.05	10[b]	10.1 ± 0.05
(b)						
F^-	2	2.12 ± 0.04	5	5.09 ± 0.10	10[b]	10.3 ± 0.05
Ac^-	10[a]	10.5 ± 0.20	20[a]	20.6 ± 0.10	50[a]	50.6 ± 0.20
For^-	5[a]	5.18 ± 0.07	10[a]	10.3 ± 0.20	20[a]	20.3 ± 0.30
Cl^-	2	1.98 ± 0.05	5	4.99 ± 0.08	10[b]	9.94 ± 0.12
Br^-	2	–	5	–	10[b]	–
NO_3^-	2	–	5	–	10[b]	–
HPO_4^{2-}	2	1.78 ± 0.08	5	4.69 ± 0.10	10[b]	9.64 ± 0.09
SO_4^{2-}	2	1.83 ± 0.09	5	4.73 ± 0.06	10[b]	9.81 ± 0.12

[a] Spiked Ac^- and For^-.
[b] Without spiked Ac^- and For^-.

higher than 1 mL min^{-1}, baseline separation of Ac^- and For^- was impossible.

For the Allsep A-2 column, baseline separation of almost all investigated ions was achieved when using a mixture of 1.5 mM $NaHCO_3$ and 1.2 mM Na_2CO_3 buffer solution as an eluent, at a flow rate of 1.6 mL min^{-1}. However, under these conditions, F^- and Ac^- were not resolved sufficiently and this critical pair could not be accurately quantified. The separation was complete after 25 min and retention times of 2.5 min, 2.7 min, 3.2 min 4.8 min, 6.5 min, 8.8 min, 10.8 min, 19.7 min and 22.4 min were observed for F^-, Ac^-, For^-, Cl^-, NO_2^-, Br^-, NO_3^-, HPO_4^{2-} and SO_4^{2-}, respectively (Fig. 3). It was also noticed that when a flow rate lower than 1.5 mL min^{-1} was used, the signals of ions become broad, especially in the case of NO_3^-, HPO_4^{2-} and SO_4^{2-}.

In the case of the IC SI-50 4E column, complete baseline separation of all concerned ions was achieved by using an eluent of 1.0 mM $NaHCO_3$ plus 3.2 mM Na_2CO_3 buffer solution at a flow rate of 1.0 mL min^{-1}. Under these conditions, the separation was possible within a single run of less than 17 min with retention times of 3.5 min, 3.8 min, 4.3 min, 5.6 min, 6.9 min, 8.8 min, 10.3 min, 13.0 min and 15.2 min for F^-, Ac^-, For^-, Cl^-, NO_2^-, Br^-, NO_3^-, HPO_4^{2-}, and SO_4^{2-}, respectively (Fig. 4). The same eluent composition is also suggested for the separation with a flow rate of 0.7 mL min^{-1} by the manufacturer. However, a flow rate of 1.0 mL min^{-1} was found to be the most suitable one for the separation.

3.2. Validation of the analytical methods

In order to validate the three analytical columns, a Certified Multianion Standard Solution PRIMUS for IC was used. This standard solution did not contain Ac^- and For^-, therefore, working solutions were spiked with known amounts of these two ions. For this purpose, three validation standards regarding to low, medium and high concentrations of analytes were used. Their anion contents were in mg L^{-1}:

(1) 2 of F^-, Cl^-, Br^-, NO_3^-, HPO_4^{2-} and SO_4^{2-} each and 10 of Ac^- and 5 of For^-;
(2) 5 of F^-, Cl^-, Br^-, NO_3^-, HPO_4^{2-} and SO_4^{2-} each and 20 of Ac^- and 10 of For^-;
(3) 10 of F^-, Cl^-, Br^-, NO_3^-, HPO_4^{2-} and SO_4^{2-} each and 50 of Ac^- and 20 of For^-.

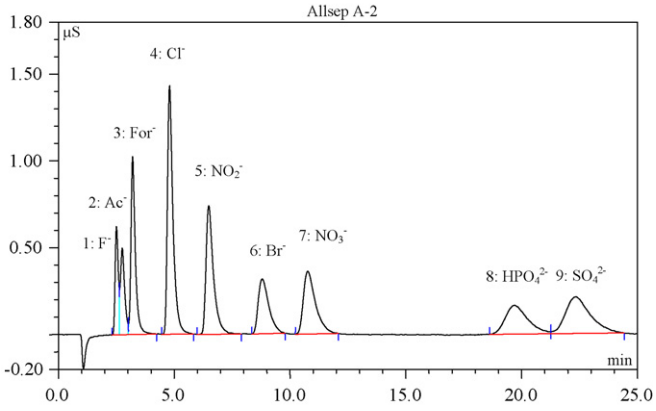

Fig. 3. Separation of 1 mg L^{-1} of F^-, 10 mg L^{-1} of Ac^-, 5 mg L^{-1} of For^-, 5 mg L^{-1} of Cl^-, NO_2^-, Br^-, NO_3^-, SO_4^{2-} each and 10 mg L^{-1} of HPO_4^{2-} standard solution on an Allsep A-2 column with an eluent mixture of 1.5 mM $NaHCO_3$ and 1.2 mM Na_2CO_3.

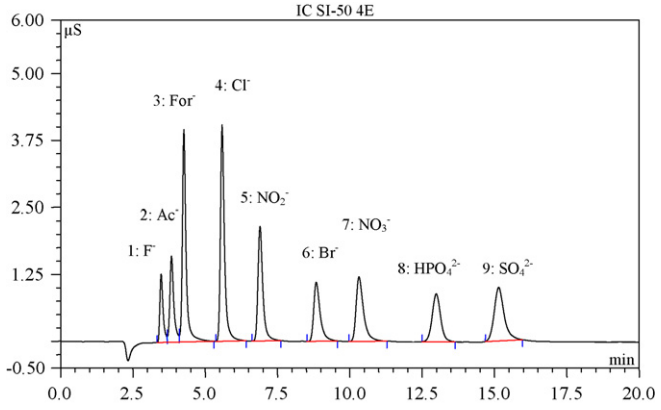

Fig. 4. Separation of 1 mg L^{-1} of F^-, 10 mg L^{-1} of Ac^-, 5 mg L^{-1} of For^-, 5 mg L^{-1} of Cl^-, NO_2^-, Br^-, NO_3^-, SO_4^{2-} each and 10 mg L^{-1} of HPO_4^{2-} standard solution on an IC SI-50 4E column using a mixture of 1.0 mM $NaHCO_3$ and 3.2 mM Na_2CO_3 as an eluent.

Table 2
Concentrations of ions detected in a certified standard solution PRIMUS after separation on the Allsep A-2 column.

Anion	Concentration, mg L^{-1} (±SD)					
	PRIMUS	Allsep A-2	PRIMUS	Allsep A-2	PRIMUS	Allsep A-2
F^-	2	2.31 ± 0.09	5	5.11 ± 0.26	10[b]	11.3 ± 0.50
Ac^-	10[a]	11.5 ± 0.30	20[a]	24.9 ± 0.60	50[a]	51.3 ± 0.90
For^-	5[a]	5.26 ± 0.05	10[a]	10.6 ± 0.20	20[a]	20.5 ± 0.10
Cl^-	2	1.98 ± 0.08	5	4.63 ± 0.08	10[b]	9.73 ± 0.06
Br^-	2	1.82 ± 0.05	5	4.70 ± 0.06	10[b]	9.59 ± 0.06
NO_3^-	2	2.02 ± 0.07	5	4.90 ± 0.08	10[b]	9.82 ± 0.07
HPO_4^{2-}	2	1.40 ± 0.10	5	4.42 ± 0.13	10[b]	9.67 ± 0.10
SO_4^{2-}	2	1.60 ± 0.10	5	4.44 ± 0.14	10[b]	9.64 ± 0.07

[a] Spiked Ac^- and For^-.
[b] Without spiked Ac^- and For^-.

Table 3
Concentrations of ions detected in a certified standard solution PRIMUS after separation on the IC SI-50 4E column.

Anion	Concentration, mg L^{-1} (±SD)					
	PRIMUS	IC SI-50 4E	PRIMUS	IC SI-50 4E	PRIMUS	IC SI-50 4E
F^-	2	2.04 ± 0.02	5	5.06 ± 0.03	10[b]	10.1 ± 0.03
Ac^-	10[a]	10.2 ± 0.20	20[a]	20.4 ± 0.10	50[a]	50.2 ± 0.10
For^-	5[a]	5.10 ± 0.09	10[a]	10.2 ± 0.10	20[a]	20.2 ± 0.10
Cl^-	2	2.01 ± 0.01	5	5.03 ± 0.04	10[b]	10.0 ± 0.01
Br^-	2	2.02 ± 0.02	5	4.96 ± 0.06	10[b]	10.1 ± 0.02
NO_3^-	2	2.00 ± 0.02	5	5.01 ± 0.01	10[b]	10.0 ± 0.05
HPO_4^{2-}	2	2.00 ± 0.04	5	5.00 ± 0.03	10[b]	10.1 ± 0.01
SO_4^{2-}	2	2.01 ± 0.01	5	5.03 ± 0.06	10[b]	10.1 ± 0.02

[a] Spiked Ac^- and For^-.
[b] Without spiked Ac^- and For^-.

The determinations were carried out with the use of optimal conditions for each column. The results with the corresponding SDs are listed in Tables 1–3. It was noted that the determined values of high concentrations of inorganic anions were obtained directly from standard solution PRIMUS without spiked Ac^- and For^- ions. A very good recovery (between 99 and 102%) of all detected ions in the measured concentrations range was observed with the use of the IC SI-50 4E column (Table 3). Also, on the IonPac AS14 column using $NaHCO_3$ plus Na_2CO_3 buffer solution as an eluent, a recovery of 99–102% was found for all ions at medium and high concentrations. In the case of anions with low concentrations a recovery till 105% was noticed (Table 1a). With the use of $Na_2B_4O_7$ solution as an eluent, a recovery of 99–103% was achieved for F^-, Ac^-, For^- and Cl^- and around 95% for HPO_4^{2-} and SO_4^{2-} when anions represented at medium and high levels. For low analyte concentrations, a recovery of 89–106% was found (Table 1b). The results obtained on the Allsep A-2 column were not satisfactory for anions in the measured concentration range and the recovery ranged from 125% for Ac^- to 70% for HPO_4^{2-} (Table 2).

3.3. Analytical performance

As a part of the method elaboration, the analytical performance of the methods, for example, the relative standard deviations (RSDs) and limits of detection (LOD – corresponding to 3 × SD (blank)/slope) for each analytical column were calculated. With the use of $NaHCO_3$ plus Na_2CO_3 buffer solution (or $Na_2B_4O_7$ solution) as an eluent for the separation on the IonPac AS14, RSDs of 2.4 (3.8), 1.2 (3.1), 1.5 (2.2), 1.2, 1.0, 1.3 (4.0) and 0.9 (3.6)% (%), and LODs of 0.03 (0.04), 0.48 (0.60), 0.15 (0.23), 0.08 (0.16), 0.05, (0.05), 0.14 (0.32), and 0.09 (0.28) mg L^{-1} (mg L^{-1}) were achieved for F^-, Ac^-, Cl^-, NO_2^-, Br^-, NO_3^-, HPO_4^{2-}, and SO_4^{2-}, respectively (for For^- RSD = 4.2% and LOD = 0.37 mg L^{-1}). Upper limit of the linear range (UL) of calibration for all investigated anions was found 100 mg L^{-1}, except Ac^- and HPO_4^{2-} – 200 mg L^{-1}. In the case of the Allsep A-2 column, RSDs of 5.0, 3.2, 3.1, 1.8, 1.6, 1.3, 1.6, 4.2 and 5.1%, and LODs of 0.03, 0.56, 0.46, 0.21, 0.12, 0.08, 0.09, 0.34 and 0.38 mg L^{-1} were obtained for F^-, Ac^-, For^-, Cl^-, NO_2^-, Br^-, NO_3^-, HPO_4^{2-} and SO_4^{2-}, respectively. For all the measured ions UL was found 100 mg L^{-1}, except Ac^- – 300 mg L^{-1} and HPO_4^{2-} – 200 mg L^{-1}. The lowest RSDs and the best LODs were achieved using the IC SI-50 4E column: for all investigated anions, the RSDs were less than 1% and the LODs were 0.02, 0.2, 0.16, 0.11, 0.06, 0.05, 0.04, 0.14 and 0.09 mg L^{-1} for F^-, Ac^-, For^-, Cl^-, NO_2^-, Br^-, NO_3^-, HPO_4^{2-} and SO_4^{2-}, respectively. The UL was found to be similar as with the used of the IonPac AS14 column, except for Ac^- – 500 mg L^{-1} and For^- – 200 mg L^{-1}.

3.4. Application of the optimized method to environmental samples

Baseline separation of all investigated ions in a single isocratic run was achieved on the IC SI-50 4E column. Therefore, this column was applied for the separation of ions in environmental samples, such as snow, hail, and rainwater. In all samples

Table 4
Typical concentrations of inorganic ions and recovery of spiked organic ions detected in real samples after separation on the IC SI-50 4E column.

Sample	Concentration, mg L^{-1} (±SD)				Recovery, % (±SD)	
	F^-	Cl^-	NO_3^-	SO_4^{2-}	Ac^-	For^-
Snow	0.12 ± 0.01	1.55 ± 0.02	1.51 ± 0.06	1.09 ± 0.03	102.9 ± 1.6	106.3 ± 3.0
Hail	0.22 ± 0.01	9.80 ± 0.07	7.71 ± 0.09	8.91 ± 0.22	104.5 ± 1.9	105.5 ± 3.5
Rain	0.10 ± 0.01	4.27 ± 0.05	0.66 ± 0.04	0.53 ± 0.03	103.0 ± 1.7	104.1 ± 1.8

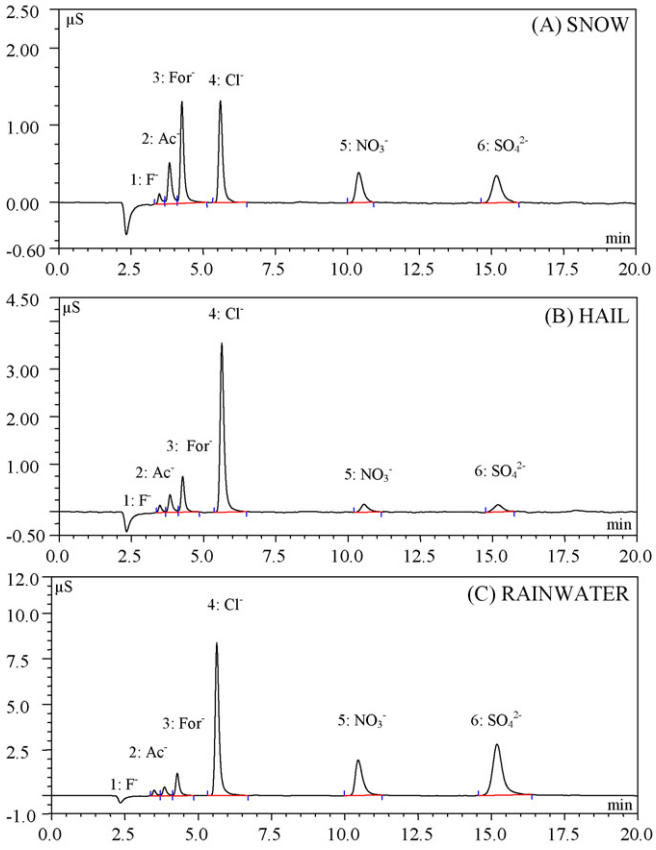

Fig. 5. Separation of low-molecular-mass organic acids and inorganic anions in real samples on an IC SI-50 4E column under optimized conditions.

taken for analysis, four inorganic ions like: F^-, Cl^-, NO_3^- and SO_4^{2-} were detected. Ions like Ac^- and For^- were found slightly higher than their LODs [9], therefore, all samples were spiked with 5 mg L^{-1} Ac^- and 2 mg L^{-1} For^-. The concentrations of the quantified inorganic anions and the recoveries of spiked organic acids are given in Table 4. Examples of chromatograms for the real samples are depicted on Fig. 5. As can be seen, for all investigated samples, the resolution was baseline and the detected peaks were sharp.

4. Conclusions

This study aimed at the separation of low-molecular-mass organic acids (i.e., Ac^- and For^-), and inorganic anions (i.e., F^-, Cl^-, NO_2^-, Br^-, NO_3^-, HPO_4^{2-}, and SO_4^{2-}) in one analytical IC cycle under isocratic elution on three different analytical columns: IonPac AS14, Allsep A-2, and IC SI-50 4E. On the IonPac AS14 column, it was impossible to separate all concerned ions in a single run. Therefore, it was necessary to apply two-step elution with different solutions as an eluent. In the first step, a buffer solution of 1.0 mM $NaHCO_3$ plus 3.5 mM Na_2CO_3 as an eluent was used for the separation of seven inorganic ions. In the second step, a solution of 2.0 mM $Na_2B_4O_7$ as an eluent for the separation of Ac^- and For^- ions was applied. In the case of the Allsep A-2 column, it was also impossible to separate all investigated ions in one run. The resolution of F^- and Ac^- was not acceptable, and it was difficult to quantify these analytes. The chromatographic signals of HPO_4^{2-} and SO_4^{2-} were broadened and these peaks had long retention times. Also, the results of the validation procedure were not satisfactory. Using isocratic elution and a mixture of 1.0 mM $NaHCO_3$ plus 3.2 mM Na_2CO_3 as an eluent, it was possible to resolve all concerned ions on the IC SI-50 4E column within a single run of fairly short analysis time. All ions were baseline separated and had sharp peaks. The validation procedure and practical analysis of the real samples proved the utility of this analytical column to the routine determination of low-molecular-mass organic acids and basic inorganic anions in a wide range of environmental precipitation samples.

Acknowledgement

One of the authors (L. Bencs) acknowledges the support of the Hungarian Scientific Research Fund (OTKA) under the project number of F67647.

References

[1] P.E. Jackson, D.H. Thomas, B. Donovan, C.A. Pohl, R.E. Kiser, J. Chromatogr. A 920 (2001) 51.
[2] R. García-Fernández, J.I. García-Alonso, A. Sanz-Medel, J. Chromatogr. A 1033 (2004) 127.
[3] J.L. Jaffrezo, N. Calas, M. Bouchet, Atmos. Environ. 32 (1998) 2705.
[4] X. Lee, D. Qin, G. Jiang, H. Zhou, Cold Regions Sci. Technol. 34 (2002) 127.
[5] T. Jauhiainen, J. Moore, P. Peramaki, J. Derome, K. Deroms, Anal. Chim. Acta 389 (1999) 21.
[6] Y.S. Fung, K.M. Lau, Talanta 45 (1998) 641.
[7] J.A. Morales, L.S. de Graterol, H. Velasquez, M.G. de Nava, B.S. de Borrego, J. Chromatogr. A 804 (1998) 289.
[8] S.R. Souza, M.F.M. Tavares, L.R.F. de Carvalho, J. Chromatogr. A 796 (1998) 335.
[9] V. Kontozova-Deutsch, A. Krata, F. Deutsch, L. Bencs, R. Van Grieken, Talanta 75 (2007) 418.
[10] A. Chebbi, P. Carlier, Atmos. Environ. 30 (1996) 4233.
[11] H. Schumann, M. Ernst, J. Chromatogr. A 640 (1993) 241.
[12] P.R. Haddad, P.E. Jackson, Ion Chromatography—Principles and Applications, Elsevier, Amsterdam, 1991.
[13] P. Papoff, A. Giacomelli, M. Onor, Microchem. J. 46 (1992) 385.
[14] E. Santoyo, S.P. Verma, F. Sandoval, A. Aparicio, R. García, J. Chromatogr. A 949 (2002) 281.
[15] L.K. Jackson, R.J. Joyce, M. Laikhtman, P.E. Jackson, J. Chromatogr. A 829 (1998) 187.
[16] P. Hatsis, C.A. Lucy, J. Chromatogr. A 920 (2001) 3.
[17] J.A. Morales, L.S. de Graterol, J. Mesa, J. Chromatogr. A 884 (2000) 185.
[18] D. Orta, P.D. Mudgett, L. Ding, M. Drybread, J.R. Schultz, R.L. Sauer, J. Chromatogr. A 804 (1998) 295.
[19] M.A.J. Curran, A.S. Palmer, J. Chromatogr. A 919 (2001) 107.
[20] P. Steinmann, W. Shotyk, J. Chromatogr. A 706 (1995) 281.
[21] P. Hoffmann, V.K. Karandashev, T. Sinner, Fresenius, J. Anal. Chem. 357 (1997) 1142.
[22] P.E. Jackson, C. Weigert, C.A. Pohl, C. Saini, J. Chromatogr. A 884 (2000) 175.
[23] C. Umile, J.F.K. Huber, J. Chromatogr. A 640 (1993) 27.
[24] V. Cheam, Analyst 117 (1992) 1137.

Talanta 79 (2009) 92–96

Contents lists available at ScienceDirect

Talanta

journal homepage: www.elsevier.com/locate/talanta

Determination of free glycerol in biodiesel at a platinum oxide surface using potential cycling technique

Leandro Maranghetti Lourenço*, Nelson Ramos Stradiotto

UNESP – São Paulo State University, Department of Analytical Chemistry, UNESP, Araraquara, SP, Brazil

ARTICLE INFO

Article history:
Received 3 December 2008
Received in revised form 3 March 2009
Accepted 4 March 2009
Available online 19 March 2009

Keywords:
Biodiesel
Free glycerol
Platinum
Potential cycling technique
Cyclic voltammetry
Quality control

ABSTRACT

A novel, inexpensive and fast method based on the electrooxidation of glycerol on platinum electrodes by the potential cycling technique has been designed for the determination of free glycerol in biodiesel. A wide range of linearity was achieved between 15 and 150 mg L^{-1} (0.16 and 1.6 mmol L^{-1}), which corresponds to concentrations ranging between 56 and 560 mg kg^{-1} (glycerol:biodiesel) for an extraction using 2 g biodiesel. A method for the fast extraction of glycerol from biodiesel with water followed by elimination of organic interferents has also been developed, so that the novel determination method can be applied to various biodiesel samples. The excellent repeatability allows determination of glycerol in numerous samples, with no need for recalibration.

1. Introduction

Biodiesel is an alternative to petroleum-derived diesel fuel. It is a renewable and biodegradable energy source composed of alkyl esters of long chain fatty acids generated from vegetable oils or animal fat. It can be used as a fuel itself or blended with diesel, thus reducing our dependence on imported oil and decreasing greenhouse gases emission as well as particulate matter discharge into the air of major cities.

Transesterification of triacylglycerols with short-chain alcohols is the most commonly employed process for biodiesel production [1]. After the reaction is completed and the mixture is allowed to rest, two phases separate: a less dense organic phase consisting of fatty acid esters, and a denser phase composed of glycerol and other residual components. After the separation process, the top layer is then repeatedly washed with water, to eliminate glycerol and unwanted impurities. However, small amounts of glycerol still remain in the organic phase, with an estimated solubility around 200 mg kg^{-1} at 0 °C. Nevertheless, because glycerol is easily dispersed in esters, solubility values between 300 and 500 mg kg^{-1} can be reached [2]. The presence of soaps in the organic phase may aggravate the situation by increasing the solubility of free glycerol in this layer.

A mixture of fatty acid esters can be commercialized as biodiesel if it meets the requirements imposed by regulations. The presence of glycerol in biodiesel is undesirable because it is responsible for lower engine performance [3], fuel tank damage, and possible release of acrolein into the atmosphere, which takes place when fuel burning occurs at temperatures above 180 °C [4]. Therefore, the amount of glycerol in the fuel should be kept to a minimum. Requirements of the Brazilian regulatory agency "Agência Nacional do Petróleo" (National Petroleum Agency, ANP) specifying the quality of biodiesel B100 (Technical regulation ANP number 1/2008), as described by the ABNT NBR 15341:2006 standard, rule that the amount of free glycerol in biodiesel should not exceed 0.02% m/m (200 mg kg^{-1}) [5]. This follows the same maximum free glycerol concentration fixed by the European EN 14214 standard (described in the tests EN 14105:2006 and EN 14106:2006) and the ASTM D6584 standard.

Many methods for the determination of free glycerol in biodiesel have been reported. Special emphasis has been given to chromatographic methods [6–12], while photometric methods are particularly interesting because of their simplicity and low cost [13,14]. An extraction phase is necessary in all the methods, except for gas chromatography. A solvent mixture, such as hexane/water [11] and hexane/hydroalcoholic mixture [2,6], or simply water under bubbling [12], is usually employed in the extraction. The well-known miscibility between glycerol and water allows for the extraction of this contaminant with water only. However, glycerol extraction with organic solvents is also often employed, so that better phase separation can be achieved after a resting

* Corresponding author. Tel.: +55 16 3301 6621; fax: +55 16 3322 7932.
E-mail address: lemarlou@iq.unesp.br (L.M. Lourenço).

0039-9140/$ – see front matter © 2009 Elsevier B.V. All rights reserved.
doi:10.1016/j.talanta.2009.03.013

period, which can last as long as 2 h. To date, only one method employing an electroanalytical technique has been reported [11], but it must be coupled with high performance liquid chromatography (HPLC). In this method [11], glycerol is extracted from biodiesel by a hexane/water mixture, followed by stirring, decantation, and separation between the aqueous and organic phases. The aqueous phase is then injected into an HPLC system (mobile phase = NaOH 0.5 mol L^{-1}) coupled with an electrochemical detector that employs pulse amperometry. Gold is used as working electrode.

The electrochemical behavior of alcohols on platinum and gold electrodes and the problems related to their electrooxidation have been long known [15]. It is common knowledge that adsorbed alcohol molecules are oxidized at all applied potentials, and the generated products depend mainly on the applied potential and the pH of the electrolyte. At potentials close to the oxygen evolution reaction, the dissociative oxidation of glycerol occurs, leading to the formation of formic acid, oxalic acid, and glycolic acid. When the potential is fixed at values around 0.75 V *versus* RHE, glyceraldehyde is produced [16]. Only platinum electrodes are electroactive in acidic medium. Both platinum and gold electrodes, particularly the latter, give relatively high current densities in alkaline medium [17]. The electrocatalytic activity of platinum has also been demonstrated to significantly increase when Pt–Au alloy electrodes are employed, being the maximum electroactivity obtained when 35% gold is present in the electrode composition [18]. The proposed mechanisms involve adsorbed hydroxyl radicals, which are assumed to participate in the oxygen transfer step [17,19].

The adsorption and oxidation of glycerol on platinum electrodes has already been investigated by cyclic voltammetry coupled with *in situ* FTIR spectroscopy. The results demonstrated that the oxidation of glycerol at the platinum electrode is a complex surface process that includes dehydrogenation, adsorption and dissociation stages [20].

In view of the present interest in the design of novel precise, fast methods for the determination of free glycerol in biodiesel and because electroanalytical methods in this field are lacking, we have developed a new reliable, inexpensive electroanalytical method for the determination of glycerol based on glycerol oxidation at a platinum electrode.

2. Experimental details

2.1. Apparatus and reagents

Glycerol (99.5% purity) and acetone (PA) were acquired from Synth. A solution prepared from $HClO_4$ 70%, purchased from Merck, was employed as the supporting electrolyte. All the solutions were prepared with water purified in a Milli-Q (Millipore, USA) system.

A freshly prepared glycerol standard solution 10.01 ± 0.01 g L^{-1} was used to construct the analytical curves.

The soybean oil biodiesel samples were obtained from the Paraná's Technological Institute (TECPAR) in Brazil.

Voltammetric measurements were carried out in an AutoLab, Model PGSTAT 30 potentiostat. A conventional 25 mL electrochemical cell was employed, using a three-electrode arrangement. The working electrode was a platinum disk with an area of 0.125 cm^2, the auxiliary electrode was a platinum electrode, and $Ag/AgCl_{(sat)}$ was the reference electrode.

Samples were vortex-mixed in a FANEM model 251 vortex mixer. Centrifugation was carried out in a FANEM EXCELSA BABY I model 206 centrifuge.

Solid-phase extractions were accomplished in Agilent Technologies AccuBond II ODS-C18 Cartridges 500 mg/6 mL.

2.2. Electroanalytical procedures

The working electrode was polished with alumina (0.3 μm) prior to the electrochemical measurements and thoroughly washed with deionized water. The clean platinum electrode was then submitted to an activation process that consisted in 50 consecutive voltammetric cycles between −0.14 and +1.3 V *versus* $Ag/AgCl_{(sat)}$ in $HClO_4$ 100 mmol L^{-1} solution, at a sweep rate of 100 mV s^{-1}. In the studies where different acidity values were evaluated, activation in acidic medium was carried out as described above, using the same acid concentrations as those that were going to be employed in the determinations. The peak current values used during the electroanalytical measurements were those that fell between 0.4 and 0.8 V *versus* $Ag/AgCl_{(sat)}$.

Twenty consecutive voltammetric cycles were performed for each different sample of the analytical curve and in the quantitative determinations, in triplicate. Only the last measurement was recorded. The $HClO_4$ concentration employed for construction of the analytical curves was 100 mmol L^{-1}.

The baseline obtained by extrapolation of the linear region prior to the peak was employed for determination of the peak current values in the cyclic voltammograms.

Concentration values in the quantifications were obtained from the interpolation of the signal obtained in the analytical curve equation by application of the least squares method.

In order to build the analytical curve depicted in Section 3.2, 12 samples with glycerol concentrations ranging between 1.80 and 150 mg L^{-1} (1.95×10^{-2} and 1.63 mmol L^{-1}) were obtained from a freshly prepared glycerol standard solution 10.01 ± 0.01 g L^{-1}.

2.3. Extraction procedures

Biodiesel B100 (2 g) was weighed in screw-cap test tubes with a precision of 0.1 mg. Water (6.00 mL) was then added to the tube, which was vortex-mixed for 5 min, followed by centrifugation for 10 min. The aqueous phase, containing glycerol and other impurities, was drained and eluted in a C18 cartridge previously conditioned with acetone (6 mL) and water (24 mL). The aqueous phase was submitted to elution in the C18 cartridge, in order to retain any traces of organic salts/compounds that might interfere with the developed electrochemical method in the solid phase. Then, a volume of exactly 4.00 mL was evaporated in a rotary evaporator until almost complete dryness.

Rotary evaporation was carried out at 200 mmHg (*ca.* 26.7 kPa) and 80 °C for 7 min, which was required for the volume to be reduced to slightly less than 1 mL. Rotary evaporation was accomplished in order to eliminate traces of methanol that are naturally present in the acetone, which could interfere with the electrochemical measurements. The evaporated sample was quantitatively transferred to a 5.00 mL volumetric flask containing $HClO_4$ at a concentration of 100 mmol L^{-1}.

The extraction procedure described above can be safely employed for a biodiesel mass of up to 4 g, if necessary.

2.4. Preparation of the control sample

2.4.1. A glycerol-free matrix

In order to obtain a glycerol-free biodiesel sample, approximately 50 mL of the biodiesel were transferred to a separatory funnel and washed with 50 mL portions of hot deionized water until the aqueous phase became clear. Then, aliquots of the organic phase with traces of water were drained and centrifuged, to achieve a more satisfactory phase separation. The organic phases were then drained and placed in a distilling flask at 105 °C for 3 h, to ensure total elimination of the residual water. Analysis of the treated

biodiesel by the method developed here confirmed the absence of free glycerol.

2.4.2. Biodiesel sample with known free glycerol concentration

A glycerol-free biodiesel sample (10 g, weighed with a precision of 0.1 mg, prepared as described in Section 2.4.1) was transferred to a screw-cap test tube. A glycerol standard solution (160 μL from 10.01 ± 0.01 g L^{-1}) was then added to this sample, and the resulting sample was vortex-mixed for homogenization. The mixture was then placed in a distilling flask at 105 °C for 3 h, to ensure total elimination of residual water. The biodiesel prepared in this way had a known concentration of glycerol of 160 mg kg^{-1}.

3. Results and discussion

3.1. Glycerol electrochemical behavior

The voltammetric behavior of a platinum electrode in the absence and in the presence of glycerol can be seen in Fig. 1.

Inhibition of the hydrogen adsorption/desorption (cathodic/anodic sweep) peaks due to glycerol chemisorption is observed at potentials lower than 0.11 V *versus* $Ag/AgCl_{(sat)}$, in the presence of glycerol. During the cathodic potential sweep, a low glycerol oxidation current at potentials in the double layer region can be seen followed by a peak (A), between 0.4 and 0.8 V *versus* $Ag/AgCl_{(sat)}$. This peak corresponds to the direct oxidation of glycerol on the electrode surface. There is also a small peak (B) between 0.7 and 1.3 V *versus* $Ag/AgCl_{(sat)}$, due to the simultaneous anodic desorption of adsorbed glycerol and intermediates and the formation of surface oxide on the Pt electrode. No peaks are observed between 1.3 and 0.7 V *versus* $Ag/AgCl_{(sat)}$ during the cathodic sweep, which indicates that there is no activity of the oxide-covered surface for glycerol oxidation. As for the 0.70–0.45 V *versus* $Ag/AgCl_{(sat)}$ potential range (C), there is cathodic reduction of the generated oxide layer, followed by a new oxidation between 0.45 and 0.20 V *versus* $Ag/AgCl_{(sat)}$ (D).

According to Roquet *et al.* [16], who conducted a study on the kinetics and mechanisms of the electrocatalytic oxidation of glycerol using a glycerol concentration of 0.1 mol L^{-1}, the quasi-superimposition of the curves during the positive and the negative potential sweeps suggests small poisoning effects. But the fact that the curves are not perfectly superimposed is presumably due to a limiting rate of glycerol adsorption on the freshly reduced Pt surface during the relatively rapid negative potential sweep.

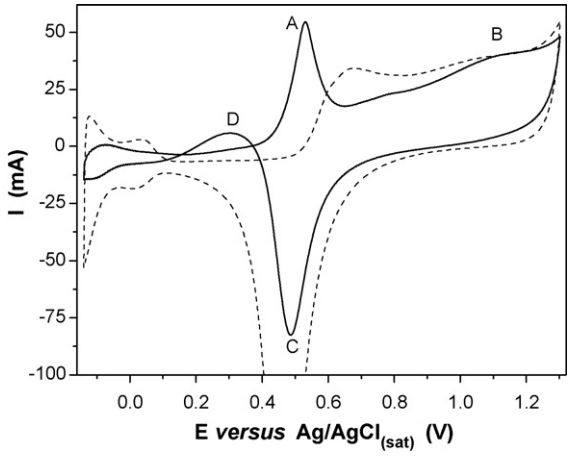

Fig. 1. Voltammograms of a smooth platinum electrode in 100 mmol L^{-1} $HClO_4$; $\nu = 100$ mV s^{-1}; without (– – – –) and with (——) 1.54 mmol L^{-1} glycerol (after 20 consecutive cycles).

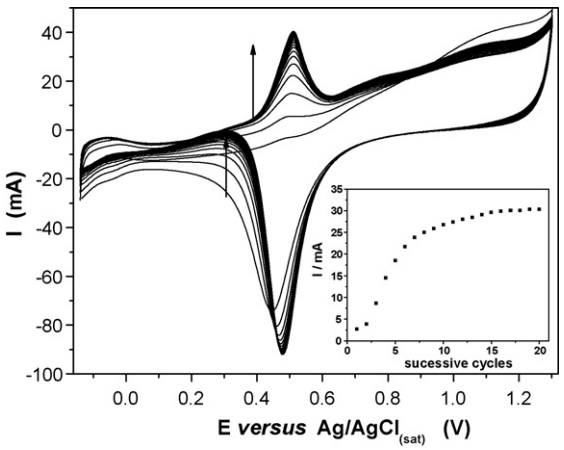

Fig. 2. Consecutive voltammograms of a 1.08 mmol L^{-1} glycerol solution in $HClO_4$ 100 mmol L^{-1}; $\nu = 100$ mV s^{-1}.

The oxidation peaks A and D increase with glycerol concentration; however, only peak A was chosen for the quantitative measurements because it is better defined and more sensitive in the concentrations employed in the present work. Fig. 2 shows that there is an increase in the current of peak A upon consecutive cycles, but it becomes stable after 20 consecutive voltammetric cycles. Peaks A and D cannot be detected in the first voltammetric cycle in the case of the studied glycerol concentration. The phenomenon responsible for more intense oxidation peak currents as a function of the number of voltammetric cycles is related to oxide growth on the platinum electrode surface in the presence of adsorbed glycerol.

The formation of platinum oxides by potential cycling between critical limits has been investigated by Burke and Roche [21] in 1.0 mol L^{-1} H_2SO_4 solution between 0 and 1.6 V *versus* RHE. The authors concluded that the potential cycling technique is a much more effective procedure for the growth of multilayer oxides. According to these authors, one of the major advantages of thick oxide growth under potential cycling conditions is that there is no need for abrasive pretreatment. In this kind of pretreatment, the generation of mechanical stress on the surface (by grinding with emery paper) is necessary for growth of a thick film. The authors explained that stress on the electrode surface is not necessary under potential cycling conditions because the formation and subsequent reduction of the monolayer film leaves the metal atoms at the surface in a disturbed state. On subsequent reoxidation, the compact oxide layer is regenerated by oxidation of the underlying bulk metal lattice, while the dispersed platinum atoms are more fully oxidized and converted to the hydrous state. This possibly occurs by repeated oxidation and reduction at the compact oxide/hydrous oxide interface.

It was necessary to perform consecutive voltammetric cycles for each measurement accomplished in the presence of glycerol because this easy re-oxidizability decays rapidly if the reduced electrode is allowed to remain on open-circuit for any appreciable time length. This fact has also been observed by James in his works on platinum oxide [22].

For practical purposes, we verified whether it was possible to use the 10th consecutive voltammetric cycle instead of the 20th for the quantitative measurements. In tests carried out at a sweep rate of 100 mV s^{-1} in $HClO_4$ 100 mmol L^{-1}, application of the least squares method to our data furnished the following straight line equation for the 10th cycle: I (μA) $= 6.6 \pm 0.5 + 0.294 \pm 0.007 \times C$ (mg L^{-1}), with $r = 0.9987$. As for the 20th cycle, the equation was I (μA) $= 6.6 \pm 0.2 + 0.301 \pm 0.003 \times C$ (mg L^{-1}), with $r = 0.9998$. These results confirm the possibility of using the 10th consecutive voltammetric cycle, although data obtained in the 20th cycle are more

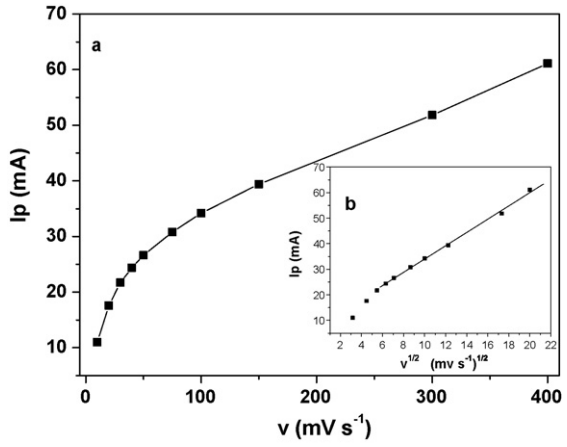

Fig. 3. Influence of the sweep rate on peak current (a), and peak current as a function of the square root of the sweep rate (b), as measured during the 20th voltammetric cycle, 1.08 mmol L^{-1} glycerol in $HClO_4$ 100 mmol L^{-1}.

precise and the linear correlation coefficient of the analytical curve is better.

Fig. 3 depicts the peak current variation as a function of the sweep rate (Fig. 3a) and the square root of the sweep rate (Fig. 3b). The results suggest that a diffusion-controlled mass transport predominates in the case of sweep rates higher than 40 mV s^{-1}.

Tests revealed that the type of mass transport is not altered for $HClO_4$ concentrations ranging between 10 and 100 mmol L^{-1}. Nevertheless, for quantitative purposes, analytical curves obtained at an acid concentration of 100 mmol L^{-1} gives better linear correlation coefficients. We selected the sweep rate 100 mV s^{-1} because it resulted in better defined voltammograms, with more intense peak currents.

3.2. Analytical curve

To verify the linearity of the electroanalytical method developed here, an analytical curve of glycerol in $HClO_4$ 100 mmol L^{-1} solution was built as described in Section 2.2. The concentration range selected for curve construction considered concentrations that might be found in real biodiesel samples submitted to the extraction technique designed here. The obtained graph is depicted in Fig. 4.

This analytical curve displays a large linearity interval between 15 mg L^{-1} (0.16 mmol L^{-1}) and 150 mg L^{-1} (1.6 mmol L^{-1}). The linear correlation coefficient is $r = 0.99965$ in this concentration

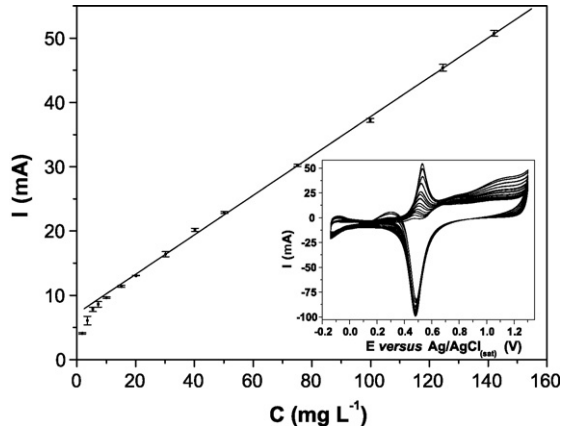

Fig. 4. Glycerol analytical curve obtained in $HClO_4$ 100 mmol L^{-1} and v = 100 mV s^{-1}.

Table 1
Determination of glycerol concentrations from simulation of the rotary evaporation process.

	Expected concentration	Obtained concentration
Free glycerol concentration (mg L^{-1})	34.9	28 ± 5
	69.5	67 ± 4
	100	100 ± 3

range. The straight line equation obtained by application of the least squares method was I (μA) = 7.16 ± 0.24 + 0.306 ± 0.003 × C (mg L^{-1}). From the obtained data, a detection limit of 2.3 mg L^{-1} (2.5 × 10^{-2} mmol L^{-1}) can be achieved.

The linearity range obtained with this method is reproducible for various electrode surface polishings. However, the obtained linear equations are strictly valid for a specific surface, which is particular of each polishing process. This justifies the preparation of a new analytical curve every time a new polishing is necessary.

In precision studies (repeatability) accomplished for glycerol concentrations of 20, 75, and 100 mg L^{-1}, in the same electrochemical conditions established in Section 2.2, current peak values of 13.2 ± 0.1, 30.5 ± 0.2, and 37.7 ± 0.2 μA were obtained, respectively, with a reliability limit of 95% for the 20 measurements.

Considering the analytical curve and the extraction method proposed in Section 2.2, which employs 2 g of biodiesel, the linearity interval between 15 and 150 mg L^{-1} corresponds to 56–560 mg kg^{-1} (glycerol:biodiesel). This includes a wide concentration range with values well below and well above the maximum tolerated by regulatory agencies; that is, 200 mg kg^{-1}. In the case of a biodiesel sample, this working range depends on the mass of biodiesel weighed before the extraction procedure, so it can be altered according to sample quality and the desired precision. A working range of 37.5–375 or 28–280 mg kg^{-1} may be employed for a biodiesel sample weighing 3 or 4 g, respectively.

The equation relating the free glycerol concentration in mg L^{-1} with the concentration in mg kg^{-1}, taking the dilution steps involved in the extraction procedure into account, is C (mg kg^{-1}) = 15/2 × C (mg L^{-1})/m (g), where m = actually weighed biodiesel mass.

3.3. Simulation of glycerol loss during rotary evaporation

To verify whether rotary evaporation causes glycerol loss, a simulation with known amounts of glycerol in water was carried out.

Nine test samples were prepared (three different concentrations, in triplicate) and placed directly in the rotary evaporator. This was done by transferring amounts of the glycerol stock solution that would allow us to obtain glycerol concentrations of 35, 70, and 100 mg L^{-1} in $HClO_4$ 100 mmol L^{-1} solution after the evaporation process and subsequent quantitative transfer to a 5.00 mL volumetric flask.

Before the electrochemical measurements were carried out, the working electrode was submitted to the cleaning and activation stages described in Section 2.2. Then, a new current *versus* glycerol concentration analytical curve was built for glycerol concentrations ranging between 15 and 100 mg L^{-1} in $HClO_4$ 100 mmol L^{-1} solution. The results are summarized in Table 1.

The results show that the obtained concentration values are very close to the expected ones, being the relative error lower for higher concentrations. The errors may be attributed to sample handling and dilution. From these considerations, we can conclude that there is no glycerol loss in the rotary evaporation process.

3.4. Determination of free glycerol in biodiesel

Three aliquots of 2 g biodiesel containing a known amount of glycerol, prepared as described in Section 2.4.2, were submitted to

Table 2
Determination of free glycerol levels in a matrix containing a known concentration of glycerol.

	Expected concentration	Obtained concentration	Average recovery
Free glycerol ($mg\,L^{-1}$)	42.7	45.7 ± 4	
Free glycerol ($mg\,kg^{-1}$)[a]	160	171 ± 15	107%
Free glycerol (wt%)	0.0160	0.017 ± 0.002	

[a] $C\,(mg\,kg^{-1}) = 15/2 \times C\,(mg\,L^{-1})/m\,(g)$ where m = mass of biodiesel.

the extraction procedure reported in Section 2.3. The electroanalytical procedure described in Section 2.2 was carried out parallel to the aforementioned procedure, to obtain an analytical curve falling within the linear concentration range, resulting in the linear equation $I\,(\mu A) = 1.01 \pm 0.50 + 0.295 \pm 0.007 \times C\,(mg\,L^{-1})$ with $r = 0.99948$.

The obtained concentrations are depicted in Table 2.

The results confirm the efficiency of the electrochemical method and the extraction procedure developed in this work, with satisfactory recovery.

4. Conclusion

A novel, alternative electroanalytical method for determination of free glycerol in biodiesel has been developed. The extraction method designed here is fast and environmentally friendly, since only a mixture of biodiesel and water and a single solid-phase extraction stage using acetone are necessary. The rotary evaporation procedure adopted here is fast and satisfactory for the analyses. As for the electroanalytical procedures, the use of consecutive voltammetric cycles (potential cycling technique) enables detection of glycerol in concentrations well below the ones that can be measured with a single voltammetric cycle. The developed extraction method gives good linearity for glycerol concentrations ranging between 15 and 150 $mg\,L^{-1}$ (0.16 and 1.6 $mmol\,L^{-1}$), which corresponds to concentrations falling within 56–560 $mg\,kg^{-1}$(glycerol:biodiesel) when a mass of biodiesel equal to 2 g is employed for extraction. This therefore includes a wide linearity range with values well below and well above the maximum amount tolerated by the regulatory agencies, which is 200 $mg\,kg^{-1}$.

The electroanalytical method is highly repeatable for a long period, thus enabling determination of glycerol in a large number of samples, with no need for recalibration.

The procedures involving extraction, sample handling, and electrochemical measurements in triplicate take up 80 min (not considering the preparation of the platinum electrode, *ca.* 75 min that is accomplished in parallel with the extraction procedure and includes platinum surface cleaning and activation as well as construction of the analytical curve). Although the procedure developed here comprises various stages, the analysis time is relatively short compared with the time necessary to carry out chromatography [8,9], which is around 30 min for a single analysis in a single chromatographic run.

Acknowledgements

The authors are grateful to CAPES for financial support and Cynthia Maria de Campos Prado Manso for linguistic advice.

References

[1] L.C. Meher, D.V. Sagar, S.N. Naik, Renew Sust. Energ. Rev. 10 (2006) 248.
[2] P. Bondiolli, L.D. Bella, Eur. J. Lipid Sci. Technol. 107 (2005) 153.
[3] M. Mittelbach, Bioresour. Technol. 56 (1996) 7.
[4] A. Neher, et al., USPTO Patent Full, Patent 5,387,720 (1995).
[5] ANP, Agência Nacional de Petróleo. Resolução no. 7 de 19 de Março de 2008, Regulamento Técnico ANP no. 1/2008, Brasília, Diário Oficial da União.
[6] P. Bondiolli, C. Mariani, A. Lanzani, E. Fedeli, S. Veronese, Riv. Ital. Sostanze Gr. 69 (1992) 7.
[7] R.W. Heiden, Analytical methodologies for the determination of biodiesel ester purity—determination of total methyl esters, Final report, NBB CONTRACT: 520320-l, 1996, website: http://www.biodiesel.org/resources/reportsdatabase/reports/gen/19960227_gen-221.pdf.
[8] C. Plank, E. Lorbeer, J. Chromatogr. A 697 (1995) 461.
[9] M. Mittelbach, G. Roth, A. Bergmann, Chromatographia 42 (1996) 431.
[10] M. Mittelbach, Chromatographia 37 (1993) 623.
[11] P. Lozano, N. Chirat, J. Graille, D. Pioch, Fresenius J. Anal. Chem. 354 (1996)319.
[12] M. Hájek, F. Skopal, J. Machek, Eur. J. Lipid Sci. Technol. 108 (2006) 666.
[13] J. Bailer, K. Hueber, Fresenius J. Anal. Chem. 340 (1991) 186.
[14] P. Bondioli, D. Bella, Eur. J. Lipid Sci. Technol. 107 (2005) 153.
[15] Yu.B. Vasilïev, V.S. Bagotskii, Toplivn. Elementy (1964) 108.
[16] L. Roquet, E.M. Belgsir, J.-M. Léger, C. Lamy, Electrochim. Acta 39 (1994) 2387.
[17] A. Kahyaoglu, B. Beden, C. Lamy, Electrochim. Acta 29 (1984) 1489.
[18] C.B. Roy, D.K. Nandi, K.V. Rao, Indian J. Chem. A 24A (1985) 742.
[19] J.E. Vitt, L.A. Larew, D.C. Johnson, Electroanalysis 2 (1990) 21.
[20] S. Shigang, Y. Dongfang, T. Zhaowu, Acta Chim. Sin. 50 (1992) 533.
[21] L.D. Burke, M.B.C. Roche, J. Electroanal. Chem. 137 (1982) 175.
[22] S.D. James, J. Electrochem. Soc. 116 (1969) 1681.

Talanta 79 (2009) 10–15

Contents lists available at ScienceDirect

Talanta

journal homepage: www.elsevier.com/locate/talanta

Extraction of polycyclic aromatic hydrocarbons from smoked fish using pressurized liquid extraction with integrated fat removal

Mette Lund[a,b], Lene Duedahl-Olesen[a], Jan H. Christensen[b,*]

[a] DTU, National Food Institute, Department of Food Chemistry, Mørkhøj Bygade 19, 2860 Søborg, Denmark
[b] University of Copenhagen, Faculty of Life Sciences, Department of Basic Sciences and Environment, Thorvaldsensvej 40, 1871 Frederiksberg C, Denmark

ARTICLE INFO

Article history:
Received 20 October 2008
Received in revised form 1 February 2009
Accepted 20 February 2009
Available online 5 March 2009

Keywords:
Pressurized liquid extraction
Smoked fish
Polycyclic aromatic hydrocarbons
Method validation
Principal component analysis

ABSTRACT

Quantification of polycyclic aromatic hydrocarbons (PAHs) in smoked fish products often requires multiple clean-up steps to remove fat and other compounds that may interfere with the chemical analysis. We present a novel pressurized liquid extraction (PLE) method that integrates exhaustive extraction with fat retention in one single analytical step. The PLE parameters: type of fat retainer, flush volume, solvent composition, fat-to-fat retainer ratio (FFR), and the dimensions of the extraction cells were the most important factors for obtaining fat-free extracts with high recoveries of PAHs. A 100 mL extraction cell filled with 18 g activated silica gel, dichloromethane:hexane (15:85, v/v) as extraction solvent, FFR of 0.025 and 100% flush volume was the best analytical setup for integrated extraction and fat retention.

The one-step procedure provided a more rapid and cost-efficient alternative with minimization of waste generation compared to the standard reference method that is based on a multi-step procedure. Furthermore, the analytical quality of the two methods are comparable, while the new integrated approach for extraction and cleanup is less prone to analytical errors (random and systematic) because of fewer analytical steps.

1. Introduction

Polycyclic aromatic hydrocarbons (PAHs), of which some are genotoxic and/or carcinogenic, are formed during incomplete combustion processes both spontaneously in nature and owing to fossil fuel combustion. The route to human exposure is manifold, since the PAHs can enter the food chain by both deposition and transfer from soil, air, and water. PAHs may therefore constitute a food safety problem. The most important factor for human exposure—and the factor of interest in this study—is the cooking procedure for food products. PAHs can be generated during drying, smoking, grilling, roasting, and frying. Smoked food products are directly exposed to PAHs during the smoking process, and the amount of PAHs transferred by smoke depends on the temperature of smoke, type of wood, length of time of smoking, and whether the smoking is indirect or direct [1–5].

Lipids interfere with the chemical analysis by gas chromatography–mass spectrometry (GC–MS) and may have severe effects on reproducibility, robustness, and PAH recovery [6]. It is therefore often necessary to remove lipids prior to the chemical analysis, which is typically done in a tiered approach: Extraction of PAHs by Soxhlet [3,7,8]; sonication [7,8]; supercritical fluid extraction [8–10] or pressurized liquid extraction (PLE) [11–13]; gel permeation chromatography (GPC) [12,14,15] and/or solid phase extraction (SPE) [3,11,15] to remove lipids and other interferences; and quantification by GC–MS [10,11,13] or high-performance liquid chromatography (HPLC) [8,9,14].

The large number of analytical steps results in high consumption of hazardous organic solvents, high costs, prolonged analysis time [12,16], an increased risk of analyte losses, decreased reproducibility, and biases. These drawbacks are also experienced in the standard reference method (SRM) for PAH sample preparation used at DTU FOOD, Denmark: PLE extraction, clean-up by GPC and SPE, and quantification by GC–MS [17], although the use of PLE can integrate extraction with fat removal [6,18–20], thereby reducing the number of analytical steps. A one-step PLE method can be achieved by adding a stationary phase (e.g. silica or alumina) directly to the PLE extraction cell. This method has previously been used in the analysis of polychlorinated biphenyls (PCBs) in fish samples [6,18–20].

The aim of this study was therefore to develop and validate a new one-step PLE method that integrates exhaustive extraction of PAHs with fat removal. The new method would be quicker than the SRM and minimize waste generation, while its analytical quality would be comparable to the SRM. Both the levels and patterns of PAHs in food products are of interest, and the method was therefore developed for analysis of 2–6 ringed PAHs. Reproducibility and accuracy of the one-step PLE method was further validated by comparing the

* Corresponding author. Tel.: +45 35332456; fax: +45 35332398.
E-mail address: jch@life.ku.dk (J.H. Christensen).

0039-9140/$ – see front matter © 2009 Elsevier B.V. All rights reserved.
doi:10.1016/j.talanta.2009.02.048

measured concentrations in 10 smoked fish samples between the two methods.

2. Experimental

2.1. Samples

Pork lard and raw trout were bought from the local butcher and fishmonger, respectively, and samples were then homogenized. Thin layers of the pork lard were scraped off to facilitate homogenization. After removal of head and skin, the fish fillets were homogenized for 10 min using a stainless steel blender (Broendum, Copenhagen, Denmark). In addition, homogenized samples of 10 fish that had been smoked by Danish fishmongers were obtained from the Danish Veterinary and Food Administration (DVFA) in Aarhus. All samples were stored at −18 °C prior to analysis.

2.2. Chemicals and reagents

Toluene, *n*-hexane (HPLC grade), and sulphuric acid were obtained from Merck (Darmstadt, Germany) and acetone, dichloromethane (HPLC grade), and *n*-pentane from Rathburn (Walkerburn, Scotland). Silica gel 60 (0.063–0.200 mm) was purchased from Merck (Darmstadt, Germany), florisil (60–100 mesh) from Fluka (Buchs, Switzerland), and neutral, basic and acidic alumina (150 mesh) from Sigma–Aldrich (Steinheim, Germany). Pre-rinsed silica gel, alumina and florisil were activated at 130–140 °C over night and stored at 120 °C. Sulphuric acid impregnated silica was prepared by adding sulphuric acid to cold silica gel (2:3, w/w). Anhydrous sodium sulphate was obtained from Merck (Damstadt, Germany), polyacrylic acid from Sigma–Aldrich (Steinheim, Germany), and Ottawa sand (20–30 mesh) from AppliChem (Darmstadt, Germany). Ottawa sand was precleaned by heating at 500 °C for 5 h.

Different spike, recovery, and internal standard solutions were applied, each consisting of PAHs or deuterated PAHs (d-PAHs) purchased from Ehrenstorfer (Augsburg, Germany) and Cambridge Isotope Laboratories (Cambridge, UK). Details on the standard solutions are listed in Table 1 in the supporting information (Table S1). To determine the optimal fat retainer (Section 3.1), PAH quantification was performed using one-point calibrations. To investigate the effects of PLE parameters (Section 3.3) and for validation (Section 3.4), the internal standard method was used, with six calibration solutions ranging from 50 to 250 ng/mL and eight calibration solutions ranging from 0 to 250 ng/mL, respectively.

Table 1
ASE settings for the final one-step PLE method.

Sample preparation	PLE settings	Analysis
100 mL extraction cell	Solvent composition: 85:15 (hexane:dichloromethane)	ASE extracts are evaporated by vacuum evaporator (35 °C) until 2 mL
Sample mixed with 5 g Ottawa sand and 10 g polyacrylic acid	Time of each static cycle: 5 min	The extracts are quantitatively transferred to GC–MS vials and evaporated by nitrogen steam
18 g silica as fat retainer	Number of static cycles: 2	The GC–MS vials are added toluene and the final volume evaporated to 100 μL by nitrogen steam
FFR value: 0.025	Polar solvent: dichloromethane Apolar solvent: hexane Flush volume: 100% Temperature: 100 °C Purge: 60 s Pressure: 1500 psi	

2.3. Fat determination

The fat content of pork lard and fish homogenates was determined in triplicates. For wet trout and smoked fish homogenate, a mixture of 10 g sample, 10 g Ottawa sand, and 20 g polyacrylic acid was added to a 66 mL ASE cell and extracted using an ASE 300 System (Dionex, Sunnyvale, CA) with instrument settings of 100 °C, 2 static cycles of 5 min, 75% flush volume, and an extraction solvent of hexane:acetone (1:1, v/v). The fat content was determined gravimetrically at 70 °C.

2.4. PLE parameters

ASE cells with volumes of 33 mL (ASE 200) and 100 mL (ASE 300) were packed with one cellulose filter at the bottom followed by the fat retainer. For fish homogenates, 2 g of polyacrylic acid was placed on top of the fat retainer to avoid deactivation of the fat retainer by water. Pork lard was ground with sodium sulphate until dry, and 5 g wet trout was ground with 5 g Ottawa sand and 10 g polyacrylic acid. The dried samples were transferred to the ASE cells, and spike standards were added (see Table S1 for details). The void volume was filled with Ottawa sand. The fat retainer, solvents, solvent composition, and flush volume were optimized, while the fat-to-fat retainer ratio (FFR) (0.025), temperature (100 °C), pressure (1500 psi), number of static cycles (2 of 5 min each), and purging time (60 s with nitrogen) were fixed throughout the study. Since the FFR was fixed, the amount of sample weighed for each extraction varied according to the fat content.

2.5. Preparation of extracts

Extracts were evaporated to 80 mL using a rotary evaporator at 35 °C and transferred quantitatively to 100 mL volumetric flasks, which were filled to the mark with pentane. Ten mL was used for fat determination. For quantification, the solvent was further reduced to 2 mL using a rotary evaporator (35 °C) and transferred to GC vials that were placed under a stream of nitrogen. The recovery standard (see Table S1 for details) and 200 μL toluene were added, and the total volume was reduced to 100 μL.

2.6. GC–MS analysis

Extracts were analysed on an Agilent 6890N gas chromatograph that was connected to an Agilent 5975B mass spectrometer with electron ionization. The gas chromatograph was equipped with a 40 m ZB-5 capillary column with special dimensions (0.18 mm id × 0.25 μm film). Helium was used as carrier gas at a flow rate of 0.8 mL/min, and 1 μL aliquots were injected in splitless mode. Injector, ion source, and quadropole temperatures were 330, 230, and 150 °C. The oven programme was: 100 °C (held for 2 min), increased to 230 °C (6 °C/min), and then 1 °C/min to 245 °C, 6 °C/min to 268 °C, 2 °C/min to 300 °C, and 6 °C/min to 330 °C. Selected ion monitoring was used to analyze 18 *m*/*z* values in the range *m*/*z* 128–316, divided into 5 groups with 4–7 ions in each.

2.7. Validation

The new method was validated by comparing its precision (repeatability), accuracy, PAH recoveries, limits of detection (LOD), and limits of quantification (LOQ) to those of the SRM. The determination of these values was based on six extractions of sub-samples of homogenized and dried trout samples spiked with 3 ng of each of the 26 PAHs/g wet tissue (see Table S1) and three method

blanks. Furthermore, robustness was estimated with respect to fat-retention capacity, as the method was applied to six fish homogenates of 5 g each combined with 18 g silica (between 5 and 30% fat). All samples were extracted and quantified in random order in two batches during two days.

2.8. Data

Concentrations of 17 PAHs in 63 smoked fish samples (viz. herrings, salmons, mackerels, and trouts) collected from smoking facilities in Denmark were measured by DVFA using the SRM (for method details, see ref. [17]). Nine of the 63 smoked fish samples and four replicates of one sample were analysed using the new one-step PLE method. Concentrations below LOD were set to zero. Because of the low concentrations, some 5–6 ring PAHs were collected in groups based on physicochemical similarities, Toxic/4 (Σbenzo[*a*]anthracene and chrysene), Toxic/5 (Σcyclopenta[*cd*]pyrene, benzo[*b*]fluoranthene, benzo[*j*]fluoranthene and benzo[*k*]fluoranthene), Toxic/6 (Σindeno[1,2,3-*cd*]pyrene and benzo[*ghi*]perylene), Toxic/T (ΣToxic/4, Toxic/5, Toxic/6 and benzo[*a*]pyrene) and PAH ($\Sigma PAHs_{26}$), giving a total of 14 PAH variables. The complete data set was divided into two sets: the 'training set' consisting of 63 smoked fish samples × 14 PAH concentrations analyzed by the SRM, and the 'test set' comprised of the 13 samples × 14 PAH concentrations analysed by the one-step PLE method.

2.9. Principal component analysis

Principal component analysis (PCA) [21,22] was used to assess the accuracy of the one-step PLE method compared to the SRM. Seven of the 63 samples analysed by the SRM were removed because of outliers in influence plots. The training set was autoscaled and analysed by PCA with full cross validation. Based on an explained variance plot and the scores and loadings, two principal components were chosen. The 'test set' (X_{new}) was then projected on the model loadings using Eq (1) to obtain the scores T_{new}.

$$T_{new} = X_{new}P \quad (1)$$

PCA was performed in MatLab 7.4.0 using the PLS toolbox 4.1.1 (www.eigenvector.com).

3. Results and discussion

3.1. Selection of fat retainer

Silica impregnated with sulphuric acid is the most frequently used fat retainer for integrated extractions of organic contaminants [6,18,19], but florisil [23] and neutral alumina [24] have also been used. A recent study of the fat-retention capacity of sulphuric-acid-impregnated silica, florisil, and basic, neutral, and acidic alumina showed that all fat retainers, except basic alumina (1.4%), yielded fat-free or nearly fat-free extracts (<1%) with FFR = 0.022 [20].

Hence, to identify a material with both high fat retention capacity and high PAH recoveries, several retainers were tested: activated silica, 2% deactivated silica, florisil, 1% deactivated florisil, alumina (neutral, basic, and acidic), 3% deactivated alumina, and sulphuric-acid-impregnated silica. The ASE 200 system with 33 mL extraction cells, pork lard, and 8 g of each fat retainer were used in this initial study. Based on previous studies [6,19,20] a FFR of 0.025, a flush volume of 70%, and an extraction solvent of dichloromethane:hexane (15:85, v/v) were employed. The amount of co-eluted fat was detected by browning reactions after adding sulphuric-acid-impregnated silica to aliquots of each extract [25].

The use of activated silica yielded both fat-free extracts (no browning reaction) and high recoveries for all PAHs (Fig. 1). Sulphuric-acid-impregnated silica gave fat-free extractions, but led to low recoveries of acenaphthylene, acenaphthene, and anthracene, as previously shown by Wang et al. [13].

Neutral, basic and acidic alumina also provided effective fat retention (limited browning reactions), but the recoveries of the high-molecular-weight (HMW) PAHs were generally low (Fig. 1, see neutral alumina). Because future optimization of the PLE parameters could lead to improved recoveries, alumina as fat retainer could not be ruled out. Neutral alumina gave the most limited browning reaction and was therefore further investigated.

A noticeable browning reaction was observed in the florisil extract, indicating an insufficient fat-retention capacity. The fat-retention capacity of florisil generally increases with lower extraction temperatures [23], but because lower temperatures decreases extraction efficiency [12,26,27], and the recoveries of HMW PAHs were already low (Fig. 1), other extraction temperatures were not tested. Remarkably strong browning reactions and fat droplets in the collection vials were observed for all the deactivated fat-retainers, demonstrating their low fat retention capacity.

3.2. Fat retention capacity

The fat retention capacity of silica and neutral alumina (hereafter denoted alumina) were compared quantitatively. The experimental settings were repeated, except that pork lard was replaced by wet trout and that the amount of fat retainer was scaled to a 100 mL ASE cell using an ASE 300 system (i.e., 5 g wet trout and 18 g fat retainer to obtain an FFR of 0.025). Activated silica gave fat-free extracts, while 27 ± 8 mg fat (6% of the total fat content) was not retained by alumina. Silica was therefore preferred as fat retainer.

The elution of fat from alumina was unexpected, since no browning reactions with sulphuric acid were observed in these extracts during the initial selection of fat retainers (cf. Section 3.1). However, in extracts where the amount of activated silica was reduced by a factor 2 and the FFR was retained, a noticeable browning reaction was also observed. This suggests that the fat retention capacity depends on the length of the chromatographic column as well as the FFR.

Recoveries obtained from activated silica using pork lard in 33 mL cells and an ASE 200 system (Fig. 1) correspond to the recoveries obtained using trout in 100 mL cells on the larger ASE 300 system (results not shown). It thus seems possible to scale the amounts of activated silica from one cell type to another with respect to recovery. However, as the length of the two cells is approximately equal, a similar ratio between the amount of fat and the length of the chromatographic column is obtained. The shorter 34 mL cell (ASE 300) results in a considerably shorter chromatographic column. This difference affects the fat retention capacity, as the FFR may be increased when changing from a 34 mL cell to the longer 100 mL cell (same diameter) [18]. As the higher density

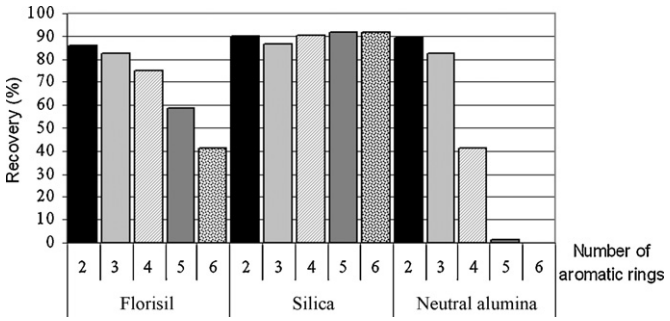

Fig. 1. PAHs recoveries from pork lard using florisil, silica, or alumina as fat retainers. The PAHs are grouped based on the number of aromatic rings. The recoveries are calculated from single measurements.

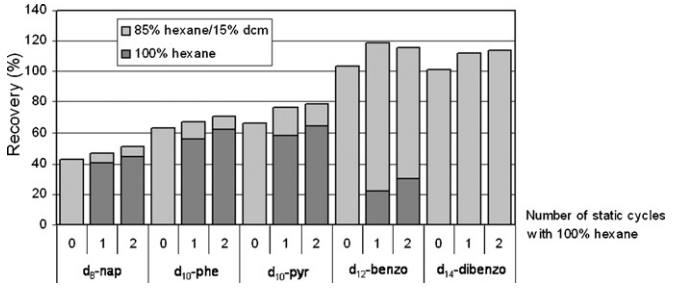

Fig. 2. Recoveries of deuterated PAHs (based on single measurements) after initial purification–0, 1 and 2 indicates the number of static cycles with pure *n*-hexane before applying 2 static cycles of dichloromethane:hexane (15:85).

of alumina compared to silica results in a shorter chromatographic column, this might explain why more than 18 g of alumina is required.

3.3. PLE parameters

One static PLE cycle with *n*-hexane has previously been used to remove apolar interferences prior to extraction of corticosteroids from bovine liver [28]. Introduction of such an additional cleanup step in the extraction procedure would be favourable and was therefore tested in this study. The test was performed by applying 0–2 cycles of 5 min with *n*-hexane prior to extraction with two cycles with dichloromethane:hexane (15:85, v/v). The flush volume was set to 70% and 100 mL ASE cells were packed with 5 g trout and 18 g silica. The results shown in Fig. 2 demonstrate that initial purification with *n*-hexane (dark columns) is inappropriate, since the recovery, especially of low-molecular-weight (LMW) PAHs (represented by d_8-naphthalene, d_{10}-phenanthrene and d_{10}-pyrene), was between 40 and 60% already for the first *n*-hexane extraction cycle.

The extraction efficiencies for HMW PAHs (represented by d_{12}-benzo[*a*]pyrene and d_{14}-dibenzo[*a*,*i*]pyrene) were between 0 and 30% in the *n*-hexane fractions, but close to 100% in the dichloromethane:hexane (15:85, v/v) fraction (Fig. 2, light columns), which indicates that the polarity of the solvent mixture is adequate for exhaustive extraction, and no further optimization is required.

The study also reveals that the recoveries of LMW PAHs (Fig. 2) are significantly lower than those observed during the initial method optimization, which is most likely caused by evaporation during the extensive pre-concentration step (i.e., the final volume was reduced to 100 μL) [29]. However, as LMW PAHs are eluted before HMW PAHs thorough activated silica, and the recoveries for 5–6 ringed PAHs were close to 100%, the one-step PLE method seems to provide an exhaustive extraction of 2–6 ringed PAHs. Any loss during the pre-concentration step can be corrected for by the use of internal standards.

PLE extraction efficiency of PAHs increases with temperature [26], while fat retention capacity is reduced [19]. Hence, the extraction temperature has to be chosen with care to obtain both high recoveries of PAHs and fat-free extracts. 100 °C seems appropriate for PAH extraction, a conclusion that is also supported by others [13].

The number of static cycles has minor effects on the extraction efficiency when using sulphuric-acid-impregnated silica for PCB extractions [6]. However, two cycles have been used most frequently [6,17,20,23], and this practice was also used here.

The flush volume divided by the number of cycles determines the amount of fresh solvent added between each extraction cycle. The flush volume may have a significant effect on recovery, especially during extractions where the ASE cells are packed with a stationary phase, as this may increase retention of the analytes. Hence, the effects of flush volumes between 70 and 130% on the PAH recoveries were tested in a system comprised of 100 mL ASE cells packed with 5 g trout and 18 g silica with dichloromethane:hexane (15:85, v/v) as extraction solvent. Note that all the extracts were fat-free. The results, shown in Fig. 1 in the supporting information (Figure S1), demonstrate that the recoveries of PAHs with 2–4 aromatic rings were unaffected by the flush volume. In contrast, increasing the flush volume from 70 to 100% significantly ($p = 0.025$) increases the recoveries of 5- and 6-ring PAHs (see Figure S1) from 102 to 107% and 76 to 92%, respectively. A flush volume of 100% was therefore chosen for the method.

Replacement of dichloromethane and *n-hexane* with less hazardous solvents (viz. acetone and pentane, respectively) was investigated. The use of acetone instead of dichloromethane led to extensive elution of fat, while replacement of *n*-hexane with *n*-pentane gave only a minor increase in fat elution, as has previously been observed by others [19]. However, as the pre-concentration step is extensive, even a small increase in fat elution should be avoided. On the other hand, in a study of integrated PLE of PAHs and fat removal from gastropods, it was found that 5% dichloromethane and 95% *n*-pentane resulted in high recoveries of 2–6 ring PAHs and insignificant elution of fat (FFR = 0.025 (unpublished data from our laboratory). Thus, using this solvent composition could make the replacement possible, since lower polarity decreases fat elution, but this was not tested further here.

The final settings of the one-step PLE method are summarised in Table 1.

3.4. Validation

The PAH recoveries were generally high (>70%), except for fluoranthene and pyrene (Table 2).

Considering that the concentrations of HMW PAHs were generally close to the LOQ, the precisions were acceptable, with relative standard deviations (RSDs) between 4 and 15%. In contrast, mainly owing to high laboratory blank values, the RSDs for naphthalene, phenanthrene, pyrene, and fluoranthene were high, between 45 and 87% (see Table 2).

The analytical quality of the SRM and the one-step PLE method is compared in Table 2. Both the recoveries and the precisions are within the same range for all compounds. Similar results are also observed for LOD and LOQ, taking into account that the calculations for the one-step PLE method were based on three times higher concentrations than those used for the SRM. The new method, however, meets the proposed EU method criteria that quote an acceptable recovery between 50 and 120%, a maximum LOD of 0.3 μg/kg and a maximum LOQ of 0.9 μg/kg for methods analysing benzo[*a*]pyrene in foods [30].

The FFR is an important parameter for optimal fat retention. Minor elution of fat (0.4%) was observed when increasing the FFR from 0.025 to 0.032; an increase to 0.043 resulted in a fat elution of 0.5%, while 6.6% was eluted using FFR = 0.082 (see Table 2 in supporting information, Table S2). Thus, the use of an additional clean-up step is most likely necessary when using an FFR greater than 0.025.

Accuracy was assessed from two extractions of a standard reference material of freeze-dried mussel tissue (NIST 2799) and by comparison of PAH concentrations in 10 smoked fish samples analyzed by both the SRM and the one-step PLE method. The bias for the 10 PAHs included in the NIST samples were between 5 and 79%, which exceeds the criteria required by NIST for 8 of 10 compounds (except for phenanthrene and benzo[*a*]pyrene). Conversely, a comparison of the PAH concentrations in the selected smoked fish samples analysed by both methods clearly indicates a high correspondence between the two sets of measurements for 7 out of 10

Table 2
List of recoveries, precision, accuracy, LOD, LOQ and linearity of the calibration curves. LOD and LOQ were calculated as 3 and 10 s respectively. $\bar{x}$ = average concentration, s = standard deviation, *a* is data obtained using the SRM and *b* is data obtained using the one-step PLE method.

PAH	Internal standard	Linearity (R^2)	$\bar{x}$ (ng/g)	s (ng/g)	Recovery (%)		Precision (%)		LOD (ng/g)		LOQ (ng/g)		Accuracy (%)
					a	*b*	*a*	*b*	*a*	*b*	*a*	*b*	
Naphthalene		0.996	2.5	1.5	70	83	95	59	5.3	4.4	17.7	14.6	
Acenaphthylene		1.000	2.2	0.3	93	74	6	15	0.4	1.0	1.3	3.2	
Acenaphthene	d_8-acenaphthylene	0.998	2.6	0.6	96	86	27	25	1.5	1.9	5.0	6.4	
Fluorene		0.999	2.4	0.5	89	83	16	21	1.0	1.6	3.3	5.3	−39
Phenanthrene		0.998	2.2	1.2	142	72	80	56	4.6	3.7	15.3	12.2	−6
Anthracene		0.999	3.0	0.5	104	99	5	17	0.3	1.5	1.0	5.1	
Fluoranthene		0.997	1.6	1.4	82	53	41	87	0.8	4.2	2.7	14.0	−79
Pyrene		0.998	2.0	0.9	81	66	29	45	1.7	2.7	5.7	9.0	−54
Benzo[*c*]fluorene		0.998	2.4	0.2	–	83	–	9	–	0.6	–	2.2	
Benzo[*a*]anthracene	d_{12}-benzo-[*a*]anthracene	0.996	2.5	0.2	92	82	4	7	0.2	0.5	0.7	1.7	−29
Chrysene		0.995	2.9	0.2	95	82	4	6	0.4	0.5	1.3	1.6	
Cyclopenta[*cd*]pyrene		0.997	2.5	0.4	102	85	15	14	0.8	1.1	2.7	3.5	
5-methylchrysene		0.998	2.8	0.2	101	94	9	8	0.5	0.7	1.7	2.3	
Benzo[*b*+*j*+*k*]fluoranthene		0.998	8.4	0.7	–	94	–	8	–	2.1	–	7.0	
Benzo[*e*]pyrene	d_{12}-benzo-[*a*]pyrene	0.998	2.7	0.2	88	91	9	8	0.5	0.6	1.7	2.1	−13
Benzo[*a*]pyrene		0.999	3.1	0.1	86	103	6	3	0.4	0.3	1.3	0.9	6
Perylene		0.997	4.1	0.2	83	108	6	6	0.5	0.7	1.7	2.4	−34
Indeno[1,2,3-*cd*]pyrene		0.998	2.4	0.1	91	82	6	3	0.4	0.2	1.3	0.7	−42
Dibenzo[*a*,*h*]anthracene	d_{12}-indeno-[1,2,3-*cd*]-pyrene	0.998	2.4	0.2	90	78	7	9	0.4	0.6	1.3	2.1	
Benzo[*ghi*]perylene		0.999	2.3	0.2	83	77	12	7	0.7	0.5	2.3	1.5	−41
Dibenzo[*a*,*l*]pyrene		0.997	3.1	0.1	112	107	13	3	0.4	0.3	1.3	0.9	
Dibenzo[*a*,*e*]pyrene	d_{14}-dibenzo-[*a*,*i*]pyrene	0.999	2.9	0.1	108	101	10	3	0.6	0.3	2.0	1.0	
Dibenzo[*a*,*i*]pyrene		0.999	2.9	0.1	98	99	8	3	0.4	0.3	1.3	1.0	
Dibenzo[*a*,*h*]pyrene		0.999	2.8	0.2	93	95	10	8	0.5	0.6	1.7	2.2	

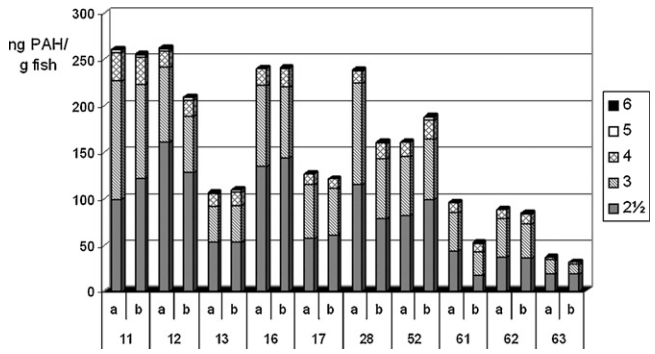

Fig. 3. PAH concentrations in 10 fish samples measured by the SRM (a) and the one-step PLE method (b). Numbers refer to samples in a larger data set obtained from DVFA.

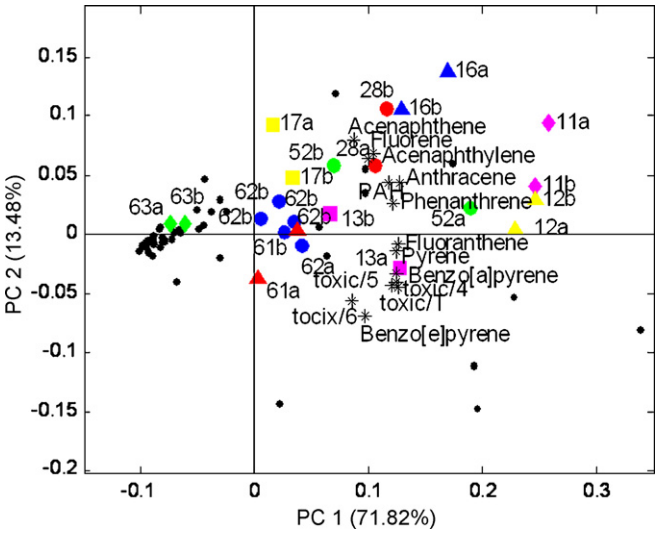

Fig. 4. Bi-plot of PC1 vs. PC2 for the scores and loadings obtained from an auto-scaled PCA model. The model was calculated for the training set and the test set samples were projected on the model. Identical samples measured by the SRM (a) and the one-step PLE method (b) are marked with identical signs.

samples (Fig. 3), indicating a high accuracy of the PLE method based on comparison with the SRM. The deviations in the three remaining samples (namely 12, 28 and 61) were mainly due to higher total PAH concentrations in the samples measured by the SRM, while the relative composition of 2½–6 ringed PAHs were similar. The variations in total PAH concentrations are most likely due to insufficient homogenization, resulting in high sample heterogeneity.

The PCA of the training set and prediction of the test set provides an additional comparison of the two analytical methods (accuracy and reproducibility). The bi-plot of PC1 vs. PC2 is shown in Fig. 4.

Samples marked with identical enlarged legends represent the same samples measured using the SRM (a) and the one-step PLE method (b), respectively. The chemical interpretation of the principal component loadings for the 14 PAH variables is straightforward: PC1 describes the PAH concentrations, since all variables have positive PC1 loadings, while PC2 explains variations related to compound sizes and physicochemical properties (i.e., HMW PAHs have negative PC2 loadings and LMW PAHs have positive PC2 loadings). Variability between the two methods is presented as the distances between identical samples, and because autoscaling unifies the importance of each individual compound in the PCA model, the correspondence between the methods confirms the high accuracy that is seen in Fig. 3. In addition, the correspondence between replicate analyses (sample 62b) indicates a high repeatability of the one-step PLE method.

4. Conclusions

The one-step PLE method is both rapid and cost-effective and minimizes waste generation compared to the SRM. The time required in the laboratory is reduced to half by combining the extraction and the two clean-up steps (i.e., GPC and SPE) in one single PLE step, which reduces the risk for bias because of fewer analytical steps. Furthermore, validation confirms that the one-step PLE method is able to replace the SRM because the analytical quality is comparable. Activated silica was found to be the preferred fat retention material, but it should be noticed that the amounts that were used cannot be directly scaled to other cell volumes. Further optimization is therefore required when using other cell types or ASE Systems.

Acknowledgements

We thank Jette Petersen for technical assistance and Kathleen Gail Jensen for proofreading. This study was supported financially by the Torkil Holm Foundation (consumables) and the COWI foundation and Ib Henriksens foundation (for funding the ASE-200 system).

Appendix A. Supplementary data

Supplementary data associated with this article can be found, in the online version, at doi:10.1016/j.talanta.2009.02.048.

References

[1] P. Šimko, Mol. Nutr. Food Res. 49 (2005) 637.
[2] I. Stumpe-Viksna, V. Bartkevics, A. Kukara, A. Morozovs, Food Chem. 110 (2008) 794.
[3] B.H. Chen, Y.S. Lin, J. Agric. Food Chem. 45 (1997) 1394.
[4] H. Karl, M. Leinemann, Zeitschrift für Lebensmittel Untersuchung und Forschung A 202 (1996) 458.
[5] P. Šimko, M. Gombita, J. Karovicová, Die Nahrung 35 (1991) 103.
[6] A.E. Müller, E. Björklund, C. von Holst, J. Chromatogr. A 925 (2001) 197.
[7] M. Jánská, M. Tomaniová, J. Hajslová, V. Kocourek, Anal. Chim. Acta 520 (2004) 93.
[8] O.P. Heemken, N. Theobald, B.W. Wenclawiak, Anal. Chem. 69 (1997) 2171.
[9] M.A. Yusty, J.L.C. Davina, Food Control 16 (2005) 59–64.
[10] M.Y. Ali, R.B. Cole, Anal. Bioanal. Chem. 374 (2002) 923.
[11] B. Veyrand, A. Brosseaud, L. Sarcher, V. Varlet, F. Monteau, P. Marchand, F. Andre, B. Le Bizec, J. Chromatogr. A 1149 (2007) 333.
[12] V. Yusà, O. Pardo, P. Marti, A. Pastor, Food Addit. Contam. 22 (2005) 482.
[13] G. Wang, A.S. Lee, M. Lewis, B. Kamath, R.K. Archer, J. Agric. Food Chem. 47 (1999) 1062.
[14] M. Ciganek, J. Neca, Veterinarni Medicina 51 (2006) 239.
[15] W. Jira, Eur. Food Res. Technol. 218 (2004) 208.
[16] P. Mottier, V. Parisod, R.J. Turesky, J. Agric. Food Chem. 48 (2000) 1160.
[17] L. Duedahl-Olesen, F. Ghorbani, Polycyclic Aromat. Compd. 28 (2008) 282.
[18] S. Sporring, C. von Holst, E. Björklund, Chromatographia 64 (2006) 553.
[19] S. Sporring, E. Björklund, J. Chromatogr. A 1040 (2004) 155.
[20] E. Björklund, A. Müller, C. von Holst, Anal. Chem. 73 (2001) 4050.
[21] R.G. Brereton, Applied Chemometrics for Scientists, John Wiley & Sons, West Sussex, England, 2007.
[22] T. Næs, T. Isaksson, T. Fearn, T. Davies, Multivariate Calibration and Classification, NIR Publications, Chichester, UK, 2004.
[23] J.L. Gómez-Ariza, M. Bujalance, I. Giraldez, A. Velasco, E. Morales, J. Chromatogr. A 946 (2002) 209.
[24] R. Draisci, C. Marchiafava, E. Ferretti, L. Palleschi, G. Catellani, A. Anastasio, J. Chromatogr. A 814 (1998) 187.
[25] E. Björklund, S. Sporring, K. Wiberg, P. Haglund, C. von Holst, Trends Anal. Chem. 25 (2006) 318.
[26] S. Lundstedt, B. van Bavel, P. Haglund, M. Tysklind, L. Öberg, J. Chromatogr. A 883 (2000) 151.
[27] M.M. Schantz, J.J. Nichols, S.A. Wise, Anal. Chem. 69 (1997) 4210.
[28] R. Draisci, C. Marchiafava, L. Palleschi, P. Cammarata, S. Cavalli, J. Chromatogr. B 753 (2001) 217.
[29] A. Filipkowska, L. Lubecki, G. Kowalewska, Anal. Chim. Acta 547 (2005) 243.
[30] European Union, Official Journal of the European Union L88 (2007) 29.

Talanta 79 (2009) 103–108

Contents lists available at ScienceDirect

Talanta

journal homepage: www.elsevier.com/locate/talanta

Preparation and time-gated luminescence bioimaging application of ruthenium complex covalently bound silica nanoparticles

Cuihong Song[a], Zhiqiang Ye[b], Guilan Wang[b], Dayong Jin[c], Jingli Yuan[a,b,*], Yafeng Guan[a,*], James Piper[c]

[a] Department of Instrumentation & Analytical Chemistry, Dalian Institute of Chemical Physics, Chinese Academy of Sciences, Dalian 116023, PR China
[b] State Key Laboratory of Fine Chemicals, Department of Chemistry, Dalian University of Technology, Dalian 116012, PR China
[c] MQ Photonics Centre, Faculty of Science, Macquarie University, Sydney, NSW 2109, Australia

ARTICLE INFO

Article history:
Received 9 January 2009
Received in revised form 6 March 2009
Accepted 7 March 2009
Available online 19 March 2009

Keywords:
Ruthenium complex
Luminescent nanoparticles
Bioimaging
Time-gated luminescence
Environmental pathogen

ABSTRACT

Luminescent ruthenium(II) complex covalently bound silica nanoparticles have been prepared and used as a probe for time-gated luminescence bioimaging. The new nanoparticles were prepared by copolymerization of a luminescent Ru(II) complex tris(5-amino-1,10-phenanthroline)ruthenium(II) conjugated with 3-aminopropyl(triethoxy)silane (APS-Ru conjugate), free (3-aminopropyl)triethoxysilane (APS) and tetraethyl orthosilicate (TEOS) in a water-in-oil reverse microemulsion consisting of Triton X-100, n-octanol, cyclohexane and water in the presence of aqueous ammonia. Characterization by transmission electron microscopy indicates that the nanoparticles are monodisperse, spherical and uniform in size, 64 ± 4 nm in diameter. Compared with the dye-doping nanoparticles, dye leakage of the new nanoparticles was remarkably decreased. In addition, it was found that the Ru(II) complex luminescence could be effectively enhanced with a longer luminescence lifetime (~2.3 μs) after forming the nanoparticles, which enables the nanoparticles to be suitable as a bioprobe for time-gated luminescence bioimaging applications. The nanoparticle-labeled streptavidin was prepared and successfully used for time-gated luminescence imaging detection of an environmental pathogen, *Giardia lamblia*, with high specificity and sensitivity.

1. Introduction

Time-gated luminescence bioimaging technique has become a useful tool in life science and microbial ecology in recent years [1–4]. The main advantage of this technique is that the short-lived background fluorescence from the raw biological samples can be effectively eliminated, hence the specific long-lived signal can be selectively imaged with a high signal-to-noise ratio. In general, this technique requires lanthanide (Eu^{3+} and Tb^{3+}) complexes that have long-lived luminescence as the detection probes. However, since optical excitation window of most luminescent lanthanide probes is limited to the UV region, a major obstacle of the technique [5,6], it has been highly desirable to develop other visible-light sensitized probes suitable for time-gated luminescence detection. For this purpose, luminescent Ru(II) complexes are considered to replace lanthanide complexes because of their visible-light excitation and emission, larger Stokes shift and relatively longer luminescence lifetime properties [7,8].

On the other hand, the recent researches have shown that luminophore-doped silica nanoparticles are very useful luminescent probes for bio-analysis and biotechnology applications [9–12]. One of the main advantages of the silica nanoprobes is that silica matrix can effectively shield the luminophores from the outside environment, such as solvent molecules and free radicals caused by light exposure, and therefore significantly improve the photostability of luminophores inside. In addition, the surface of silica nanoparticles can be easily modified with various functional groups, such as amino, thiol and carboxylic groups, to produce biocompatible nanoprobes. In recent years, the Ru(II)–bipyridine complex, $[Ru(bpy)_3]Cl_2$, doped silica nanoparticles have been applied for the selective tagging of a wide range of biomedically important targets, such as bacteria, cancer cells and individual biomolecules [12–16]. Because of the presence of a number of luminophores encapsulated within one nanoparticle, the $Ru(bpy)_3Cl_2$-doped silica nanoprobe showed higher photo-stability and stronger luminescence, providing a remarkable improvement for the detection sensitivity [11]. However, due to the lack of covalent attachment between the $Ru(bpy)_3Cl_2$ molecules and silica matrix, the dye leaking problem of $Ru(bpy)_3Cl_2$-doped silica nanoprobe is inevitable, which might result in the decrease of per-particle brightness and the increase of background levels in bioassay processes [17].

* Corresponding authors: Tel.: +86 411 84706293/84379590; fax: +86 411 84706293/84379590.
E-mail addresses: jingliyuan@yahoo.com.cn (J. Yuan), guanyafeng@dicp.ac.cn (Y. Guan).

0039-9140/$ – see front matter © 2009 Elsevier B.V. All rights reserved.
doi:10.1016/j.talanta.2009.03.018

Giardia lamblia, one of the most prevalent and epidemic water-borne pathogens, has caused a number of diarrheal disease outbreaks worldwide [18]. The main spreading pathway of the *giardiasis* is contaminated water and food. *Giardia* cysts can survive for weeks to months in cold water and are resistant to conventional water treatment methods such as chlorination and ozonolysis, and therefore can be present in city reservoirs, even clean-looking mountain streams [19–22]. Thus, fast and efficient identification of them in water and biological fluids is an important task for both clinical diagnostics and environmental science. Some methods have been developed for the detection and genetic characterization of a variety of parasites in recent years [23]. Of the methods, amplification-based and hybridization-based ones are more mature and commercially available. Noteworthily, the advance in fluorescence microscopy in the last few decades opened the possibility of examining the structural organization of biological systems in more detail. However, due to the low dose required for infection, the detection of *Giardia lamblia* in environmental water bodies requires the concentration of large volumes of water. Owing to the presence of large amounts of fluorescent mineral particles, plant debris, algae, and other microorganisms in the highly concentrated (10,000-fold) water sample, the identification of fluorescently stained *Giardia lamblia* is often difficult and laborious [1,24,25].

In this work, luminescent silica nanoparticles covalently bound with a Ru(II) complex were prepared by using a new Ru(II)–diimine complex, tris(5-amino-1,10-phenanthroline)ruthenium(II) hexafluorophosphate $[Ru(NH_2\text{-phen})_3](PF_6)_2$, as a luminophore core. The amino group of the Ru(II) complex was converted into carboxylic group by succinic anhydride, and then the complex was covalently bound to (3-aminopropyl)triethoxylsilane (APS) to form the functionalized precursor (APS-Ru conjugate) that can be copolymerized with APS and tetraethoxysilane (TEOS) by the catalysis of aqueous ammonia in water-in-oil (W/O) microemulsion. The obtained nanoparticles are spherical, uniform in size (64 ± 4 nm in diameter), and highly luminescent with better photo-stability and longer luminescence lifetime than those of the free Ru(II) complex. In addition, the amino groups on the surface of the nanoparticles make surface modification and bioconjugation of the nanoparticles easier. The nanoparticle-labeled streptavidin (SA) was prepared and used for time-gated luminescence imaging detection of *Giardia lamblia*. The results show that the imaging using the new nanoparticles as a probe can effectively eliminate background fluorescence and accurately identify *Giardia lamblia* in a complex environmental sample.

2. Experimental

2.1. Materials and physical measurements

The Ru(II) complex dichlorotetrakis(dimethyl sulphoxide) ruthenium(II) $[Ru(DMSO)_4Cl_2]$ and the ligand 5-amino-1,10-phenanthroline (NH_2-phen) were prepared using the previous methods [26–29]. Triton X-100, (3-aminopropyl)triethoxylsilane (APS), tetraethyl orthosilicate (TEOS), N-hydroxysuccinimide (NHS) and 1-ethyl-3-(3-dimethylaminopropyl) carbodiimide hydrochloride (EDC) were purchased from Acros Organic. Tris(2,2′-bipyridyl)dichlororuthenium(II) hexahydrate $[Ru(bpy)_3]Cl_2{\bullet}6H_2O$ was obtained from Sigma. Streptavidin (SA) was purchased from Chemicon International Inc. *Giardia lamblia* and its mouse monoclonal antibody were purchased from Biotech Frontiers Pty. Ltd. Biotinylated rabbit anti-mouse IgG antibody was prepared and used according to a previous method [30]. Unless otherwise stated, all chemicals were purchased from commercial sources and used without further purification.

^{1}H NMR spectra were measured on a Bruker DRX 400 spectrometer (400 MHz). Mass spectra were recorded on a HP1100LC/MSD electrospray ionization mass spectrometry (ESI/MS). Elemental analysis was carried out on a Vanio-EL CHN analyzer. UV–vis absorption spectra were measured on a PerkinElmer Lambda 35 UV–vis spectrometer. Luminescence excitation and emission spectra were recorded on a PerkinElmer LS 50B luminescence spectrometer. Emission lifetimes were measured on an ISS-Chronos multifrequency cross-correlation phase and modulation lifetime spectrometer. Luminescence quantum yields (ϕ) were measured in the air saturated aqueous solution using $[Ru(bpy)_3]Cl_2$ complex as a standard ($\phi = 0.028$) [31]. All spectra were recorded at room temperature. The shape and size of the nanoparticles were characterized using a JEOL JEM-2000EX transmission electron microscope (TEM). All normal luminescence imaging and time-gated luminescence imaging measurements were carried out on a laboratory-use luminescence microscope [2]. The microscope, equipped with a 100 W mercury lamp, a B-2A filters (excitation filter, 450–490 nm; dichroic mirror, 505 nm; emission filter, >520 nm) and a color CCD camera system, was used for the normal luminescence imaging measurement with an exposure time of 10 s. The microscope, equipped with a 30 W xenon flashlamp, B-2A filters and a time-gated digital black-and-white CCD camera system (gate resolution of 0.2 μs), was used for the time-gated luminescence imaging measurement with the conditions of delay time, 1.4 μs; gate time, 10 μs; lamp pulse width, 6 μs; exposure time, 20 s.

2.2. Synthesis of tris(5-amino-1,10-phenanthroline)ruthenium(II) hexafluorophosphate

The 10 mL ethanol solution containing 33.8 mg $Ru(DMSO)_4Cl_2$ (0.07 mmol) and 44.9 mg NH_2-phen (0.23 mmol) was refluxed for 15 h under N_2 in the dark. After the solution was cooled to room temperature, 10 mL of water was added, and the mixture was filtered. To the filtrate was added 114 mg NH_4PF_6 (0.7 mmol) dissolved in 10 mL water with stirring, the orange-yellow precipitate was collected and washed with water and ether, and then purified by silica gel chromatography using an elution of CH_3CN–H_2O (saturated with KNO_3) with a gradient of water increasing from 0 to 10%. After adding 91 mg NH_4PF_6 (0.56 mmol) dissolved in 2 mL water, 45 mg pure Ru(II) complex, $[Ru(NH_2\text{-phen})_3](PF_6)_2$, was obtained after filtering and drying (66% yield). ^{1}H NMR (acetone-d_6) for $[Ru(NH_2\text{-phen})_3](PF_6)_2$, δ (ppm): 6.38 (s, 6H, amino protons), 7.30 (s, 3H), 7.54 (m, 3H), 7.76 (m, 3H), 7.90 (m, 3H), 8.40–8.29 (m, 6H), 8.90 (d, 3H). Anal. Calcd. for $[Ru(NH_2\text{-phen})_3](PF_6)_2$ (%): C, 44.27; H, 2.79; N, 12.90. Found (%): C, 44.41; H, 2.92; N, 12.74. ESI-MS: m/z 832.0 $[M\text{-}PF_6]^+$, 343.5 $[M\text{-}2PF_6]^{2+}$.

2.3. Preparation of the Ru(II) complex covalently bound silica nanoparticles

Before the nanoparticle preparation, the APS-Ru conjugate was prepared as follows. To a solution consisting of 5 mg $[Ru(NH_2\text{-phen})_3](PF_6)_2$ in 350 μL anhydrous DMF was added a mixture of 2 mg succinic anhydride and 20 μL triethylamine in 50 μL anhydrous DMF. The solution was stirred for 12 h at room temperature. After 80 μL anhydrous ethanol solution containing 8.2 mg EDC and 4.0 mg NHS was added, the solution was agitated for 1 h, and then 6.5 μL APS was added with stirring. The reaction was kept for another 3 h. The obtained solution containing APS-Ru conjugate was used in the next step without further manipulation.

The Ru(II) complex covalently bound silica nanoparticles were prepared in a water-in-oil reverse microemulsion with the following procedure. To a flask were added 1.77 g Triton X-100, 1.6 mL n-octanol and 7.5 mL cyclohexane with stirring to form a homoge-

nous solution. To the solution were added an appropriate amounts of APS-Ru conjugate solution (20, 40, 60, 80, 100, 120 and 140 μL, respectively) and water (total amount of APS-Ru solution and H_2O was controlled to be 400 μL). After 100 μL TEOS and 5 μL APS were added with vigorous stirring, the polymerization reaction was initiated by adding 60 μL concentrated aqueous ammonia (25–28%). The reaction was allowed to continue for 24 h at room temperature. The nanoparticles were isolated from the microemulsion by adding acetone, followed by centrifuging and washing with ethanol and water several times to remove any surfactant molecules and physically adsorbed dye molecules from the particle's surface.

2.4. Preparation of the nanoparticle-labeled SA

To 0.8 mL of 0.1 M phosphate buffer of pH 7.1 containing 2.0 mg of BSA were added 1.0 mg of the nanoparticles and 0.2 mL of 1% glutaraldehyde. After stirring for 24 h at room temperature, the nanoparticles were centrifuged and washed with the phosphate buffer, and then added to 1.0 mL of the phosphate buffer containing 0.2 mg of SA. After 0.2 mL of 1% glutaraldehyde was added and the reaction mixture was stirred for 22 h at 4 °C, 2.0 mg of $NaBH_4$ was added and the solution was incubated for another 2 h at room temperature. The nanoparticle-labeled SA was centrifuged and washed three times with the phosphate buffer, diluted with 1.0 mL of 0.05 M Tris–HCl buffer of pH 7.8 containing 0.2% BSA, 0.1% NaN_3, and 0.9% NaCl, and then stored at 4 °C before use.

2.5. Luminescence imaging of Giardia lamblia

To 6 μL *Giardia lamblia* solution (10^6 cysts/mL) were added 16 μL of anti-*Giardia* monoclonal antibody (~50 μg/mL), 16 μL of biotinylated rabbit anti-mouse IgG antibody (~50 μg/mL) and 10 μL of the nanoparticle-labeled SA (~200 μg/mL) in a tube. After incubation for 2 d at room temperature in the dark, the cysts were separated by centrifugation (<500 rpm) and washed with 100 μL of distilled water several times to remove the unreacted nanoparticle-SA conjugate. The cysts were mixed with 20 μL of an environmental water sample [6], and then spotted on a glass slide for luminescence microscopy imaging detection. To confirm the non-specific binding of the nanoparticles on *Giardia* cysts, a control experiment in the absence of anti-*Giardia* antibody was also carried out with the same method.

3. Results and discussion

3.1. Preparation and characterization of the nanoparticles

The preparation principle of the Ru(II) complex covalently bound silica nanoparticles is presented in Fig. 1. After the amino group of the complex was converted into carboxylic group by reacting with succinic anhydride, the complex was covalently coupled with APS in the presence of EDC and NHS to form a functionalized precursor, APS-Ru conjugate. Then, the Ru(II) complex covalently bound silica nanoparticles were prepared by hydrolysis copolymerization of the precursor with TEOS and APS catalyzed by aqueous ammonia in a W/O microemulsion. The resulting suspensions were clear and stable over months if stored in the dark at 4 °C, indicating the superb dispersibility of the nanospheres in the solution.

The nanoparticles are characterized with TEM and spectroscopic methods. The results of Fig. 2 show that the average particle size can be controlled by the precursor (APS-Ru conjugate) concentration, increasing from 47 to 64 nm as the volume of added precursor solution is increased from 20 to 120 μL (the sizes in diameter of the nanoparticles prepared using 20, 40, 60, 80, 100 and 120 μL of APS-Ru conjugate solutions are 47 ± 3, 51 ± 3, 55 ± 4, 58 ± 4, 61 ± 3 and 64 ± 4 nm, respectively). The particle shape is perfectly spherical with a smooth morphology and narrow size distribution. However, the particle shape became less spherical when higher volume (>120 μL) of precursor solution was used (Fig. 2d). Thus the nanoparticles prepared using 120 μL of APS-Ru conjugate solution (64 ± 4 nm in diameter, corresponding to 1.2 mg of Ru(II) complex) were selected for further characterization and application because of their satisfactory shape and luminescence intensity. For comparison, the Ru(II) complex physically encapsulated silica nanoparticles using the same amount of luminophore (1.2 mg Ru(II) complex) and the same W/O microemulsion system were also prepared. In this case, spherical nanoparticles of 81 ± 4 nm in diameter were obtained (Fig. 2e). Higher resolution images shown in the insets of Fig. 2a–d show that, unlike physically doped nanoparticles (Fig. 2e), no black spots are found inside the nanoparticles, which indicates that the covalently bound Ru(II) complex molecules are distributed evenly throughout the silica network rather than form clusters in the nanoparticles. To the best of our knowledge, this is the first report on preparing silica-based luminescent Ru(II)–diimine complex nanoparticles by covalent binding method in W/O microemulsion.

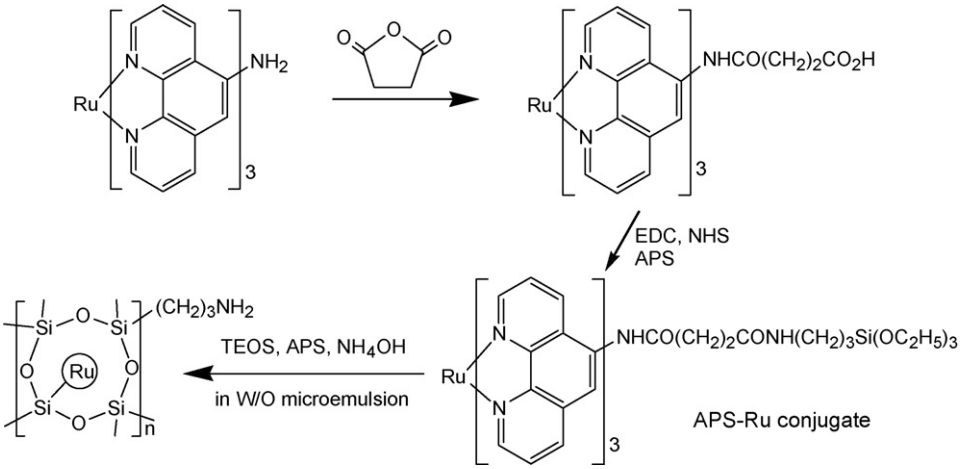

Fig. 1. Preparation principle of the Ru(II) complex covalently bound silica nanoparticles.

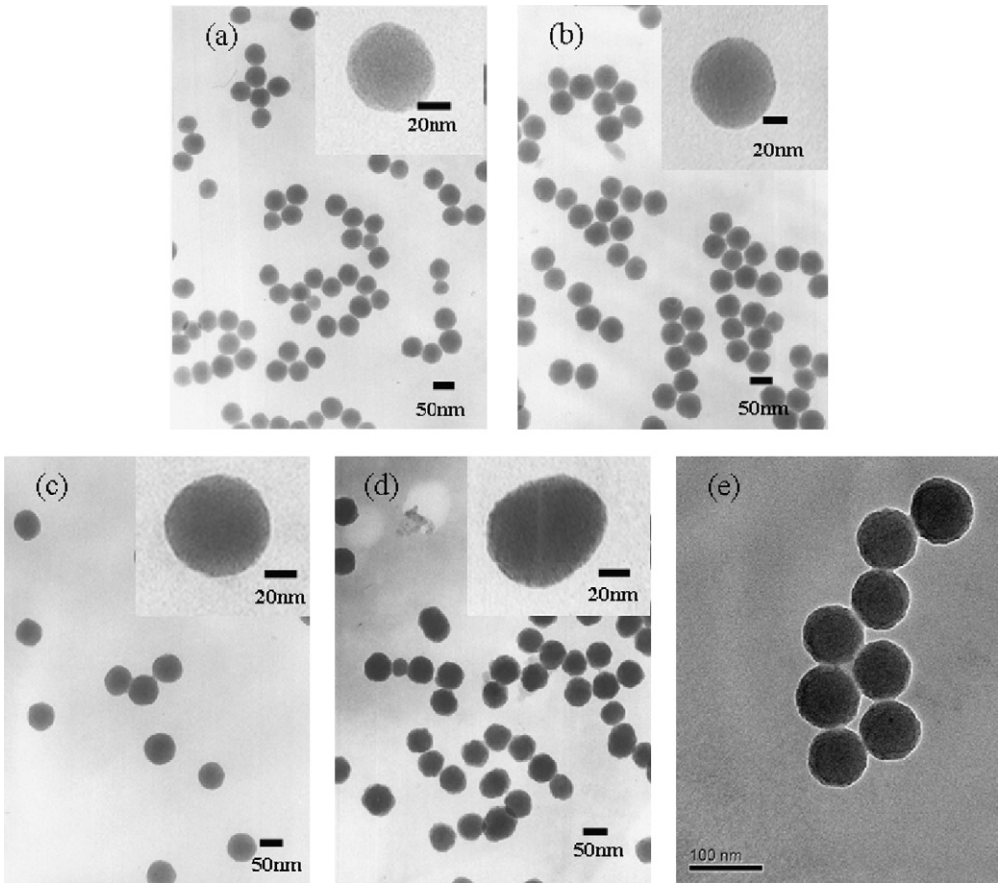

Fig. 2. Representative TEM images of the Ru(II) complex covalently bound (a–d, 20, 80, 120 and 140 μL of APS-Ru conjugate solutions were used, respectively) and physically encapsulated (e) silica nanoparticles. Insets in (a)–(d) are higher resolution images of the same particles.

The excitation and emission spectra of free $[Ru(NH_2\text{-phen})_3]^{2+}$ complex and the nanoparticles in the aqueous solution were measured. As shown in Fig. 3, free $[Ru(NH_2\text{-phen})_3]^{2+}$ complex shows emission band centered at 604 nm at room temperature, which is characteristic metal-to-ligand charge transfer (MLCT)-based luminescence typically observed in the spectra of Ru(II)–diimine complexes. The excitation spectrum of the nanoparticles remains almost the same to the free Ru(II) complex, but the maximum emission wavelength of the nanoparticles is ~9 nm shifted toward the shorter wavelength compared with the free complex. It might be due to the weak interaction between the Ru(II) complex and the silica matrix. To give the dye amount in the covalent binding nanoparticles, the number of $[Ru(NH_2\text{-phen})_3]^{2+}$ molecules in a 64-nm nanoparticle is estimated [30] to be about 3300, showing the remarkable signal amplification effect of the nanoparticles compared with a single dye molecule if they are used as bioprobes.

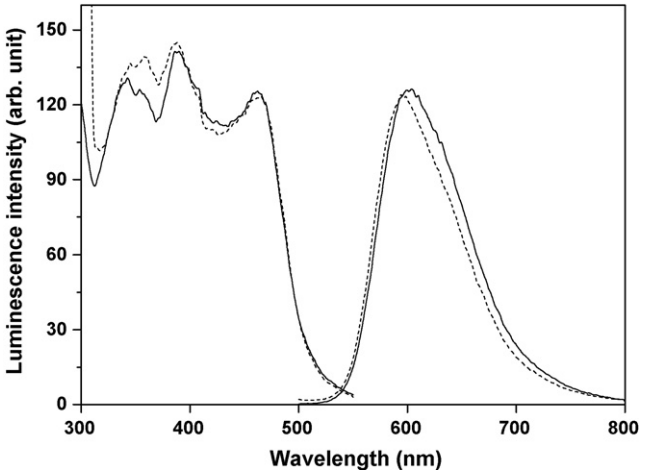

Fig. 3. Excitation (300–550 nm) and emission (500–800 nm) spectra of free $[Ru(NH_2\text{-phen})_3]^{2+}$ complex (solid lines, 20 μM) and the nanoparticles (dash lines, 100 mg/L) in 0.01 M phosphate buffer of pH 7.4 at room temperature.

Ru(II)–diimine complexes, such as $[Ru(bpy)_3]^{2+}$ and $[Ru(phen)_3]^{2+}$, have been used for oxygen-sensing applications [32] because their luminescence can be quenched by molecular oxygen. It is believed that the encapsulation of the complex molecules in silica nanoparticles can effectively increase the emission efficiency, lifetime and photostability of the complex since the silica matrix can provide a chemically and mechanically stable vehicle. Indeed, the emission quantum yield (ϕ) of either the covalently bound nanoparticles (ϕ, ~6.0%) or the physically encapsulated nanoparticles (ϕ, ~4.0%) was determined to be much higher than that of the free $[Ru(NH_2\text{-phen})_3]^{2+}$ complex (ϕ, ~2.5%) in the air saturated aqueous solution, using $[Ru(bpy)_3]Cl_2$ (ϕ, 2.8%) as the reference [31]. Moreover, the Ru(II) complex covalently bound silica nanoparticles show a longer luminescence lifetime (2.28 μs), 3-fold longer than that of the free Ru(II) complex (0.77 μs) in the air saturated aqueous solution using $Ru(bpy)_3Cl_2$ (0.43 μs) as a standard [33], indicating that the new nanoparticles can be used as a probe for time-gated luminescence bioimaging application.

To evaluate the photostability of the nanoparticles, the photostabilities of free $[Ru(NH_2\text{-phen})_3]^{2+}$ complex, the covalently bound

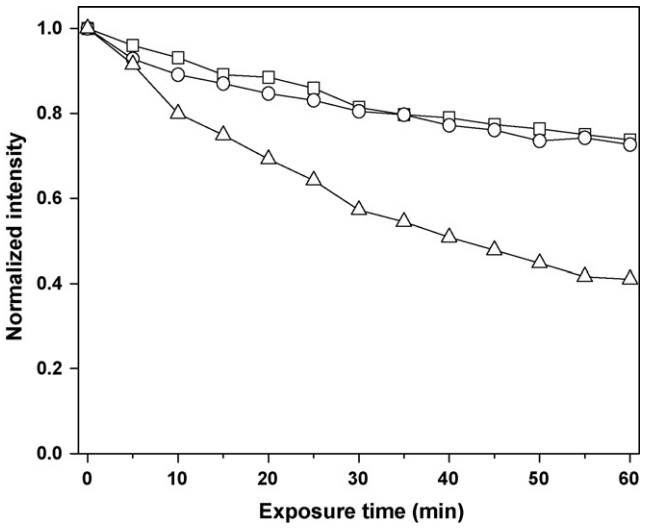

Fig. 4. Photobleaching experiments: free $[Ru(NH_2\text{-}phen)_3]^{2+}$ complex (triangle), the Ru(II) complex covalently bound nanoparticles (square) and physically encapsulated nanoparticles (circle) in aqueous solution phase with a 30 W deuterium lamp as excitation source.

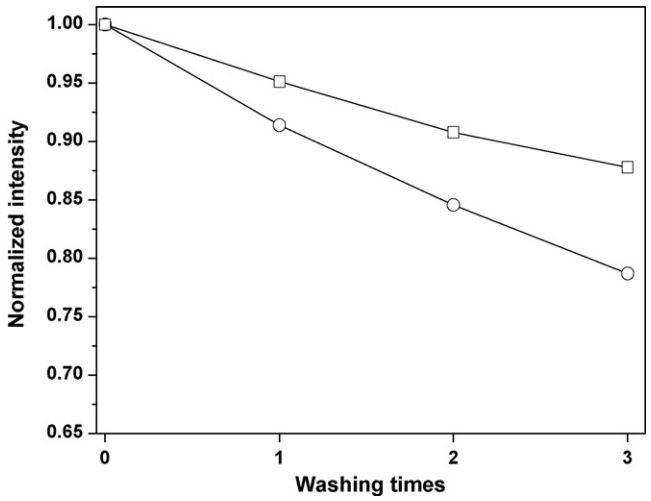

Fig. 5. Leakage experiments: the Ru(II) complex covalently bound nanoparticles (square) and physically encapsulated nanoparticles (circle).

and physically encapsulated nanoparticles in 0.01 M phosphate buffer of pH 7.4 against photobleaching were measured by using a 30 W deuterium lamp as an excitation source. The emission intensity was recorded at 5 min intervals for a period of 1 h. The results are shown in Fig. 4. After 1 h excitation, the emission intensity of the free complex was decreased 60%, whereas the emission intensities of the covalently bound and physically encapsulated nanoparticles were only decreased 26% and 27%, respectively. The high photostability of the nanoparticles is caused by the fact that the Ru(II) complex in the nanoparticles is surrounded by silica, which isolates the complex from the outside environment, such as solvent molecules and free radicals caused by light exposure, and therefore effectively protects the complex from photodecomposition.

The dye leakages for the covalently bound and physically encapsulated nanoparticles were investigated in the aqueous solution. A typical experiment procedure is as follows. Firstly, the suspension of the nanoparticles was prepared and its luminescence intensity was measured. After the nanoparticles were centrifuged down (14,000 rpm) for 10 min, and ultrasonically redispersed in water, the luminescence intensity was measured again. Such a procedure was repeated for three times keeping the same suspension volume. As shown in Fig. 5, the luminescence intensity of the physically encapsulated nanoparticles is 21% decreased after washing three times, whereas that of the covalently bound nanoparticles is only 12% decreased when treated in the same way. These results clearly indicate that the dye leakage from the silica matrix can be effectively reduced since the complex molecules are covalently bound to silicon atoms in the nanoparticles.

3.2. Time-gated luminescence imaging for Giardia cysts

The nanoparticle-labeled SA was used for time-gated luminescence imaging of *Giardia* cysts in a complex environmental water sample. Firstly, a control experiment was carried out using *Giardia* cysts incubated with biotinylated secondary antibody and the nanoparticle-labeled SA. No binding event was found for the nanoparticles onto the *Giardia* cysts surface, indicating the non-specific absorption of the nanoparticles onto the cysts is negligible. After *Giardia* cysts were incubated with the anti-*Giardia* antibody, biotinylated secondary antibody and the nanoparticle-labeled SA, the bright-field, normal luminescence and time-gated luminescence imagings (excited at 450–490 nm) of *Giardia* cysts were carried out. As shown in Fig. 6a, it is very difficult to identify the single *Giardia* cyst from the bright-field image. Compared with the normal luminescence image (Fig. 6b), the time-gated luminescence image (Fig. 6c) shows only the specific luminescence signal from the *Giardia* cyst and the short-lived background fluorescence from the other non-target co-existing substances can be gated off effectively. The above results demonstrate that the new nanoparticles can be used as a visible-light excitation bioprobe for the detection of microorganisms in complicated environmental samples. In addition, the clear image excited with 450–490 nm also indicate the availability of the new Ru nanoparticle-based luminescence probe in routine time-gated luminescence bioassays because its excitation can be accomplished by the semiconductor light sources like light-emitting diodes (LEDs) or laser diodes (LDs) with maximum outputs at violet to blue wavelengths, which can be expected to sufficiently decrease the damage of excitation light to biological samples in comparison with the UV excitation.

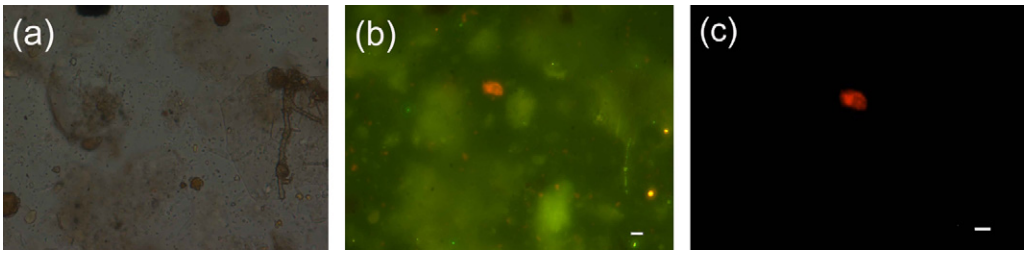

Fig. 6. Bright-field (a), luminescence (b) and time-gated luminescence (c) images of *Giardia lamblia* stained by the nanoparticle-labeled SA in a complex environmental water sample. Scale bars, 10 μm. The time-gated luminescence image is shown in pseudo-color (wavelength of 615 nm) treated by a SimplePCI software [2].

4. Conclusions

In this work, luminescent silica nanoparticles covalently bound with a Ru(II) complex were prepared for the first time by using the reverse microemulsion method. The preparation is highly reproducible and easily controllable. The nanoparticles are monodisperse, spherical, uniform in size, highly luminescent in aqueous solution and have a longer luminescence lifetime. Compared with the physically encapsulated nanoparticles, dye leakage of the covalent binding nanoparticles is remarkably decreased because the dye molecules are covalently bound to the silica matrix. Due to the presence of surface amino groups, the nanoparticles are also easily conjugated with biomolecules. The availability of the new biocompatible nanoparticles was demonstrated by the highly specific time-gated luminescence imaging detection of an environmental pathogen, *Giardia lamblia*. In addition, it is noteworthy that the new Ru nanoparticle-based luminescent probe offers the advantages of visible-light excitation and emission and a longer luminescence life-time in comparison with most UV excitation lanthanide probes. With the further development of the detection system, it can be expected that the new nanoparticles serve as an efficient probe for the identifications of microorganisms and living cells in complex environmental and biological samples.

Acknowledgements

The present work was supported by the National Natural Science Foundation of China (Nos. 20575069, 20835001), the Specialized Research Fund for the Doctoral Program of Higher Education of China (200801410003), and Macquarie University Research Fellowship Scheme.

References

[1] R. Connally, D. Veal, J. Piper, Microsc. Res. Tech. 64 (2004) 312.
[2] B. Song, G.L. Wang, M.Q. Tan, J.L. Yuan, J. Am. Chem. Soc. 128 (2006) 13442.
[3] K. Hanaoka, K. Kikuchi, S. Kobayashi, T. Nagano, J. Am. Chem. Soc. 129 (2007) 13502.
[4] D. Jin, R. Connally, J. Piper, Cytometry A 71A (2007) 797.
[5] J. Wu, G.L. Wang, D.Y. Jin, J.L. Yuan, Y.F. Guan, J. Piper, Chem. Commun. (2008) 365.
[6] J. Wu, G.L. Wang, D.Y. Jin, J.L. Yuan, Y.F. Guan, J. Piper, J. Mater. Chem. 19 (2009) 1258.
[7] D.S. Tyson, J. Bialecki, F.N. Castellano, Chem. Commun. (2000) 2355.
[8] E.A. Medlycott, G.S. Hanan, Chem. Soc. Rev. 34 (2005) 133.
[9] L. Wang, K. Wang, S. Santra, X. Zhao, L.R. Hilliard, J.E. Smith, J. Wu, W. Tan, Anal. Chem. 78 (2006) 646.
[10] X. Zhao, D.R. Tapec, W. Tan, J. Am. Chem. Soc. 125 (2003) 11474.
[11] J. Wu, Z. Ye, G. Wang, J. Yuan, Talanta 72 (2007) 1693.
[12] L. Wang, W. Zhao, M.B. O'Donoghue, W. Tan, Bioconjugate Chem. 18 (2007) 297.
[13] S. Santra, P. Zhang, K. Wang, R. Tapec, W. Tan, Anal. Chem. 73 (2001) 4988.
[14] X. Zhao, L.R. Hilliard, S.H. Mechery, Y. Wang, R.P. Bagwe, S. Jin, W. Tan, Proc. Natl. Acad. Sci. U.S.A. 101 (2004) 15027.
[15] X. Hun, Z. Zhang, Talanta 73 (2007) 366.
[16] X. He, J. Ge, K. Wang, W. Tan, H. Shi, C. He, Talanta 76 (2008) 1199.
[17] A. Burns, H. Owb, U. Wiesner, Chem. Soc. Rev. 35 (2006) 1028.
[18] M.S. Wolfe, Clin. Microbiol. Rev. 5 (1992) 93.
[19] R.M. Mariante, R.G. Vancini, A.L. Melo, M. Benchimol, Exp. Parasitol. 110 (2005) 62.
[20] J. Kim, S. Sim, T. Yong, S. Park, Parasitol. Res. 103 (2008) 1459.
[21] F.E. Lucy, T.K. Graczyk, L. Tamang, A. Miraflor, D. Minchin, Parasitol. Res. 103 (2008) 1369.
[22] I.A. Rosa, M. Einicker-Lamas, R.R. Bernardo, M. Benchimol, Exp. Parasitol. 120 (2008) 215.
[23] P.T. Monis, S. Giglio, A.R. Keegan, R.C.A. Thompson, Trends Parasitol. 21 (2005) 340.
[24] R. Connally, D. Veal, J. Piper, J. Biomed. Opt. 9 (2004) 725.
[25] R. Connally, D.Y. Jin, J. Piper, Cytometry A 69 (2006) 1020.
[26] I.P. Evans, A. Spencer, G. Wilkinson, J. Chem. Soc., Dalton Trans. (1973) 204.
[27] P. Lenaerts, K. Driesen, R.V. Deun, K. Binnemans, Chem. Mater. 17 (2005) 2148.
[28] K. Binnemans, P. Lenaerts, K. Driesen, C.J. Gorller-Walrand, Mater. Chem. 14 (2004) 191.
[29] J.P. Lecompte, A. Kirsch-De Mesmaeker, M. Demeunynck, J.J. Lhomme, Chem. Soc., Faraday Trans. 89 (1993) 3261.
[30] Z.Q. Ye, M.Q. Tan, G.L. Wang, J.L. Yuan, Anal. Chem. 76 (2004) 513.
[31] K. Nakamaru, Bull. Chem. Soc. Jpn. 55 (1982) 2697.
[32] E.R. Carraway, J.N. Demas, B.A. DeGraff, J.R. Bacon, Anal. Chem. 63 (1991) 337.
[33] L. Qian, X. Yang, Adv. Funct. Mater. 17 (2007) 1353.

Talanta 79 (2009) 38–45

Contents lists available at ScienceDirect

Talanta

journal homepage: www.elsevier.com/locate/talanta

Amperometric biosensor for hydrogen peroxide based on coimmobilized horseradish peroxidase and methylene green in ormosils matrix with multiwalled carbon nanotubes

A.K. Upadhyay, Tzu-Wei Ting, Shen-Ming Chen*

Department of Chemical Engineering and Biotechnology, National Taipei University of Technology, No. 1, Section 3, Chung-Hsiao East Road, Taipei 106, Taiwan, ROC

ARTICLE INFO

Article history:
Received 31 December 2008
Received in revised form 1 March 2009
Accepted 2 March 2009
Available online 14 March 2009

Keywords:
Multiwalled carbon nanotubes
Methylene green
Ormosils
Horseradish peroxidase
Hydrogen peroxide

ABSTRACT

A novel amperometric biosensor for the analytical determination of hydrogen peroxide was developed. The fabrication of the biosensor was based on the coimmobilization of horseradish peroxidase (HRP), methylene green (MG) and multiwalled carbon nanotubes within ormosils; 3-aminopropyltrimethoxysilane (APTMOS), 2-(3,4-epoxycyclohexyl)ethyltrimethoxysilane (ETMOS) and phenyltrimethoxysilane (PHTMOS). APTMOS determined the hydrophilicity/hydrophobicity of the ormosils and PHTMOS and ETMOS increased the physical and mechanical strength of the ormosil matrix. The ormosil modified electrodes were characterized with SEM, UV–vis spectroscopy and electrochemical methods. Cyclic voltammetry and amperometric measurements demonstrated the MG coimmobilized with HRP in this way, displayed good stability and could efficiently shuttle electrons between immobilized enzyme and electrode, and MWCNTs facilitated the electrocatalytic reduction of H_2O_2 at reduced over potential. The Micheaelis constant of the immobilized HRP was 1.8 mM, indicating a high affinity of the HRP to H_2O_2 without loss of enzymatic activity in ormosil matrix. The prepared biosensor had a fast response of H_2O_2, less than 10 s, and excellent linear range of concentration from 5×10^{-7} to 2×10^{-5} M with the detection limit of 0.5 μM (S/N = 3) under the optimum conditions. At the same time, the influence of solution pH, effect of enzyme amount, steady-state applied potential and temperature on the biosensor were investigated. The enzyme electrode retained about 90% of its initial activity after 30 days of storage in a dry state at 4 °C. The preparation of the developed biosensor was convenient and showed high sensitivity with good stability.

1. Introduction

The rapid, accurate, reliable and simple analytical determination of hydrogen peroxide is of great importance in clinical, industrial, pharmaceutical, food industry and environmental [1–5] analyses. Conventional hydrogen peroxide determination methods, such as fluorimetry [6,7], titrimetry [8], spectrometry [9] and chemiluminescence [10,11] are generally time consuming and cumbrous for operation. Now the electrochemical method displays better prospects due to its advantages of easy preparation, fast detection, low consumption of reagents and high selectivity and sensitivity [12]. Nowadays, horseradish peroxidase (HRP) has been widely used for the fabrication of ormosil based amperometric biosensors to the detection of H_2O_2 due to its high purity, sensitivity, low cost and easy availability [13–15].

Carbon nanotubes (CNTs) have attracted considerable study since their discovery [16]. Due to their high electrical conductivity, strong absorptive properties, good mechanical strength and excellent biocompatibility, currently biomolecules have been successfully integrated with MWCNTs. The integration of biomolecules with MWCNTs enables the use of such hybrid system as electrochemical biosensors (enzymes electrodes, DNA sensors or immune sensors) [17–20]. The MWCNT-based biosensors offer substantially greater signals especially at low potential, reflecting the electrocatalytic activity of MWCNTs. Such low-potential operation of MWCNT-based biosensor results in a wide linear range and fast response time. Several number of amperometric peroxide biosensors have been fabricated based on NAD^+ and SWNT modified electrode [21], poly(TB)/HRP/MWCNT/chitosan modified electrode [22], MWCNT/polysulfone modified electrode [23], MWCNT/BSA/HRP/ferrocene modified electrode [24], MWCNT/HRP/MB modified electrode [25], silica-hydroxyapatite/HRP nanocomposite modified electrodes [26], TiO_2/DNA/thionin nanocomposite modified electrode [27], Au-modified TiO_2 nanotube arrays/HRP modified electrode [28] and

* Corresponding author.
E-mail address: SMChen78@ms15.hinet.net (S.-M. Chen).

0039-9140/$ – see front matter © 2009 Elsevier B.V. All rights reserved.
doi:10.1016/j.talanta.2009.03.010

CNT/ABTS/HRP based modified electrode [29]. Xie and co-workers developed third-generation biosensor for H_2O_2 on the basis of the immobilization of horseradish peroxidase (HRP) in a nanocomposite film of tetrathiafulvalene–tetracyanoquinodimethane (TTF–TCNQ)/multiwalled carbon nanotubes (MWCNTs) modified gold electrode [30]. A series of water soluble organic dyes have been used as mediators in solution, due to their excellent mediating ability and low cost. But in solution, dye molecules will not only pollute the reference electrode and counter electrode, also decrease the analytical sensing ability of sensor, due to deposition it on the electrode surface. Therefore, it would be preference to immobilize the dye on the electrode surface. To overcome this critical issue, we used organically modified sol–gel glasses (ormosils) to encapsulate the dyes/biomolecules. The dye strongly interacts with the silanol groups of the porous surface and remains in a more restricted environment at the ormosils than it is at the gel–glass cage. This observation indicates the ormosils would be a suitable host for dyes. Several redox dyes such as, methylene blue [31], methylene green (MG) [32], meldola blue [33] and Celestine blue [34] can be used as electron transfer mediators when immobilized on the electrode surfaces. The leaching of biomolecules from the electrode surface during electrochemical characterization is a crucial problem in the fabrication of electrochemical biosensor. Ormosils are the unique matrices to encapsulate the biomolecules [35–38], due to their inert chemical nature, high mechanical strength, excellent optical properties, strong adhesion properties to its surface support and ease of modification. The incorporation of organic moieties increases the crosslinking in the matrix and provides improved electron transportation. The ormosil modified electrodes possesses a large potential window, low and almost constant background current over a large potential window, and fast kinetics for a large number of electrochemical mediators. The intersection of ormosil with MWCNT will be a valuable asset in the field of development of biosensor because the ormosils are the appropriate matrices for the encapsulation of biomolecules (enzyme, protein, DNA, etc.) and MWCNTs provide better conductivity than graphitic carbon to its unique physical and chemical properties.

In this article we prepared a highly sensitive and selective H_2O_2 biosensor using three types of ormosils; 2-(3,4-epoxycyclohexyl) ethyltrimethoxysilane (ETMOS) phenyltrimethoxysilane (PHTMOS), and 3-aminopropyltrimethoxysilane (APTMOS). Methylene green (as mediator) and HRP were coimmobilized within the ormosils matrix with MWCNTs. The presence of organic functional moieties in the ormosil, provide strong cage to the encapsulating small molecular size enzymes to remove the leaching problem. The widely present amino groups in ormosils provide a hydrophilic microenvironment that is compatible with the biomolecules [39] and increase the stability of the biosensor. Cyclic voltammetric and amperometric measurements were carried out to demonstrate the feasibility of MG as an electron shuttle between the immobilized peroxidase and a glassy carbon electrode. MWCNTs incorporated within ormosils facilitating the electron-transfer reaction between the enzyme and the electrode. The resulting biosensor exhibited high sensitivity and much better stability than the developed biosensor based on the coimmobilization of horseradish peroxidase and methylene blue on a CNT modified electrode [25], and methylene blue/SiO_2 nanocomposite modified electrode [40].

2. Experimental

2.1. Reagents and materials

Peroxidase from horseradish (POD, EC 1.11.1.7 type VI) was obtained from Sigma; methylene green was purchased from Fluka. phenyltrimethoxysilane, 3-aminopropyltrimethoxysilane, 2-(3,4-epoxycyclohexyl)ethyltrimethoxysilane, *N,N*-dimethylformamide (DMF) and multiwalled carbon nanotubes (10–15 nm diameter) were purchased from Aldrich Chemical Co. Hydrogen peroxide (30%, w/v solution) was purchased from Wako Pure Industrial Co., Japan. The concentrations of more diluted hydrogen peroxide solutions were determined by titration with cerium(IV) to a ferroin end point. Phosphate buffer solutions (PBS) of various pH were prepared with 0.1 M KH_2PO_4 and 0.1 M Na_2HPO_4 with supporting electrolyte 0.1 M KCl. All other chemicals employed were of analytical grade. All the solutions were prepared with doubly distilled water.

2.2. Apparatus

The electrochemical measurements were performed with a computer controlled CHI750A (TX, USA) electrochemical system. Cyclic voltammetry and amperometric measurements were done with a three electrode system comprising the MG/HRP/GCE and MWCNTs/MG/HRP/GCE as a working electrode, an Ag/AgCl reference electrode and platinum wire as counter electrode. All electrochemical measurements were carried out in 5 ml (0.1 M, pH 7.2) phosphate buffer solution (PBS). All experimental solutions were thoroughly deoxygenated by bubbling nitrogen through the solution for at least 15 min. Hitachi scientific instruments (Japan) Model S-3000H scanning electron microscope and Hitachi scientific instruments (Japan) Model U-3300 UV–vis spectrophotometer were used for surface image and UV–vis spectra measurements, respectively.

2.3. Fabrication of H_2O_2 biosensor

A glassy carbon electrode (GCE, 3 mm in diameter) was polished with 1.0, 0.3 and 0.05 μm Al_2O_3 slurry successively followed by rinsing thoroughly with double distilled water until a mirror-like surface was obtained. Then it was washed ultrasonically in 1:1 nitric acid, absolute ethanol and double distilled water, each for 5 min, and allowed to dry at room temperature. Two types of ormosils modified electrodes (OME) were fabricated based on the composition given in Table 1.

(A) MWCNTs/MG/HRP/GCE: 75 μl of 3-aminopropyltrimethoxysilane, 10 μl (1 mM) of methylene green and 225 μl of doubly distilled water were mixed in a cell with constant stirring, followed by the addition of 50 μl (1 mg/ml) of horseradish peroxidase (HRP) and 30 μl (1 mg/ml in DMF) of MWCNTs in same solution and stirred for 5 min to get homogeneous solution. After that 2-(3,4-epoxycyclohexyl)ethyltrimethoxysilane,

Table 1
Composition of Ormosils modified electrodes.

OME	APTMOS (μl)	ETMOS (μl)	PHTMOS (μl)	MG (1 mM) (μl)	HRP 1 mg/ml (μl)	DD water (μl)	MWCNTs (1 mg/ml in DMF) (μl)	HCl (μl)
1	75	10	5	10	50	225	–	10
2	75	10	5	10	50	225	30	10

OME: ormosils modified electrode, APTMOS: 3-aminopropyltrimethoxysilane; ETMOS: 2-(3,4-epoxycyclohexyl)ethyltrimethoxysilane; PHTMOS: phenyltrimethoxysilane; MG: methylene green; HRP: horseradish peroxidase; MWCNTs: multiwalled carbon nanotubes.

phenyltrimethoxysilane and 0.1N, 10 μl HCl were mixed and stirred for 10 min to allow to completion of hydrolysis. The prepared ormosil film was smooth and crackfree.1.4 μg of HRP enzyme was deposited on the electrode surface.

(B) MG/HRP/GCE: This ormosils modified electrode was prepared as the same procedure mentioned for ormosils modified electrode A and differ only the absence of MWCNTs. 10 μl of the prepared homogeneous solution was added over the glassy carbon electrode followed by multiwalled carbon nanotubes modified ormosils formation for 6–7 h at room temperature. The OMEs were washed in phosphate buffer (0.1 M, pH 7.2) followed by incubation of electrodes for 4 h in same buffer.

3. Result and discussion

3.1. Physical characterization

3.1.1. SEM and AFM of ormosil modified composite

The physical morphology also affects the response of the enzyme electrode. Thus, the study of surface morphology of the ormosils modified matrix is an important factor affecting its analytical performance. Fig. 1a and b shows the SEM of different surfaces. Fig. 1a is the image of ormosils immobilized with spherical particles of HRP. The immobilized HRP ormosils electrode surface was smooth and indicates that the enzyme was successfully incorporated within ormosils matrix. Fig. 1b displays the SEM image of MWCNTs and HRP within ormosils matrix. It was shown that the MWCNTs (diameter in the range of 30–50 nm) was spread around and equally distributed in the ormosil matrix. The surface of the MWCNTs became rough due to presence of enzyme. It suggested that HRP enzymes disperse along the side walls of MWCNTs in the ormosils film. Therefore, the uniform and open nanostructure provided a significant increase of effective surface for HRP enzyme loading and a good preparation reproducibility of the biosensor.

Typical AFM image (tapping mode) of the MWCNTs/MG/HRP in ormosil composite was shown in Fig. 1c. The thickness of MWCNTs/MG/HRP/Ormosils layer was about 100–108 nm (estimated from the AFM image) and showed an island-like structure. The height difference between the bright region and the dark ground was about 20 nm. The AFM measurement of HRP immobilized in MWCNTs/MG/Ormosil indicated that the deposited enzyme formed a uniform layer with globular shape. The bright regions indicated the presence of MWCNTs in the ormosil film. These features would help in retaining of dopants for long time and improving the electrochemical behavior of the film.

3.1.2. UV–visible spectra of ormosil modified composite

Fig. 2 shows the UV–vis spectra of the MG in water and MG incorporated with HRP in ormosils from 300 to 800 nm. The UV–vis spectrum for the MG head peaks at 664 and 610 nm (Fig. 2, curve a). In the case of MG incorporated within ormosils composites (Fig. 2, curve b), the absorption peaks at 664 nm disappeared, due to interaction between MG and SiO_2 present in ormosils, whereas the peak at around 610 nm shifted slightly towards lower wavelength at 590 nm (blue shift, by about 20 nm) and showed the dimeric form of the dye [41]. The absorption observed at 403 nm corresponds to the HRP heme group absorption and revealed that the HRP was successfully immobilized within the matrix and retained enzymatic properties in ormosil film.

3.2. Electrochemical studies of MWCNTs/MG/HRP/GCE

Fig. 3 displays the typical cyclic voltammograms of MG/HRP/GCE and MWCNTs/MG/HRP/GCE incorporated within ormosils, over a potential range from 0.0 to −0.4 V in 0.1 M PBS (pH 7.2) at different

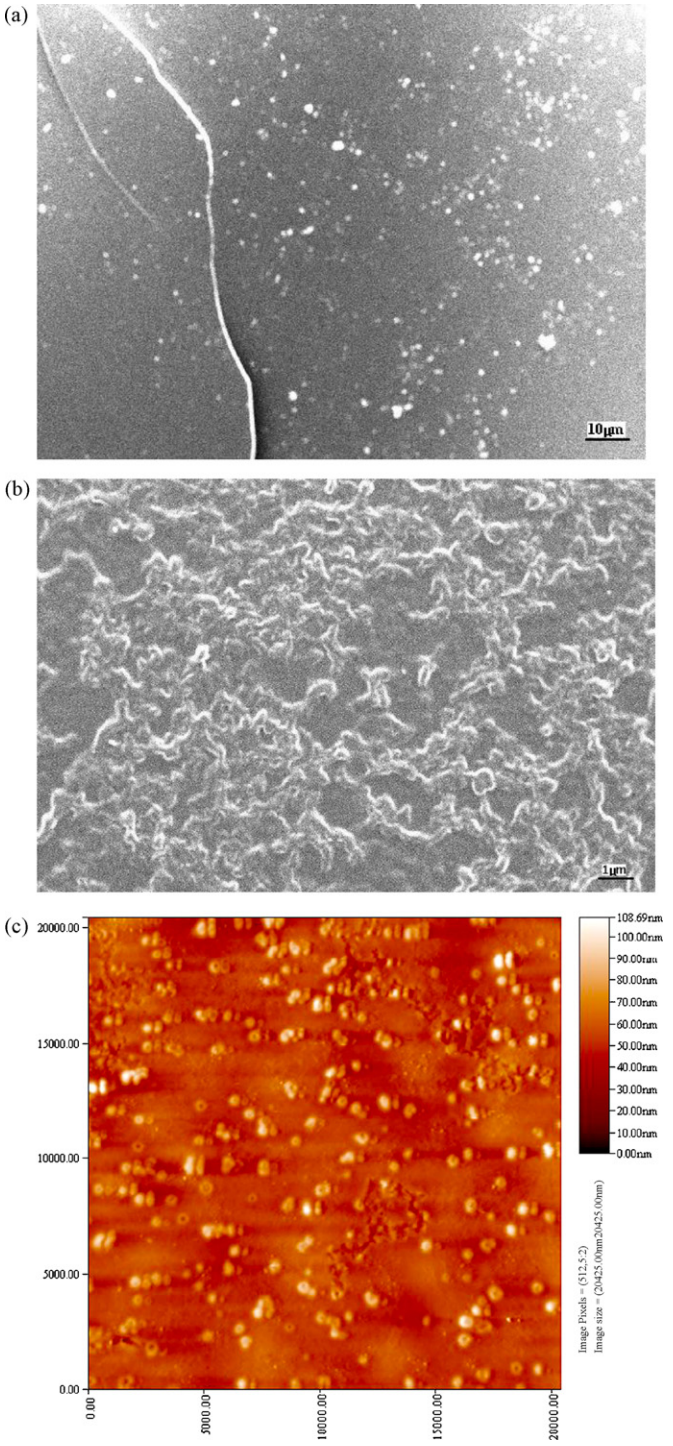

Fig. 1. Typical SEM of ormosils/HRP in the absence of MWNTs (a) presence of MWCNTs (b) composite film on the surface of ITO glass and (c) AFM image of the MWCNTs/MG/HRP composite film coated on ITO glass.

scan rates. Fig. 3b illustrated the remarkable significance of MWCNTs in the electrochemical behavior of modified electrode. The modified electrode with MWCNTs shows a well defined reversible voltammogram corresponding to the redox reaction of MG. Multiwalled carbon nanotubes not only increase the peak current, also improved the redox nature of methylene green incorporated within ormosils because the MWCNTs increase the effective surface area of modified electrode. The peak separation (ΔE_p) was typically small (~35 mV) and the ratio of anodic and cathodic

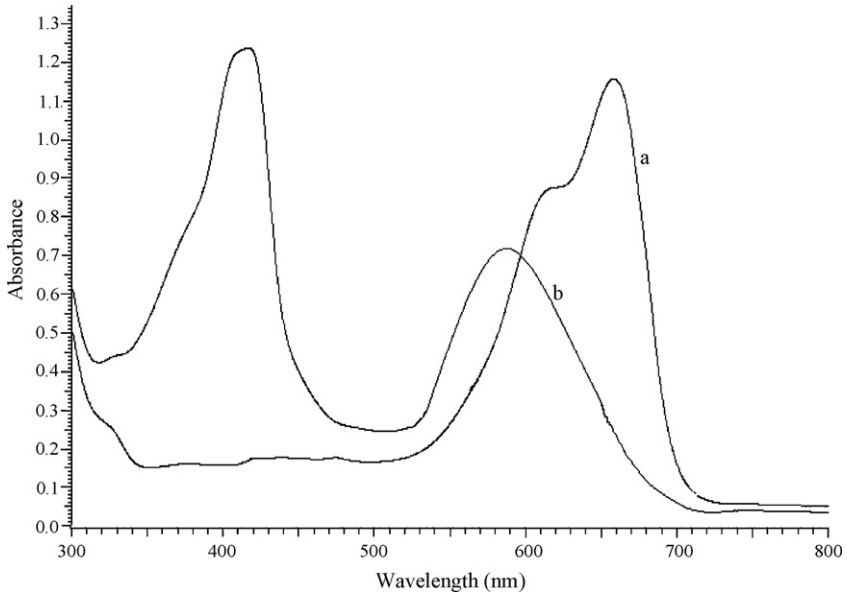

Fig. 2. UV–vis spectra of methylene green in solution (a) and in ormosil immobilized with HRP.

peak current was close to unity for MWCNTs modified electrode. It was clear that the peak potential was independent of the scan rate in the range between 10 and 200 mV s^{-1}. On the other hand, the MG/HRP/GCE shows poor electrochemical response for MG (Fig. 3a). As shown, the anodic and cathodic peaks were rather broad and the magnitude of the peak current was significantly lower than that observed on the MWCNTs composite electrode. Furthermore, the ΔE_p at the MG/HRP/GCE was relatively large, suggesting a sluggish electron transfer kinetics. From this result, we confirmed that MWCNTs/MG/HRP composites have good electrochemical reversibility. Both the anodic peak current and cathodic peak current were proportional to scan rate at the above scan range, suggesting that peak currents were surface confined. This suggested that redox dye as mediator was immobilized on the surface of the electrode successfully. The electrochemical behavior of MG modified with MWCNTs, without incorporated within ormosils was also investigated. MG molecules at once leached out from the electrode surface and no significant signal was observed (data not shown). To overcome this shortcomes, we used excellent ormosils matrix to encapsulate the MG and enzyme to increase the sensitivity and stability of hydrogen peroxide biosensor.

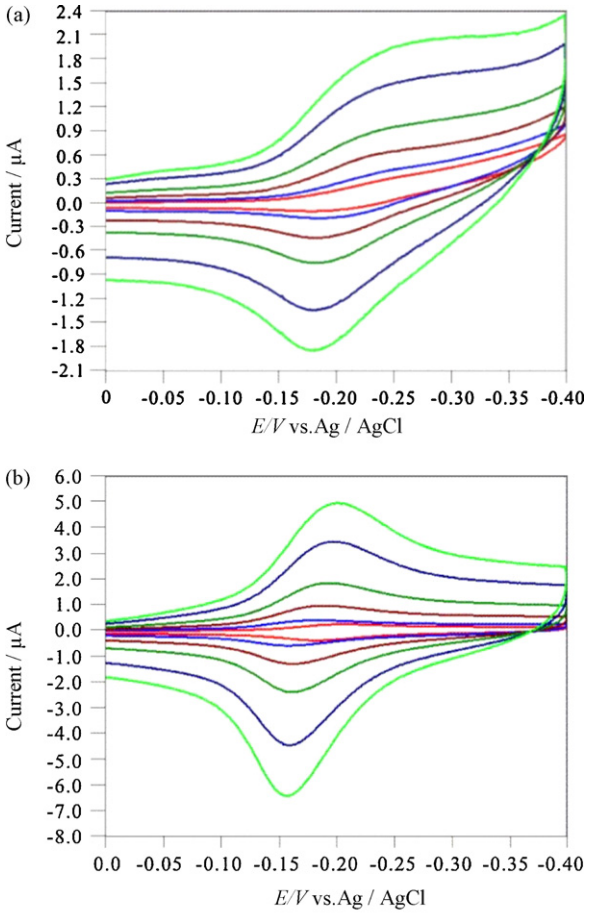

Fig. 3. Cyclic voltammograms of methylene green immobilized in ormosil in the absence (a) and presence (b) of MWCNTs in 0.1 M PBS (pH 7.2) at the scan rate of 5, 10, 20, 50, 100 and 200 mV s^{-1}.

Surface coverage (Γ) for the electroactive species was estimated by using Eq. (1)

$$\Gamma = \frac{Q}{nFA} \quad (1)$$

where A (0.70 cm^2) is the area of the working GCE, n (=1) the number of electron per reactant molecule, Q the charge obtained by integrating the anodic peak at low voltage scan rate (10 mV s^{-1}), and F is the Faraday Constant. In the present case, the calculated surface coverage for the electroactive species was 1.59×10^{-11} mol cm^{-2}.

3.3. Electrocatalysis of H_2O_2 on the MWCNTs/MG/HRP/GCE

At bare GC electrode, there was no response in the presence of H_2O_2. Fig. 4 displays the cyclic voltammograms of plane MG modified electrode without addition of H_2O_2 (curve A), and MG/HRP/GCE (curve B), MWCNTs/MG/HRP/GCE (curve C) in the presence of 0.5 mM H_2O_2 in 0.1 M PBS (pH 7.2) at the scan rate of 50 mV s^{-1}. It can been seen (Fig. 4, curve B) a small response was observed for MG/HRP/GCE in the potential range −0.05 to −0.18 V in the presence of 0.5 mM H_2O_2, but the modified electrode MWCNTs/MG/HRP/GCE (Fig. 4, curve C) showed a remarkable increased cathodic current in the same amount of H_2O_2. The reduction catalytic current of hydrogen peroxide starts at 0.0 V and obvious catalytic reduction peak appears at the potential of −0.18 V. This observation illustrated

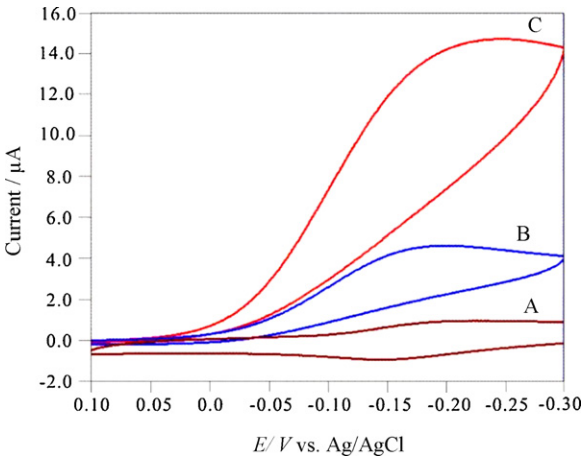

Fig. 4. Cyclic voltammograms of (A) plane MG incorporated in ormosil (B) and (C) are the CVs of MG/HRP/GCE and MWCNTs/MG/HRP/GCE respectively in the presence of 0.5 mM H_2O_2 in 0.1 M PBS (pH 7.2) at the scan rate of 50 mV s^{-1}.

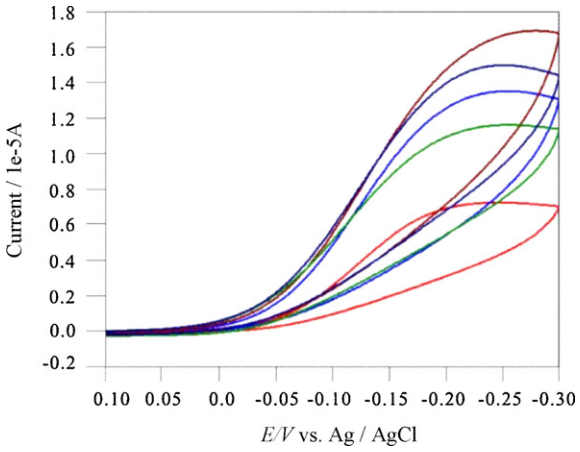

Fig. 5. Cyclic voltammograms of MWCNTs/MG/HRP/GCE in the presence of different concentration of H_2O_2: 0.3 0.5, 0.7, 1.0, 1.2 mM in 0.1 M PBS (pH 7.2) at the scan rate of 50 mV s^{-1}.

that MWCNTs played a significance role and facilitated the electrocatalysis of hydrogen peroxide on the modified electrode. MWCNTs not only increased the catalytic current, but also lowered the overpotential to reduce the interferences in the measurements. Fig. 5 presents the CVs of addition of various concentration of hydrogen peroxide at the scan rate of 50 mV s^{-1} in (0.1 M, pH 7.2) PBS. The cathodic peak current was dramatically increased and anodic peak current disappeared, indicated the fast electrocatalytic reduction of peroxide on the MWCNTs modified electrode.

The mechanism of the sensor can be summarized as follows. The peroxidase (POD) reduces hydrogen peroxide to water.

$$H_2O_2 + POD_{(red)} \rightarrow H_2O + POD_{(ox)}$$

Then the oxidized peroxidase converts MGH to MG^+

$$POD_{(ox)} + MGH \rightarrow POD_{(red)} + MG^+ + H^+$$

This overall reduction reaction of $POD_{(ox)}$ included two separate steps:

$$POD(I) + MGH \rightarrow POD(II) + MG^{\bullet}$$

$$POD(II) + MG^{\bullet} \rightarrow POD_{(red)} + MG^+$$

Where one electron was donated at a time, POD(I) was $POD_{(ox)}$ and $MG^{\bullet}$ represented the free radical formed during the reaction.

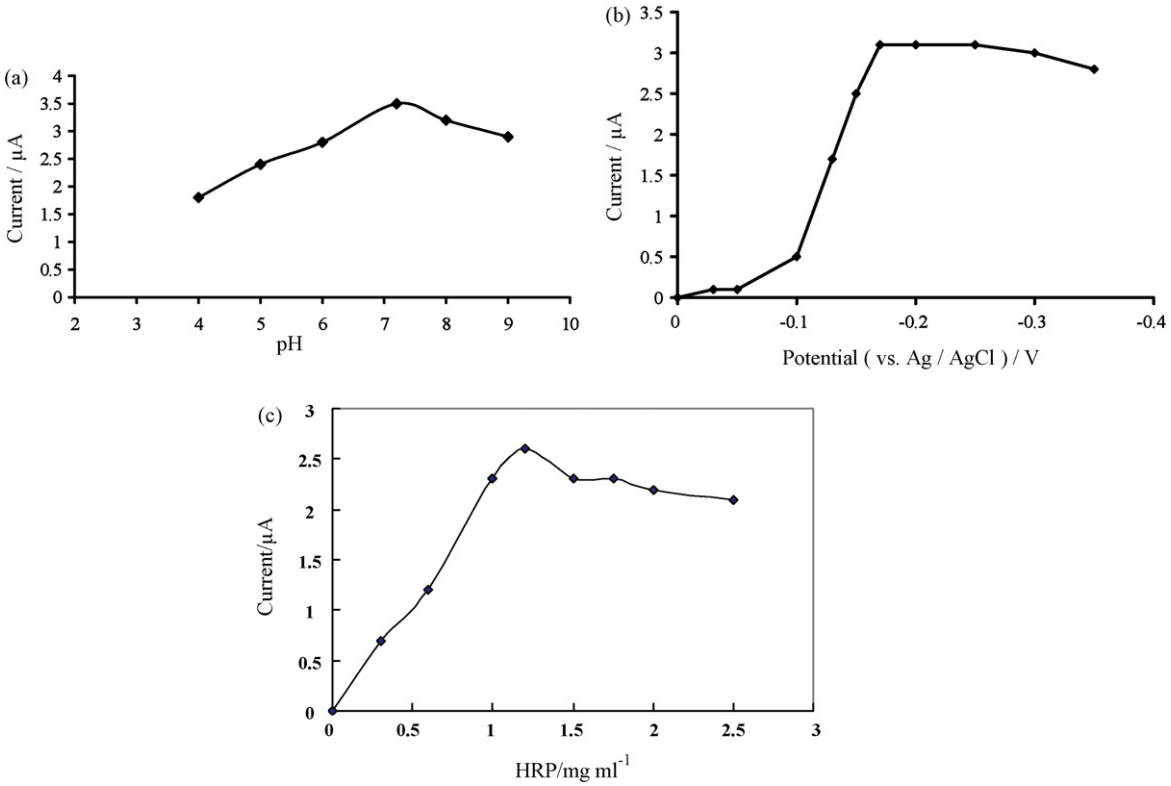

Fig. 6. (a) Influence of pH on the H_2O_2 sensor, study-state current measured in the presence of 0.5 mM H_2O_2 in 0.1 M PBS (pH 7.2) at applied potential of −0.18 at 25 °C. (b) Effect of potential on the sensor response for 0.5 mM H_2O_2 in 0.1 M PBS (pH 7.2). (c) Influence of the amount of HRP on the fabrication of biosensor.

MG^+ reduced at the sensor, resulting in a cathodic current.

$$MG^+ + H^+ + 2e \rightarrow MGH$$

3.4. Optimization of experimental conditions

3.4.1. Influence of pH and temperature on the sensor

It is well known that pH is a critical parameter of the enzyme activity and the stability in aqueous media [42]. The influence of the solution pH in the overall reaction for the electroanalysis of (0.5 mM) H_2O_2 using 0.1 M, PBS at pH 4.0 to 9.0 was studied Fig. 6a. The current and potential of the peak depended on the solution pH. The experimental results showed that the current response was higher at pH 7.2, when pH > 7.2/pH < 7.2, the current response became smaller. This was attributed to the higher activity of HRP in slight alkaline pH solution. Thus, the optimum pH for further studies was sit at 7.2.

The effect of temperature on the sensor had been examined between 15 and 45 °C. The response signal of the H_2O_2 sensor increased as the temperature varied from 15 to 37 °C. But at temperature lower than 20 °C, the activity of the enzyme was rather lower and the response time was relatively longer. On the other hand, at temperatures higher than 37 °C, the activity of enzyme decreased rapidly due to the partial denaturation of the enzyme. Taking both the lifetime and response time into consideration, 25 °C was the selected temperature for this work.

3.4.2. Effect of applied potential on the sensor

The applied potential has an important influence over the sensor response, because the applied potential contributes to the sensitivity and selectivity of the system [43]. The steady-state response to 0.5 mM H_2O_2 was measured at several applied potential values in 0.1 M, PBS buffer at pH 7.2, as shown in Fig. 6b. Electroreduction of H_2O_2 was observed already at approximately −0.18 V, and the steady-state current increased slowly with applied potential decreasing from −0.10 V to −0.18 V which can be attributed to the increasing driving force for the fast reduction of compounds. The current approaches a maximum value at −0.18 V and constant till −0.25 V, and then started decline. To avoid interferences and reduction of oxygen at high negative applied potential, −0.18 V was selected as the applied potential for amperometric measurement. This potential was superior to the previous reported work [44].

3.4.3. Influence of HRP amount on sensor fabrication

The amount of the enzyme in composite is a vital factor affecting the analytical sensitivity of the biosensor. The influence of amount of immobilized HRP on the analytical characteristics of the enzyme electrode was studied using CVs. Fig. 6c displays the effect of the amount of HRP enzyme in the MWCNTs modified electrode. The current response increases as the enzyme amount is increased and was maximum at 1.2 mg ml^{-1}. For higher amounts than 1.2 mg ml^{-1}, a reduction of the biosensor sensitivity is observed due to diffusion limitation. So, an optimum loading of 1.2 mg ml^{-1} HRP was used for subsequent experiment.

3.5. Kinetic analysis

The apparent Michaelis constant (K_M), which gives an indication of the enzyme-substrate kinetics, can be calculated from the electrochemical version of the Lineweaver–Burk equation

$$\frac{1}{I_{ss}} = \frac{1}{I_{max}} + \frac{K_M}{I_{max}}\frac{1}{C}$$

where I_{ss} is the steady-state current after the addition of substrate, C is the bulk concentration of the substrate and I_{max} is the maximum current measured under saturated substrate condition. The

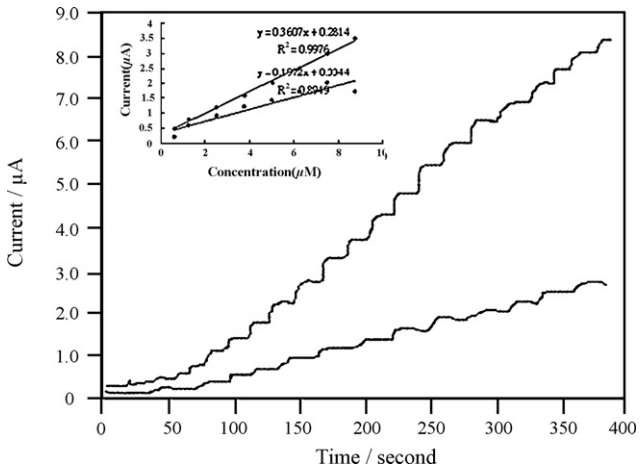

Fig. 7. Amperometric response of (a) MWCNTs/MG/HRP/GCE and (b) MG/HRP/GCE in a stirred 0.1 M PBS (pH 7.2) after successive hydrogen peroxide additions at applied potential −0.18 V vs. Ag/AgCl. Inset shows the linear calibration plot of catalytic currents vs. hydrogen peroxide concentrations.

K_M value was determined by analysis of the slope and intercept for the plot of the reciprocals of the cathodic current versus H_2O_2 concentration. The K_M value of the H_2O_2 sensor was determined by steady-state amperometric response and found to be 1.8 mM, which was smaller than those of 7.6 mM for HRP on nanoscopic gold tubes arrays modified nanoelectrode [45], 4.6 mM for HRP immobilized in sol–gel/hydrogel modified electrode [46], 4.3 mM for HRP in multilayer QPVP film [51], 4.51 mM for HRP on AuNP/CHIT/SPCE [47], 4.04 mM for HRP on TTF/TCNQ/MWCNTs modified electrode [30], 2.5 mM for HRP immobilized on a ferrocene containing polymer electrochemically deposited onto a Pt electrode [48], 5.12 mM for SBP (soybean peroxidase) immobilized in sol–gel thin film [49] and was close to 2.0 mM for HRP immobilized on FMC-BSA/MWCNTs ormosil composite-modified GC electrode [50] and 2.1 mM for sol–gel/nafion/MG electrode [32]. The smaller value of K_M value means that the immobilized HRP possesses higher enzyme activity, and the present modified electrodes exhibit higher affinity to H_2O_2. The immobilization of HRP in ormosils mentioned appears to be beneficial to improving the biosensor's performance.

4. Analytical characterization of H_2O_2 sensor

Fig. 7 presents the dynamic amperometric response of the sensor at a working potential of −0.18 V with successive injections of 0.5 mM H_2O_2 in 0.1 M PBS (pH 7.2) on MG/HRP/GCE and MWCNTs/MG/HRP/GCE. The trace clearly demonstrated the fast response and high sensitivity of the MWCNTs/MG/HRP/GCE to H_2O_2 than MG/HRP/GCE, suggested that the MWCNTs facilitated the electron transfer in the matrix and enhanced the electrocatalytic properties of modified electrode. The response time was less than 10 s (t = 95% of I_{max}), which was much lower than that earlier reported for H_2O_2 biosensor [52,53]. Fig. 6 (inset) shows the calibration plot of the biosensor. The response to H_2O_2 was linear in the range from 5×10^{-7} to 2×10^{-5} M with a correlation coefficient of 0.998 (n = 10), with the lower limit of detection 0.5 μM at a signal to noise ratio of 3. The higher sensitivity of the sensor may result from the biocompatible microenvironment around the enzyme [54]. The linear range, response time and limit of detection observed with MWCNTs/MG/HRP film electrode is in general comparable with most of the modified electrode reported in the literature (Table 2). The recovery rate was also estimated with the basic method of slandered recovery test. The recovery data were obtained as 98.6%.

Table 2
Comparison of the efficiency of MWCNTs/MG/HRP modified electrode used in determination of H_2O_2.

Electrode	Method	Electrolyte	LOD (μM)	LCR (M)	RT (s)	Ref.
MWCNT/MB/HRP/GCE	CV	pH 7 PBS	1	4×10^{-6} to 2×10^{-3}	<30	25
MWCNT/PS/HRP/SPE	CV	pH 7 PBS	25	2×10^{-5} to 5×10^{-4}	–	23
MWCNT/FMC-BSA/HRP/GCE	CV, FIA	pH 6.8 PBS	5	2×10^{-5} to 4.5×10^{-3}	20	24
PDDA-Au/DNA-Ag/HRP	CV	pH 6 PBS	2	7×10^{-6} to 7.8×10^{-3}	15	50
SG/MG/nafion/HRP/GCE	CV	pH 7 PBS	0.1	5×10^{-7} to 1.6×10^{-3}	20	32
MB/HRP/GA/GPE	CV	pH 7 PBS	3	9.9×10^{-6} to 6.49×10^{-4}	–	55
Ag-nano/PVA/Pt	CV	pH 7 PBS	10	45×10^{-6} to 6×10^{-3}	–	56
Gelatine/MB/HRP/GCE	CV	pH 7 PBS	4	1×10^{-5} to 1.2×10^{-3}	<20	40
NMB/HRP/GCE	CV	pH 7 PBS	2.07	2.5×10^{-6} to 1×10^{-4}	<20	57
MG/HRP/zeolite/GCE	CV	pH 7 PBS	0.5	2.5×10^{-6} to 2.4×10^{-4}	40	44
MWCNT/MG/HRP/GCE	CV	pH 7.2 PBS	0.5	5×10^{-7} to 2×10^{-5}	<10	Present work
PEGDGE/SBP/GCE	CV	pH 7.4 PBS	–	1×10^{-7} to 2×10^{-4}	–	58

LCR: linear concentration range; LOD: limit of detection; RT: response time.

Table 3
Interferences studies.

Interferents	Current ratio
Uric acid	1.01
Glucose	1.00
Cysteine	1.00
Dopamine	1.03
Ascorbic acid	1.00
Oxalic acid	0.97
NADH	1.00
Citric acid	0.99

4.1. Stability of the biosensor

The stability of the biosensor was examined by amperometric measurements in the presence of 6 μM H_2O_2 periodically. It was found that the biosensor retained its 90% response after 1 month of testing. When the biosensor was not in use, it was stored under dry conditions at 4 °C in a refrigerator. The good long-term stability can be attributed to the great stability of MG and the excellent biocompatibility and the stabilizing microenvironment around the HRP provided by the organically modified sol–gel composite matrix.

4.2. Selectivity against interferences

The selectivity of this H_2O_2 biosensor was evaluated by H_2O_2 determinations in the presence of some potentially coexisting compounds of H_2O_2 in biological systems. In this experiment, six interfering substances including uric acid, dopamine, ascorbic acid, glucose, cysteine, oxalic acid, NADH and citric acid were tested and the results were listed in Table 3. It can be observed that the eight tested interferents exerted neglectable influences on the determination of H_2O_2.

5. Conclusion

We have developed a novel MWCNTs/ormosils based electrochemical biosensor for the analytical detection of hydrogen peroxide. HRP and MG were successfully incorporated within ormosils matrix. The experimental results proved that the MWCNTs imparting the electrocatalytic property of modified electrode due to enhance the rate of electron transportation within omosils film. The modified electrode MWCNTs/MG/HRP/GCE showed stable and reproducible electrochemical behavior, long stability and excellent electrochemical reversibility. This modified electrode showed excellent electrocatalytic activity for H_2O_2 reduction at reduced over potential with fast response time (<10 s) with very low limit of detection. So, this novel and efficient strategy, that is, successful coimmobilization of HRP, MG as a mediator, and MWCNTs within ormosils for the construction of the hydrogen peroxide biosensor, opens up a new approach to construct verity of organically modified sol–gel glasses amperometric biosensors.

Acknowledgement

This work was financially supported by the National Science Council of Taiwan.

References

[1] S.Q. Liu, H.X. Ju, Biosens. Bioelectron. 19 (2003) 177.
[2] X.B. Lu, J.H. Jhou, W. Lu, Q. Liu, J.H. Li, Biosens. Bioelectron. 23 (2008) 1236.
[3] X.H. Shu, Y. Chen, H.Y. Yuan, S.F. Gao, D. Xiao, Anal. Chem. 79 (2007) 3695.
[4] X. Cui, G. Liu, Y. Lin, J. Biomed. Nanotechol. 1 (2005) 1.
[5] X.L. Luo, J.J. Xu, W. Zhou, H.Y. Chen, Biosens. Bioelectron. 19 (2004) 1295.
[6] M.C.Y. Chang, A. Pralle, E.Y. Isacoff, C.J. Chang, J. Am. Chem. Soc. 126 (2004) 15392.
[7] J. Li, P.K. Dasgupta, G.A. Tarver, Anal. Chem. 75 (2003) 1203.
[8] N.V. Klassen, D. Marchington, H.C.E. McGovan, Anal. Chem. 66 (1994) 2921.
[9] A. Lobnik, M. Cajlakovuc, Sens. Actuators B 74 (2001) 194.
[10] S.H. Chen, R. Yuan, L.Y. Zhang, N. Wang, X.L. Li, Biosens. Bioelectron. 22 (2007) 1268.
[11] J. Li, C. Lau, M. Morizono, K. Ohta, M. Kai, Anal. Chem. 73 (2001) 5979.
[12] A.A. Karyakin, Electroanal. 13 (2001) 813.
[13] J. Wang, M. Gu, J. Di, Y. Gao, Y. Wu, Y. Tu, Biopro. Biosyst. Eng. 30 (2007) 289.
[14] W. Li, R. Yuan, Y. Chai, L. Zhou, S. Chen, Na Li, J. Biochem. Biophys. Methods 70 (2008) 830.
[15] V. Lvovich, A. Scheeline, Anal. Chem. 69 (1997) 454.
[16] S. Iijima, Nature 354 (1991) 56.
[17] L.Q. Rong, C.Y.Q.Y. Qian, X.H. Xia, Talanta 72 (2007) 819.
[18] N. Zhu, Z. Chang, P. He, Y. Fang, Anal. Chim. Acta 545 (2005) 21.
[19] K. Gong, Y. Dong, S. Xiong, Y. Chen, L. Mao, Biosens. Bioelectron. 20 (2004) 253.
[20] J. Manso, M.L. Mena, P. Yanez-Sedeno, J. Pingarron, J. Electroanal. Chem. 603 (2007) 1.
[21] A. Salimi, L. Miranzadeh, R. Hallaj, H. Mamkhezri, Electroanalysis 20 (2008) 1760.
[22] Y. Liu, J. Lei, H. Ju, Talanta 74 (2008) 965.
[23] S. Sanchez, M. Pumera, E. Cabruja, E. Fŕbregas, Analyst 132 (2007) 142.
[24] V.S. Tripathi, V.B. Kandimalla, H. Ju, Biosen. Bioelectron. 21 (2006) 1529.
[25] Jin. Xu, J. Zhu, Q. Wu, Z. Hu, H. Chen, Electroanalysis 15 (2003) 219.
[26] B. Wang, J.J. Zhang, Z.Y. Pan, X. Tao, H. Wang, Biosen. Bioelectron. 24 (2009) 1141.
[27] Po.H. Lo, S.A. Kumar, S.M. Chen, Colloid Surf. B: Biointerfaces 66 (2008) 266.
[28] A.K.M. Kafi, G. Wu, A. Chen, Biosen. Bioelectron. 24 (2008) 566.
[29] J.L. Lyon, K.J. Stevenson, Electron. Chim. Acta 53 (2008) 6714.
[30] Z. Cao, X. Jiang, Q. Xie, S. Yao, Biosen. Bioelectron. 24 (2008) 222.
[31] J. Liu, S.L. Mu, Synth. Met. 107 (1999) 159.
[32] B. Wang, S. Dong, Talanta 51 (2000) 565.
[33] A. Vasilescu, S. Andreescu, C. Bala, S.C. Litescu, T. Naguer, J.L. Martr, Biosens. Bioelectron. 18 (2003) 781.
[34] A. Noorbakhsh, A. Salimi, E. Sharifi, Electroanalysis 20 (2008) 1788.
[35] R. Gupta, N.K. Chaudhury, Biosen. Bioelectron. 22 (2007) 2387.
[36] T. Coradin, J. Livage, Acc. Chem. Res. 40 (2007) 819.
[37] D. Avnir, O. Lev, J. Livage, J. Mater. Chem. 16 (2006) 1013.
[38] S. Xu, Z. Jiang, H. Wu, S. Huang, Progr. Chem. 16 (2004) 443.
[39] A.F. Groboilot, C.P. Champagne, G.D. Darling, D. Poncelet, R.J. Neufild, Biotechnol. Bioeng. 42 (1993) 1157.
[40] H. Yao, N. Li, S. Xu, Jin. Xu, J.J. Zhu, H. Chen, Biosen. Bioelectron. 21 (2005) 372.
[41] S. Jockusch, N.J. Turro, Macromolecules 28 (1995) 7416.
[42] G. Bicketstaff, Methods in Biotech, Humana Press, New Jersey, 1997.
[43] E. Csoregi, G. Jonsson-Petersson, L. Gorton, J. Biotechnol. 30 (1993) 315.
[44] B. Liu, F. Yan, J. Kong, J. Deng, Anal. Chim. Acta 386 (1999) 31.

[45] M. Delvaux, A. Walcarius, S. Demoustier-Champagne, Anal. Chim. Acta 525 (2004) 221.
[46] B. Wang, J. Zhang, G. Cheng, S. Dong, Anal. Chim. Acta 407 (2000) 111.
[47] T. Tangkuaram, C. Ponchio, T. Kangkasomboon, P. Katikawong, W. Veerasai, Biosen. Bioelectron. 22 (2007) 2071.
[48] M.P.G. Armada, J. Losada, I. Cuadrado, B. Alonso, B. González, C.M. Casado, J. Zhang, Sens. Actuators B 101 (2004) 143.
[49] Q. Wang, G. Lu, B. Yang, Anal. Chem. 71 (1999) 1935.
[50] L. Ma, R. Yuan, Y. Chai, S. Chen, J. Mol. Catal. B 56 (2009) 215.
[51] C. Sun, W. Li, Y. Sun, X. Zhang, J. Shen, Electrochim. Acta 44 (1999) 3401.
[52] H. Liu, Y. Liu, J. Qian, T. Yu, J. Deng, Talanta 43 (1998) 111.
[53] C. Lei, J. Deng, Ana. Chem. 68 (1996) 3344.
[54] B.Q. Wang, B. Li, Q. Deng, S.J. Dong, Anal. Chem. 70 (1998) 170.

Talanta 79 (2009) 72–76

Contents lists available at ScienceDirect

Talanta

journal homepage: www.elsevier.com/locate/talanta

Au NPs-aptamer conjugates as a powerful competitive reagent for ultrasensitive detection of small molecules by surface plasmon resonance spectroscopy

Jianlong Wang, Ahsan Munir, H. Susan Zhou*

Department of Chemical Engineering, Worcester Polytechnic Institute, 100 Institute Road, Worcester, MA 01609, United States

ARTICLE INFO

Article history:
Received 3 February 2009
Received in revised form 2 March 2009
Accepted 3 March 2009
Available online 14 March 2009

Keywords:
Aptamer
Small molecules
Au nanoparticles
Surface plasmon resonance

ABSTRACT

Features of Au NPs-aptamer conjugates as a powerful competitive reagent to substitute antibody in enhancing surface plasmon resonance spectroscopy (SPR) signal for the detection of small molecule are explored for the first time. In order to evaluate the sensing ability of Au NPs-aptamer conjugates as a competitive reagent, a novel SPR sensor based on indirect competitive inhibition assay (ICIA) for the detection of adenosine is constructed by employing the competitive reaction between antiadenosine aptamer with adenosine and antiadenosine aptamer with its partial complementary ss-DNA. The partial complementary ss-DNA of antiadenosine aptamer is firstly immobilized on SPR gold film as sensing surface. When the Au NPs-antiadenosine aptamer conjugates solution is added to SPR cell in the absence of adenosine, Au NPs-antiadenosine aptamer conjugates is adsorbed to SPR sensor by the DNA hybridization reaction, and results in a large change of SPR signal. However, the change of SPR signal is decreased when the mixing solution of adenosine with Au NPs-antiadenosine aptamer conjugates is added. This is because adenosine reacts with antiadenosine aptamer in Au NPs-antiadenosine aptamer conjugates and changes its structure from ss-DNA to tertiary structure, which cannot hybridize with its partial complementary ss-DNA immobilized on SPR gold surface. Based on this principle, a SPR sensor for indirect detection of adenosine can be developed. The experimental results confirm that the SPR sensor possesses a good sensitivity and a high selectivity for adenosine, which indirectly confirms that Au NPs-aptamer conjugates is a powerful competitive reagent. More significantly, it can be used to develop other SPR sensors based on ICIA to detect different targets by changing the corresponding type of aptamer in Au NPs-aptamer conjugates.

Published by Elsevier B.V.

1. Introduction

Indirect competitive inhibition assay (ICIA) has been receiving increased attention in surface plasmon resonance spectroscopy (SPR) because it can greatly enhance the sensitivity of SPR for detecting small molecules [1–3]. The most critical point for the ICIA technique is to find an excellent competitive reagent to amplify SPR signal for indirect detection of small molecules. An excellent competitive reagent should not only bind well with small molecules, but should also result in a large change of SPR signal after it has been adsorbed on the SPR gold film [4]. At present, SPR sensors based on ICIA technique for detecting small molecules employ analyte (small molecule)-antibody system [5–7]. In this system antibody is used as a competitive reagent to induce SPR signals. However, it is well known that the change of SPR signals resulting from antibody adsorption is not very large. Furthermore, the types of antibody responding to small molecules are limited, which restricts the extensive application of ICIA in SPR sensors for detection of small molecules. Thus, it is imperative to explore novel competitive reagents that can not only extend the application of ICIA, but can also enhance the sensitivity the SPR sensors for detecting small molecules.

Recently, techniques based on aptamers are taking a very significant role in the development of specific detectors for different kinds of analytes, especially for small molecules [8–16]. Many reports have confirmed that aptamers can be used to substitute antibodies in bioanalytical sensing [17–24]. However, there have been little or no efforts made to utilize aptamer as a competitive reagent of ICIA in place of antibody in SPR spectroscopy. Maybe the reason comes from the fact that the change of SPR signal resulted from the adsorption of aptamer is smaller than that of antibody because the molecule weight of most aptamer is smaller than antibody. However, this problem is easy to be overcome by the amplifying effect of gold nanoparticles (Au NPs). Many reports had confirmed that Au NPs can greatly enhance the sensitivity of biosensor [25–31]. Furthermore, many literatures had also confirmed that aptamer is very easy to be tagged by Au NPs [32–34]. Therefore, utilizing Au NPs-aptamer conjugates as a competitive reagent of ICIA to substi-

* Corresponding author. Tel.: +1 508 831 5275; fax: +1 508 831 5936.
E-mail address: szhou@wpi.edu (H.S. Zhou).

0039-9140/$ – see front matter. Published by Elsevier B.V.
doi:10.1016/j.talanta.2009.03.003

tute antibody for enhancing the sensitivity of SPR for the detection of small molecule is expected to be a promising approach.

In this work, we adopt adenosine and antiadenosine aptamer as a model system to evaluate the sensing ability of Au NPs-aptamer conjugates as a competitive reagent. We design a novel SPR sensor based on ICIA to detect adenosine. Our results confirmed Au NPs in Au NPs-aptamer conjugates greatly enhance the sensitivity of present SPR sensor for detection of adenosine; antiadenosine aptamer in Au NPs-aptamer conjugates promise the selectivity of present SPR sensor for adenosine. Thus, the application of Au NPs-aptamer conjugates can combine the advantage of aptamer technique and amplifying effect of Au nanoparticles, which will be benefit to extend the application of SPR spectroscopy for detection of small molecules.

2. Experimental

2.1. Materials

Trisodium citrate, hydrogen tetrachloroaurate (III) ($HAuCl_4$), 6-mercaptohexan-1-ol (MCH), adenosine, uridine, cytidine and guanosine were purchased from Sigma and used as received. All DNA molecules were obtained from Integrated DNA Technologies (IDT). The sequence of the adenosine-binding aptamer was 5′-SH-C_6-AGA GAA CCT GGG GGA GTA TTG CGG AGG AAG GT-3′ (aptamer), the sequence of its part complementary strand was 5′-SH-C_6-ACC TTC CTC CGC-3′ (ss-DNA). DNA solutions were prepared by dissolved DNA in 50 mM pH 8.0 Tris–HCl buffer including 138 mM NaCl. Different concentrations of adenosine and 1 mM uridine, cytidine, guanosine were all prepared in the Tris–HCl buffer.

2.1.1. The synthesis and modification of Au NPs with a diameter of ~13 nm

All glassware used in the following procedures was cleaned in a bath of freshly prepared 3:1 HCl:HNO_3 (aqua regia) and rinsed thoroughly in H_2O prior to use. Au NPs stabilized with citrate were synthesized according to our previous work [35]. That is, 100 mL of 1 mM $HAuCl_4$ (4 mL 1% (w/w) $HAuCl_4$ solution dissolved in 96 mL H_2O) was brought to a reflux while stirring and then 10 mL of a 38.8 mM trisodium citrate (10 mL 1.14% (w/w) trisodium citrate) solution was added quickly, which resulted in a color change of the solution from pale yellow to deep red. After the color change, the solution was refluxed for an additional 15 min and left to cool to room temperature. The diameter of Au NPs was detected by dynamic light scattering. The data was shown in Fig. 1.

Au NPs-aptamer conjugates were prepared according to the literature with some modification [36]. That is, transfer 3 mL of the already prepared Au NPs to the NaOH-treated glass vials and then add 120 μL 10 μM aptamer with magnetic stirring to facilitate the reaction for 16 h. The final Tris–HCl concentration is ~50 mM.

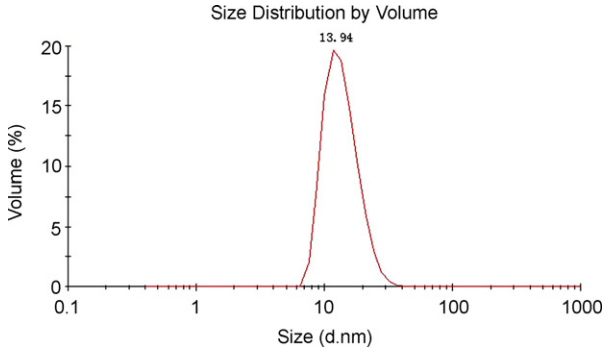

Fig. 1. The diameter of Au NPs detected by dynamic light scattering.

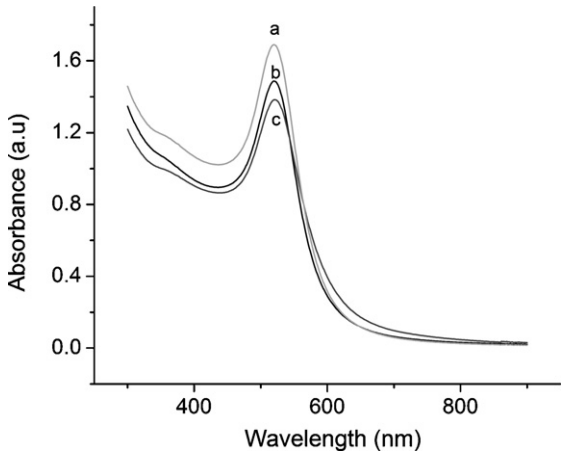

Fig. 2. UV–vis absorption of (a) Au NPs, (b) Au NPs-aptamer conjugates, and (c) Au NPs-aptamer conjugates after MCH treatment.

Centrifuge Au NPs-aptamer conjugates at 14,000 × *g* at room temperature for 25 min twice to remove the free aptamer. And then, disperse the Au NPs-aptamer conjugates in 2 mL of buffer containing 138 mM NaCl, 50 mM Tris–HCl, pH 8.0.

MCH treatment of Au NPs-aptamer. The prepared Au NPs-aptamer conjugates were treated with MCH according to Li et al.'s report [37]. Briefly, MCH was added to the prepared Au NPs-aptamer conjugates solution to give a final MCH concentration of ~4 μM. The MCH treatment was performed at room temperature for 30 min. The reaction was quenched by two washes with equal volumes of ethylacetate, which removed excess MCH from solution. A similar centrifugal procedure was used to collect the Au NPs-aptamer conjugates. At last, the Au NPs-aptamer conjugates were dispersed in 2 mL of buffer containing 138 mM NaCl, 50 mM Tris–HCl, pH 8.0 again.

UV–vis absorption spectrum is used to observe the change of Au NPs status after aptamer labeling and MCH treating. The results were shown in Fig. 2. We can see that the absorbance of Au nanoparticles at 519 nm did not change greatly after aptamer labeling and MCH treating, it means these modifications do not affect the character of Au NPs. The decrease of peak intensity mainly comes from the loss of Au nanoparticles during the process of centrifugation.

2.2. In situ SPR measurement

The SPR experiments were done using Eco Chemie Autolab SPR systems (Brinkmann Instruments, New York, USA). It works with a laser diode fixed at a wavelength of 670 nm, using a vibrating mirror to modulate the angle of incidence of the p-polarized light beam on the SPR substrate. The instrument is equipped with a cuvette. Gold sensor disk (25 mm in diameter) was mounted on the hemicylindrical lens (with index-matching oil) to form the base of the cuvette. An O-ring (3 mm inner diameter) between the cuvette and disk prevents leakage. An auto-sampler (Eco Chemie) with controllable aspirating–dispensing–mixing pipette was used to add samples into the cuvette and provide constant mixture by aspiration and dispensing during measurements. This experimental arrangement maintains a homogenous solution and reproducible hydrodynamic conditions.

For detailed experiment, the SPR gold film was firstly immersed into the ss-DNA solution for 12 h in order to assemble the monolayer of ss-DNA. Then the modified gold film was thoroughly rinsed with 50 mM Tris–HCl buffer and water to remove the weakly adsorbed ss-DNA. Ss-DNA modified SPR gold film was immersed in 100 μM 6-mercapto-hexanol for 1 h to block the uncovered gold surface. This gold film was used as a sensing surface to detect the amount

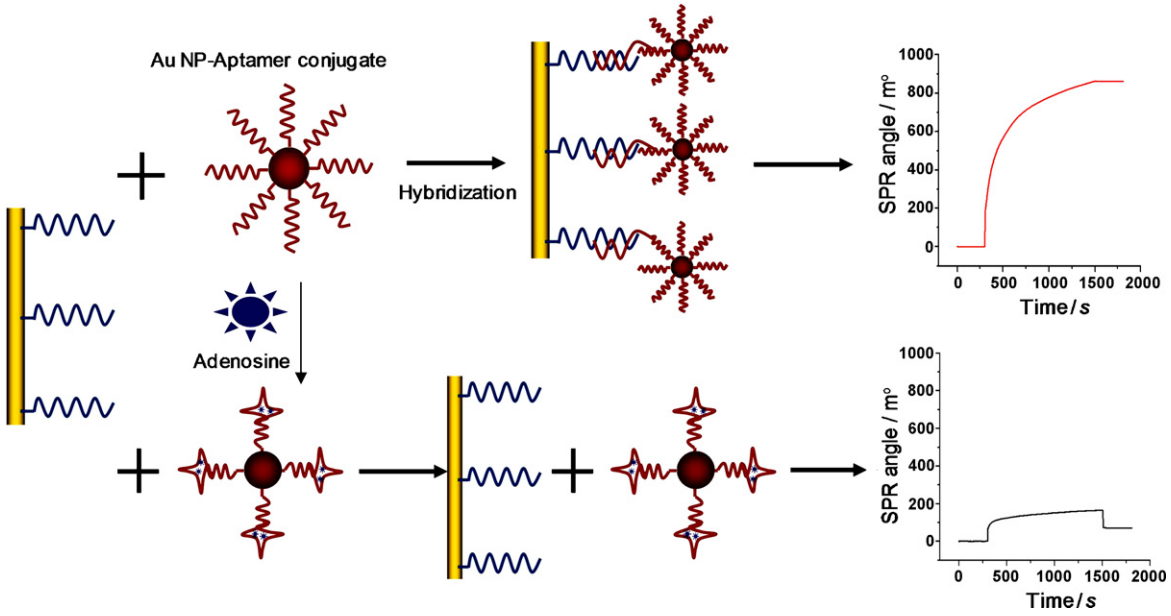

Fig. 3. Schematic representation of the SPR biosensor for the detection of the small molecules that utilize Au NPs-aptamer conjugates as competitive reagent.

of aptamer possessing ss-DNA structure on Au NPs-aptamer conjugates, which can be adjusted by the concentration of adenosine adding to Au NPs-aptamer conjugates solution. The detection procedure is made up of two steps. At first, Au NPs-aptamer conjugates solution was mixed with different concentrations of adenosine for 30 min. After that, the mixing solution was injected to SPR cell and record SPR angle–time curve. The inject rate for all samples are 10 μL/s, the volume for all samples dispensed in SPR cell are 40 μL, the mixing rate for all samples during the process of experiment are 10 μL/s.

3. Results and discussion

3.1. The detection principle of SPR biosensor

In order to evaluate the ability of Au NPs-aptamer conjugates as a competitive reagent, it is necessary to construct a SPR sensor based on aptamer technique for detecting small molecules by ICIA. Before constructing SPR sensor, how to fabricate the sensing surface that can specifically and rapidly bind Au NPs-aptamer conjugates existed in solution for ICIA of small molecule should be considered. The reaction of small molecule with aptamer in the solution will induce aptamer change its structure from ss-DNA structure to tertiary structure, and small molecules will be embedded inside the aptamer. So different from antibody-based ICIA [5–7], where the reaction can be achieved by adsorbing antibody on small molecule-modified-SPR gold film, the conformation change of the aptamer will be inhibited if small molecules are immobilized on SPR gold surface because of the strong stereo-hindrance effect between aptamer and SPR gold film. Thus, it is difficult to fabricate a sensing surface on SPR gold film for aptamer. However, aptamer being a ss-DNA makes it easy to hybridize with its complementary ss-DNA sequence. Therefore if aptamer's complementary ss-DNA sequence is immobilized on the SPR gold film as a sensing surface for detection of aptamer possessing ss-DNA structure in solution, which can be controlled by adding different concentration of small molecule, a SPR sensor for small molecule based on ICIA using aptamer as competitive regent is feasible.

Based on this principle, we select a simple system (adenosine/its aptamer which was tagged by Au NPs) to construct a SPR sensor for detecting adenosine by ICIA. The detection process of this SPR sensor is shown in Fig. 3. The SPR gold film was first modified with a ss-DNA which is complementary to the aptamer. When Au NPs-aptamer conjugates were added to the SPR reaction cell, Au NPs-aptamer conjugates will be adsorbed on the surface of SPR gold film through the hybridization reaction between ss-DNA and aptamer, which will result in an obvious change in SPR signal. However, this change will decrease when the mixed solution of Au NPs-aptamer conjugates with adenosine is added to the SPR reaction cell because adenosine reacts with aptamer and makes the aptamer on Au NPs change its structure from ss-DNA to tertiary. The aptamer possessing tertiary structure cannot hybridize with ss-DNA immobilized on SPR gold film. Thus, the change of SPR signal will decrease with the increase of the number of Au NPs-aptamer conjugates possessing tertiary structure, which is proportional to the concentration of adenosine.

3.2. SPR spectroscopy detects the concentration of adenosine by using Au NPs-aptamer conjugates as competitive reagents

During our experiments, we utilize the SPR angle–time curve to monitor the hybridization reaction between ss-DNA immobilized on SPR gold film and Au NPs-aptamer conjugates after Au NPs-aptamer conjugates are reacted with different concentrations of adenosine for 30 min. The results are shown in Fig. 4. In the absence of adenosine, Au NPs-aptamer conjugates in solution directly hybridize with ss-DNA immobilized on SPR gold film, resulting in a largest SPR angle shift (∼0.861°). This angle shift is much larger that of angle shift by the adsorption of antibody that is generally used as competitive reagent in ICIA [1–3]. Thus, maybe a higher detection range can be obtained with present SPR sensor by using Au NPs-aptamer conjugates as competitive reagent. The SPR angle shift resulted from the binding of Au NPs-aptamer conjugates decreases (∼0.832°) after Au NPs-aptamer conjugates solution are reacted with 0.1 nM adenosine for 30 min. This is because parts of aptamers on Au NPs react with adenosine and form its tertiary structure, which cannot hybridize with its complementary ss-DNA. In general, a ss-DNA will hybridize with its complementary ss-DNA from its 3′ end or its 5′ end. However, the 3′ end and the 5′ end of aptamer possessing tertiary structure will locate on the surface of Au NPs with the introduction of adenosine. This structure inhibit the reaction of aptamer possessing tertiary structure

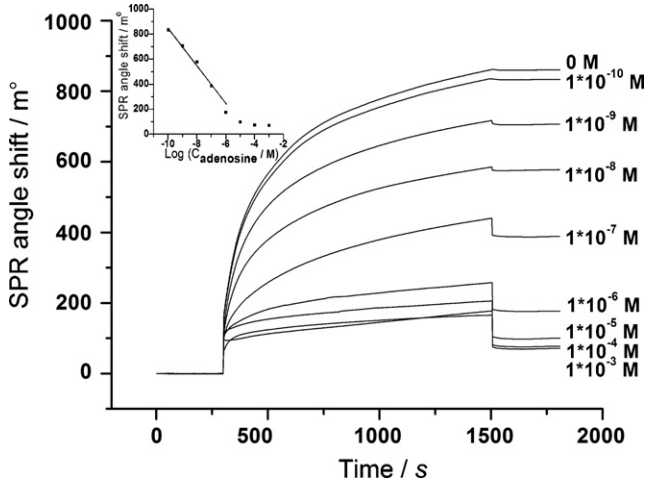

Fig. 4. SPR angle–time curves for the detection of the binding process between ss-DNA and Au NPs-aptamer conjugates after Au NPs-aptamer conjugates are reacted with different concentrations of adenosine for 30 min. Inset: A curve describing the linear relationship between the SPR angle shift and the adenosine concentrations.

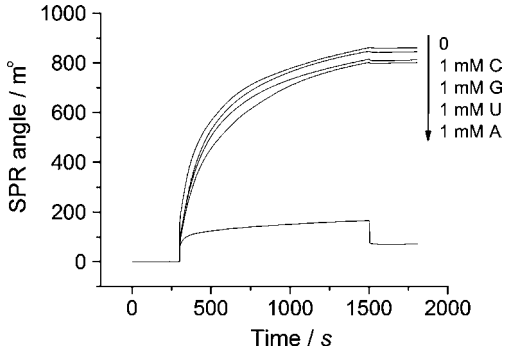

Fig. 5. SPR angle–time curves for the detection of the binding process between ss-DNA and Au NPs-aptamer conjugates after Au NPs-aptamer conjugates are reacted with different kinds of analytes for 30 min.

on Au NPs with its complementary ss-DNA immobilized on SPR gold surface because ss-DNA is inaccessible to 3′ or 5′ of aptamer possessing tertiary structure. Therefore, ss-DNA immobilized on SPR gold film only hybridizes with the rest of aptamers possessing free coil structure on Au NPs. When the concentration of adenosine adding to Au NPs-aptamer conjugates solution is further increased, we can observe the SPR angle shift gradually decreases. However, the decreasing trend will reduce after adenosine with high concentrations are added, especially when the concentration of adenosine is larger that 10^{-6} M. By analyzing the change of SPR angle shift with the concentrations of adenosine, we obtain a good linear relationship between the logarithms of adenosine concentrations and the SPR angle shift over a range of 1×10^{-10}–1×10^{-7} M (shown in the inset of Fig. 4). The detection result of this present SPR sensor that utilize Au NPs-aptamer conjugates as a competitive reagent for analyzing the concentration of adenosine are comparable with other optical and electrochemical aptasensor and are much superior to the detection results obtained by general SPR sensor based on molecularly imprinted technique [38,39]. It must be pointed out that a nonspecific adsorption can be found in this SPR biosensor. From Fig. 4, we can see that SPR angle–time curves for the detection of the binding process between ss-DNA and Au NPs-aptamer conjugates still change about 0.07° even when Au NPs-aptamer conjugates react with 1 mM adenosine for 30 min. The main reason for this phenomenon may come from the stereo-hindrance effect of aptamer possessing different structures. After adenosine is added to Au NPs-aptamer conjugates, most of free-coiled aptamer react with adenosine and form its tertiary structure. However, the formation of tertiary structure of aptamer maybe will inhibit the further reaction between its adjacent free-coiled aptamer and adenosine. Thus, the nonspecific adsorption occurs after the mixing solution of Au NPs-aptamer conjugates with adenosine is added. Besides that, we also evaluate the selectivity of present SPR sensor that utilizes Au NPs-aptamer conjugates as a competitive reagent. Fig. 5 exhibits different SPR angle–time binding curves between ss-DNA immobilized on SPR gold film and Au NPs-aptamer conjugates after Au NPs-aptamer conjugates reacted with different analytes for 30 min. From Fig. 5, we can see the SPR binding curves of ss-DNA with Au NPs-aptamer conjugates after Au NPs-aptamer conjugates reacted with 1 mM cytidine, guanosine and uridine for 30 min slightly decrease. However, the SPR angle shift dramatically decreases after addition of 1 mM adenosine. From these results, we confirm that Au NPs-aptamer conjugates can not only specifically react with its target small molecule, but can also greatly enhance the sensitivity of SPR for detection of small molecule, which perfectly meet the requirements of an excellent competitive reagent.

4. Conclusion

In conclusion, we present an idea that using Au NPs-aptamer conjugates as a competitive reagent to substitute the application of antibody in SPR detection of small molecule based on ICIA. In order to evaluate the sensing ability of Au NPs-aptamer conjugates as a competitive reagent of ICIA in SPR sensor, we first combine the competition reaction between aptamer/its target small molecule and aptamer/its complementary ss-DNA to design a SPR sensor for detection of adenosine by ICIA. Our results confirm that Au NPs-aptamer conjugates are a powerful competitive reagent, which can not only greatly enhance the sensitivity of SPR for detecting adenosine based on ICIA, but also possess excellent specificity toward its target small molecules. More significantly, it can be used to develop different kinds of SPR sensor to detect other targets by changing the kind of aptamer in Au NPs-aptamer conjugates. Therefore, it is expected that the application of Au NPs-aptamer conjugates as a competitive reagent may offer a new direction in designing high performance SPR biosensors for sensitive and selective detection of small molecules by ICIA.

Acknowledgement

This work is supported by National Science Foundation (EEC-0823974).

References

[1] J. Homola, Chem. Rev. 108 (2008) 462.
[2] D.R. Shankaran, K.V.A. Gobi, N. Miura, Sens. Actuators B 121 (2007) 158.
[3] D.R. Shankaran, N. Miura, J. Phys. D: Appl. Phys. 40 (2007) 7187.
[4] D.R. Shankaran, K.V. Gobi, K. Matsumoto, T. Imato, K. Toko, N. Miura, Sens. Actuators B 100 (2004) 450.
[5] T. Masadome, Y. Yano, T. Imato, Anal. Lett. 41 (2008) 640.
[6] M. Tanaka, K. Sakamoto, H. Nakajima, N. Soh, K. Nakano, D.H. Chung, T. Imato, Bunseki Kagaku 5 (2007) 705.
[7] D.R. Shankaran, K.V. Gobi, T. Sakai, K. Matsumoto, K. Toko, N. Miura, Biosens. Bioelectron. 20 (2005) 1750.
[8] N.K. Navani, Y. Li, Curr. Opin. Chem. Biol. 10 (2006) 272.
[9] B. Shlyahovsky, D. Li, E. Katz, I. Willner, Biosens. Bioelectron. 22 (2007) 2570.
[10] D. Li, B. Shlyahovsky, J. Elbaz, I. Willner, J. Am. Chem. Soc. 129 (2007) 5804.
[11] M. Zayats, Y. Huang, R. Gill, C.A. Ma, I. Willner, J. Am. Chem. Soc. 128 (2006) 13666.
[12] C. Lin, E. Katilius, Y. Liu, J. Zhang, H. Yan, Angew. Chem. Int. Ed. 45 (2006) 5296.
[13] R. Nutiu, Y. Li, Methods 37 (2005) 16.
[14] R. Nutiu, J.M. Yu, Y. Li, ChemBioChem 5 (2004) 1139–1144.
[15] R. Nutiu, Y. Li, Chem.-Eur. J. 10 (2004) 1868.
[16] N. Rupcich, W. Chiuman, R. Nutiu, S. Mei, K.K. Flora, Y. Li, J.D. Brennan, J. Am. Chem. Soc. 128 (2006) 780.

[17] E.N. Brody, M.C. Willis, J.D. Smith, S. Jayasena, D. Zichi, L. Gold, Mol. Diagn. 4 (1999) 381.
[18] K. Feng, Y. Kang, J.J. Zhao, Y.L. Liu, J.H. Jiang, G.L. Shen, R.Q. Yu, Anal. Biochem. 378 (2008) 38.
[19] P.L. He, L. Shen, Y.H. Cao, D.F. Lia, Anal. Chem. 79 (2007) 8024.
[20] I. Willner, M. Zayats, Angew. Chem. Int. Ed. 46 (2007) 6408.
[21] O. Stoevesandt, M.J. Taussig, Proteomics 7 (2007) 2738.
[22] N.S. Que-Gewirth, B.A. Sullenger, Gene Ther. 14 (2007) 283.
[23] Y.C. Huang, B.X. Ge, D. Sen, H.Z. Yu, J. Am. Chem. Soc. 130 (2008) 8023.
[24] I. Willner, B. Shlyahovsky, M. Zayats, B. Willner, Chem. Soc. Rev. 37 (2008) 1153.
[25] L.A. Lyon, D.J. Pena, M.J. Natan, J. Phys. Chem. B 103 (1999) 5826.
[26] S. Link, M.A. El-Sayad, J. Phys. Chem. B 103 (1999) 4212.
[27] L. He, M.D. Musick, S.R. Nicewarner, F.G. Salinas, S.J. Benkovic, M.J. Natan, C.D. Keating, J. Am. Chem. Soc. 122 (2000) 9071.
[28] L.A. Lyon, M.D. Musick, M.J. Natan, Anal. Chem. 70 (1998) 5177.
[29] K. Tamada, F. Nakamura, M. Ito, X.H. Li, A. Baba, Plasmonics 2 (2007) 185.
[30] J. Zhao, X.L. Zhu, T. Li, G.X. Li, Analyst 133 (2008) 1242.
[31] J. Wang, W.Y. Meng, X.F. Zheng, S.L. Liu, G.X. Li, Biosens. Bioelectron. 24 (2009) 1598.
[32] M. Liss, B. Petersen, H. Wolf, E. Prohaska, Anal. Chem. 74 (2002) 4488.
[33] M. Hendrix, E.S. Priestley, G.F. Joyce, C.H. Wong, J. Am. Chem. Soc. 119 (1997) 3641.
[34] S.H.L. Verhelst, P.J.A. Michiels, G.A. van der Marel, C.A.A. van Boeckel, J.H. van Boom, ChemBioChem 5 (2004) 937.
[35] J.L. Wang, H.S. Zhou, Anal. Chem. 80 (2008) 7174.
[36] Y.L. Wang, H. Wei, B.L. Li, W. Ren, S.J. Guo, S.J. Dong, E.K. Wang, Chem. Commun. (2007) 5220.
[37] W.A. Zhao, W. Chiuman, J.C.F. Lam, et al., J. Am. Chem. Soc. 130 (2008) 3610.
[38] K. Taniwaki, A. Hyakutake, T. Aoki, M. Yoshikawa, M.D. Guiver, G.P. Robertson, Anal. Chim. Acta 489 (2003) 191.
[39] M. Yoshikawa, M.D. Guiver, G.P. Robertson, J. Mol. Struct. 739 (2005) 41.

Talanta 79 (2009) 62–67

Contents lists available at ScienceDirect

Talanta

journal homepage: www.elsevier.com/locate/talanta

Development of an enrofloxacin immunosensor based on label-free electrochemical impedance spectroscopy

Ching-Chou Wu [a,b,*], Chia-Hung Lin [a], Way-Shyan Wang [c]

[a] Department of Bio-industrial Mechatronics Engineering, National Chung Hsing University, No. 250, Kuo Kuang Road, Taichung 402, Taiwan
[b] Institute of Biomedical Engineering, National Chung Hsing University, No. 250, Kuo Kuang Road, Taichung 402, Taiwan
[c] Department of Veterinary Medicine, National Chung Hsing University, No. 250, Kuo Kuang Road, Taichung 402, Taiwan

ARTICLE INFO

Article history:
Received 30 December 2008
Received in revised form 26 February 2009
Accepted 3 March 2009
Available online 14 March 2009

Keywords:
Enrofloxacin
Electrochemical impedance spectroscopy
Label-free
Equivalent circuit
Immunosensor

ABSTRACT

Enrofloxacin is the most widespread antibiotic in the fluoroquinolone family. As such, the development of a rapid and sensitive method for the determination of trace amounts of enrofloxacin is an important issue in the health field. The interaction of the enrofloxacin antigen to a specific antibody (Ab) immobilized on an 11-mercapto-undecanoic acid-coated gold electrode was quantified by electrochemical impedance spectroscopy. Two equivalent circuits were separately used to interpret the obtained impedance spectra. These circuits included one resistor in series with one parallel circuit comprised of a resistor and a capacitor (1R//C), and one resistor in series with two parallel RC circuits (2R//C). The results indicate that the antigen-antibody reaction analyzed using the 1R//C circuit provided a more sensitive resistance increment against the enrofloxacin concentration than that of the 2R//C circuit. However, the 2R//C circuit provided a better fitting for impedance spectra, and therefore supplies more detailed results of the enrofloxacin-antibody interaction, causing the increase of electron transfer resistance selectively to the modified layer, and not the electrical double layer. The antibody-modified electrode allowed for analysis of the dynamic linear range of 1–1000 ng/ml enrofloxacin with a detection limit of 1 ng/ml. The reagentless and label-free impedimetric immunosensors provide a simple and sensitive detection method for the specific determination of enrofloxacin.

1. Introduction

A wide variety of antibiotics have been used to treat or prevent bacterial infection in food-producing animals. The use of antibiotics can effectively control the occurrence of disease and maintain the growth of animals. Enrofloxacin, a specific type of fluoroquinolone antibacterial, possesses a broad spectrum of activity against most Gram-negative pathogens, including *Pseudomonas aeruginosa* and *Enterobacteriaceae*, and some Gram-positive bacteria [1]. It is frequently used to treat urinary, pulmonary and digestive infections in veterinary medicine due to a long half-life and its wide distribution to different tissues [2–5]. According to a report of the World Health Organization (WHO) meeting in 1998, enrofloxacin was the most extensively approved antibiotic of the fluoroquinolones family for livestock, poultry, fish, or pet animals globally [6]. However, with increasing use of enrofloxacin, the sanitary issues, including drug residues in edible tissues of food-producing animals and the bacterial resistance being transferred from animals to human, have occurred significantly [7,8]. In order to protect consumers' health, the European Union has established maximum residue limit (MRL) for enrofloxacin, which is fixed at 100 μg/kg in several edible animal tissues [9]. Moreover, the USA Food and Drug Administration (FDA) withdrew the approval of enrofloxacin for poultry in 2005, because scientific data have indicated that the use of enrofloxacin causes the emergence of resistance in *Campylobacter*, that could result in the ineffective treatment of human diseases [10]. As such, the development of precise, specific, and sensitive methods for the detection of enrofloxacin in veterinary and medical fields has become an important issue.

Different detection strategies have been employed for the determination of enrofloxacin levels. These include adsorptive stripping voltammetry [11], spectrophotometry [12–14], capillary electrophoresis with diode-array detector [15–17] or mass spectrometry [18], high performance liquid chromatography (HPLC) using ultraviolet adsorption [19–21] or fluorescence detection [21–25], and enzyme-linked immunosorbent assay (ELISA) with UV–vis spectrometry [26–28] or fluorescence detection [29]. Among these, the lowest detection limit of enrofloxacin was 0.1 ng/ml, obtained with the ELISA method with fluorescence detection [29]. ELISA is a sensitive, fast, and specific method for the detection of enrofloxacin in the veterinary field by means of the interaction of an antigen and an antibody (Ab). However, in direct or

* Corresponding author. Tel.: +886 4 2285 1268; fax: +886 4 2287 9351.
E-mail address: ccwu@dragon.nchu.edu.tw (C.-C. Wu).

0039-9140/$ – see front matter © 2009 Elsevier B.V. All rights reserved.
doi:10.1016/j.talanta.2009.03.006

indirect competitive ELISA methods, experimental procedures such as the preparation of antigen- or antibody-enzyme conjugates and the reaction of enzymes with their specific substrates are complicated and time-consuming. A label-free impedimetry that allows for real-time detection and eliminates the labeling and catalyzing process of enzyme has been widely applied to the detection of specific antigen-antibody interaction [30–33]. The method works by using the simulation and fitting of equivalent circuit models for experimental impedance spectra. As such, the electrochemical properties of electrode-solution interface can be explained by using the circuit element [30–35]. Thavarungkul et al. obtained a detection limit of 3×10^{-15} M penicillin G in milk by calculating the changes in the imaginary part of impedance [32]. Ionescu et al. immobilized the monoclonal antibody of ciprofloxacin on the poly(pyrrole-NHS) membrane to obtain a detection limit of 10 pg/ml for ciprofloxacin by the analysis of two parallel RC equivalent circuits [33]. Additionally, Ding et al. adopted one parallel RC equivalent circuit to directly detect endotoxin by using polymyxin B-immobilized gold electrodes. As mentioned above, the label-free impedimetric immunosensor can provide a cost-effective, sensitive, and rapid detection based on the impedance analysis of antigen-antibody interaction.

To the best of our knowledge, relatively little research on the use of enrofloxacin immunosensors with label-free impedimetric detection has been reported. In the present work, we have covalently immobilized anti-enrofloxacin antibodies on a self-assembled monolayer (SAM)-coated gold electrode and used an electrochemical impedance system to directly quantify the response of the enrofloxacin-antibody interaction. Moreover, two types of equivalent circuits for fitting of the experimental impedance spectra were compared to detect the changes in resistive and capacitive parameters of equivalent circuit during the immunosensor development.

2. Materials and methods

2.1. Materials

Highly specific monoclonal anti-enrofloxacin antibodies (IgG1), initially reported by Wang et al. [28] and Watanabe et al. [29], were kindly provided by the Wang laboratory. Bovine serum albumin (BSA), 11-mercapto-undecanoic acid (MUA), 1-ethyl-3-(3-dimethylamino-propyl) carbodiimide HCl (EDC), *N*-hydroxysuccinimide (NHS), and 2-(N-morpholino) ethanesulfonic acid (MES) were purchased from Sigma. Enrofloxacin was obtained from Bayer. MUA solutions were prepared by dissolving in absolute ethanol. The supporting electrolyte was Dulbecco's phosphate buffered saline (PBS, pH 7.4) contained 8 g of NaCl, 0.2 g of KCl, 0.2 g of KH_2PO_4, and 1.15 g of Na_2HPO_4 per liter of H_2O. Fifteen millimolar MES solution (pH 5.0) was buffered with 1 M NaOH. All solutions were prepared with double distilled water purified through a Milli-Q system. All chemicals were of analytical grade and were used without further purification.

2.2. Modification processes of gold electrode

A 1.6-mm diameter gold electrode (Bioanalytical System Corp.) was manually polished with a 0.05 μm alumina slurry, and then ultrasonically cleaned in acetone and distilled water. Next, the electrode was electrochemically cleaned in 0.5 M H_2SO_4 using a cycling potential from 0 V to +1.5 V vs. a Ag/AgCl reference electrode with a scanning rate of 500 mV/s for 10 cycles. The electropolished electrode was dried and dropped with 20 μl 5 mM MUA at 37 °C for 20 min in an incubator of 15% relative humidity, and then the residual MUA molecules were ultrasonically removed in a 95% ethanolic solution. The MUA-modified electrode was soaked in 0.6 ml 15 mM MES (pH 5.0) containing 30 mM EDC and 2 mM NHS for 30 min to activate the COOH-terminated group of MUA. Next, 20 μl 0.2 mg/ml anti-enrofloxacin antibodies in PBS (pH 7.4) were placed on the activated MUA monolayer for 30 min, and then cleaned with distilled water. Finally, the electrode was reacted in 1% (w/v) BSA, which had been previously prepared in PBS for 30 min to prevent the electrode surface from the non-specific adsorption. The antibody-immobilized gold electrodes were rinsed with PBS (containing 0.05% Tween-20). The different concentrations of enrofloxacin, ranging from 1 μg/ml to 1 ng/ml, were prepared in PBS solution. After a 30 min incubation period with enrofloxacin antigen at room temperature, the experimental impedance spectra were measured.

2.3. Electrochemical measurements

All electrochemical experiments were performed with the IM-6 impedance analyzer (Zahner Electrik Corp.). Cyclic voltammetry (CV) and electrochemical impedance spectroscopy (EIS) were performed in a conventional three-electrode cell. An Ag/AgCl and a Pt wire were used as reference electrode and counter electrode, respectively. An equimolar $Fe(CN)_6^{3-/4-}$ mixture (2.5 mM) in a PBS solution (pH 7.4) was used to probe the electrochemical properties of modified electrodes. A cyclic voltammetric potential ranged from −0.1 V to +0.5 V at a scanning rate of 20 mV/s. Impedance measurements were carried out in the frequency range of 1 Hz to 100 kHz at a +0.21 V potential added with a 5 mV amplitude sine wave. The acquisition and analysis of impedance spectra, and the simulation of equivalent circuits were carried out with the IM-6/THALES software package.

3. Results and discussion

3.1. Electrochemical characteristics of modified electrodes

The changes in the electrochemical characteristics on the modified gold electrode were investigated by using CV and EIS. The $Fe(CN)_6^{3-/4-}$ redox couple was used as an electrochemical probe to detect the integrity of the immobilized layers after a variety of modifying steps [31,32,34,35]. Fig. 1 shows the cyclic voltammograms of the bare gold electrode followed by modification of MUA, immobilization of antibodies, and blocking of BSA for the

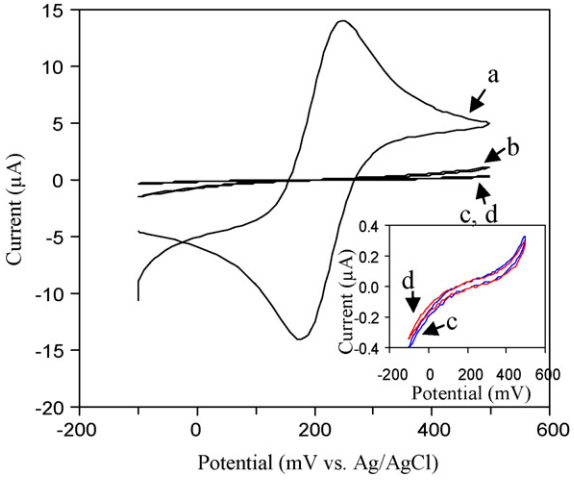

Fig. 1. Cyclic voltammograms recorded on bare gold electrodes (a), followed by MUA modification (b), antibody immobilization (c), and BSA blocking (d) in a 10 mM PBS solution containing 2.5 mM equimolar $Fe(CN)_6^{3-/4-}$ from −0.1 V to +0.5 V vs. Ag/AgCl with a scanning rate of 20 mV/s.

remaining adsorption-reactive sites. Some well-defined characteristic waves of $Fe(CN)_6^{3-/4-}$ are observed on the bare gold electrode. A peak-potential separation (ΔE_p) of 68 mV was measured and confirmed to be reversible. After modifying the MUA SAM on the gold electrode, the redox reaction of $Fe(CN)_6^{3-/4-}$ decreased due to the electrostatic repulsion of the negatively charged carboxyl group of the MUA (p*K*a value of 4.8) [36] and the hydrophobic effect of the long hydrocarbon chain of MUA. The results indicate that the direct drop-coating method of MUA for only 20 min can effectively insulate the bare gold surface, which is consistent with a previous study reported by Ding and co-workers [34]. Subsequently, the carboxyl groups of MUA were activated by EDC and NHS in MES solution (pH 5.0) to form stable aminoacyl esters, which can react with the amino groups of the antibody [37]. After coupling, the Faradaic current measured for the antibody-modified electrode became smaller than that for the MUA-modified electrode. Subsequently, the electrode provided a smaller redox current than that for the antibody-modified electrode, with the BSA blocking, as shown in the inset of Fig. 1. The decreasing current may result from increasing thickness and structural hindrance of the modified layer to the $Fe(CN)_6^{3-/4-}$ molecules. The behavior of the Faradaic current was further confirmed by EIS measurements.

3.2. Impedimetric measurement for modified electrodes

Electrochemical impedance spectroscopy is a sensitive method used to explore the interface properties between electrode and solution [30–35]. The electrochemical impedimetric properties of each modification step in the development of enrofloxacin immunosensors were examined in PBS (pH 7.4) solution containing 2.5 mM $Fe(CN)_6^{3-/4-}$. Fig. 2 shows the results of the impedimetric measurement of the gold electrodes with various modification processes. As previously established, impedance plots of the bare gold electrode, as depicted in curve (a) of Fig. 2, present a Faradaic system including a linear correlation of Z_{re} and Z_{im} at lower frequency, indicating a diffusion-controlled section corresponding to the Warburg impedance, and a semicircle region at higher frequency, indicating a kinetic part determined by the electron transfer resistance [30]. After modifying the gold electrode surface by MUA, the diffusion-controlled part in the impedance spectrum fully disappeared, and the diameter of semicircle obviously increased. Even at the frequency range of impedance measurement down to 0.1 Hz, the diffusion-controlled part was not observed. In order to minimize time consuming procedures, the following measurements were implemented from 1 Hz to 100 kHz. The disappearance of the diffusion-transport part and an increase of the electron transfer resistance are attributed to the effective insulation of MUA layer for $Fe(CN)_6^{3-/4-}$ mediator. The phenomenon also suggests that a non-Faradaic interface is present in the MUA-modified gold electrode. Followed by the procedures of antibody immobilization, BSA blocking, and incubation of 1–1000 ng/ml enrofloxacin, the diameter of semicircle on the impedance plots increased gradually. Compared with CV, EIS provided a more sensitive detection for different modifying processes. In order to completely realize the electrode-solution interface properties of the impedimetric immunosensors, two equivalent electrical circuits were designed for fitting the impedance spectra.

3.3. Equivalent circuits for EIS analysis

The Randles equivalent circuit is frequently used to elucidate the electrochemical properties of electrode-solution interfaces with the occurrence of Faradaic current and diffusion transport [30]. However, Warburg's impedance part was absent after the MUA modification of the gold electrode, as shown in curve (b–e) of Fig. 2. This indicates that there is no Faradaic current present and the Randles circuit does not suffice in explaining the following impedance experiments with the MUA layer. A non-Faradaic circuit consisting of one resistor (solution resistance (R_s)) in series with one parallel circuit comprised of a resistor (electron transfer resistance (R_{et})) and a capacitor (constant phase element (CPE)) [30,34,35] was designated as the 1R//C model, and is illustrated in Fig. 3(a). A CPE was used in place of a pure capacitor to explain the inhomogeneity on the electrode surface [34,35]. The impedance of CPE can be expressed by

$$Z_{CPE}(\omega) = Z_0(j\omega)^{-\alpha}$$

where Z_0 is a constant, j is the imaginary number, ω the angular frequency, and $0 < \alpha < 1$. When α is closer to 1, CPE becomes more capacitive.

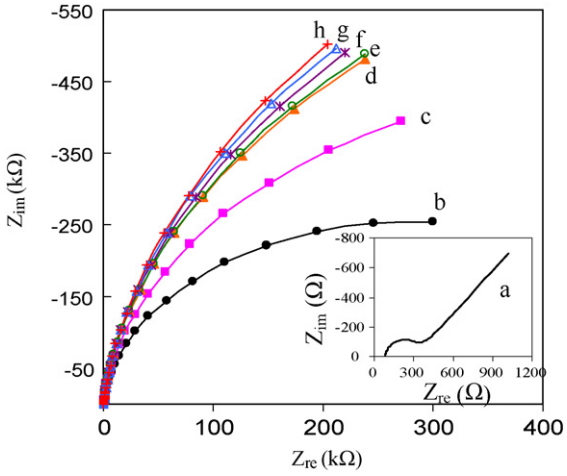

Fig. 2. Nyquist plot (Z_{im} vs. Z_{re}) of the bare gold electrode (a), following MUA modification (b), antibody immobilization (c), BSA blocking (d), 1 ng/ml enrofloxacin deposited onto the antibody/BSA–MUA film (EDAF) (e), 10 ng/ml EDAF (f), 100 ng/ml EDAF (g), and 1000 ng/ml EDAF (h) at a +0.21 V potential vs. Ag/AgCl and 5 mV ac signal in PBS (pH 7.4) containing 2.5 mM $Fe(CN)_6^{3-/4-}$.

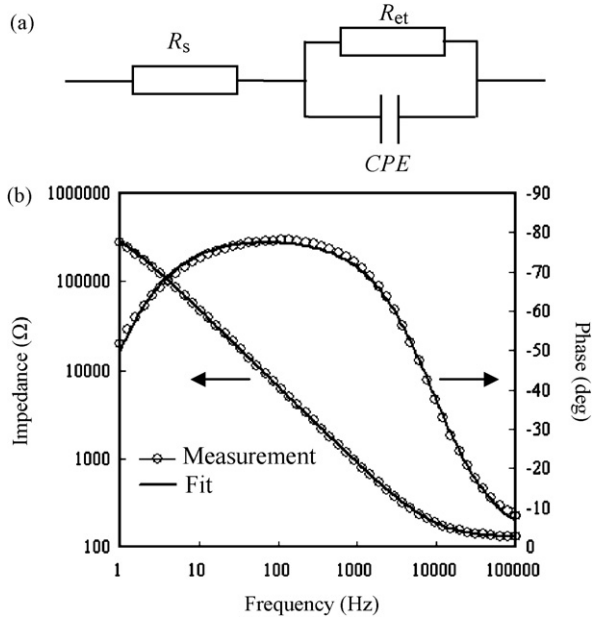

Fig. 3. 1R//C equivalent electrical circuit diagram (a) used to fit the impedance spectra (b) for the BSA-blocked gold electrode. R_s, solution resistance; R_{et}, electron transfer resistance; CPE, constant phase element. Circle lines and solid lines represent the experimental measurement and the computer fitting of impedance spectra, respectively.

Table 1
Values of the circuit elements fitted from the experimental spectra by the 1R//C model after Ab immobilization, BSA blocking, and incubation of 1 ng/ml enrofloxacin. The statistical values of the mean ± standard deviation were calculated in four repetitions.

	R_s (Ω)	R_{et} (kΩ)	CPE (nF)
Ab	87.8 ± 0.1	974.0 ± 5.8	183.0 ± 0.5
Ab/BSA	88.1 ± 0.0	1447.5 ± 2.9	180.8 ± 0.3
Enrofloxacin-Ab/BSA	87.6 ± 0.1	1476.0 ± 4.4	182.4 ± 0.4

Fig. 3(b) shows the impedance spectra for the BSA-blocked gold electrode obtained from computer fitting using the 1R//C circuit and the experimental measurement. In order to compare the 1R//C circuit-fitted curves with the experimental spectrum in detail, the fitting result only displayed a small deviation vs. the experimental data below 1 kHz, and was in good agreement with the experimental data above 1 kHz to 100 kHz. Table 1 shows the element values of the 1R//C circuit for the processes of antibody immobilization, BSA blocking, and immunoreaction of 1 ng/ml enrofloxacin. The values of mean error and maximum error for the fitting data simulated by the 1R//C circuit were 0.45% and 6.72%, respectively. The mean error value of 0.45% indicates a small difference between the experimental results and the simulated data. To compare the element values listed in Table 1, R_s values were kept nearly constant even with different biomolecule modifications on the gold electrode; R_s represents the solution resistance. In addition, we observed that the R_{et} value increases significantly while the CPE value did not vary with the different processes. The result suggests that the electron transfer to the electrode-solution interface is slowed primarily due to the spatial hindrance of the biomolecules. Consequently, the electron transfer resistance is a useful indicator of the quantify of immunoreaction of enrofloxacin onto antibody-modified gold electrodes.

In practice, the electron transfer resistance is the combination of modified layer resistance (R_m) and double layer resistance (R_{dl}) in series [34,35,38]. Similarly, the CPE element of the 1R//C circuit contains the contributions of both the modified layer capacitance (C_m) and the double layer capacitance of the modified layer-solution interface (C_{ms}) [34,35,38]. In Ding's [35] and Patolsky's studies [38], the CPE was treated as two capacitances, C_m and C_{ms}, in series with each other. Therefore, we tried to directly replace R_{et} by the series of R_m and R_{dl} and CPE by the series of C_m and C_{ms} in the 1R//C circuit model, respectively. Unfortunately, the 1R//C circuit substituted with R_m, R_{dl}, C_m, and C_{ms} appeared with a larger mean error, approximately 0.63%, and the values of R_m and R_{dl} averagely shared the value of R_{et}. Further, the fitting result did not reflect the corresponding electrochemical properties of modified layer.

We consulted Ionescu's study related to the circuit network for the antibody-immobilized electrode by using two parallel RC circuits instead of the parallel RC part of 1R//C circuit [33]. A diagram of the two parallel RC circuit, as shown in Fig. 4(a), is defined as the 2R//C circuit. Our 2R//C circuit differed distinctly from Ionescu's study [33] in terms of the definition and denomination of circuit elements. From our studies, the 2R//C circuit separately explains the electrical properties of the modified layer-solution interface and the modified layer. With respect to the circuit network arrangement, our 2R//C circuit is compatible with the practical electrical properties between solution and electrode, specifically the solution resistance (R_s), the R_{ms}, and the CPE_{ms} of the modified layer-solution interface and the R_m and the CPE_m of the modified layer. Fig. 4(b) shows the fitting curve obtained by using the 2R//C circuit vs. the experimental data for the BSA-blocked gold electrode. It is evident that the simulated data computed by the 2R//C circuit provided a better agreement with the experimental measurement in the overall spectra than that computed by the 1R//C circuit. Moreover, the mean error and maximum error of the fitting data simulated by the 2R//C circuit was 0.13% and 3.26%, respectively.

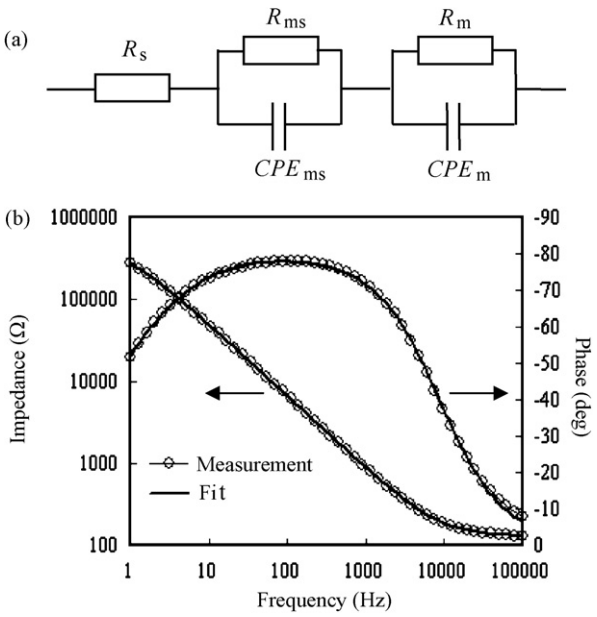

Fig. 4. 2R//C equivalent electrical circuit diagram (a) used to fit the impedance spectra (b) for the BSA-blocked gold electrode. R_s, solution resistance; R_{ms} and CPE_{ms}, resistance and CPE of membrane-solution interface, respectively; R_m and CPE_m, resistance and CPE of modified layer, respectively. Circle lines and solid lines represent the experimental measurement and the computer fitting of impedance spectra, respectively.

The smaller fitting error values suggest that the fitting of the 2R//C model is significantly more accurate than that of the 1R//C model for elucidating the electrical properties of the antibody/BSA-immobilized electrode.

Table 2 shows the element values of the 2R//C circuit for the processes of antibody immobilization, BSA blocking, and immunoreaction of 1 ng/ml enrofloxacin. The R_s values obtained from the 2R//C circuits were the same as the R_s of the 1R//C circuit. The results clearly demonstrate that the R_s element of the 2R//C circuit only represents the solution resistance and not the sum of the solution resistance and the modified layer resistance, as described in Ionescu's study [33]. In the comparison of capacitive elements, the value of CPE_{ms} was about five times larger than that of CPE_m, resulting from a smaller thickness and a larger permittivity of the electrical double layer relative to those of the antibody/BSA-modified layer. However, R_m was larger than R_{ms}. This is attributed to the denser structure of the modified layer toward hindering the electron transfer relative to that of the electrical double layer. Among the circuit elements of the 2R//C model, only the values of R_m increased with antibody and BSA immobilization. In contrast, the capacitive elements displayed only a weak change. Before and after BSA blocking, the R_m value increased significantly from 940.5 ± 6.8 kΩ to 1377.5 ± 3.5 kΩ with $p < 0.05$ (t-test analysis). This is attributed to the effective blocking of BSA toward the remaining adsorption-reactive sites on the electrode surface. Subsequently, with incubation of 1 ng/ml enrofloxacin, the R_m value increased to 1393.7 ± 2.1 kΩ. Therefore, R_m of the 2R//C circuit can be used to evaluate the enrofloxacin-antibody interaction on the immunosensor.

3.4. EIS for enrofloxacin detection

The antigen-antibody specific interaction can be quantified by using label-free impedimetric analysis [32,33,35]. The antibody-immobilized gold electrode was incubated with the enrofloxacin antigen at different concentrations ranging from 1 ng/ml to 1 μg/ml, for 30 min and then used in the impedance measurement. The cal-

Table 2
Values of the circuit elements fitted from the experimental spectra by the 2R//C model after Ab immobilization, BSA blocking and incubation of 1 ng/ml enrofloxacin. The statistical values of mean ± standard deviation were calculated in four repetitions.

	R_s (Ω)	R_{ms} (kΩ)	CPE_{ms} (nF)	R_m (kΩ)	CPE_m (nF)
Ab	87.6 ± 0.1	21.1 ± 0.2	1085.3 ± 2.5	940.5 ± 6.8	220.0 ± 0.6
Ab/BSA	87.3 ± 0.1	22.0 ± 0.3	1035.8 ± 1.3	1377.5 ± 3.5	218.4 ± 1.1
Enrofloxacin-Ab/BSA	86.8 ± 0.1	20.1 ± 0.4	1043.0 ± 1.0	1393.7 ± 2.1	220.7 ± 1.3

ibration curves corresponding to the differences in the R_{et} of the 1R//C circuit and the R_m and the R_{ms} of the 2R//C circuit as a function of the enrofloxacin concentration are shown in Fig. 5. Each experimental condition was assayed in quadruplicate. The change in the R_{et} value is calculated by the following equation:

$$\Delta R_{et} = R_{et,Enr\text{-}Ab/BSA} - R_{et,Ab/BSA}$$

where $R_{et,Enr\text{-}Ab/BSA}$ and $R_{et,Ab/BSA}$ are the values of the electron transfer resistance after and before enrofloxacin incubation onto the antibody-modified electrode, respectively. The values of ΔR_m and ΔR_{ms} are calculated using the same formula as above. The calibration curves indicated that the difference in ΔR_{et} and ΔR_m increased positively with the concentration of enrofloxacin, while the ΔR_{ms} was independent of enrofloxacin concentration. The results suggest that enrofloxacin-antibody binding does not change the electron transfer rate to the membrane-solution interface, but predominately hinders the electron transfer to the modified layer due to the geometric effect [33]. Furthermore, the high ionic strength of PBS used might make the change of electrical double layer insignificant. Therefore, the changes in ΔR_m present the interaction of the enrofloxacin and the immunosensor. Although the change in R_{ms} against the antigen concentration in the present study differs from the resistor (R_{FS}) of film-solution interface used in Ionescu's study [33], we propose that it results from different denominations of the same circuit elements. For example, no matter the denomination of the element used in our study of Ionescu's study [33], the resistive element of the rightmost R//C part of the 2R//C circuit, as shown in Fig. 4a, presented a positive correlation with the antigen concentration. Moreover, the resistive element of the middle R//C part of the 2R//C circuit was independent of the antigen concentration. After comparison with Ionescu's study [33], the element definition and physical explanation utilized in the study is more compatible for the actual electrode-solution interface.

To further clarify the linearity over the 1–1000 ng/ml concentration range, linear regression analysis of ΔR_{et} and ΔR_m against the enrofloxacin concentration had an equation of $\Delta R_{et} = 105.3 \log[\text{Enrofloxacin}] + 36.8$ with $R^2 = 0.9933$, and $\Delta R_m = 94.0 \log[\text{Enrofloxacin}] + 30.8$ with $R^2 = 0.9927$, respectively. The high correlation coefficient indicated a linear relationship between the values of ΔR_{et} and ΔR_m and the enrofloxacin concentration. Specifically, the sensitivity of the regressive line obtained from ΔR_{et} was larger than that from ΔR_m. This suggests that the use of the 1R//C circuit provides a larger resistive response corresponding to the same enrofloxacin concentration. The resistance increment of R_{et} and R_m after and before incubation with 1 ng/ml enrofloxacin was 28.5 kΩ and 16.2 kΩ (calculated from Tables 1 and 2), respectively. The accuracy of the R_{et} and the R_m (i.e. the standard deviation of repeated measurements) without enrofloxacin was 2.9 kΩ and 3.5 kΩ, respectively. Therefore, the limit of detection (LOD) obtained by both of the 1R//C model and the 2R//C model was at least 1 ng/ml, based on the IUPAC recommendation [39]. Although the LOD of the label-free impedimetric immunosensor is higher than that of the ELISA method [27–29], the detection range of the immunosensors contains the MRL of enrofloxacin recommended by European Union [9]. Moreover, the preparation procedure of the impedimetric immunosensor presents easier fabrication and less reagent requirement than that of ELISA.

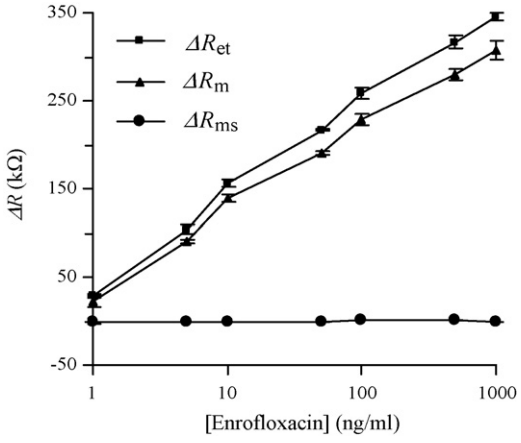

Fig. 5. Changes in the electron transfer resistance (R_{et}) of the 1R//C circuit and the modified layer resistance (R_m), as well as the membrane-solution interface resistance (R_{ms}) of the 2R//C circuit as a function of enrofloxacin concentration ranging from 1–1000 ng/ml.

3.5. Selectivity experiment

In order to investigate the selectivity of the label-free impedimetric immunosensor for the enrofloxacin detection, the effect of interfering compounds ciprofloxacin and norfloxacin on the immunosensor response was explored. These compounds of ciprofloxacin, norfloxacin and enrofloxacin belong to the second generation quinolone antibacterial. Therefore, ciprofloxacin and norfloxacin antibiotics have similar physical and chemical characteristics to enrofloxacin. The immunoreaction of ciprofloxacin and norfloxacin to the enrofloxacin immunosensor was implemented in PBS. The EIS results showed that no significant changes in the impedimetric responses of R_{et} element were observed for the ciprofloxacin and the norfloxacin antibiotics ranging from 1 ng/ml to 1000 ng/ml. Furthermore, enrofloxacin antibiotics were solubilized in a commercial porcine serum (Cat.26250084, Bibco, Invitrogen Corp.) to simulatedly estimate the sensor response of enrofloxacin in a real sample. The linear regression equation of ΔR_{et} ($\Delta R_{et} = R_{et,Enr\text{-}Ab/serum} - R_{et,Ab/serum}$) against enrofloxacin of the 1–1000 ng/ml concentration range was $\Delta R_{et} = 115.2 \log[\text{Enrofloxacin}] + 98.7$ with $R^2 = 0.9888$. The selectivity results proved the high specificity of the immunosensor and its potential to operate in real blood samples.

4. Conclusion

Anti-enrofloxacin antibodies are readily and rapidly immobilized on the surface of gold electrodes followed MUA modification and the EDC/NHS activation. The antigen-antibody affinity reaction can be quantified by the R_{et} element of the 1R//C circuit and the R_m element of the 2R//C circuit. Compared with the sensitivity of ΔR_m against the enrofloxacin concentration, analysis of ΔR_{et} provides a more sensitive response to the antigen-antibody interaction. How-

ever, the 2R//C circuit has a better fitting for the impedance spectra and provides more detailed results of the enrofloxacin-antibody interaction. This results in an increase in the electron transfer resistance to the modified layer, but not to the electrical double layer. The LOD of enrofloxacin is at least as low as 1 ng/ml on the antibody-immobilized electrode. Moreover, the linear detection range of the immunosensors covers the MRL of enrofloxacin set by the European Union. The reagentless and label-free impedimetric immunosensors can perform simple and sensitive detections to specifically measure the enrofloxacin concentration.

Acknowledgment

We gratefully acknowledge the partial support by the grants from the National Science Council (NSC96-2313-B-005-044-MY3), the Taichung Veterans General Hospital, and the National Chung Hsing University (TCVGH-NCHU 967609), and from the Ministry of Education, Taiwan, R.O.C. under the ATU plan.

References

[1] F.J. Angulo, K.R. Johnson, R.V. Tauxe, M.L. Cohen, Microb. Drug Resist. 6 (2000) 77.
[2] P.M. Vancutsem, J.G. Babish, W.S. Schwark, Cornell Vet. 80 (1990) 173.
[3] B. Martinsen, T.E. Horsberg, Antimicrob. Agents Chemother. 39 (1995) 1059.
[4] J.C. Yorke, P. Froc, J. Chromatogr. A 882 (2000) 63.
[5] J. Duan, Z. Yuan, J. Agric. Food Chem. 49 (2001) 1087.
[6] Use of quinolones in food animals and potential impact on human health, WHO/EMC/ZDI/98.10, 1998, pp. 9–10.
[7] W.H. Sheng, Y.C. Chen, J.T. Wang, S.C. Chang, K.T. Luh, W.C. Hsieh, Diagn. Microbiol. Infect. Dis. 43 (2002) 141.
[8] S. Pakpinyo, J. Sasipreeyajan, Vet. Microbiol. 128 (2007) 59.
[9] European commission Regulation 99/508/EEC, Off. J. European Commission L60, 9 March 1999, p. 305.
[10] Withdrawal of Approval of The New Animal Drug Application for Enrofloxacin in Poultry Docket No. 2000N-1571, Department of Health and Human Services, U.S. Food and Drug Administration, USA, 28 July 2005, p. 22.
[11] A. Navalón, R. Blanc, L. Reyes, N. Navas, J.L. Vílchez, Anal. Chim. Acta 454 (2002) 83.
[12] M. Lizondo, M. Pons, M. Gallardo, J. Estelrich, J. Pharm. Biomed. Anal. 15 (1997) 1845.
[13] S. Mostafa, M. El-Sadek, E.A. Alla, J. Pharm. Biomed. Anal. 27 (2002) 133.
[14] S. Mostafa, M. El-Sadek, E.A. Alla, J. Pharm. Biomed. Anal. 28 (2002) 173.
[15] D. Barrón, E. Jiménez-Lozano, J. Cano, J. Barbosa, J. Chromatogr. B 759 (2001) 73.
[16] M. Hernández, C. Aguilar, F. Borrull, M. Calull, J. Chromatogr. B 772 (2002) 163.
[17] H.-W. Sun, P. He, Y.-K. Lv, S.-X. Liang, J. Chromatogr. B 852 (2007) 145.
[18] F.J. Lara, A.M. García-Campaña, F. Alés-Barrero, J.M. Bosque-Sendra, L.E. García-Ayuso, Anal. Chem. 78 (2006) 7665.
[19] M.J. Souza, C.F. Bittencourt, L.M. Morsch, J. Pharm. Biomed. Anal. 28 (2002) 1195.
[20] E. Turiel, A. Martín-Esteban, J.L. Tadeo, Anal. Chim. Acta 562 (2006) 30.
[21] S.-W. Hung, C.-W. Shih, B.-R. Chen, C.-Y. Tu, Y.-F. Ling, L.-T. Tsou, S.-P. Ho, W.-S. Wang, J. Food Drug Anal. 15 (2007) 71.
[22] O.R. Idowu, J.O. Peggins, J. Pharm. Biomed. Anal. 35 (2004) 143.
[23] S. Zhao, H. Jiang, X. Li, T. Mi, C. Li, J. Shen, J. Agric. Food Chem. 55 (2007) 3829.
[24] E.A. Christodoulou, V.F. Samanidou, J. Sep. Sci. 30 (2007) 2421.
[25] S.J. Zhao, H.Y. Jiang, S.Y. Ding, X.L. Li, G.Q. Wang, C. Li, J.Z. Shen, Chromatographia 65 (2007) 539.
[26] Z. Wang, Y. Zhu, S. Ding, F. He, R.C. Beier, J. Li, H. Jiang, C. Feng, Y. Wan, S. Zhang, Z. Kai, X. Yang, J. Shen, Anal. Chem. 79 (2007) 4471.
[27] A.-C. Huet, C. Charlier, S.A. Tittlemiers, G. Singh, S. Benrejeb, P. Delahaut, J. Agric. Food Chem. 54 (2006) 2822.
[28] W.-S. Wang, C.-W. Shih, S.-W. Hung, Y.-F. Ling, C.-Y. Tu, B.-R. Chen, S.-P. Ho, Taiwan Vet. J. 32 (2006) 391.
[29] H. Watanabe, A. Satake, Y. Kido, A. Tsuji, Analyst 127 (2002) 98.
[30] J.S. Daniels, N. Pourmand, Electroanal 19 (2007) 1239.
[31] M. Wang, L. Wang, G. Wang, X. Ji, Y. Bai, T. Li, S. Gong, J. Li, Biosens. Bioelectron. 19 (2004) 575.
[32] P. Thavarungkul, S. Dawan, P. Kanatharana, P. Asawatreratanakul, Biosens. Bioelectron. 23 (2007) 688.
[33] R.E. Ionescu, N. Jaffrezic-Renault, L. Bouffier, C. Gondran, S. Cosnier, D.G. Pinacho, M. -Pilar Marco, F.J. Sánchez-Baeza, T. Healy, C. Martelet, Biosens. Bioelectron. 23 (2007) 549.
[34] S.-J. Ding, B.-W. Chang, C.-C. Wu, M.-F. Lai, H.-C. Chang, Anal. Chim. Acta 554 (2005) 43.
[35] S.-J. Ding, B.-W. Chang, C.-C. Wu, M.-F. Lai, H.-C. Chang, Electrochim. Acta 50 (2005) 3660.
[36] K. Sugihara, T. Teranishi, K. Shimazu, K. Uosaki, Electrochemistry 67 (1999) 1172.
[37] D. Sehgal, I.K. Vijay, Anal. Biochem. 218 (1994) 87.
[38] F. Patolsky, M. Zayats, E. Katz, I. Willner, Anal. Chem. 71 (1999) 3171.
[39] A.J. Cunningham, Introduction to Bioanalytical Sensors, John Wiley & Sons, Inc., New York, 1998, p. 40.

Talanta 79 (2009) 68–71

Contents lists available at ScienceDirect

Talanta

journal homepage: www.elsevier.com/locate/talanta

A simplified ion exchange bead-based KOH electrodialytic generator for capillary ion chromatography

Bingcheng Yang[a,*], Feifang Zhang[a], Xinmiao Liang[a,b,*]

[a] School of Pharmacy, East China University of Science and Technology, Shanghai 200237, China
[b] Dalian Institute of Chemical Physics, Chinese Academy of Sciences, Dalian 116023, China

ARTICLE INFO

Article history:
Received 22 January 2009
Received in revised form 26 February 2009
Accepted 3 March 2009
Available online 14 March 2009

Keywords:
Electrodialytic eluent generator
Capillary ion chromatography
Ion exchange bead

ABSTRACT

A simple potassium hydroxide electrodialytic generator (EDG) with singe membrane configuration is described. In this setup, one cation exchange resin (CER) bead is used to fabricate the EDG in place of the common membrane sheet. The device is implemented simply in a commercial stainless steel (SS) Tee which serves as both the EDG cartridge and the cathodic electrode. The present EDG has much lower internal volume (~0.16 (L), which is well suited with capillary ion chromatography system. The device has been tested up pressures to 3200 psi and could be directly deployed on the high-pressure side of the pump. The electrolysis gas can be effectively removed by a segment of PTFE tubing. In the tested range of 0–100 mM, the KOH concentration is generated linearly with the applied current being near-Faradaic efficiency. The device permits both isocratic and gradient operation with good reproducibility, as demonstrated by the analysis of anions.

1. Introduction

One of the developments achieved in recent years in the field of ion chromatography (IC) was the introduction of eluent electrodialytic generator (EDG) [1–5]. In IC, acids, bases (or salts of weak acids) are commonly used as chromatographic eluents. Until the advent of the EDG, eluent preparation was strictly manual. This is tedious, contamination-prone and subject to operator errors. Preparing hydroxide eluents commonly used for suppressed anion chromatography is especially problematic, as they are easily contaminated by atmospheric CO_2. An online EDG not only eliminates the above problems, it renders gradient elution a simple matter of current programming, the EDG, rather than mechanical blending of solutions. Over the past several years, EDG-equipped IC systems have gained much popularity.

Capillary ion chromatography (CIC) has aroused much interests in recent years due to some advantages over conventional counterparts [6], although CIC equipment or columns are not commercially available at the present time. The development of capillary ion exchange columns have been extensively investigated [7–10]. And little concern has been made for the EDG applied for CIC. Dasgupta and co-workers first introduced a micro-scale NaOH EDG for CIC and successfully demonstrated its benefits for the analysis of anions [5]. However, the use of membrane sheet in this design led to the limited ability of bearing backpressure (<800 psi). The similar micro-scale NaOH generators in post-suppressor applications was also used to provide improved quantitation and identification of anions of very weak acids in ion chromatography [11]. Liu et al. reported a miniaturized version of Dionex commercial EDG for CIC, in which membrane sheets are stacked together to withstand high-pressure [12]. Similar performance of this device with that of common counterpart was observed by the analysis of anions.

Recently we presented a novel KOH EDG for CIC, in which ion exchange resin beads were used to fabricate EDG in place of the common membrane sheet [13]. The dual ion exchanger configuration ensures the production of gas-free eluent, obviating the need of a gas removal device. The subsequent paper demonstrated the device could behave a multifunctional EDG by generation of diverse eluents such as $Na_2CO_3/NaHCO_3$, CH_3SO_3H, and KNO_3 [14]. However, three drawbacks of the design should be mentioned. First, limited choice of the available sources of anion beads with suitable size (e.g. 0.7–0.9 mm diameter) and suitable mechanical strength (crosslinking is recommended to be ≥8%). Second, a constant current source with wide range of operation voltage is suggested when higher constant current or higher flow rate is used. In the previous setup [13,14], the EDG was powered by a constant current source with output voltage range of 0–36 V. Due to higher electric resistance of the bead and limited voltage range, the current was always broken down when operation current was larger than ~300 μA. One way to this problem is use of higher concentration of feed solu-

* Corresponding author at: School of Pharmacy, East China University of Science and Technology, Shanghai 200237, China.
E-mail addresses: bcyang06@hotmail.com (B. Yang), liangxm@dicp.ac.cn (X. Liang).

0039-9140/$ – see front matter © 2009 Elsevier B.V. All rights reserved.
doi:10.1016/j.talanta.2009.03.004

tion, while it leads to higher consumption of feed solution. Third, the dual membrane configuration appeared to be complicated relative to the single membrane configure. To solve the drawbacks mentioned above, the previous design was simplified by using single membrane configuration, in which one cation exchange resin (CER) bead is used to fabricate EDG. There are many available commercial cation beads matching the requirements. By a constant current source with 0–36 V output voltage, the EDG can easily generate up to 100 mM KOH at 3 μL/min. The EDG is implemented simply in a commercial stainless steel (SS) Tee and its nominal internal volume is ~0.16 μL, which is well suited with CIC system. The electrolysis gas can be effectively removed by a segment of PTFE tubing.

2. Experimental

2.1. Chemicals

Analyte solutions were prepared in the form of either sodium or potassium salts. Typically, these were regent grade chemicals, used as received from the manufacturer. Ultra-pure water (Milli-Q, USA) was used throughout with a specific receptivity of about 18.2 MΩ cm.

2.2. Fabrication of EDG

The fabrication of the EDG was similar to that previously described [13]. Briefly, a commercial SS Tee (VICI Corp., Prod no., ZT1C) was used as the EDG housing. For a segments of PEEK tubing (0.020 in. i.d. × $^1/_{16}$ in. o.d.), a cavity (1 mm i.d. × 1 mm depth) was made at the terminal bore. CER beads (Rexyn 101 H^+-type for the cation exchange resin) were dried prior to use. One CER bead with the diameter of ~1.0 mm was placed in the drilled out cavity in the PEEK tubing and wetted with water whereupon it expanded and lodged tightly in the cavity. The bead-bearing PEEK tube were placed at the perpendicular arm and fixed in place with 10–32 nuts and ferrules, water inlet and eluent outlet tubes were then similarly connected, respectively at the other two arms. A platinum needle (0.25 mm i.d. × 0.45 mm o.d. × 1 in. long, Hamilton Co. Reno, NV) was put in all the way into the PEEK tubing, (almost) touching the bead. The Pt-needle functioned both as the electrode and the liquid inlet tube; the liquid outlet was provided by a 0.25 mm i.d. silica capillary. The nominal internal volume of the EDG, without considering the space that the protrusion of the spherical beads may consume, is ~0.16 μL. The schematic diagram was shown in Fig. 1.

The feed solution was pumped pneumatically by N_2 pressure sufficient to establish a flow of ~0.2 mL/min through each donor chamber. The feed solution could in principle be recycled but was presently allowed to go to waste.

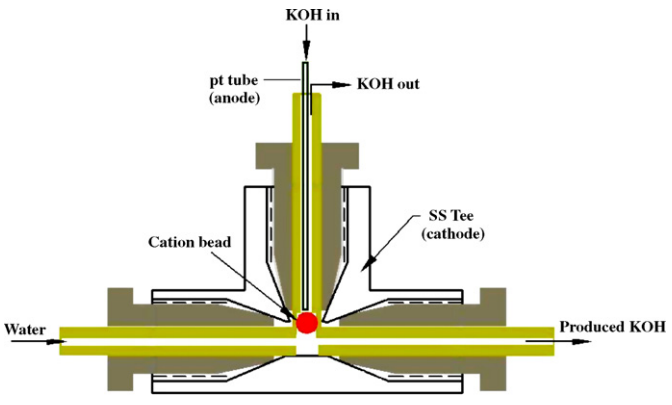

Fig. 1. Schematic diagram of bead-based EDG.

2.3. Chromatography system

The CIC system was similar to that previously described [13]. In brief, a Nano-HPLC pump (Micro-Tech Scientific Inc. S/N 011208-167, USA) was used for pumping pure water. An internal loop injector (200 nL) was used for sample injection (P/N CI4W.2, VICI, Houston, TX). The flow rate of 3 μL/min was used throughout unless otherwise stated. A laboratory-made anion exchange monolithic column (coated by AS18 latex, 0.25 mm i.d. × 250 mm long) was used to evaluate the performance of the EDG. The column was butt-jointed to a homemade Nafion fiber-based suppressor (80 μm i.d. × 200 mm o.d., 30 mm long) using 10 mM H_2SO_4 as the regenerant. A contactless capacitance detector (CCD) was used essentially as a conductance detector for analyte detection in a suppressed conductometric mode [15].

2.4. High-pressure conductivity cell calibration

At high electrolyte concentrations, the relationship between conductance and concentration is not linear. The concentration of the generated eluent was measured on line by conductivity measurement using a high-pressure conductivity cell (for details of construction process see ref. [5]). The high-pressure conductivity cell (cell constant measured to be 21.6 cm^{-1}) was calibrated with 1–100 mM KOH. The conductance G (in mS/cm) could be expressed as a quadratic function of the concentration C (mM KOH)

$$G\,(\mathrm{mS/cm}) = -0.000852C^2 + 0.2298C + 0.01785, \quad R = 0.9999 \quad (1)$$

with a multiple correlation coefficient of better than 0.9999. This equation was used to calculate the concentration of KOH generated.

3. Results and discussion

3.1. Pressure tolerance

Spherical ion-exchange resin beads can function well as balls in miniature "ball-on-seat" valves, thus making fabrication of high-pressure devices in a miniature format simple. As EDG is typically used in the chromatographic system, it is necessary to examine its ability to bear high backpressure. In our previous report [13,14], dual bead-based KOH EDG fabricated by one anion and cation bead were used to has been tested up pressure to about 2000 psi. As mentioned in the Section 1, anion bead is always the limiting factor of either available sources or mechanical strength. This means that anion bead always determines the possible maximal operation pressure. In addition, the cation bead used here (with the diameter of ~1 mm) has slightly bigger size than that of the anion bead used previously (with the diameter of 0.6–0.8 mm). It is known that the bigger bead always means higher mechanical strength. Thus the EDG fabricated here is in principle capable of bearing higher operation pressure. Based on the method described previously [13,14], we tested the pressure tolerance by connecting the EDG with a packed PEEK capillary column (0.15 mm i.d. × 1.6 mm o.d. × 16 cm long, Micro-Tech Scientific Inc., USA). The system backpressure varied linearly with the flow rate (R^2 = 0.9953) over a flow rate range of 0.3–1.8 μL/min reaching a pressure of 3260 psi at 1.8 μL/min, indicating good mechanic stability. Much higher flow rate was not explored due to the restriction of the pump used in the experiment. At the high flow rate end, the terminal exit flow was measured with and without the column (with and without backpressure) and found to be almost same. And we also measured any leakage of fluid through the capillaries in the electrode chambers over 30-min-long periods. There was no observable leakage.

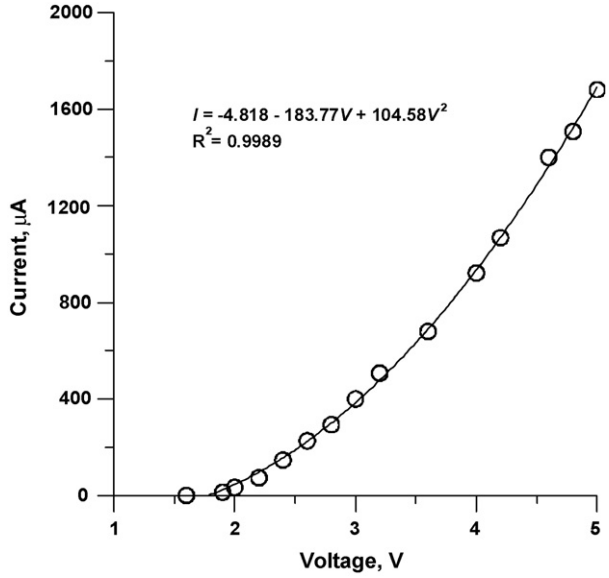

Fig. 2. Current–voltage curve of the EDG.

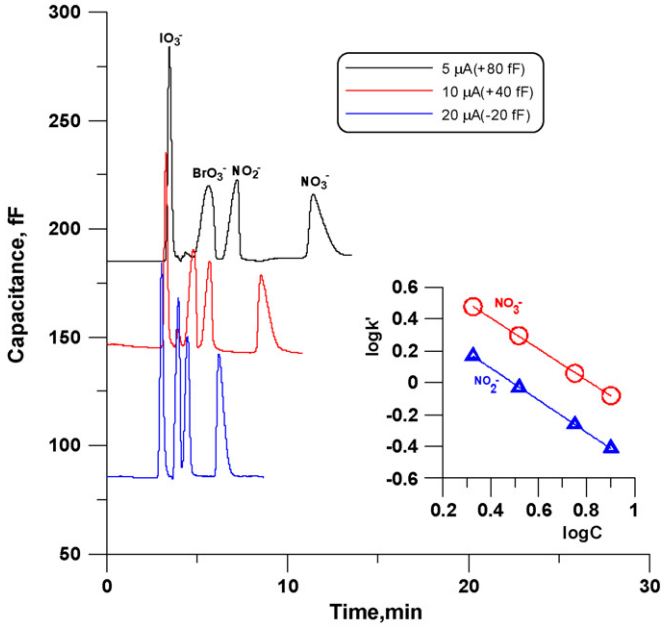

Fig. 3. Effect of applied current on the retention times of analytes. Conditions: flow rate, 3 μL/min; column, monolithic column (0.36 mm o.d. × 0.25 mm i.d. × 250 mm, ΔP = 560 psi) functionalized by Dionex AS18 latex particle; injection volume, 200 nL; 0.5 mM of each ion. Suppressed mode, fiber chemical suppressor with 10 mM H_2SO_4 regenerating solution; Detector, CCD. Plots of log k versus log[KOH] for nitrate and nitrite are shown in the inset.

3.2. Voltage–current behavior

The current–voltage relationship of the EDG was depicted in Fig. 2. In this experiment, 200 mM KOH feed solution flowed in the donor channel and water flowed in the eluent channel. The EDG was connected with a 150 Ω resistor in series. When a given voltage was applied to the system, the voltage drop across the resistor was monitored by a Multimeter and then the corresponding current could be calculated. I–V curve of the device achieved showed a quadratic function. The threshold voltage at which the electrodialytic reaction starts to work is about 1.8 V. Relative to the dual bead configuration, the present device shows lower electric resistance and then can easily be operated in the cases of higher KOH concentration generated is required.

3.3. EDG performance

Due to unperfect Donnan rejection, some undesired pentration (open circuit penetration, OCP) of feed electrolyte is unavoidable even when no current is applied [16]. Obvously, such a leakage is undesirable for good gradient chromatography; commonly an OCP value of <1 mM is desirable for practical gradient IC. For the EDG presented here, the OCP for 200 mM KOH feed soltuion was essentially zero and no change in background conductance was measurable. This resulted from the smaller surface area and significant thickness of cation bead, which was well suited with our previous characterization of dual bead-based EDG [13,14].

With 200 mM KOH as feed and a central channel flow rate of 3 μL/min, the generated KOH concentration C (up to 100 mM was generated) varied linearly with the applied current i (μA):

$$C(\text{mM}) = 0.202i + 1.926, \quad R^2 = 0.9996 \qquad (2)$$

The ideal Faradaic efficiency at this flow rate was 0.207 mM/μA. Small difference was within the combined accuracy of experimental measurement. In addition, good linear correlation between the applied current and the KOH concentration generated was also demonstrated by varying the applied current and plotting log k versus log[KOH] (*note*: (1) [KOH] was calculated by the calibration equation of the applied current and the concentration generated; (2) k denoting capacity factor). These plots were shown in inset in Fig. 3, and the slopes are −0.976 (R^2 = 0.9997) and −1.008 (R^2 = 0.9998) for NO_3^- and NO_2^- respectively, which are in well agreement with the theoretical slope of −1.0 for anion exchange elution of a singly charged anion with a singly charged eluent anion.

3.4. Chromatographic properties

The EDG presented here belongs to single membrane configuration, in which hydrogen gas is accompanied with the generated KOH eluent. Removal of the gas is necessary when the EDG is coupled with chromatography system. One method to remove the gas is the use of porous membrane tubing since pressurized gases can permeate through polymeric material. Sjögren et al. demonstrated

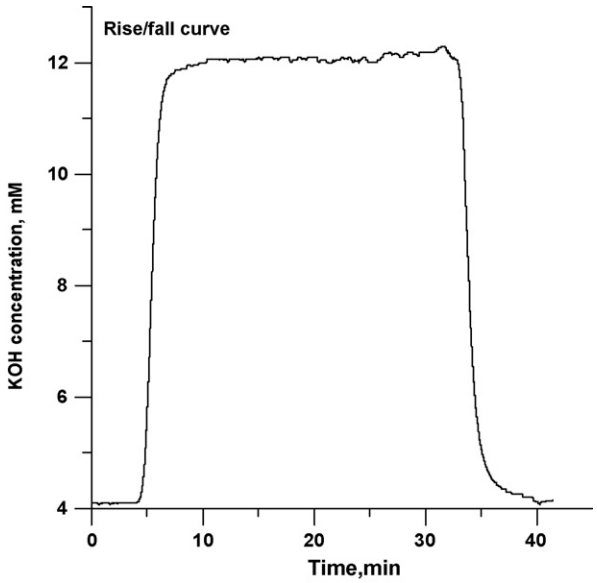

Fig. 4. Rise/fall curve of the EDG. Conditions: at t = 0 min, the current was increased from 10 μA to 50 μA, and at t = 30 min decreased from 50 μA to 10 μA.

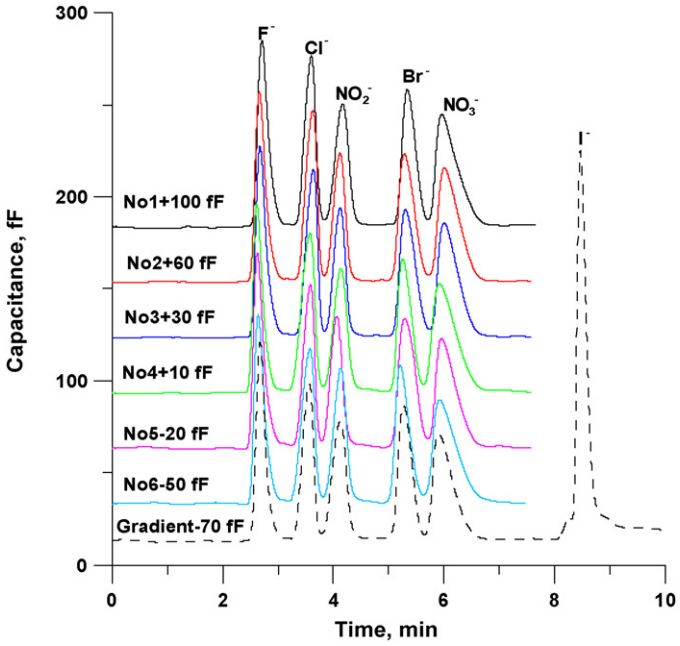

Fig. 5. Chromatogram achieved by KOH EDG. Conditions: isocratic mode, $I = 20\ \mu A$; gradient mode, temporal current programming, 20 μA for 0–4.8 min, with a step change to 90 μA thereafter; other conditions as in Fig. 3.

this by the use of small length of PTFE tube to remove the electrolysis hydrogen gases in their design of NaOH EDG [5]. In the present study, a segment of PTFE tube similar to that described by Sjögren et al. was placed between the outlet of generator cartridge and the inlet of the injector to remove electrolysis gases. We found it was sufficient to remove the electrolytically generated hydrogen, at least to an extent that no problems were encountered with bubble formation in the detectors.

A rise/fall test was performed to study the change in KOH concentration when the current is increased and decreased in abrupt steps. The results were shown in Fig. 4. The lag time, the time it takes for the solution to travel from the generator and reach the conductivity cell, is significant, ~5 min. However, thereafter the eluent concentration responds rapidly. The biggest contributor to the lag time and any dispersion in the gradient is the H_2 removal tube and the high-pressure conductivity cell. In practice, the first can be shortened. The second, the larger contributor, is really an optional item. As has previously been pointed out [1], as long as the EDG devices perform reproducibly, specifying generator current is sufficient; one need not know the precise eluent concentration.

Isocratic and gradient chromatograms obtained with the EDG were shown in Fig. 5. The latter based on temporal current programming, 20 μA for the first 4.8 min, with a step change to 90 μA thereafter. We measured retention reproducibility under isocratic conditions; this ranged in relative standard deviation from 0.6% for nitrate to 1.34% for fluoride ($n = 6$). It should be noted that, as the current programming started at 4.8 min and the delay time existed, the retention times of the first five peaks in the chromatogram achieved in gradient mode matched well with those of the peaks in the isocratic mode. Two repetitive gradient operation showed good repeatability and more explorations were not performed. Actually, the generated KOH concentration is highly related with the applied current, as demonstrated above, the operation repeatability can be guaranteed if the applied current is exact.

From Fig. 5, it can be seen that the peak height of iodide ion is much higher than that of the other ions. It probably resulted from the use of higher applied current (equivalent to higher KOH concentration), then leading to higher elution strength. This could also be confirmed by Fig. 3. The peak height of five anions increased with increasing applied current (from 5 μA to 20 μA).

In summary, a simple CER bead-based EDG is presented for CIC that is easy to be fabricated. The device can bear pressure up to ~3200 psi and could be directly deployed on the high-pressure side of the pump. Low nominal internal volume of the device will be beneficial to the chromatographic gradient operation. The KOH concentration is readily generated linearly with applied current with near-Faradaic efficiency, up to 100 mM. It is believed that the device can find the useful applications in CIC.

Acknowledgements

This research was supported by National Natural Science Foundation of China (no.20805047). It was partially supported by National Key Technology R&D Program in the 11th 5-year Plan of China (no. 20707026).

References

[1] D.L. Strong, P.K. Dasgupta, K. Friedman, J.R. Stillian, Anal. Chem. 63 (1991) 480.
[2] D.L. Strong, P.K. Dasgupta, J. Membr. Sci. 57 (1991) 321.
[3] D.L. Strong, C.U. Joung, P.K. Dasgupta, J. Chromatogr. 546 (1991) 159.
[4] Y. Liu, N. Avdalovic, C. Pohl, J. Madden, N. Shirakawa, Am. Lab. 30 (1998) 48C.
[5] A. Sjögren, C.B. Boring, P.K. Dasgupta, I.V.J.N. Alexander, Anal. Chem. 69 (1997) 1385.
[6] P. Kuban, P.K. Dasgupta, J. Sep. Sci. 27 (2004) 1441.
[7] Y. Ueki, T. Umemura, J.X. Li, T. Odake, K. Tsunoda, Anal. Chem. 76 (2004) 7007.
[8] E. Sugrue, P.N. Nesterenko, B. Paull, J. Chromatogr. A 1075 (2005) 167–175.
[9] P. Zakaria, J.P. Hutchinson, N. Avdalovic, Y. Liu, P.R. Haddad, Anal. Chem. 77 (2005) 417.
[10] P. Kuban, P. Pelcova, V. Kuban, L. Klakurkova, P.K. Dasgupta, J. Sep. Sci. 31 (2008) 2745.
[11] A. Sjögren, C.B. Boring, P.K. Dasgupta, Anal. Chim. Acta 384 (1999) 135.
[12] Y. Liu, V. Barreto, C. Pohl, 58th PittCon Presentation, Chicago, USA, 2007.
[13] B.C. Yang, M. Takeuchi, P.K. Dasgupta, Anal. Chem. 80 (2008) 40.
[14] B.C. Yang, F.F. Zhang, X.M. Liang, P.K. Dasgupta, J. Chromatogr. A 1216 (2009) 2412.
[15] M. Takeuchi, Q.Y. Li, B.C. Yang, P.K. Dasgupta, V.E. Wilde, Talanta 76 (2008) 617.
[16] P.K. Dasgupta, R.Q. Bligh, J. Lee, V. D'Agostino, Anal. Chem. 57 (1985) 253.

Talanta 79 (2009) 46–53

Contents lists available at ScienceDirect

Talanta

journal homepage: www.elsevier.com/locate/talanta

Pressurized liquid extraction versus other extraction techniques in micropreparative isolation of pharmacologically active isoflavones from *Trifolium* L. species

Grażyna Zgórka*

Department of Pharmacognosy with Medicinal Plant Unit, Medical University of Lublin, 1 Chodzki Street, 20-093 Lublin, Poland

ARTICLE INFO

Article history:
Received 6 October 2008
Received in revised form 23 February 2009
Accepted 3 March 2009
Available online 14 March 2009

Keywords:
Pressurized-liquid extraction
Ultrasound-assisted extraction
Trifolium L.
Isoflavones
Phytoestrogens

ABSTRACT

As a new sample preparation technique, pressurized liquid extraction (PLE), in combination with reversed-phase liquid chromatography (RP-LC) and photodiode-array (PDA) detection were used for the isolation and determination of phytoestrogenic isoflavones in hydrolyzed extracts obtained from aerial parts of five *Trifolium* L. (clover) species. To optimize the effectiveness of PLE procedure, variable extraction parameters: methanol and acetone (or their 75% aqueous solutions), as extraction solvents, temperatures (75, 100 and 125 °C) and the changeable number of static extraction cycles were tested. Additionally, two other micropreparative techniques: ultrasound-assisted extraction (UAE), and conventional solvent extraction (CSE), under optimized conditions, were also used and compared. Optimum extraction efficiency, expressed in the highest yield of biochanin A, formononetin, daidzein and genistein from plant material, with PLE, using methanol–water (75:25, v/v) as an extraction solvent, an oven temperature of 125 °C and three 5-min static extraction cycles, was obtained.

1. Introduction

Trifolium L. (clover) is an important genus of the Leguminosae (Fabaceae) family as containing some species rich in isoflavone constituents. This group of plant phenolics (flavonoids), therapeutically belonging to the class of phytoestrogens, had been the subject of considerable scientific research in recent years, especially in relation to soy isoflavones. Nowadays, besides the health benefits related to menopausal problems, there is an interest in the possible preventive role of these compounds as regards to breast and prostate cancer, osteoporosis, as well as cardiovascular disease, combined with atheromatosis [1–5]. For isoflavone glycosides and malonylglycosides are metabolized in mammalian and human small intestine, releasing pharmacologically active aglycones [6], effective extraction techniques, followed by appropriate hydrolytic procedures are needed to determine the real, total concentration of non-glycosidic isoflavone phytoestrogens in plant samples examined. Knowledge on verified, factual amounts of isoflavone aglycones is undoubtedly of special importance in the establishment of the proper dosage of clover extracts, while performing *in vivo* experiments or clinical studies, and for further accurate evaluation of pharmacological activity of these constituents.

Generally, to isolate isoflavone compounds from plant material, traditional solvent extraction (with or without stirring), using methanol, ethanol, acetonitrile or their aqueous mixtures [7–9], overnight maceration in a suitable solvent [10] or continuous extraction in a Soxhlet apparatus [11,12] have been reported.

In comparison with traditional extraction techniques, for a long time used in sample preparation, extraction enhanced by sonication (UAE) has been applied in increasing number of newer analytical studies (mainly concerning soy isoflavones). Rostagno and co-workers developed and optimized UAE for isolation of isoflavones from soybeans [13] and soy beverages blended with fruit juices [14]. Tian et al. [15] performed extraction of isoflavones from natural sources and nutritional supplements by sonicating raw materials in cold 80% aqueous methanol for 10 min. In last decade, three studies have been reported documenting the UAE use for extraction of isoflavones from *Trifolium pratense* L. (red clover) or dietary supplements, deriving from aforementioned species [16–18].

Another modern extraction technique – PLE (also known by its trade name: Accelerated Solvent Extraction – ASE), started to be utilized at the end of the twentieth century [19]. The application of elevated temperatures and pressures under an inert, nitrogen atmosphere devoid of light, guarantees safe, quick and very efficient extraction of sample constituents in this method, combined with low or minimal use of toxic solvents and reduced waste generation [20].

Recent analytical applications of PLE, focusing in extraction of other groups of isoflavonoids from plant material, were described

* Tel.: +48 817423713; fax: +48 817423809.
E-mail address: gzgorka@pharmacognosy.org.

0039-9140/$ – see front matter © 2009 Elsevier B.V. All rights reserved.
doi:10.1016/j.talanta.2009.03.011

only in two papers published in last decade. Rostagno and coworkers [21] isolated isoflavone derivatives from soybeans by means of PLE using 0.1 g freeze-dried sample of plant material (mixed with sand) and 70% ethanol as extracting solvent, subjected to three static PLE cycles at 100 °C. Klejdus et al. [22] elaborated two-step procedure, with hexane followed by 60% methanol with 0.3% formic acid as PLE solvents, used in two 5-min cycles, at 100 °C, for extraction of isoflavones from soybean food.

Till the present day, the application of PLE to isolation of isoflavones from any clover species has not been reported. In this study, taking into account advantages and disadvantages of UAE and CSE, PLE was selected as a primary extraction method and compared with the aforementioned techniques as regards to their effectiveness in the process of micropreparative isolation of isoflavone compounds. Based on quantitative results of earlier experiments done [23], aboveground parts of red clover and four other *Trifolium* species, rich in isoflavone compounds were chosen. Although the isoflavone profile of red clover (predominant amounts of formononetin and biochanin A) is known to vary from that observed in soybeans (main isoflavones: daidzein and genistein) their final metabolites, showing phytoestrogenic properties in humans are similar [24,25]. Hence, the results of the studies done may be the indication of new, alternative and valuable sources of isoflavone compounds useful for medicinal and dietary purposes.

2. Experimental

2.1. Reagents, solvents and materials

LC-grade solvents and reagents (acetonitrile, phosphoric acid) were purchased from J.T. Baker (Deventer, The Netherlands). Methanol (MeOH), acetone (MeCOMe), hydrochloric acid (HCl) and sodium hydroxide (NaOH), obtained from POCh (Gliwice, Poland), were of analytical grade. In all experiments deionized water (18.2 MΩ resistance), produced by a Simplicity™ (Millipore, Molsheim, France) purification system, was used. Isoflavone standards: daidzein (99% purity, determined by LC), genistein (99% purity, determined by LC), formononetin (95% purity, determined by LC) and biochanin A (99% purity, determined by LC) were purchased from ChromaDex (Santa Ana, CA, USA). The chemical structures of these compounds were shown in Fig. 1. Phenyl BakerBond cartridges (500 mg, 3 mL), used for SPE procedure, were supplied by J.T. Baker (Phillipsburg, NJ, USA). Minisart SRP 15 syringe filters, with pore size of 0.45 μm, were purchased from Sartorius (Goettingen, Germany).

2.2. Plant material

Aboveground, green parts of five *Trifolium* species: *T. arvense* L. (Tarv), *T. medium* L. (Tmed), *T. pannonicum* L. (Tpan), *T. pratense* L. (Tpra) and *T. rubens* L. (Trub) were obtained during their flowering period, either from clovers growing in natural habitat (near Lublin) or cultivated and collected in the Medicinal Plant Unit of the Department of Pharmacognosy (Medical University of Lublin, Poland). Voucher specimens of the particular species were identified taxonomically and deposited in the Department of Pharmacognosy (Medical University of Lublin). Clover samples were dried immediately just after collection in a drying oven at a temperature of 40 °C for 24 h, then ground, milled and finally sieved to obtain a particle size of 0.75 mm.

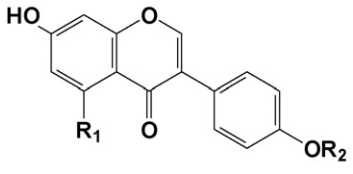

Isoflavones	R_1	R_2
daidzein	H	H
formononetin	H	CH_3
genistein	OH	H
biochanin A	OH	CH_3

Fig. 1. Chemical structures of isoflavone aglycones examined.

2.3. PLE procedure

A newly elaborated PLE procedure was performed using an ASE 100 Accelerated Solvent Extractor (Dionex Corporation, Sunnyvale, CA, USA). The bottom part of a 10-mL stainless-steel extraction cell was protected with a circular glass fiber filter, then each clover sample (0.5 g) was introduced and covered with a small plug of quartz wool. Finally, the cell was tightly closed and placed in the heating oven. Extractions ($n = 4$, per each clover sample) were carried out at an operating pressure of 10 MPa, using extraction solvents: MeOH, MeOH–water (75:25, v/v), MeCOMe and MeCOMe–water (75:25, v/v) at three temperature levels: 75, 100 and 125 °C. A 5-min static time, a 100-s purge time and a flush volume of 60% were programmed for each extraction cycle. In optimization of PLE process, one to four extraction cycles, for samples of *T. pratense* ($n = 6$) extracted with 75% MeOH at 75 °C, were examined. All PLE extracts were evaporated under vacuum to dryness and subjected to acidic hydrolysis.

2.4. UAE procedure

As the first reference method, UAE was performed using a Sonorex ultrasonic bath produced by Bandelin Electronic GmbH (Berlin, Germany). The apparatus generated ultrasounds with a stable frequency of 35 kHz.

Powdered herb samples (2 g) of five clover species were transferred into 250-mL round-bottom flasks, and poured with 75% or 100% (v/v) MeOH (50 mL). Each vessel was placed under reflux in an ultrasonic bath. Samples, immersed in solvent, were sonicated for 30 min at a controlled temperature of 75 °C. Then, after cooling, methanolic extracts were carefully decanted into collecting flasks and the whole extraction process was repeated twice (for 15 min) for the same sample to guarantee total removing of isoflavones from plant material. Combined extracts were evaporated till dryness under vacuum. Four simultaneous UAEs per one clover sample were done.

2.5. CSE procedure

As the second reference method, CSE was carried out for aerial parts of five *Trifolium* species, using four replicates for each sample. Pulverized clover herbs (2 g) were placed in 250-mL round-bottom flasks and treated with 75% or 100% (v/v) MeOH (50 mL). Samples, dipped in adequate solvent, were extracted under reflux, at a temperature of 75 °C in a heating extraction mantle with a programmed temperature controller (Multiserv, Lublin, Poland) for a period of 30 min. In the next step, cooled, methanolic extracts were carefully decanted into collecting flasks and, under the same conditions, the 15-min extraction was repeated twice for the plant residue. Combined extracts were evaporated till dryness in vacuo and submitted to hydrolytic procedure.

2.6. Acid hydrolysis and neutralization of hydrolyzed clover extracts

Each of dry residues, obtained by vacuum evaporation of PLE, UAE and CSE clover extracts, was dissolved in 75% MeOH (6 × 10 mL) and all liquid portions were transferred quantitatively to a 250-mL round-bottom flask. Afterwards, 5 mL of 36–38% HCl was added to the whole medium and finally the flask was placed in a heating

mantle under a reflux condensor. Sample hydrolysis has been performed from the beginning of liquid boiling for a period of 1 h. Then, hydrolyzed extracts were allowed to cool to room temperature and neutralized to pH ~ 2.5 by adding, drop by drop, 25 mL of 2 M NaOH aqueous solution, all the time stirring. Neutralized extracts were filtered through Filtrak paper and evaporated in vacuo to dryness. Dry residues were washed with 75% MeOH and filtered using Minisart SRP 15 syringe filters into 10-mL volumetric flasks and adjusted to nominal volume using the same solvent. Afterwards, hydrolyzed extracts were subjected to SPE procedure.

2.7. Sample clean-up using SPE

To remove other co-extractive, high molecular weight matrix components (e.g. chlorophyll) present in PLE, UAE and CSE clover extracts, quick and efficient SPE procedure was employed, based on earlier experiments done, giving very high recoveries (>96%) of all four isoflavones examined [23]. A 12-port vacuum manifold processor (system Baker SPE-12G) connected with a vacuum pump (AGA-Labor, Warsaw, Poland) was used for SPE. Two mL samples of clover extracts in 75% MeOH were transferred into phenyl J.T. Baker cartridges, activated previously with MeOH (10 mL), followed by equilibration with 75% (v/v) MeOH (10 mL). Extract samples were drawn through the solid phase under vacuum (−0.01 MPa). Using these conditions, analytes could directly flow through the sorbent beds, while the interfering substances (chlorophyll, waxes) were retained. Main eluate fractions were collected and the residual isoflavones, adsorbed on SPE columns, were washed with 3 mL of 75% MeOH into the same collection vials. All combined eluates were further filtered into 10-mL calibrated flasks using 0.45-μm Minisart SRP 15 filters (Sartorius, Goettingen, Germany) and finally (after diluting to 10 mL with 75% MeOH) analyzed by LC.

2.8. LC analysis and method validation

The chromatographic system consisted of an Agilent Technologies (Waldbronn, Germany) Model 1100 liquid chromatograph, equipped with a PDA detector, a Rheodyne 20-μL loop injector (10-μL samples were injected) and an on-line vacuum degasser. The separation of isoflavone compounds was performed on an ODS Hypersil column (250 mm × 4.6 mm I.D.; d_p = 5 μm) produced by ThermoHypersil (Runcorn, Cheshire, UK). A gradient mobile phase system, with acetonitrile (A) and 1 mM phosphoric acid (B) was used as followed: 0 min/25; 5 min/35; 15 min/45; 20 min/95 and 25 min/95% A in B. The flow rate was of 1.0 mL min^{-1}. The temperature of thermostatted column compartment was maintained at 20 °C during the whole separation process. Isoflavones were detected at 260 nm.

Quantitative analysis of isoflavones was performed based on an external standard method. The linearity of calibration curves, obtained for biochanin A, formononetin, daidzein and genistein, was assessed using regression coefficients (R^2) estimated for particular seven-point curves, constructed for increasing concentration levels of aforementioned reference compounds, prepared as solutions in 75% (v/v) MeOH. The repeatability of peak areas obtained for isoflavones was checked by RSD evaluation (not higher than 3%) obtained in intra- and inter-day (n = 3) assays. Additionally, LOD and LOQ values were determined for all four isoflavone aglycones examined.

The variability of the quantitative LC results for particular isoflavone aglycones was analyzed based on *T. pratense* extracts obtained by PLE under optimized extraction conditions (75% MeOH, t = 125 °C, 3 static extraction cycles). The inter-day precision was verified using three replicates a day of *T. pratense* sample, repeated for three consecutive days (n = 9) and determining the RSD values. The intra-day precision was assessed using six sample replicates per day, during different 3 days, with final RSD calculation.

The method accuracy was evaluated including only the results of recovery tests for PLE, UAE and CSE, as the recoveries for hydrolytic and SPE procedures have been earlier reported [23]. Stock methanolic solutions containing combined reference isoflavones: biochanin A, formononetin, daidzein and genistein have been prepared at three concentration levels (0.2, 0.4 and 0.6 mg mL^{-1}) and 0.2-mL volumes of particular aliquots (signed as fortification levels 1, 2 and 3, respectively) have been added to powdered samples of clover examined (n = 5, for each fortification level), placed previously in extraction vessels. Samples were left at room temperature for 10 min to enable MeOH evaporation. Afterwards, they were subjected to PLE, UAE or CSE, using in all techniques 75% (v/v) MeOH as an extraction solvent, at a temperature of 75 °C, followed by hydrolytic and SPE procedures described above. Isoflavone recoveries were obtained by calculating the percent ratio of determined amount to added amount together with RSD.

3. Results and discussion

3.1. Validation of LC method

To evaluate the effectiveness of PLE, UAE and CSE, quick and reliable LC procedure of isoflavone qualitation and quantitation have been developed and validated. Calibration curves for biochanin A, formononetin, daidzein and genistein showed very good linear regression (R^2 > 0.9995) and the linear ranges, estimated for all four standards examined, were from ~0.01 to ~0.4 mg mL^{-1}. The optimal gradient LC conditions, obtained on an ODS Hypersil column, enabled the quick separation of flavonoid compounds within 25 min. As baseline separation of isoflavone compounds was achieved and no interfering peaks were detected, therefore the selectivity of the elaborated procedure was also appropriate (Figs. 2 and 3). Low LOD and LOQ values indicate that instrument parameters (detector wavelength set at 260 nm and noise level) were in accordance with analytical rules (Table 1). The combination of PLE and LC methods provided good reproducibility with overall intra- and inter-day precision less than 5% and 6%, respectively (Table 2).

3.2. Optimization of PLE procedure

For obtaining the maximum efficiency of PLE technique some crucial parameters have been optimized, including extraction temperature, the composition of extraction solvent and number of extraction cycles.

3.2.1. Temperature as a factor affecting PLE efficiency

As it was documented during the first step of PLE optimization, at stable pressure of extraction process (10 MPa), the use of elevated temperatures (100 and 125 °C) significantly increased the kinetics of PLE process and the ability of extraction solvents to dissolve all four isoflavones, thanks to easier solvent penetration of plant matrix and higher rates of mass transport. This phenomenon was independent on the plant material, i.e. particular clover species examined. The highest extraction efficiency for daidzein, genistein, formononetin and biochanin A at 125 °C was reported (Fig. 4). Moreover, under higher temperature conditions tested, no thermal degradation of the analytes was observed.

3.2.2. PLE and the composition of extraction solvents

The selection of proper organic solvents or their mixtures with water in PLE was prerequisite to obtain high yields of isoflavones from plant material, however this problem had not been deeply

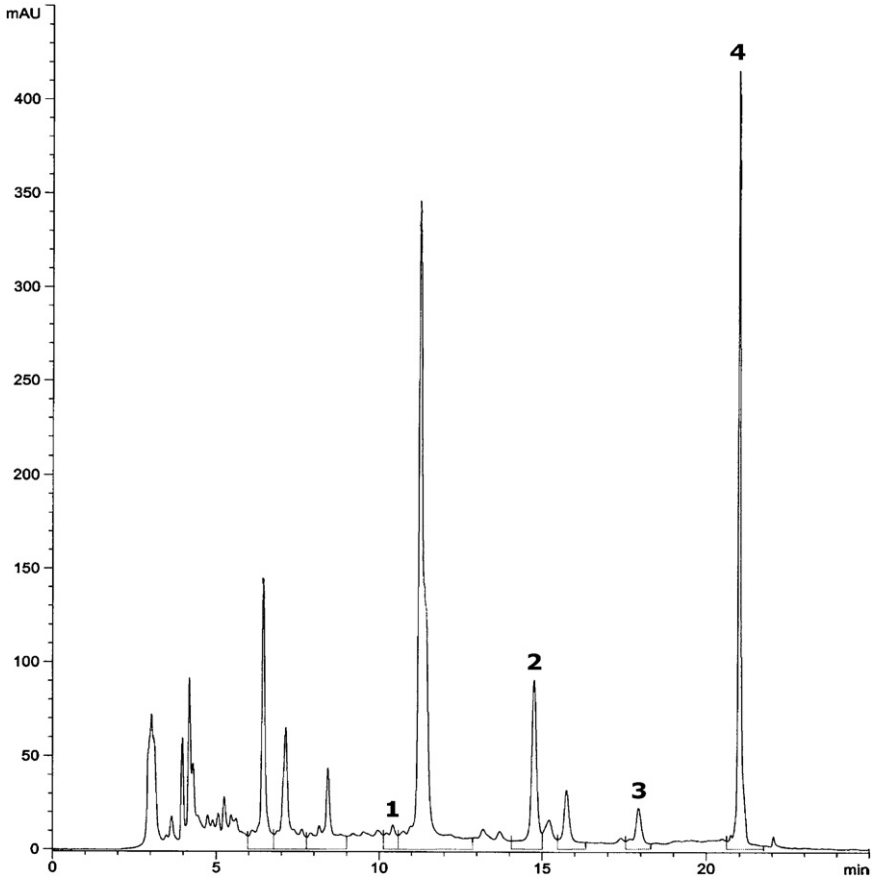

Fig. 2. LC chromatogram of flavonoid compounds isolated from the aerial parts of *T. medium* by means of PLE (75% MeOH as an extraction solvent; $t = 125\,^{\circ}C$). Isoflavones: **1** = daidzein; **2** = genistein, **3** = formononetin, **4** = biochanin A.

Table 1
Parameters of calibration curves ($y = ax + b$): slope (a), intercept (b), regression coefficient (R^2) together with LOD (S/N = 3) and LOQ (S/N = 10) values estimated for four isoflavone aglycones.

Isoflavone	a	b	R^2	LOD		LOQ	
				ng mL^{-1}	μg g^{-1}	ng mL^{-1}	μg g^{-1}
Biochanin A	86492.2	76.4	0.99994	24	1	81	3
Formononetin	65046.7	−19.7	0.99989	55	3	182	9
Daidzein	61349.2	−63.9	0.99989	25	1	83	3
Genistein	83688.7	105.3	0.99994	39	2	131	7

studied and documented in scientific literature as regards to this class of natural compounds. In this study, MeOH (from a group of simple alcohols) and MeCOMe (a representative of simple ketones), and their 75% (v/v) aqueous solutions, were chosen as solvents traditionally used for extraction of various plant polyphenolics. The results presented in Fig. 5, showing PLE efficiency at 100 °C, depending on the type of extraction liquids, were surprising in relation to low isoflavone yield using MeCOMe, because it is the basic organic solvent recommended by the 6th European Pharmacopea to be used in standard extraction procedure of flavonoids, later analyzed by spectrophotometric method. Slightly higher amounts of all four isoflavones were also isolated from clover herbs using MeCOMe–H_2O (75:25, v/v) as an extraction solvent. Notable changes were only reported when MeCOMe was replaced by MeOH. It lead to about two-fold higher PLE efficiency in relation to all analytes examined. In details, for more hydrophobic isoflavones: formononetin and biochanin A, maximum amounts extracted with MeOH were comparable with those obtained using 75% (v/v) MeOH, whereas for more polar compounds: daidzein and genistein, the latter solvent resulted in the highest PLE efficiency (Fig. 5).

Table 2
Results (μg g^{-1} dry wt) of intra- and inter-day precision tests for isoflavone compounds isolated from *T. pratense* herb using PLE and determined by RP-HPLC.

Isoflavone	Intra-day ($n = 6$)						Inter-day ($n = 9$)	
	1st day		2nd day		3rd day		Mean	RSD(%)
	Mean	RSD(%)	Mean	RSD(%)	Mean	RSD(%)		
Biochanin A	2430	3.4	2529	3.3	2495	3.4	2489	4.2
Formononetin	2417	4.1	2496	3.9	2434	4.0	2431	4.6
Genistein	339	4.6	371	4.5	358	4.8	363	5.1
Daidzein	55	4.8	60	4.7	57	4.9	58	5.8

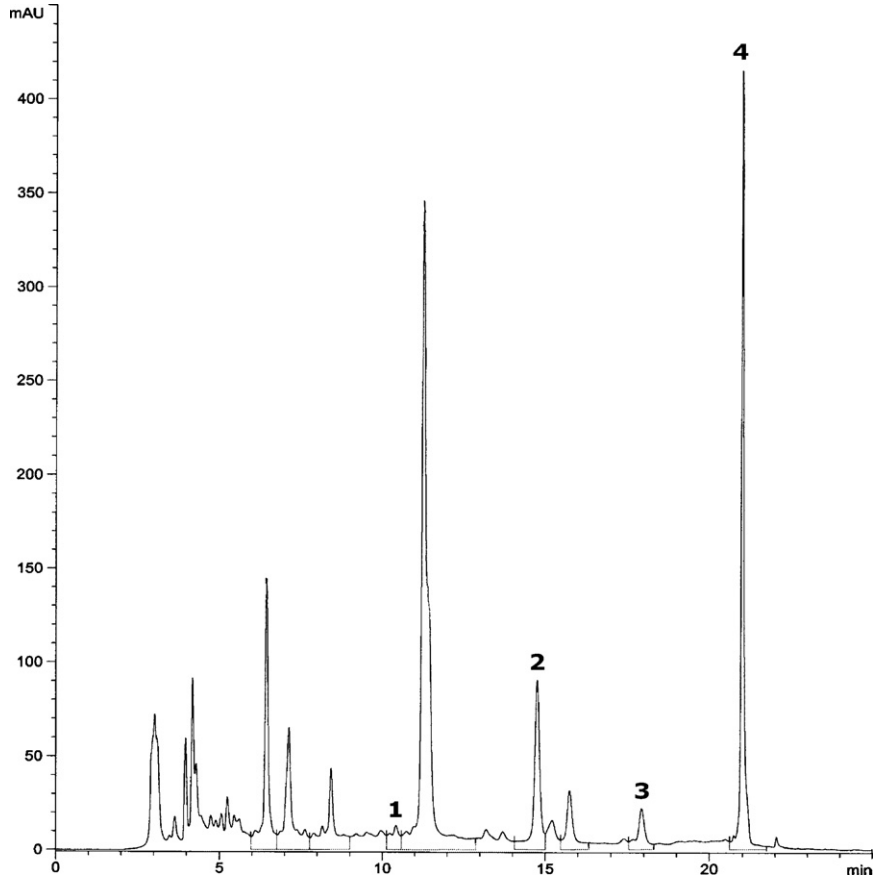

Fig. 3. LC chromatogram of flavonoid compounds isolated from the aerial parts of *T. arvense* by means of UAE (75% MeOH as an extraction solvent; $t = 75\,^{\circ}C$). Isoflavones: **1** = daidzein; **2** = genistein, **3** = formononetin, **4** = biochanin A.

3.2.3. Number of extraction cycles and PLE efficiency

Because of the low weight (0.5 g) of clover samples used, with a constant particle size of 0.75 mm, a 5-min extraction time for one cycle was established. In order to guarantee the exhausting extraction of plant material, the increasing number of extraction cycles (from 1 to 4) was tested. As it was presented in Table 3, the full extraction of all four isoflavones examined has been already completed after third cycle and the use of the fourth one turned out to be needles. Therefore, in all further experiments three 5-min static extraction cycles were used for optimum efficiency of PLE.

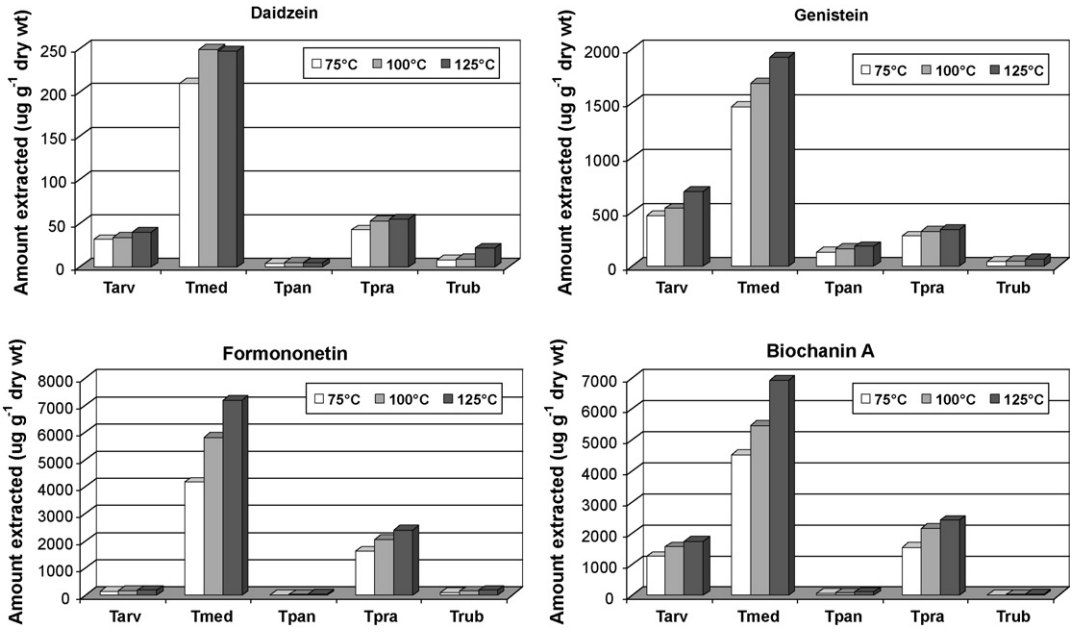

Fig. 4. Influence of extraction temperature on the effectiveness of PLE procedure (extraction solvent: 75% MeOH; 3 extraction cycles).

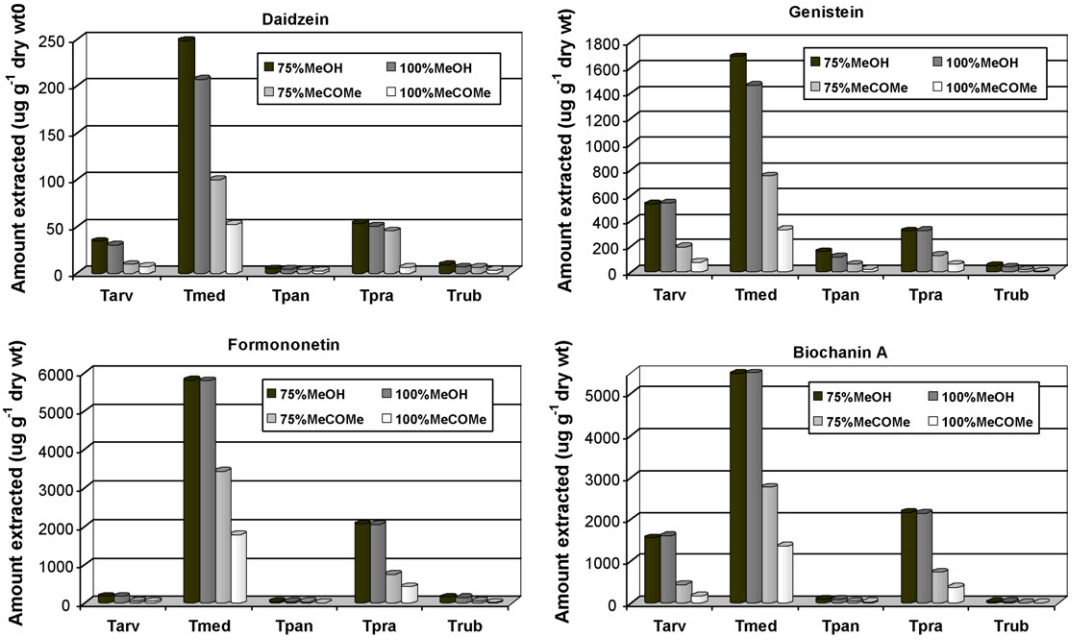

Fig. 5. Influence of various extraction solvents on the effectiveness of PLE procedure (extraction temperature: 100 °C; 3 extraction cycles).

3.3. Effectiveness of PLE technique in comparison with UAE and CSE

The advantages of PLE over UAE and CSE included less time required for preparing the extract, the ability of process automation and full temperature control. Besides, it was observed that PLE, using the same organic solvents as traditional techniques, used them much more efficiently. Hence, the reduction of solvent consumption by up to 90%, giving significant savings for each operation, has been documented for PLE.

With the aforementioned technique, the time required for exhausting extraction of isoflavones was shortened four-fold, i.e. from 1 h (reported for UAE and CSE) to 15 min.

The relative extraction efficiency, determined for PLE, UAE and CSE, indicated that PLE produced the highest yields of four isoflavones examined at the same extraction temperature of 75 °C (Fig. 6). Additionally, for all these techniques, the comparison of extraction solvents revealed the higher yield of more polar isoflavones: genistein and daidzein using 75% (v/v) MeOH, whereas for more hydrophobic: formononetin and biochanin A, 100% MeOH turned out to be the best extraction solvent. In general, for CSE, relative extraction efficiency did not exceeded 74%, while for UAE, it was comprised in the range from 66.3% to 94.4% (Fig. 6).

CSE lead to cleaner extracts than PLE and UAE, however the risk of obtaining greater amounts of co-extracted hydrophobic compounds was avoided by using the effective SPE clean-up procedure.

Table 3
Efficiency of PLE procedure, depending on the number of static extraction cycles, expressed as amount of extracted isoflavones (μg g^{-1} dry wt ± SD; $n = 6$); PLE conditions: 0.5 g sample of *T. pratense*, 75% (v/v) MeOH as extraction solvent, temperature of 75 °C.

Compound	Number of static extraction cycles			
	1	2	3	4
Daidzein	30 ± 2	37 ± 2	42 ± 2	42 ± 3
Genistein	196 ± 10	234 ± 12	278 ± 13	283 ± 13
Biochanin A	1307 ± 99	1495 ± 114	1627 ± 116	1600 ± 116
Formononetin	1229 ± 96	1411 ± 104	1541 ± 106	1539 ± 100

3.4. Isoflavone recoveries in PLE, UAE and CSE

The comparison of the mean recoveries of biochanin A, daidzein, formononetin and genistein (Table 4) showed similar and very good (close to 100%) accuracy in determination of four isoflavones using PLE, UAE and CSE in combination with RP-LC. As it was reported, the recoveries tested for the second and third fortification level were a little bit higher in relation to the first one. The lowest RSD values (in the range of 3.9–5.1%) for CSE were recorded.

3.5. Application of PLE and RP-LC to determination of isoflavones in clovers

Once PLE method had been developed and its advantages over UAE and CSE had been documented, it was used under optimum extraction conditions (comprising extraction temperature of 125 °C, 75% (v/v) MeOH as the extraction solvent and three 5-min static extraction cycles) to prepare aqueous-alcoholic isoflavone fractions from aerial parts of five clover species and to determine the qualitative and quantitative profile of these analytes by RP-LC. Graphical

Table 4
Mean recoveries (% ± RSD, %; $n = 5$) of four isoflavone aglycones determined for clover samples fortified at levels 1, 2 and 3 and subjected to PLE, UAE and CSE procedures.

Isoflavone	Mean recovery (%) ± RSD, (%); $n = 5$		
	PLE	UAE	CSE
Biochanin A	96.6 ± 4.9[1]	96.3 ± 5.1[1]	97.2 ± 4.7[1]
	101.3 ± 5.0[2]	102.3 ± 4.8[2]	99.3 ± 4.6[2]
	100.1 ± 4.9[3]	100.3 ± 4.6[3]	101.3 ± 4.0[3]
Daidzein	94.6 ± 6.0[1]	93.8 ± 5.4[1]	96.9 ± 4.8[1]
	97.3 ± 5.0[2]	98.2 ± 4.7[2]	99.0 ± 4.5[2]
	97.6 ± 5.2[3]	98.0 ± 4.9[3]	98.1 ± 4.0[3]
Formononetin	98.1 ± 3.8[1]	97.9 ± 4.2[1]	98.8 ± 3.9[1]
	99.7 ± 5.2[2]	100.2 ± 4.6[2]	99.6 ± 4.0[2]
	100.9 ± 4.9[3]	101.3 ± 4.8[3]	102.1 ± 4.5[3]
Genistein	93.8 ± 5.8[1]	96.9 ± 5.4[1]	97.1 ± 5.1[1]
	96.2 ± 6.1[2]	97.1 ± 5.0[2]	98.3 ± 4.9[2]
	97.1 ± 5.6[3]	97.9 ± 5.1[3]	98.2 ± 5.0[3]

1, 2, 3 Numbers of fortification levels.

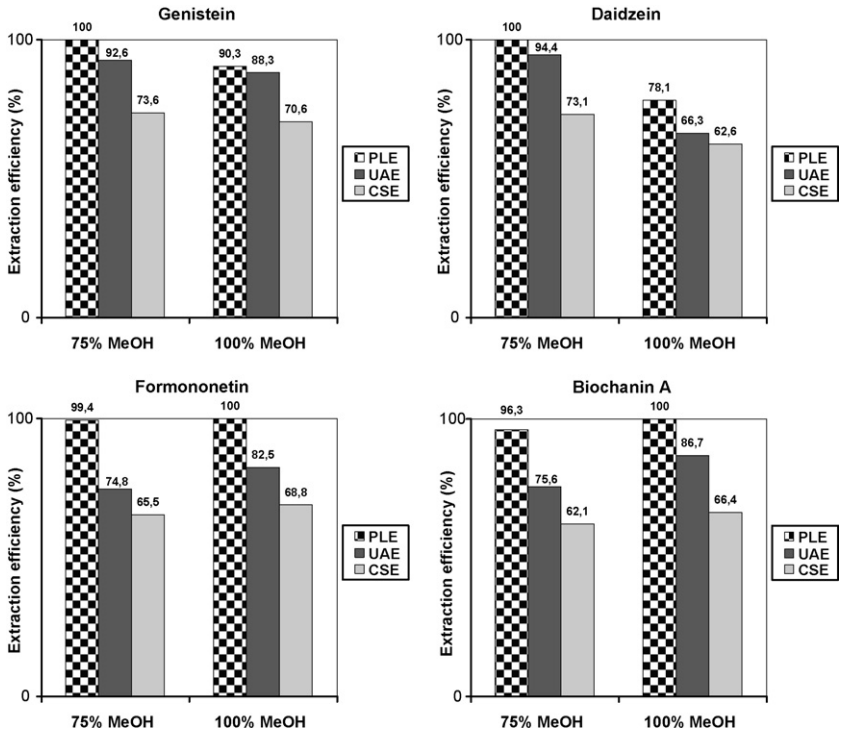

Fig. 6. Comparison of relative extraction efficiency determined for PLE, UAE and CSE techniques at extraction temperature of 75 °C.

presentation of the results obtained (Fig. 7) revealed a new clover species (Tmed), that, similarly to common red clover (Tpra), might be important from the medicinal point of view as containing very high amounts (above 1.6% dry wt) of total aglycone forms of pharmacologically active isoflavones. In all five clover species examined predominant amounts of hydrophobic isoflavones (formononetin and biochanin A) have been documented. This observation entitles for the statement, that quantitative profile of isoflavone aglycones in clovers is quite different from that in soya beans reported. In more general sense, the elaborated PLE technique, thanks to a very high efficiency of the extraction procedure, can be used for quick preparation of extracts from a great number of plant samples containing isoflavones and to establish the real amounts of these analytes by optimized RP-LC method.

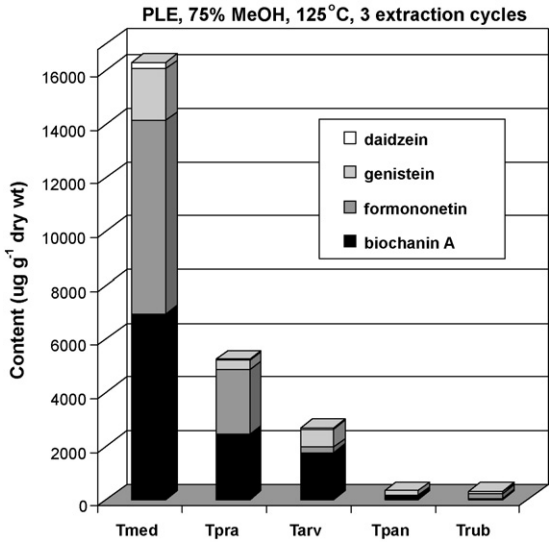

Fig. 7. Total and individual content of particular isoflavone aglycones in five clover species obtained under optimized PLE conditions.

4. Conclusions

In this work, the impact of variable extraction methodology on the recoveries of isoflavone compounds from five clover species was investigated and compared. The PLE proved to be a modern sample preparation technique, providing significant advantages such as optimum efficiency with lower costs of reagents and high yield of isoflavone aglycones with good precision and accuracy, in relation to other conventional extraction methods (CSE), also those assisted by ultrasonication (UAE).

This is the first report describing the use of PLE in micropreparative isolation of isoflavones from plants representing *Trifolium* L. genus. The quantitative results, obtained thanks to the employment of the aforementioned extraction method and its combination with RP-LC, revealed new and rich herbal sources of pharmacologically active isoflavones for medicinal purposes.

Acknowledgements

Special acknowledgements to the Polish Ministry of Science and Higher Education for the financial support of this research project (Grant No 2 P05F 006 29) and to Mr. Jaroslaw Cislo for his help in plant collection and technical assistance.

References

[1] V. Beck, U. Rohr, A. Jungbauer, J. Steroid Biochem. Mol. Biol. 94 (2005) 499.
[2] F. Occhiuto, R. De Pasquale, G. Guglielmo, D.R. Palumbo, G. Zangla, S. Samperi, A. Renzo, C. Circosta, Phytother. Res. 21 (2007) 130.
[3] M. Imhof, A. Gocan, F. Reithmayr, M. Lipovac, C. Schimitzek, P. Chedraui, J. Huber, Maturitas 55 (2006) 76.
[4] C. Atkinson, J.E. Compston, N.E. Day, M. Dowsett, S.A. Bingham, Am. J. Clin. Nutr. 79 (2004) 326.
[5] P.B. Clifton-Bligh, R.J. Baber, G.R. Fulcher, M.L. Nery, T. Moreton, Menopause 8 (2001) 259.
[6] K.D.R. Setchell, L. Zimmer-Nechemias, J. Cai, J.E. Heubi, Am. J. Clin. Nutr. 68 (1998) 1453S.
[7] P.A. Murphy, T.T. Song, G. Buseman, K. Barua, G.R. Beecher, D. Trainer, J. Holden, J. Agric. Food Chem. 45 (1997) 4635.
[8] P.A. Murphy, K. Barua, C.C. Hauck, J. Chromatogr. B 777 (2002) 129.

[9] S.H. Kim, W.S. Jung, J.K. Ahn, I.M. Chung, Eur. Food Res. Technol. 220 (2005) 207.
[10] L. Liggins, A. Mulligan, S. Runswick, S.A. Bingham, Eur. J. Clin. Nutr. 56 (2002) 961.
[11] T. Nguyenle, E. Wang, A.P. Cheung, J. Pharm. Biomed. Anal. 14 (1995) 221.
[12] L.S. Hutabarat, H. Greenfield, M. Mulholland, J. Chromatogr. A 886 (2000) 55.
[13] M.A. Rostagno, M. Palma, C.G. Barroso, Anal. Chim. Acta 597 (2007) 265.
[14] M.A. Rostagno, M. Palma, C.G. Barroso, J. Chromatogr. A 1012 (2003) 119.
[15] F.F. Tian, Y.X. Zhu, F.M. Xie, H. Long, C.T. Duda, E.M. Janle, P.T. Kissinger, J. Liq. Chromatogr. Rel. Technol. 25 (2002) 475.
[16] E. de Rijke, A. Zafra-Gómez, F. Ariese, U.A.Th. Brinkman, C. Gooijer, J. Chromatogr. A 932 (2001) 55.
[17] P. Delmonte, J. Perry, J.I. Rader, J. Chromatogr. A 1107 (2006) 59.
[18] N.M.M. Saviranta, M.J. Anttonen, A. von Wright, R.O. Karjalainen, J. Sci. Food Agric. 88 (2008) 125.
[19] B.E. Richter, B.A. Jones, J.L. Ezzell, N.L. Porter, Anal. Chem. 68 (1996) 1033.
[20] R. Carabias-Martínez, E. Rodríguez-Gonzalo, P. Revilla-Ruiz, J. Hernández-Méndez, J. Chromatogr. A 1089 (2005) 1.
[21] M.A. Rostagno, M. Palma, C.G. Barroso, Anal. Chim. Acta 522 (2004) 169.
[22] B. Klejdus, J. Vacek, V. Adam, J. Zehnalek, R. Kizek, L. Trnková, V. Kubáň, J. Chromatogr. B 806 (2004) 101.
[23] G. Zgórka, J. Sep. Sci. 32 (2009) 965.
[24] N.L. Booth, C.R. Overk, P. Yao, S. Totura, Y. Deng, A.S. Hedeyat, J.L. Bolton, G.F. Pauli, N.R. Farnsworth, J. Agric. Food Chem. 54 (2006) 1277.
[25] N. Tsunoda, S. Pomeroy, P. Nestel, J. Nutr. 132 (2002) 2199.

Talanta 79 (2009) 27–31

Contents lists available at ScienceDirect

Talanta

journal homepage: www.elsevier.com/locate/talanta

Label-free genotyping of single-nucleotide polymorphisms for DNA and RNA targets using a cationic polythiophene derivate

Yali Zhang[a,b], Zhengping Li[a,*], Yongqiang Cheng[a], Yucong Wang[a]

[a] Key Laboratory of Medicine Chemistry and Molecular Diagnosis, Ministry of Education; College of Chemistry and Environmental Science, Hebei University, No. 180, East Wusi Road, Baoding 071002, Hebei Province, PR China
[b] College of Sciences, Hebei University of Science and Technology, Shijiazhuang 050018, Hebei Province, PR China

ARTICLE INFO

Article history:
Received 31 October 2008
Received in revised form 25 February 2009
Accepted 28 February 2009
Available online 13 March 2009

Keywords:
Single-nucleotide polymorphisms
Cationic polythiophene
DNA
RNA

ABSTRACT

By using the specific primer extension reaction, a new assay for genotyping of single-nucleotide polymorphisms (SNPs) has been demonstrated. The assay relies on the conformational and colorimetric change of water-soluble polythiophene derivative, poly[3-(3′-*N*,*N*,*N*-triethylamino-1′-propyloxy)-4-methyl-2,5-thiophene hydrochloride] (PMNT), upon forming interpolyelectrolyte complex with extended double strand DNA and non-extended single strand DNA. All three kinds of SNP genotypes can be colorimetrically identified with one primer extension reaction in homogeneous solution. Moreover, combining with the specific digestion of RNA strands in the RNA/DNA hybrids, the proposed assay can also be applied to SNP genotyping for RNA templates. The SNP genotyping assay does not require chemical modification of oligonucleotide probes and nucleic acid targets and any separation step. It would be useful for routinely SNP detection in ordinary laboratories.

1. Introduction

Single-nucleotide polymorphisms (SNPs) are the most common type of human genetic variation. Due to their high-density and relatively even distribution, SNPs as high-resolution genetic marks have been used for candidate gene association studies and fine mapping disease loci [1]. SNP detection has become increasingly important to identify disease-causing genes and for early disease diagnosis. As more and more SNPs of known relevance for disease are being identified, such as the SNPs associated with the Alzheimer's disease [2] and the mutations in the p53 gene associated with a variety of human cancers [3], the disease-associated SNP detection is likely to be routinely applied to secure diagnoses of patients [4]. From point-of-care clinical diagnostic, a number of selected SNP markers in disease-related genes need to be routinely genotyped. To meet the demand, the simple, robust, and low-cost genotyping assays are desirable.

Up to date, a wide variety of techniques have been proposed for SNP detection [4–6]. However, most of the currently existing SNP genotyping assays need to label the oligonucleotide probes or dNTPs/ddNTPs to produce detectable signals. The widespreadly used labels include radioactive isotope [7], fluorescent dyes [8–10], electrochemical redox-labels [11], nanoparticles [12,13] and enzymes [14]. The label process generally limits the application of SNP detection to the routine diagnoses due to its sophisticated preparation, high cost and the low stability of labeled probes. As a way to circumvent the limitations, intense researches have recently been carried out worldwidly with the goal of developing efficient label-free methods for SNP detection, which include electrochemical [15–17], colorimetric [18], surface plasmon resonance [19,20] and capillary electrochromatography [21]. However, these label-free methods still need the complex protocol to immobilize the oligonucleotide probes on the surfaces of electrodes or nanomaterials, or long-time electrochromatographic process. Moreover, all these methods are based on the hybridization with allele-specific oligonucleotide (ASO) probes, which suffer the disadvantage of low specificity because the ASO methods identify SNPs only based on the differences in thermal stability between one-base mismatched and perfectly matched hybrids of the targets and ASO probes. In contrast, the primer extension methods are based on the high specificity of DNA polymerase to catalyze the DNA synthesis reaction. The 3′-terminal of a pair of allele-specific primers is designed to respectively match the nucleotide at the polymorphic site of wild and mutant targets. Under appropriate conditions, only the primer whose 3′-terminus perfectly matches the interrogated sequence can be extended catalyzed by the DNA polymerase. Generally, the primer extension methods offer 10 times

Abbreviations: SNPs, single-nucleotide polymorphisms; dNTPs, total of dATP, dTTP, dCTP and dGTP; RTase, reverse transcriptase; RNase H⁻, absence activity of ribonuclease H; RUs, repeat units; DEPC, diethypyrocarbonate; ssDNA, single strand DNA; dsDNA, double strands DNA; PMNT, poly[3-(3′-*N*,*N*,*N*-triethylamino-1′-propyloxy)-4-methyl-2,5-thiophene hydrochloride].

* Corresponding author. Fax: +86 312 5079403.
E-mail address: lzpbd@hbu.edu.cn (Z. Li).

0039-9140/$ – see front matter © 2009 Elsevier B.V. All rights reserved.
doi:10.1016/j.talanta.2009.02.056

higher genotype discrimination than the ASO methods [22]. Furthermore, the primer extension methods are robust, they only require two oligonucleotide probes and can be easily optimized [23]. The mini-pyrosequencing assays [24] and mass spectrometry-based detection [25] can combine the label-free detection with high specificity of primer extension reaction. However, the pyrosequencing assays need the sophisticated conversion reactions and expensive biochemical and bioluminescent reagents. Mass spectrometry instrument is too expensive to use in the routinely clinical laboratories.

Due to their optical signal amplification effect, cationic conjugated polymers (CCPs) have been widely used to fabricate biological sensors [26], and have been recently designed to genotype SNPs [27,28] with FRET detection. However these SNP assays also need fluorescently labeled dNTPs. Recently, Leclerc and coworkers [29,30] and Nilsson and Inganás [31] groups developed new water-soluble polythiophene derivatives, which can produce the conformational changes upon forming interpolyeletrolyte complex with DNA strands and can transduce the complex formation into optical (colorimetric or fluorometric) signal without any labeling of the DNA probe or the target. Therefore, the water-soluble polythiophene derivatives can offer a unique platform for label-free biological detections, such as DNA hybridization [29,31], human α-thrombin [30], S1 nuclease activity and DNA damage [32]. Taking the advantages of the label-free detection of polythiophene derivative and the high specificity and robustness of primer extension reaction, herein, we demonstrate a simple and reliable SNP genotyping assay for DNA targets in a homogeneous manner. Furthermore, combining with the specific digestion of RNase H, the proposed assay can also be applied to SNP detection of RNA targets.

2. Experimental

2.1. Apparatus and reagents

PAGE-purified DNA and RNA oligonucleotides, reverse transcriptase (RTase) M-MLV (RNase H^-) and dNTPs were purchased from TaKaRa Biotechnology Co. Ltd. (Dalian, China). The concentration of the oligonucleotides was determined by measuring the absorbance at 260 nm in a 100 μL quartz cuvette. A TU1901 UV–visible spectrophotometer (Purkinje General Instrument Co. Ltd., Beijing, China) was used to measure the absorption spectra. The primer extension reactions were carried out in 200 μL PCR microtubes and the reaction temperature was controlled by a T1 Thermal Cycler (Biometra, Germany). DEPC water and Millipore filtration system-purified (18.2 MΩ) and sterilized water were respectively used for SNP genotyping assays of RNA and DNA. Cationic water-soluble poly[3-(3′-*N*,*N*,*N*-triethylamino-1′-propyloxy)-4-methyl-2,5-thiophene hydrochloride] (PMNT) was prepared from an oxidative polymerization in chloroform with $FeCl_3$ as the oxidizing agent according to the procedure in the literatures [29,33].

2.2. Procedures

For the primer extension reaction with DNA targets as the template, 2.0 μL target DNA (1.0×10^{-4} M), 2.0 μL primer (1.0×10^{-4} M), and 100 μL Tris–HCl buffer (10 mM Tris–HCl, 50 mM KCl, 1.5 mM $MgCl_2$, pH 8.3) were mixed in a 200 μL PCR microtube. The solution was heated at 70 °C for 5 min and cooled at room temperature for 10 min. Afterward, 2.0 μL dNTPs (including 2.5×10^{-3} M of dATP, dCTP, dGTP and dTTP) and 100 Unit RTase M-MLV were added in the solution. The mixed solution was incubated at 42 °C for 30 min to perform the primer extension reaction. After naturedly cooling to room temperature, 5.0 μL 1.0×10^{-3} M (monomer repeat units (RUs)) PMNT was transferred in the reaction product. After mixing, the UV–vis absorption spectrum was measured in a 100 μL quartz cuvette with a TU 1901 spectrophotometer. The SNP genotypes experiment were the same as the above procedure, except for three kinds of SNP genotypes targets which were 2.0 μL target DNA T_1 (1.0×10^{-4} M), 1.0 μL target DNA T_1 (1.0×10^{-4} M) and 1.0 μL target DNA T_2 (1.0×10^{-4} M) and 2.0 μL target DNA T_2 (1.0×10^{-4} M) according to primer 1 and primer 2 respectively.

For the primer extension reaction with RNA targets as the templates, the mixture solution of 2.0 μL target RNA (1.0×10^{-4} M), 2.0 μL primer (1.0×10^{-4} M) and 100 μL buffer (50 mM Tris–HCl, 75 mM KCl, 3 mM $MgCl_2$, 10 mM DTT, pH 8.3) in a 200 μL PCR microtube was heated at 70 °C for 5 min, 50 °C for 1.5 h, and cooled at room temperature for 10 min. 2.0 μL dNTPs (2.5×10^{-3} M of each dNTP), 100 unit RTase M-MLV and 1.0 μL (40 units) Ribonuclease Inhibitor (TakaRa Biotechnology Co. Ltd. Dalian, China) were then transferred in solution and incubated at 42 °C for 1 h to perform the primer extension reaction. Afterward, 3 Unit RNase H was added in the solution and incubated at 30 °C for 10 min to specifically digest the RNA strands in the RNA/DNA hybrids. Finally, 3.0 μL PMNT (1.0×10^{-3} M in RUs) was mixed with the reaction product and the UV–vis absorption spectrum was measured.

3. Results and discussion

3.1. Principle of SNP detection

Our new SNP genotyping strategy is illustrated in Fig. 1a. Here four types of oligonucleotides are used: a primer 1 (P_1: 5′-gTC CTg ggA gAg ACC-3′), a wild DNA target (T_1: 5′-Cgg AgA TTC TCT TCC TCT gTg CgC Cgg TCT CTC CCA ggAC-3′); a primer 2 (P_2: 5′-gTC CTg ggA gAg ACT-3′), and a mutant DNA target (T_2: 5′-Cgg AgA TTC TCT TCC TCT gTg CgC CAg TCT CTC CCA ggAC-3′). The oligonucleotides T_1 and T_2 are the fragments of p53 exon 8 containing a polymorphic site (Arg282Trp), where the nucleotide G (underlined in T_1) in a wild-type target is replaced by A (underlined in T_2) in a mutant. The 3′-terminal nucleotides of P_1 and P_2 are designed to be complementary to the T_1 and T_2 respectively at the polymorphic site. When P_2 is mixed and hybridized with the DNA targets (including T_1 and T_2), the primer extension reaction will be taken place along T_2 template (situation A of Fig. 1a) in the presence of reverse transcriptase (RTase) and dNTPs to produce double-stranded DNA (dsDNA). In situation B, the 3′-terminal nucleotide of P_2 is not complementary to the wild DNA target T_1, thus the primer extension reaction cannot take place and T_1 remains single stranded DNA (ssDNA) conformation. Certainly, if P_1 is used for the primer extension reaction, T_2 will remain ssDNA and T_1 will produce dsDNA.

A water-soluble poly[3-(3′-*N*,*N*,*N*-triethylamino-1′-propyloxy)-4-methyl-2,5-thiophene hydrochloride] (PMNT, Fig. 1b) is employed to transduce the primer extension event into colorimetric signal. The absorption spectra of PMNT itself and the mixture of PMNT, RTase M-MLV and dNTPs were respectively measured in the same experimental conditions. As shown in Fig. 2, the absorption spectrum of PMNT is almost the same as that of the mixture, indicating that the RTase M-MLV and dNTPs do not affect the colorimetric properties of PMNT. Therefore, the colorimetric effects (i.e., color changes) described in this paper should be originated from the interaction between PMNT and nucleic acid molecules.

The PMNT itself takes a random-coil conformation in an aqueous solution. As shown in Fig. 3a, the PMNT solution exhibits maximum absorption at a short wavelength (λ_{max} = 379 nm, yellow color) as any twisting of the conjugated backbone leads to a decrease in the effective conjugation length [29,32]. The PMNT can form an interpolyelectrolyte complex (triplex) with dsDNA produced from the primer extension reaction of P_2/T_2 through strongly electrostatic

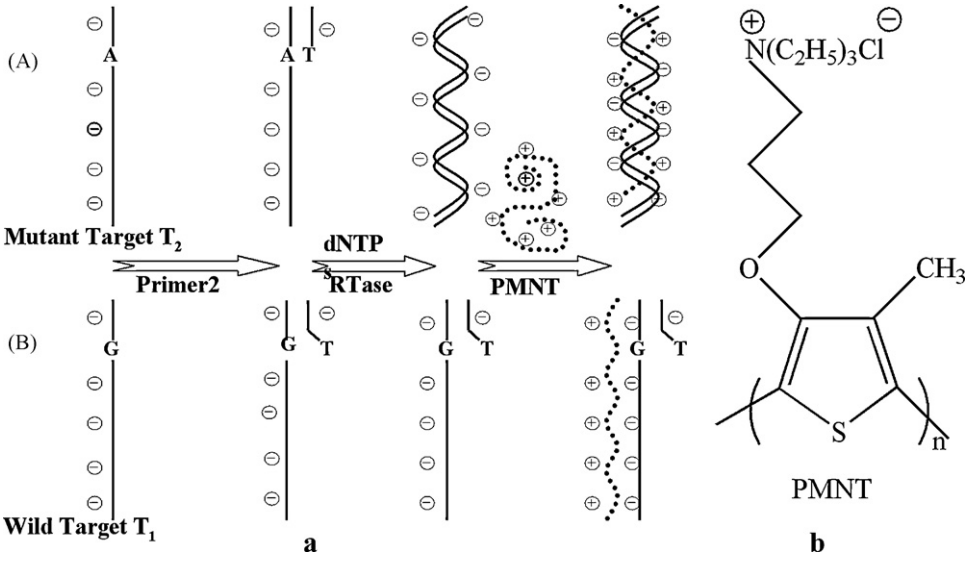

Fig. 1. (a) Schematic representation of the SNP genotyping assay for DNA target; (b) chemical structure of PMNT.

interaction, in which the PMNT takes a right-handed helical orientation due to the binding of the polymer to the negatively charged phosphate backbone of dsDNA [29]. Thus, the maximum absorption of the triplex is red-shifted to 412 nm (Fig. 3b) and the solution is orange. When the PMNT electrostatically combines with the ssDNA in the non-extended P_2/T_1, it takes planar conformation and the polythiophene backbone is highly conjugated. As a result, the much red-shift (λ_{max} = 472 nm, Fig. 3c) and clear color change (from yellow to pink–red) can be observed. Thus the colorimetric effects of PMNT can be used to probe the primer extension reaction and should be conveniently applied to SNP genotyping.

3.2. SNP genotyping of DNA target

For the DNA targets used in the studies, three kinds of SNP genotypes are generally possible: homozygous G (only wild DNA T_1), heterozygous G/A (wild DNA T_1 and mutant DNA T_2), and homozygous A (only mutant DNA T_2). When the P_2 is used as the primer to perform the extension reaction in the presence of RTase and dNTPs, the DNA target in homozygous G type will remain ssDNA conformation, half of the DNA target in heterozygous G/A type can form dsDNA, and all of the DNA target for homozygous A type will form dsDNA. Fig. 4 compares the colorimetric effects of the three SNP types upon addition of PMNT after the primer extension reaction with P_2, where the absorbance ratio of 412 nm to 472 nm ($A_{412\,nm}/A_{472\,nm}$) is used to represent the absorbance changes. As shown in Fig. 4 that three kinds of genotypes could be clearly distinguished by measurement of $A_{412\,nm}/A_{472\,nm}$. Moreover, the SNP genotyping could also be well accomplished with P_1 extension reaction in the same experimental conditions (Fig. 4). These results give evidence that the proposed method is accurate and versatile to identify SNP genotypes. More importantly, with the proposed method, all three kinds of SNP genotypes can be identified in one primer extension reaction by measuring the absorbance of $A_{412\,nm}/A_{472\,nm}$.

3.3. SNP genotyping of RNA target

To investigate SNP genotyping assay for RNA, the wild RNA target (T_1': 5′-Cgg AgA UUC UCU UCC UCU gUg CgC Cgg UCU CUC CCA ggAC-3′) and mutant RNA target (T_2': 5′-Cgg AgA UUC UCU UCC

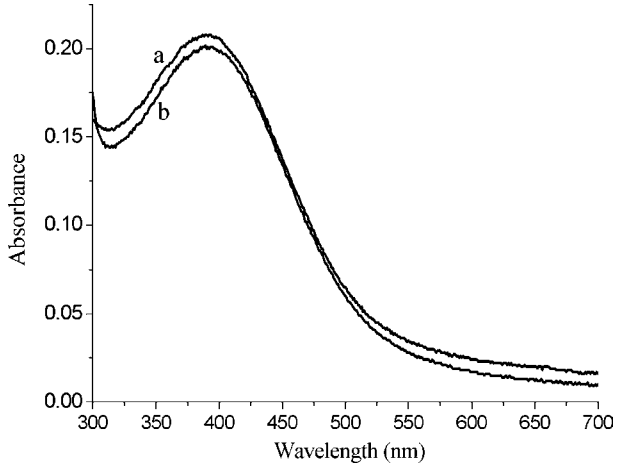

Fig. 2. UV–vis absorption spectra of (a) PMNT and (b) the mixture of PMNT, RTase M-MLV, and dNTPs. The solution a is prepared by addition 5.0 μL PMNT (1.0×10^{-3} M in RUs) in 100 μL buffer solution (10 mM Tris–HCl, 50 mM KCl, 1.5 mM $MgCl_2$, pH 8.3). The solution b is prepared by mixing of 100 units RTase M-MLV, 2.0 μL dNTPs (containing each dNTP of 2.5×10^{-3} M), 5.0 μL PMNT (1.0×10^{-3} M in RUs) and 100 μL buffer solution.

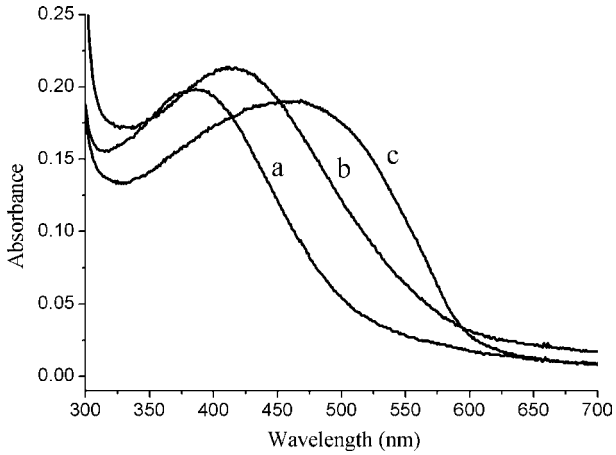

Fig. 3. UV–vis absorption spectra of (a) PMNT, (b) PMNT and primer extension reaction product of P_2/T_2, and (c) PMNT and primer extension reaction product of P_2/T_1. [PMNT] = 5×10^{-5} M in RUs, [P_2] = [T_1] = [T_2] = 2×10^{-6} M. The primer extension reactions were performed in Tris–HCl buffer (10 mM Tris–HCl, 50 mM KCl, 1.5 mM $MgCl_2$, pH 8.3) at 42 °C for 30 min in the presence 100 units RTase M-MLV and 5×10^{-5} M dNTPs.

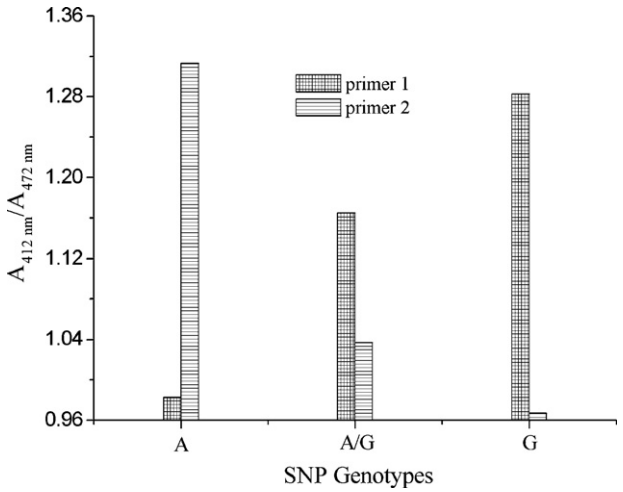

Fig. 4. The ratio of absorbance of 412 nm to 472 nm ($A_{412\,nm}/A_{472\,nm}$) as a function of homozygous A, heterozygous G/A, and homozygous G. The results are respectively acquired by using primer 1 and primer 2 as the primers for the extension reactions. The heterozygous G/A target was prepared by mixing wild target T_1 and mutant target T_2 at molar ratio of 1:1. The experimental conditions for primer extension reaction are the same as Fig. 3.

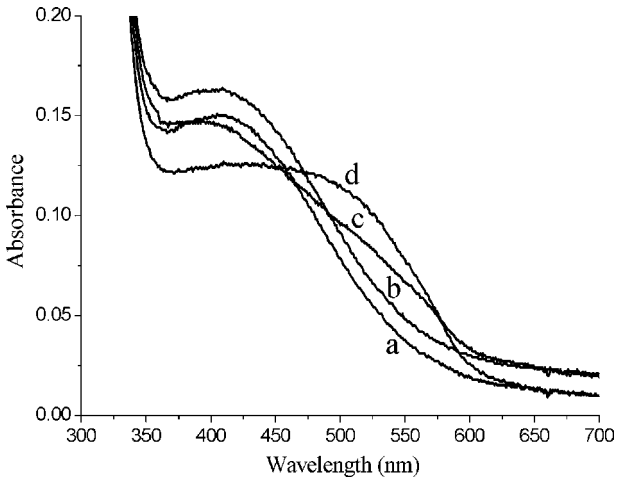

Fig. 6. UV–vis absorption spectra of (a) PMNT and T_1', (b) PMNT and the primer extension reaction product of P_1/T_1', (c) PMNT and the primer extension reaction product of P_1/T_2' after RNase H digestion, and (d) PMNT and the primer extension reaction product of P_1/T_1' after RNase H digestion.

UCU gUg CgC CAg UCU CUC CCA ggAC-3′) are used as the templates for primer extension reactions. Sequences of T_1' and T_2' are respectively the same as T_1 and T_2 except the deoxyribonucleotides and thymine in DNA targets are respectively replaced by ribonucleotides and uracil. Therefore, P_1 and P_2 can be also used as the primers for the primer extension reaction with RNA targets. The principle of SNP genotyping assay for RNA target is depicted in Fig. 5 and the experimental results are shown in Fig. 6. As shown in Fig. 6a, the absorption maximum of the duplex complex of RNA target (T_1') with PMNT appears around 410 nm, which is almost the same as that of triplex complex of dsDNA with PMNT (Fig. 3). This result indicates that PMNT conformation in RNA/PMNT duplex is similar to that in dsDNA/PMNT triplex, which can be attributed to RNA conformation easy to form secondary structure. When P_1 hybridizes with T_1' followed by extension reaction in the presence of RTase and dNTPs, the hybrid of RNA/DNA can be obtained. The absorption spectrum pattern (Fig. 6b) of the triplex of the RNA/DNA with PMNT is the same as that of RNA/PMNT duplex (Fig. 6a). RNase H specifically digests RNA only in complementary DNA/RNA hybrids. When the RNA strands in the RNA/DNA hybrids are specifically digested by ribonuclease H (RNase H), the ssDNA strand will be released. Upon addition of PMNT, the DNA/PMNT duplex can form and the much red-shifted absorption can be observed (Fig. 6d). In contrast, when the mutant RNA (T_2') is used as the template, P_1 extension reaction can not take place because the 3′-terminal base of P_1 (C) is not complementary to the base (A) of T_2 at the polymorphic site. Therefore, only P_1 can be released after the RNase H digestion. The formation of P_1/PMNT only results in a little absorption at long wavelength (Fig. 6c). One can see from Fig. 6 that the absorbance difference of a, b, c, and d reaches the maximum at 525 nm. Therefore, the col-

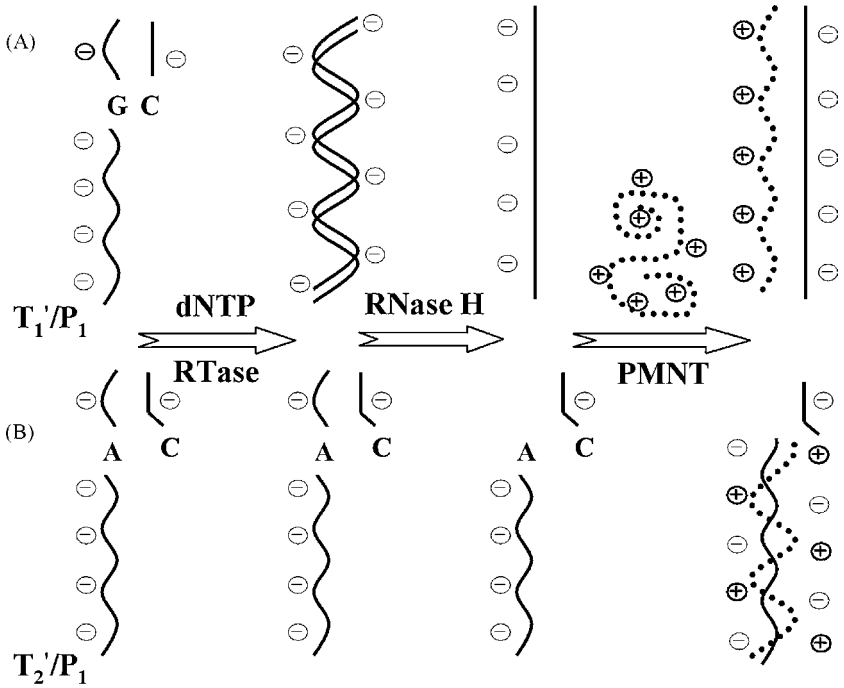

Fig. 5. Schematic representation of the SNP genotyping assay for RNA target.

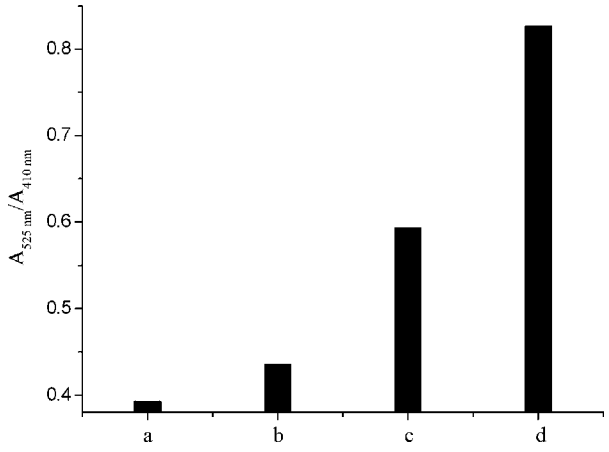

Fig. 7. The absorbance ratio of 525 nm to 410 nm ($A_{525\,nm}/A_{410\,nm}$) corresponding to the absorption spectra in Fig. 6. [PMNT] = 3×10^{-5} M in RUs, $[P_1] = [T'_1] = [T'_2] = 2 \times 10^{-6}$ M. The primer extension reactions were performed in Tris–HCl buffer (50 mM Tris–HCl, 75 mM KCl, 3 mM $MgCl_2$, 10 mM DTT, pH 8.3) at 42 °C for 1 h in the presence of 100 unit RTase M-MLV and 5×10^{-5} M dNTPs. 3.0 unit RNase H was mixed with the reaction product and incubated at 30 °C for 10 min in order to digest the RNA strands in RNA/DNA hybrids.

orimetric changes of PMNT can be characterized by the absorbance ratio of 525 nm to 410 nm ($A_{525\,nm}/A_{410\,nm}$). As shown in Fig. 7, combination of the primer extension reaction with the specific digestion of RNase H, the one-base mutation of RNA target can be clearly discriminated by measuring the colorimetric effects of PMNT.

4. Conclusion

In summary, a novel methodology for SNP genotyping assay of DNA and RNA targets has been developed based on conformational changes of the backbone of cationic polythiophene derivative. In contrast to previous reports [10], this new assay does not require any chemical modification of oligonucleotide probes and nucleic acid targets, which should significantly reduce the SNP genotyping cost. With the proposed method, all three kinds of SNP genotypes can be colorimetrically identified with one primer extension reaction in homogeneous solution. This procedure could provide simple operation without requirement of any separation steps and inexpensive instrumentation for reliable and robust SNP detection. The amplification, typically by the polymerase chain reaction (PCR), of the genomic DNA region that spans the locus of interest is a general step of SNP genotyping methods [23]. The application of the proposed method in real genomic sample analysis can be easily achieved by using standard PCR protocol. Therefore, we believe that the proposed SNP genotyping assay should be practical, especially for routinely clinical diagnoses in ordinary laboratories.

Acknowledgments

The project is supported by the National Natural Science Foundation of China (NSFC, No. 20675023), Program for New Century Excellent Talents in University (NCET-05-0258).

References

[1] The International SNP Working Group, Nature 409 (2001) 928–933.
[2] M.U. Ahmed, K. Idegam, M. Chikae, K. Kerman, P. Chaumpluk, S. Yamamura, E. Tamiya, The Analyst 132 (2007) 431–438.
[3] M. Hollstein, D. Sidransky, B. Vogelstein, C. Harris, Science 262 (1993) 1980–1981.
[4] The Wellcome Trust Case Control Consortium, Nature 447 (2007) 661–678.
[5] Z. Tsuchihashi, N.C. Pracopoli, Pharmacogenomics J. 2 (2002) 103–110.
[6] X. Chen, P.F. Sullivan, Pharmacogenomics J. 3 (2003) 77–96.
[7] R.J. Meagher, J.A. Coyne, C.N. Hestekin, T.N. Chiesl, R.D. Haynes, J.I. Won, A.E. Barron, Anal. Chem. 79 (2007) 1848–1854.
[8] G. Nallur, C. Luo, L. Fang, S. Vooley, V. Dave, J. Lambert, K. Kukanskis, S. Kingsmore, R. Lasken, B. Schweitaer, Nucleic Acids Res. 29 (2001) e118.
[9] S. Tyagi, D.P. Bratu, F.R. Kramer, Nat. Biotechnol. 16 (1998) 49–53.
[10] C. Dong, P. Zhang, R. Bi, J. Ren, Talanta 71 (2007) 1192–1197.
[11] C.E. Immoos, S.J. Lee, M.W. Gvinstaff, J. Am. Chem. Soc. 126 (2004) 10814–10815.
[12] N.L. Rosi, C.A. Mirkin, Chem. Rev. 105 (2005) 1547–1562.
[13] Y.C. Cao, R. Jin, C.S. Thaxton, C.A. Mirkin, Talanta 67 (2005) 449–455.
[14] E.S. Mansfield, J.M. Worley, S.E. Mckenzie, S. Surry, E. Rappaport, P. Fortina, Mol. Cell. Probes 9 (1995) 145–146.
[15] J. Hahm, C.M. Lieber, Nano Lett. 4 (2004) 51–54.
[16] A. Star, E. Tu, J. Niemann, J.P. Gabriel, C.S. Joiner, C. Valcke, Proc. Natl. Acad. Sci. U.S.A. 103 (2006) 921–926.
[17] H. Miyahara, K. Yamashita, M. Kanai, K. Uchida, M. Takagi, H. Kondo, S. Takenaka, Talanta 56 (2002) 829–835.
[18] H.X. Li, L.J. Rothberg, J. Am. Chem. Soc. 126 (2004) 10958–10961.
[19] T. Endo, K. Kerman, N. Nagatani, Y. Takamura, E. Tamiya, Anal. Chem. 77 (2005) 6976–6984.
[20] D.K. Kim, K. Kerman, M. Saito, R.R. Sathuluri, T. Endo, S. Yamamura, Y.S. Kwon, E. Tamiya, Anal. Chem. 79 (2007) 1855–1864.
[21] J.M. Song, A. Asthana, D.P. Kim, Talanta 68 (2006) 940–944.
[22] T. Pastinen, A. Kurg, A. Metspalu, L. Peltonen, A.C. Syvanen, Genome Res. 7 (1997) 606–614.
[23] I.K. Litos, P.C. Ioannou, T.K. Christopoulos, J. Traeger-Synodinos, E. Kanavakis, Anal. Chem. 79 (2007) 395–402.
[24] G.H. Zhou, M. Gotou, T. Kajiyama, H. Kambara, Nucleic Acids Res. 33 (2005) e133.
[25] X. Sun, H. Ding, K. Huang, B. Guo, Nucleic Acids Res. 28 (2000) e68.
[26] S.W. Thomas III, G. Joly, T.M. Swager, Chem. Rev. 107 (2007) 1339–1386.
[27] X.R. Duan, Z.P. Li, F. He, S. Wang, J. Am. Chem. Soc. 129 (2007) 4154–4155.
[28] X.R. Duan, S. Wang, Z.P. Li, Chem. Commun. 11 (2008) 1302–1304.
[29] H.A. Ho, M. Biossinot, M.G. Bergeron, G. Corbeil, K. Doré, D. Boudreau, M. Leclerc, Angew. Chem. Int. Ed. 41 (2002) 1548–1551.
[30] H.A. Ho, M. Béra-Abérem, M. Leclerc, Chem. Eur. J. 11 (2005) 1718–1724.
[31] K.P.R. Nilsson, O. Inganás, Nat. Mater. 2 (2003) 419–424.
[32] Y. Tan, F. Feng, F. He, S. Wang, Y. Li, D. Zhu, J. Am. Chem. Soc. 128 (2006) 14972–14976.
[33] H.A. Ho, M. Leclerc, J. Am. Chem. Soc. 125 (2003) 4412–4413.